Explicitly correlated random-phase approximation:
Development and application of a wave-function method

Zur Erlangung des akademischen Grades eines

Doktors der Naturwissenschaften

(Dr. rer. nat.)

von der KIT-Fakultät für Chemie und Biowissenschaften
des Karlsruher Instituts für Technologie (KIT)
genehmigte

Dissertation

von
Diplom-Chemikerin

Anna-Sophia Hehn

aus Würzburg

KIT-Dekan: Prof. Dr. W. Klopper
Referent: Prof. Dr. W. Klopper
Korreferent: Prof. Dr. J. Gauß
Tag der mündlichen Prüfung: 24. April 2017

Abstract

Development and application of a wave-function method The present thesis is concerned with the development of the random-phase approximation method aiming to overcome its slow basis-set convergence by combining it with the explicitly correlated wave-function ansatz of F12 theory. The random-phase approximation has proven as powerful approach to treat electron correlation, being capable to describe long-range interactions while exhibiting a favorable scaling of the computation time with respect to the system size. In this thesis, two ansätze are presented to further improve the computational efficiency of random-phase approximation methods, summarizing working equations, corresponding implementations and benchmark results. It is shown that basis-set convergence can be drastically accelerated when relying on the ring coupled-cluster doubles formulation. Benchmark results demonstrate that triple-zeta basis sets are sufficient to converge correlation and atomization energies to within 99% of the basis-set limit. An analogous improvement is achieved for several explicitly correlated ring coupled-cluster doubles ansätze including exact exchange. The connection to coupled-cluster theory is furthermore exploited to set up diagnostic schemes which allow to validate the applicability of the random-phase approximation depending on the system under investigation.

Keywords: *Ab initio* **quantum chemistry, random-phase approximation, F12 theory, coupled-cluster theory**

Kurzfassung

Entwicklung und Anwendung einer Wellenfunktionsmethode Gegenstand der vorliegenden Arbeit ist die Entwicklung der Random-Phase-Approximation-Methode, mit dem Ziel deren langsame Basissatzkonvergenz durch Kombination mit dem explizit korrelierten Wellenfunktionsansatz der F12-Theorie zu überwinden. Die Random-Phase-Approximation hat sich als leistungsfähiger Ansatz zur Erfassung der Elektronenkorrelation erwiesen, da sie langreichweitige Wechselwirkungen beschreiben kann und gleichzeitig eine vorteilhafte Skalierung der Rechenzeit mit der Systemgröße aufweist. Zur weiteren Verbesserung der Recheneffizienz der Random-Phase-Approximation-Methoden werden im Rahmen dieser Arbeit zwei Ansätze eingeführt und anhand einer Zusammenfassung der Arbeitsgleichungen, der zugehörigen Implementierungen und Benchmark-Ergebnisse vorgestellt. Es wird gezeigt, dass die Basissatzkonvergenz drastisch beschleunigt werden kann, wenn der Ring-Coupled-Cluster-Doubles-Ansatz zugrunde liegt. Benchmark-Ergebnisse veranschaulichen, dass triple-zeta-Basissätze ausreichen um Korrelations- und Atomisierungsenergien bis zu 99% des Basissatzlimits zu konvergieren. Eine vergleichbare Verbesserung wird für verschiedene explizit korrelierte Ring-Coupled-Cluster-Doubles-Ansätze erzielt, welche exakten Austausch berücksichtigen. Die Verbindung zur Coupled-Cluster-Theorie wird zudem verwendet um Diagnostiken zu entwickeln, die es ermöglichen die Anwendbarkeit der Random-Phase-Approximation in Abhängigkeit des zu untersuchenden Systems zu überprüfen.

Schlagwörter: *Ab-initio*-**Quantenchemie, Random-Phase-Approximation, F12-Theorie, Coupled-Cluster-Theorie**

Contents

1. Introduction

The development of a quantum-chemical method should be based on the aim of explaining, falsifying or even predicting experimental data, an undertaking which requires both broad applicability and sufficient accuracy. Applicability on the one hand to enable the investigation of larger systems, accuracy on the other hand to make rigorous and reliable quantitative predictions. Fulfilling both conditions is a major challenge in quantum chemistry: methods that reach the gold standard in terms of accuracy suffer from their complexity limiting applications to small systems. In reverse, universal applicability often comes with the charge of crucial approximations resulting in unpredictable and unreliable errors. This thesis focuses on a quantum-chemical method called random-phase approximation (RPA) which is claimed not only to yield a connection between the gold standard of accuracy and a universal, broad applicability, but also to combine both accuracy and applicability in a favorable ratio: On the one hand, RPA is an *ab initio* method not relying on empirical data, allowing to predict error ranges and therefore reliable results. Systematic improvement of the direct RPA approach is possible due to its connection to coupled-cluster methods and perturbation theory, so that accuracy can be tuned as needed by adding corrections. On the other hand, the non-perturbative RPA ansatz describes dispersion and is not sensible to small HOMO-LUMO gaps, enabling to tackle challenging systems like metal clusters or complexes with dominant van der Waals interactions. Moderate scaling of the computation time with respect to the size of the investigated system allows to exceed the computational limit of various other sophisticated wave-function methods.

These advantages motivate a further development of the RPA method and the following dissertation aims to make a contribution by combining RPA with the well-established explicitly correlated wave-function ansatz. Two different explicitly correlated RPA approaches are presented, investigating possible ansätze to improve basis-set convergence and thus computation times. Applicability is assessed with the focus on static correlation, aiming to answer the question: Can RPA treat systems with low computational cost? And is it possible to validate the applicability of RPA, a method, which is often claimed to be sufficiently accurate and universally applicable?

1.1 The random-phase approximation: climbing Jacob's ladder to touch heaven?

Universal applicability, sufficient accuracy and low computational cost are three striking qualities, which need further explanation if not intended to be meaningless. Certainly, a definition is always variable, given the fact that "sufficient" and "low" are adjectives that imply a reference or relating context, which can or even needs to be chosen depending on the examined molecular property and the field of applications. And "universal" can only be understood in the sense of "broad", as even the largest benchmark set can be controverted as insufficient. The following classification therefore has to be appraised keeping not only the vagueness in mind, but also tolerating a certain bias, as it was written from the viewpoint of wave-function theory designed to treat molecules in the gas phase. The emphasis is based on the random-phase approximation, aiming to outline and specify the wanted features "applicability, accuracy and efficiency" in reflection with the achievements and obstacles of current research.

Universal applicability

Applicability, accuracy and efficiency are always connected - high computational cost limits the applicability, applicability requires a certain accuracy and accuracy often increases the computational cost. One possibility to define universal applicability without referring to accuracy or efficiency is to interpret it as the ability of describing different sorts of correlation - defined for instance as static and dynamic correlation - in order to allow the treatment of molecular systems throughout the periodic table. A system is dominated by dynamic correlation if a single reference determinant is sufficient as zeroth-order description of the exact wave function. This is often the case for main-group compounds, where wave-function methods like coupled-cluster singles doubles (CCSD) or second-order Møller-Plesset perturbation theory (MP2) are standardly applied, based on a single Hartree-Fock (HF) determinant. In contrast, transition-metal chemistry is commonly associated with strong static correlation: due to the partially filled d shells and thereto nearly degenerate s shells, a variety of low-lying states emerge leading to a ground state with significant near-degeneracy correlation [1, 2]. In such cases, HF and the thereon relying post-HF correlation methods fail, leaving the field to multireference approaches or density-functional theory (DFT). Even though the latter is by definition a single-reference method, being based on solely one Kohn-Sham (KS) determinant, it can implicitly cover moderate static correlation through the exchange-correlation functional [3, 4]. DFT is thus claimed to be applicable to molecular systems throughout the periodic table, including transition metals [5] and f elements [6]. RPA adopts this advantage as it can equally rely on a KS determinant. Its capability to capture multireference effects goes hand in hand with its insensitivity towards small band gaps, one of the benefits where RPA takes precedence over perturbative methods like MP2 [7]. The list of RPA applications therefore includes transition-metal compounds [8], metal clusters [9, 10] and solids [11–13], demonstrating an equally broad applicability as DFT. RPA even outruns DFT when it comes to dynamic correlation, in particular dispersion interactions: The long-range forces, which are purely dynamical in character, are not captured by standard DFT functionals [14, 15], even though there has been recent progress in developing empirical corrections [16–19]. In contrast, RPA includes van der Waals interactions in a non-empirical, seamless way [20–23], enabling for example the description of the interlayer bonding in hexagonal boron nitride [24] or graphite [25] as well as the interaction between graphene and metal surfaces [26, 27]. In the latter study, both chemisorption and physisorption minima are described as well as the correct long-range asymptotics behavior. Consistent results for lattice constants and cohesive energies of noble gas solids [28], alkali, alkaline-earth and transition metals [29] support the claim that RPA accounts equally well for all bonding situations.

Sufficient accuracy

Since RPA "incorporates van der Waals interactions, but also describes ionic bonding, covalent and metallic bonding", Kresse *et al.* reason that it has the potential to be "universally applicable to solids, molecules and biological systems" [11]. However, abandoning the rather theoretical definition from above, it is certain that applicability *in practice* always requires sufficient accuracy in order to make reliable predictions.
In the most general and simple way, a method is said to be sufficiently accurate if it reproduces and confirms experimental data. As experiment also implies a certain variance or error range, the aim can only be of "chemical accuracy". This well-established landmark is fixed to 1 kcal/mol for thermochemistry of main-group compounds; for transition metals it is shifted towards 3 kcal/mol. Providing chemical or quantitative accuracy is the major advantage of coupled-cluster (CC) methods. The exponential wave-function ansatz enables a systematic improvement towards the exact result, reaching the gold standard of accuracy at the coupled-cluster singles doubles with perturbative triples (CCSD(T)) level. CCSD(T) results are considered

to be predictive and therefore standardly serve as benchmark reference circumventing a more involved, direct comparison with experiment. DFT in contrast is usually doomed to be not systematically improvable, grounded on a variety of exchange-correlation functionals which depend on empirical parameters and therefore often fail to give consistent results. An attempt to introduce a certain systematic into the huge spectrum of exchange-correlation functionals is the ordering of Jacob's ladder [30]. RPA as an orbital-dependent functional constitutes the fifth rung, thus it is located above the second rung GGA functionals TPSS [31] and PBE [32, 33] as well as third-rung hybrid functionals PBE0 [34] and B3LYP [35]. Going from GGA over hybrid functionals to RPA, one climbs Jacob's ladder from earth to heaven and based on this ordering, it is tempting to assume comparable smaller error bars. When regarding investigations on compounds over the whole periodic table, a promising but still ambiguous picture emerges:

Taking for instance a look at van-der-Waals systems, RPA convinces with its superior description of the long-range forces. Binding energies for the dispersion-dominated complexes of the S22 test set [36] deviate by a mean absolute error of 0.41 kcal/mol from the theoretical reference values [7], only slightly inferior to the fitted, dispersion-corrected B3LYP-D3 result of 0.36 kcal/mol. Relative energies of n-alkanes are found to be comparable in magnitude to CCSD(T) [23]. The mean absolute errors in lattice constants and atomization energies reduce about a factor of 2 in comparison to other semilocal and van-der-Waals corrected functionals [28, 29]. RPA binding energies of graphite or graphene-metal systems match experiment and are considered as current benchmark, used to assess the quality of DFT functionals [25, 27].

Regarding small-gap systems, like transition-metal compounds, metals or metal clusters, the performance of RPA appears more biased: Dissociation energies of third-row transition metal oxides are accurately predicted with a mean absolute deviation of 3.3 kcal/mol, outpacing the best-performing DFT functional TPSS with a comparable large error of 14.3 kcal/mol. For equilibrium bond distances and frequencies, RPA results are in contrast inferior to corresponding TPSS calculations [8]. Applications on neutral gold clusters [9] demonstrate that RPA can determine the 2D to 3D transition in structural growth, outperforming TPSS and supporting revTPSS [37] results at the same time. Cohesive energies of copper clusters are however too small and comparable to PBE0 [10], a hybrid functional which is known for its inconsistent performance concerning metals and metal clusters [38, 39]. The tendency towards underbinding is also found for atomization energies and heats of formation for a variety of semiconductors and metals; lattice constants are in contrast in good agreement with experiment, with relative errors smaller than 1% [11, 12]. Slightly larger errors are found for RPA band gaps which are only about 5% too large compared to the experimental values [13].

The selected applications not only highlight RPA's successful performance for interaction energies of dispersion-dominated compounds, but also reveal its failure when it comes to correlation and atomization energies. In general, a significant underbinding trend is found, not only for small-gap systems, but also for closed-shell main-group compounds [7, 40]. The failure is rooted in the inadequate description of short-range correlation and the self-interaction error, representing a major disadvantage of the direct RPA approach.

However, these apparently troublesome shortcomings can be cured when exploiting the method's connection to coupled-cluster and many-body perturbation theory: RPA is not only related to density-based approaches, but can equally well be derived in a wave-function framework [41–44], paving the way for systematic corrections. In the past decade, the connection served as starting point for several current research fields:

1. Various approaches have been set up to correct for exchange, either in a perturbative way [45–47] or via renormalization [8, 48–50]. The so-called approximate exchange kernel (AXK) [8, 51] is of the latter category. It successfully circumvents the self-interaction error and thus significantly improves atomization energies and ionization potentials without affecting reaction barriers. Second-order screened exchange (SOSEX) is in contrast a perturbative correction [45, 52], which corrects the self-interaction error but still suffers from numerical instabilities when applied to small-gap systems.

2. Single-excitation corrections [10, 50, 53] can be introduced to account for orbital relaxation, improving both correlation and binding energies [24, 54]. It was for instance shown by Scheffler *et al.* that the inclusion of both exchange (SOSEX) and single excitations results in a consistent improvement over RPA for test sets with dominant self-interaction, atomization energies and isogyric reactions [55].

3. A range of higher-order RPA approaches were suggested based on the generalizing polarization propagator formalism [56, 57], considering additional double excitations in the excitation manifold [58, 59] or a correlated ground state beyond a single HF determinant [60–62]. Heßelmann also investigated the impact of third-order corrections on the RPA correlation energy [63].

Numerous other beyond-RPA approaches exist (see e.g. the overviews in Refs. [7, 24]) and the number is steadily increasing, however, none of the developed approaches has so far established itself as flawless, optimal choice. This is mainly due to the fact that improvement on one side often entails certain drawbacks on the other. The inclusion of exact exchange e.g. corrects the self-interaction error, but worsens the description

of left-right correlation [64]. Moreover, most proposed schemes cannot compete with the favorable scaling of the initial direct RPA ansatz [65]. AXK for instance increases the computational cost to N^6; SOSEX scales as N^5 with respect to the system size N.

High efficiency

Low computational cost is however one of the crucial characteristics that the ideal quantum-chemical method should possess. The success of DFT is certainly aligned to its moderate scaling, for GGA functionals e.g. the computation times increase proportional to N^3 with the number of basis functions N. In comparison, the scaling of RPA is higher, showing an $N^4 \log N$ dependence [65–67], but the method is in contrast to DFT non-iterative. In practice, RPA calculations are therefore routinely faster than conventional HF or KS calculations [68], allowing to treat large systems with up to 1500 atoms. Large-scale applications are for example reported in Refs. [69, 70]. Implementations on Gaussian atomic orbitals are available in the TURBOMOLE program package [65, 71]; plane-wave implementations are provided by the CP2K simulation package [69, 72, 73] and the VASP program [28, 66, 67]. Also note that a variety of other RPA implementations exist, see e.g. Refs. [74–76], and that linear scaling RPA approaches were published only recently [77–79]. For both atomic orbital and plane-wave implementations, the moderate scaling of the direct RPA approach is achieved by exploiting resolution of the identity (RI) techniques which speeds up the calculation of the integrals and reduces the memory requirements. The so-obtained gain in efficiency is remarkable: as shown for instance in Ref. [69], RIRPA energies of condensed phase systems with up to 1500 atoms can be computed in less than one hour. Nevertheless, efficiency suffers from the slow basis-set convergence which is inherent to RPA as a wave-function method based on atomic orbitals [80, 81]. The basis-set incompleteness error, which is introduced by truncating the one-electron basis, entails the need to go for larger and larger basis sets including basis functions of higher and higher angular momentum quantum numbers. In particular, it was shown that convergence is proportional to X^3 with the angular momentum quantum number X and that basis sets of quadruple- or even quintuple-zeta quality are required to converge RPA atomization and interaction energies to the basis-set limit [40, 80]. Furthermore, the unfavorable basis-set dependence has as consequence that RPA interaction energies are often flawed by the basis-set superposition error (BSSE) [82]. The overlap of atomic basis functions results in a spurious stabilization of the dimer complex relative to its individual monomers, leading to large errors in the binding energy. Thus, both basis-set incompleteness and superposition error have to be taken into account when aiming for a robust and efficient quantum-chemical method. More precisely, the quest should be focused on equilibrating the methodological error, introduced by approximating the N-electron wave-function ansatz, with the basis-set incompleteness error, conceded through the truncation of the one-electron basis.

1.2 Tuning efficiency with explicitly correlated wave-function theory

Regarding the rapidly growing research field of more and more accurate beyond-RPA methods thus calls for equally sophisticated approaches to tackle the problem of RPA's intrinsically slow basis-set convergence. Fortunately, several remedies exist: asymptotic laws allow for instance to set up extrapolation schemes [83–85]. Fabiano *et al.* applied various extrapolation formulae to investigate the basis-set dependence of RPA [81], showing that the basis-set limit is reached for a two-point extrapolation when using quintuple- and sextuple-zeta basis sets. A corresponding extrapolation including basis sets of quadruple-zeta size was found to be insufficient and the authors therefore recommend to either increase the basis-set size or to fall back on semiempirical extrapolation schemes. Moreover, basis-set convergence can be accelerated when combining short-range RPA with long-range DFT in terms of a range-separated wave-function ansatz [86–89]. Describing the critical short-range part of the correlation hole within density-functional theory accelerates convergence, in particular, Franck *et al.* showed that both the short- and the long-range part of range-separated RPA approaches converge exponentially with the maximum angular momentum quantum number [90]. A third alternative is given by explicitly correlated wave-function methods [91–93]: the idea of F12 theory is to improve the wave-function ansatz by considering geminals in the wave-function expansion. Incorporating two-particle basis functions which depend explicitly on the interelectronic distance improves the description of the Coulomb hole, decreasing the asymptotic dependence of the correlation energy from X^{-3} to X^{-7} [94, 95].

The success story of F12 methods

During the last decades, F12 methods have therefore been established as efficient working tools in wave-function theory. The hour of birth can be seen in a series of fundamental papers by Kutzelnigg and co-

workers [93, 96–98], originating and developing the idea of an explicitly correlated wave-function ansatz. First applications of explicitly correlated MP2 theory demonstrated its usefulness and paved the way to a rapidly growing research field [97]. While the initial ansatz assumed a linear dependence on the interelectronic distance r_{12}, it later on became state of the art to work with Slater geminals, now depending exponentially on r_{12} [99, 100]. Higher efficiency was achieved by introducing auxiliary basis sets for the resolution of the identity [95, 101] and by developing a complementary auxiliary basis (CABS) [102]. It was furthermore found that keeping the geminal amplitudes fixed according to the cusp conditions reduces the scaling while the loss of accuracy is negligible [99, 103]. Different ansätze for projection operators were investigated, ensuring that the geminal excitation manifold is strongly orthogonal to the conventional HF orbitals [104]. Based on these developments, a variety of highly efficient explicitly correlated wave-function methods have been developed, reaching e.g. from MP2-F12 theory [105] to CCSD(T)(F12) [106, 107] and allowing to treat not only correlation, but also excitation energies [108, 109] as well as gradients [110, 111]. Most importantly it was shown that triple-zeta basis sets are in general sufficient to reach quintuple-zeta quality [112]. The F12 ansatz thus represents a large saving in computation time, primarily due to the computation of the Hartree-Fock wave function.

Incorporating an interelectronic property in a time-dependent mean-field approach — an outline

The aim of this thesis is to combine the explicitly correlated wave-function approach with the random-phase approximation in order to enable fast basis-set convergence for correlation energies. Given the fact that F12 geminals are standardly introduced by describing the wave-function expansion as an exponential ansatz of excitation operators acting onto the reference determinant, two derivations of explicitly correlated RPA are presented using an analogous wave-function formalism: the first is based on the equations of motion, allowing to describe the RPA ground state as a linear combination of the reference determinant, conventional doubly excited states as well as the additionally introduced geminal manifold (Chapter 3). The second approach exploits the connection of RPA and coupled-cluster theory, implying that RPA single excitation vectors can be coupled to yield a double excitation amplitude (Chapter 4). Inclusion of exchange is also investigated, regarding several approximate ring coupled-cluster schemes and investigating their sensitivity towards triplet instabilities. Furthermore, it is the goal to learn about the shortcomings of RPA theory: wave-function diagnostics which have proven to be feasible tools in coupled-cluster theory are transferred to RPA and tested on small main-group molecules in Chapter 5.

2. The starting point — a summary on achievements in the field of RPA and F12 theories

2.1 Calculating ground-state energies within the random-phase approximation

Since David Bohm and David Pines set up their approximate electron-correlation method in the 1950s [113–115], a variety of "random-phase approximation" methods have been developed. The historical development of the RPA method gives an overview over the huge spectrum of approaches, revealing and underlining the impact of Bohm and Pines' initial concept (see for example Refs. [7, 24]). All approaches are essentially based on the approximation that the electron correlation is described by the Coulomb potential and single-particle excitations only, but differ in the working equations, the treatment of exchange and the underlying reference determinant. Inconsistencies in the nomenclature exist since many methods were only shown to be equivalent to the RPA ansatz in retrospect. Using a Hartree-Fock (HF) determinant as reference and including exact exchange, the RPA eigenvalue problem is for instance equivalent to time-dependent Hartree-Fock theory [116]. To avoid misunderstandings, it therefore became a convention to refer to "direct" RPA (dRPA) when strictly speaking of the original ansatz neglecting exchange. In contrast, RPA acronyms representing approaches including exchange are in generally substituted or completed by a variety of abbreviations specifying the underlying characteristic treatment of exchange. The nomenclature in the following chapters of this thesis sticks to this convention, thus referring to RPA as a generic term for both direct and exchange methods, while specifying the latter two approaches by adding the specific acronym. Furthermore, if not stated otherwise the derived equations hold for both HF and Kohn-Sham (KS) determinants, also in cases where only one of the two is stated explicitly.

Even though the aim of the thesis is focused on calculating ground-state energies, it is necessary to review the calculation of excitation energies first, in order to introduce the basic approximations defining the RPA approach. The outline on RPA is therefore split in two parts: first deriving the RPA eigenvalue problem and subsequently introducing explicit expressions for the RPA correlation energy. For both steps, several ansätze exist, all leading to more or less equivalent working equations for excitation energies and the correlation energy. The following summary focuses on those ansätze which are used in subsequent chapters to derive explicitly correlated RPA approaches.

The RPA eigenvalue problem: Starting from the equations of motion / the hypervirial theorem

In 1977, Bouman and Hansen derived the RPA equations in a wave-function formulation based on the equations of motion [117, 118],

$$-i\frac{d}{dt}\hat{Q} = [\hat{H}, \hat{Q}]\,, \tag{2.1}$$

describing the time-dependence of an arbitrary, single-particle operator $\hat{Q}$ in terms of its commutator with the Hamiltonian $\hat{H}$. Note that atomic units are used in Eq. (2.1) and in the following. The expectation value of the commutator with respect to the complete set of orthonormal eigenstates of the Hamiltonian $|\Psi_n\rangle$ is known as the general or the off-diagonal hypervirial theorem [119],

$$\langle\Psi_n|[\hat{Q}, \hat{H}]|\Psi_n\rangle = 0\,, \tag{2.2}$$

$$\langle\Psi_m|[\hat{Q}, \hat{H}]|\Psi_n\rangle = \Omega_{nm}\langle\Psi_m|\hat{Q}|\Psi_n\rangle\,. \tag{2.3}$$

Ω_{nm} denote excitation energies corresponding to the difference of eigenvalues ε_n, $\Omega_{nm} = \varepsilon_n - \varepsilon_m$. When referring to the ground state $|0\rangle$, the second index of Ω_{n0} is in the following omitted, using the short-hand notation Ω_n. To solve Eq. (2.3) within the RPA, Bouman and Hansen chose the projection manifolds $|\Psi_m\rangle$ and $|\Psi_n\rangle$ as

$$|\Psi_m\rangle = |\Psi_0\rangle = N_0 [|\mathrm{HF}\rangle + \tfrac{1}{2} \sum_{ijab} t_{ij}^{ab} |_{ij}^{ab}\rangle] \,, \tag{2.4}$$

$$|\Psi_n\rangle = \sum_{ia} t_{ai}^n |_i^a\rangle \,. \tag{2.5}$$

The closed-shell ground state $|\Psi_0\rangle$ is thus given as the sum of the HF (or KS) determinant $|\mathrm{HF}\rangle$ (or $|\mathrm{KS}\rangle$) and the doubly excited states $|_{ij}^{ab}\rangle$, weighted by the doubles amplitudes t_{ij}^{ab} and the normalization constant N_0. The excitation manifold is described as a linear combination of singly excited states $|_i^a\rangle$, parameterized in terms of the singles amplitudes t_{ai}^n corresponding to the excited state n. Real spatial orbitals are assumed; $\{a, b, \dots\}$ indicate virtual and $\{i, j, \dots\}$ occupied orbitals. The chosen ansatz has the advantage of demonstrating that the RPA ground state is correlated, including the doubly excited states $|_{ij}^{ab}\rangle$. The role of double excitations becomes even more apparent when following the further derivation: Introducing the resolution of the identity to evaluate the commutator on the left-hand side of Eq. (2.3), one obtains an equation which depends on the left and right transition moments of the single-particle operator $\hat{Q}$, $\langle_i^a|\hat{Q}|\mathrm{HF}\rangle$ and $\langle \mathrm{HF}|\hat{Q}|_i^a\rangle$, respectively. The transition moments can be assumed to be linearly independent because the arbitrary operator $\hat{Q}$ can be written as the sum of an Hermitian and an anti-Hermitian operator. Eq. (2.3) can thus be split into a set of coupled equations,

$$\sum_{bj} (A_{ij}^{ab} X_{bj}^n + B_{ij}^{ab} Y_{bj}^n) = \Omega_n X_{ai}^n \,,$$

$$\sum_{bj} (A_{ij}^{ab} Y_{bj}^n + B_{ij}^{ab} X_{bj}^n) = -\Omega_n Y_{ai}^n \,, \tag{2.6}$$

given in matrix notation as

$$\begin{pmatrix} \mathbf{A} & \mathbf{B} \\ \mathbf{B} & \mathbf{A} \end{pmatrix} \begin{pmatrix} \mathbf{X}^n \\ \mathbf{Y}^n \end{pmatrix} = \Omega_n \begin{pmatrix} \mathbf{1} & \mathbf{0} \\ \mathbf{0} & -\mathbf{1} \end{pmatrix} \begin{pmatrix} \mathbf{X}^n \\ \mathbf{Y}^n \end{pmatrix} . \tag{2.7}$$

Details on the derivation are outlined in Refs. [51, 117] and discussed in Appendix D if crucial for the thereon based RPA-F12 method of Chapter 3. It is only noted that, for closed-shell references, the normalization of the metric to unity is in the following conserved by introducing the biorthogonal basis, indicated by an overline as $\{|_i^{\bar{a}}\rangle, |_{ij}^{\overline{ab}}\rangle, \dots\}$ and used in the following as defined in Eqs. (A.1) and (A.2) of Appendix A.

Eq. (2.7) represents an Hermitian eigenvalue problem: Ω_n are the requested excitation energies while $\mathbf{X}^n$ and $\mathbf{Y}^n$ denote the eigenvectors, here defined in connection with the double and single excitation amplitudes t_{ab}^{ij} and t_{ai}^n,

$$X_{ai}^n = N_0 t_{ai}^n \,, \tag{2.8}$$

$$Y_{ai}^n = N_0 \sum_{bj} t_{ij}^{ab} t_{bj}^n \,, \tag{2.9}$$

implying that amplitudes and coefficients are connected through

$$\mathbf{T} = \mathbf{Y}\mathbf{X}^{-1} \,. \tag{2.10}$$

The Hermitian matrix $\mathbf{A}$ represents the contraction of the Hamiltonian with singly excited determinants, resulting in a zeroth-order term of the Fock (or KS) matrix elements F_{pq} and the first-order two-electron integrals g_{qs}^{pr},

$$A_{ij}^{ab} = \langle_i^{\bar{a}}|\hat{H}|_j^b\rangle - \delta_{ab}\delta_{ij}\langle \mathrm{HF}|\hat{H}|\mathrm{HF}\rangle = \langle \mathrm{HF}|\hat{E}_{ia}[\hat{H}, \hat{E}_{bj}]|\mathrm{HF}\rangle$$

$$\overset{\mathrm{RPAX}}{=} F_{ab}\delta_{ij} - F_{ji}\delta_{ab} + 2g_{ib}^{aj} - g_{bi}^{aj} \overset{\mathrm{dRPA}}{=} F_{ab}\delta_{ij} - F_{ji}\delta_{ab} + 2g_{ib}^{aj} \,. \tag{2.11}$$

The symmetric matrix $\mathbf{B}$, in contrast, is obtained through projection onto doubly excited determinants,

$$B_{ij}^{ab} = \langle_{ij}^{\overline{ab}}|\hat{H}|\mathrm{HF}\rangle = \langle \mathrm{HF}|[\hat{E}_{ia}, [\hat{E}_{jb}, \hat{H}]]|\mathrm{HF}\rangle$$

$$\overset{\mathrm{RPAX}}{=} 2g_{ij}^{ab} - g_{ji}^{ab} \overset{\mathrm{dRPA}}{=} 2g_{ij}^{ab} \,. \tag{2.12}$$

To allow a straightforward comparison with other, in the following introduced wave-function methods, the matrix elements of $\mathbf{A}$ and $\mathbf{B}$ are expressed in terms of single-excitation operators $\hat{E}_{pq}$. For closed-shell systems, $\hat{E}_{pq}$ is defined as a linear combination of creation and annihilation operators, $\hat{a}_{p\sigma}^{\dagger}$ and $\hat{a}_{p\sigma}$, summing over both spin contributions $\sigma = \alpha, \beta$,

$$\hat{E}_{pq} = \hat{a}_{p\alpha}^{\dagger}\hat{a}_{q\alpha} + \hat{a}_{p\beta}^{\dagger}\hat{a}_{q\beta}. \tag{2.13}$$

The creation operator $\hat{a}_p^{\dagger}$ creates and the complementary operator $\hat{a}_p$ annihilates a particle in the spatial orbital ϕ_p. $\{p, q, \ldots\}$ denote the complete molecular orbital basis and the two-electron integrals are throughout the thesis defined as

$$g_{qs}^{pr} = \int\int \phi_p^*(r_1)\phi_r^*(r_2)\frac{1}{|r_1 - r_2|}\phi_q(r_1)\phi_s(r_2)\mathrm{d}r_1\mathrm{d}r_2 = \langle pr|qs\rangle. \tag{2.14}$$

Eqs. (2.11) and (2.12) summarize the matrix contributions for both direct RPA and RPAX including exchange, indicated by the label on top of the corresponding equality signs. Note that in the case of dRPA, the two-electron contribution to matrices $\mathbf{A}$ and $\mathbf{B}$ is identical since $g_{aj}^{ib} = g_{ab}^{ij} = g_{ij}^{ab}$ for real orbitals. The difference between dRPA and RPAX also has to be taken into account when drawing the corresponding Goldstone diagrams, as given in Fig. 2.1. While the Fock matrix contribution to the matrix $\mathbf{A}$, visualized in terms of the first two diagrams, is equal for both dRPA and RPAX, the two-electron integrals and the related last two diagrams require a twofold definition in order to enable a discrimination between both methods: for dRPA, the dashed line corresponds to the non-antisymmetrized two-electron interaction, whereas the antisymmetrized counterpart is required for RPAX. However, standardly, antisymmetrized Goldstone diagrams are solely used to represent open-shell equations referring to spin orbitals, while ordinary Goldstone diagrams are reserved to closed-shell cases and spatial orbitals. Interpretation rules thus have to be adopted accordingly. A detailed summary on the nomenclature for antisymmetrized and ordinary Goldstone diagrams is given in Appendix A.
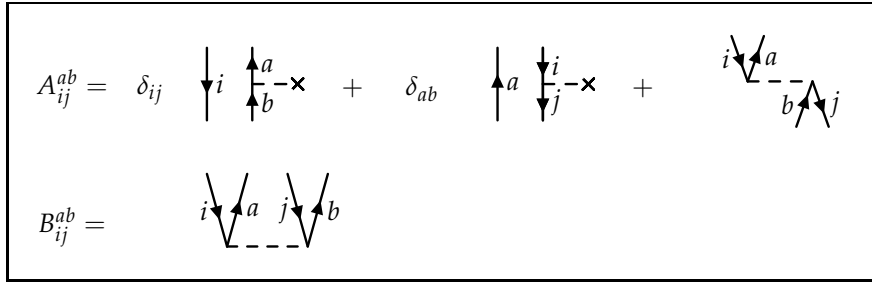

Fig. 2.1: Diagrammatic representation of the orbital rotation Hessians $\mathbf{A}$ and $\mathbf{B}$.

Due to the projection onto doubly excited determinants, it is sometimes claimed that the matrix $\mathbf{B}$ could be interpreted as a double-excitation or correlation contribution [120]. This interpretation is opposed to the picture that emerges for example from coupled-cluster (CC) theory [121]: Optimizing the connected expectation value of the coupled-cluster singles wave function with respect to the singles amplitudes leads to identical definitions for matrices $\mathbf{A}$ and $\mathbf{B}$, supporting the viewpoint that both terms arise from orbital relaxation. Indeed, they are most often referred as orbital rotation Hessians, emphasizing the connection to coupled-perturbed HF theory. This ambivalent nature of the $\mathbf{B}$ matrix has to be kept in mind when combining RPA and F12 theory. Furthermore, the discussion should not be mixed up with the interpretation of the matrices $\mathbf{X}$ and $\mathbf{Y}$: Standardly, the matrix $\mathbf{Y}$ is considered as correlation contribution. Neglecting $\mathbf{Y}$, the coupled RPA equations reduce to an uncoupled eigenvalue problem, the Tamm-Dancoff approximation (TDA) [122].

Approximating the excitation operator and the ground state - Connection to response theory and polarization propagators

Already ten years earlier than Bouman and Hansen, Rowe published a similar derivation based on the equations of motion, which solely differs by *a priori* assumed approximations [41, 42, 123]. While Bouman and Hansen specify ground and excited states in an *ad hoc* way, Rowe assumed the following two approximations for the single-particle operator $\hat{Q}$: The first is that the correlation energy can be captured by only introducing single excitations in the wave-function expansion, described via the excitation operator $\hat{Q}_n^{\dagger}$ [124],

$$\hat{Q}_n^{\dagger} = \sum_{ia}(X_{ai}^n\hat{E}_{ai} + Y_{ai}^n\hat{E}_{ia}). \tag{2.15}$$

X_{ai}^n and Y_{ai}^n are again single excitation amplitudes describing the excited state n. The second approximation is to assume boson commutation rules, ensuring a normalization of the ground state $|\Psi_0\rangle$ [125],

$$\langle \overline{\Psi}_0|[\hat{Q}_n, \hat{Q}_m^\dagger]|\Psi_0\rangle = \sum_{ai}\left[(X_{ai}^n)^{\mathrm{T}} X_{ai}^m - (Y_{ai}^n)^{\mathrm{T}} Y_{ai}^m \right] = \delta_{nm}\,, \tag{2.16}$$

a relation which is automatically fulfilled for HF (or KS) references. Based on these two assumptions, Eq. (2.3) can be formulated as

$$\langle \bar{q}|[\hat{H}, \hat{Q}_n^\dagger]|\mathrm{HF}\rangle = \Omega_n \langle \bar{q}|\hat{Q}_n^\dagger|\mathrm{HF}\rangle\,, \tag{2.17}$$

with the projection manifold of single excitations $\langle \bar{q}| = \langle 0|\delta \hat{Q}_n$. Applying standard commutation rules finally leads to the RPA eigenvalue problem of Eq. (2.7).

The ansatz of Rowe has the advantage that it is much more general, allowing to draw the connection to higher-order RPA approaches. This can be demonstrated even more apparently when reformulating the equations of motion in terms of polarization propagators, exposing RPA to be a first-order polarization propagator approach [56]. For a detailed introduction and comprehensive literature about response theory or polarization propagator methods, the reader is referred for instance to Refs. [56, 57, 124, 126, 127]. For the sake of convenience, the density matrix response function or polarization propagator $\mathbf{\Pi}(\Omega)$ is here just shortly introduced as the inverse of Eq. (2.7),

$$\mathbf{\Pi}(\Omega) = -(\mathbf{\Lambda} - \Omega\mathbf{\Sigma})^{-1}\,, \tag{2.18}$$

relying on the superoperator formulation of Eqs. (2.7) and (2.16),

$$(\mathbf{\Lambda} - \Omega_n\mathbf{\Sigma})|\mathbf{X}^n, \mathbf{Y}^n\rangle = 0\,, \tag{2.19}$$

$$\langle \mathbf{X}^n, \mathbf{Y}^n|\mathbf{\Sigma}|\mathbf{X}^m, \mathbf{Y}^m\rangle = \delta_{nm}\,, \tag{2.20}$$

with the superoperator matrices

$$\mathbf{\Lambda} = \begin{pmatrix} \mathbf{A} & \mathbf{B} \\ \mathbf{B} & \mathbf{A} \end{pmatrix} \quad \text{and} \quad \mathbf{\Sigma} = \begin{pmatrix} \mathbf{1} & \mathbf{0} \\ \mathbf{0} & -\mathbf{1} \end{pmatrix}\,, \tag{2.21}$$

and the super-column and -row vectors $|\mathbf{X}^n, \mathbf{Y}^n\rangle$ and $\langle \mathbf{X}^n, \mathbf{Y}^n|$. This result for the RPA polarization propagator can be derived by assuming the same approximations as in the derivation of Rowe: Eq. (2.18) is obtained by considering the manifold of single excitations and de-excitations only, represented by the one-electron operator $\hat{\mathbf{Q}}^\dagger = \left\{ \sum_{ai} \hat{E}_{ai}, \sum_{ai} \hat{E}_{ia} \right\}$,

$$\mathbf{\Pi}(\Omega) = -(\mathbf{Q}^\dagger|(\breve{H} - \Omega\breve{1})^{-1}|\mathbf{Q}^\dagger)\,. \tag{2.22}$$

Note that $|\mathbf{Q}^\dagger)$ is the super-row vector corresponding to the operator $\hat{\mathbf{Q}}^\dagger$ and that expectation values in the superoperator formalism represent commutators according to $(\mathbf{P}|\breve{H}|\mathbf{Q}) = \langle \Psi_0|[\hat{\mathbf{P}}^\dagger, [\hat{H}, \hat{\mathbf{Q}}]]|\Psi_0\rangle$. Superoperators $\breve{H}$ and $\breve{1}$ are defined as $\breve{H}\hat{X} = [\hat{H}, \hat{X}]$ and $\breve{1}\hat{X} = \hat{X}$. In the following, the manifold of excitation and de-excitation operators $\sum_{ia} \hat{E}_{ai}$ and $\sum_{ia} \hat{E}_{ia}$ is indicated by $\hat{\mathbf{E}}$ and $\hat{\mathbf{E}}^\dagger$.

The 2×2 super-matrix representation of $\mathbf{\Pi}(\Omega)$ [51, 128],

$$\mathbf{\Pi}(\Omega) = \begin{pmatrix} \langle\langle \hat{\mathbf{E}}^\dagger, \hat{\mathbf{E}}\rangle\rangle(\Omega) & \langle\langle \hat{\mathbf{E}}^\dagger, \hat{\mathbf{E}}^\dagger\rangle\rangle(\Omega) \\ \langle\langle \hat{\mathbf{E}}, \hat{\mathbf{E}}\rangle\rangle(\Omega) & \langle\langle \hat{\mathbf{E}}, \hat{\mathbf{E}}^\dagger\rangle\rangle(\Omega) \end{pmatrix}\,, \tag{2.23}$$

can be formulated based on the response function $\langle\langle \hat{\mathbf{E}}^\dagger, \hat{\mathbf{E}}\rangle\rangle(\Omega)$,

$$\begin{aligned} \langle\langle \hat{\mathbf{E}}^\dagger, \hat{\mathbf{E}}\rangle\rangle(\Omega) &= -(\mathbf{E}|(\breve{H} - \Omega\breve{1})^{-1}|\mathbf{E}) \\ &= -\langle \Psi_0|[\hat{\mathbf{E}}^\dagger, [\hat{\mathbf{E}}, (\hat{H} - \Omega\hat{1})^{-1}]]|\Psi_0\rangle\,. \end{aligned} \tag{2.24}$$

Within RPA, the commutator of Eq. (2.24) is approximated by choosing the HF (or KS) determinant as reference state $|\Psi_0\rangle$. Furthermore, the evaluation of the inverse in Eq. (2.24) is simplified by exploiting the resolution of the identity, projecting the equations onto the single excitation manifold $|\mathbf{h}) = \left\{ \hat{\mathbf{E}}, \hat{\mathbf{E}}^\dagger \right\}$ [56, 126],

$$\begin{aligned} \mathbf{\Pi}(\Omega) &= -(\mathbf{Q}^\dagger|\mathbf{h})(\mathbf{h}|\breve{H} - \Omega\breve{1}|\mathbf{h})^{-1}(\mathbf{h}|\mathbf{Q}^\dagger)\,, \\ &= -\begin{pmatrix} (\mathbf{E}|\mathbf{E}) & (\mathbf{E}|\mathbf{E}^\dagger) \\ (\mathbf{E}^\dagger|\mathbf{E}) & (\mathbf{E}^\dagger|\mathbf{E}^\dagger) \end{pmatrix} \begin{pmatrix} (\mathbf{E}|\breve{H} - \Omega\breve{1}|\mathbf{E}) & (\mathbf{E}|\breve{H} - \Omega\breve{1}|\mathbf{E}^\dagger) \\ (\mathbf{E}^\dagger|\breve{H} - \Omega\breve{1}|\mathbf{E}) & (\mathbf{E}^\dagger|\breve{H} - \Omega\breve{1}|\mathbf{E}^\dagger) \end{pmatrix}^{-1} \begin{pmatrix} (\mathbf{E}|\mathbf{E}) & (\mathbf{E}|\mathbf{E}^\dagger) \\ (\mathbf{E}^\dagger|\mathbf{E}) & (\mathbf{E}^\dagger|\mathbf{E}^\dagger) \end{pmatrix} \\ &= -\begin{pmatrix} \mathbf{U} & \mathbf{0} \\ \mathbf{0} & -\mathbf{U} \end{pmatrix} \begin{pmatrix} \mathbf{A} - \Omega\mathbf{U} & -\mathbf{B} \\ -\mathbf{B} & \mathbf{A} + \Omega\mathbf{U} \end{pmatrix}^{-1} \begin{pmatrix} \mathbf{U} & \mathbf{0} \\ \mathbf{0} & -\mathbf{U} \end{pmatrix}\,, \end{aligned} \tag{2.25}$$

with the already known definitions for the Hessian matrices $\mathbf{A}$ and $\mathbf{B}$ (see Eqs. (2.11) and (2.12)) and the metric $\mathbf{U}$,

$$A_{ij}^{ab} = (E_{ai}|\breve{H}|E_{bj}) = (E_{ai}^{\dagger}|\breve{H}|E_{bj}^{\dagger}) = \langle \mathrm{HF}|[\hat{E}_{ia}, [\hat{H}, \hat{E}_{bj}]]|\mathrm{HF}\rangle \,, \tag{2.26}$$

$$B_{ij}^{ab} = -(E_{ai}|\breve{H}|E_{bj}^{\dagger}) = -(E_{ai}^{\dagger}|\breve{H}|E_{bj}) = -\langle \mathrm{HF}|[\hat{E}_{ia}, [\hat{H}, \hat{E}_{jb}]]|\mathrm{HF}\rangle \,, \tag{2.27}$$

$$U_{ij}^{ab} = (E_{ai}^{\dagger}|E_{bj}) = \langle \mathrm{HF}|[\hat{E}_{ia}, \hat{E}_{bj}]|\mathrm{HF}\rangle \,. \tag{2.28}$$

The advantage of the polarization propagator formulation is that it paves the way to higher-order approaches based on the expansion of the reference state and the excitation manifold to single, double, triple etc. excitations. A perturbation analysis up to third order is for example summarized in Ref. [129]. A variety of higher-order RPA schemes were suggested, considering a correlated ground state [60–62], a two-particle, two-hole correction [58, 130, 131] or the expansion of the excitation manifold to double excitations [58, 59]. These methods closely resemble the second-order polarization propagator approximation (SOPPA) [56, 132, 133]; a diagrammatic comparison is e.g. given in Ref. [129]. It should be noted that it is also common to apply Löwdin partitioning [134] to fold the double-excitation space into the single-excitation space, reducing the dimension of the higher-order RPA eigenvalue problem and allowing to introduce additive two-particle, two-hole corrections [58, 130, 131].

The derivations presented so far define the RPA method by (1) approximating the ground state and the excited state in terms of singly and doubly excited determinants or (2) by restricting the projection manifold to single (de-)excitations and by choosing a HF (or KS) determinant as reference state. In the framework of time-dependent density-functional theory based on the density response function and the KS determinant, a third "definition" of the random-phase approximation is common: Its connection to the already introduced derivations can be highlighted by rewriting the density matrix response function in a Dyson-type form [124, 135],

$$\mathbf{\Pi}(\Omega) = \mathbf{\Pi}^0(\Omega) + \mathbf{\Pi}^0(\Omega)\left[\mathbf{V} + \mathbf{K}(\Omega)\right]\mathbf{\Pi}(\Omega) \,, \tag{2.29}$$

where $\mathbf{\Pi}^0(\Omega) = -\begin{pmatrix} \mathbf{\Delta} - \Omega\mathbf{1} & \mathbf{0} \\ \mathbf{0} & \mathbf{\Delta} + \Omega\mathbf{1} \end{pmatrix}^{-1}$ denotes the zeroth-order propagator with $\Delta_{ij}^{ab} = F_{ab}\delta_{ij} - F_{ji}\delta_{ab}$. $V_{qs}^{pr} = 2g_{qs}^{pr}$ is the bare Hartree kernel and $\mathbf{K}(\Omega)$ the frequency-dependent Bethe-Salpeter kernel [136]. To recover Eq. (2.18) and thus to obtain the propagator as approximated within *direct* RPA, exchange contributions are neglected and $\mathbf{K}(\Omega)$ is set to zero. For the connection to the Bethe-Salpeter equation and related methods see e.g. Ref. [137]. Analogously, the density response function $\chi(\Omega)$ as obtained within time-dependent density functional theory satisfies the Dyson equation

$$\chi(\Omega) = \chi^0(\Omega) + \chi^0(\Omega)\left[\frac{1}{r_{12}} + f_{\mathrm{xc}}(\Omega)\right]\chi(\Omega) \,, \tag{2.30}$$

where again the exchange-correlation kernel $f_{\mathrm{xc}}(\Omega)$ is set to zero within dRPA. dRPA is therefore often defined as the neglect of the exchange-correlation kernel within linear response theory. It should be furthermore noted that it is in fact sufficient to calculate the density response function to obtain the RPA correlation energy; only the diagonal of the density *matrix* response function is required, $\mathbf{\Pi}(\Omega, r_1, r_1, r_2, r_2) = \chi(\Omega, r_1, r_2)$. More specifically, the RPA correlation energy can be solely expressed in terms of the real-space transition densities $\rho_{0n}(r)$, which are connected to the density response function $\chi(\Omega)$ according to the Lehmann representation [124],

$$\chi(\Omega, r_1, r_2) = -\sum_{n \neq 0}\left(\frac{\rho_{0n}(r_1)\rho_{0n}(r_2)}{\Omega_n - \Omega - i\eta} + \frac{\rho_{0n}(r_1)\rho_{0n}(r_2)}{\Omega_n + \Omega + i\eta}\right) \,. \tag{2.31}$$

Ω_n are the excitation energies for all excited states n, Ω the frequency and η a positive infinitesimal ensuring convergence. The transition densities are hereby defined as the expectation value of the density operator $\hat{\rho}(r) = \sum_{pq}\phi_p(r)\phi_q(r)\hat{E}_{pq}$ with the ground and excited states $|\Psi_0\rangle$ and $|\Psi_n\rangle$,

$$\rho_{0n}(r) = \langle \Psi_0|\hat{\rho}(r)|\Psi_n\rangle = 2\sum_{ia}(\mathbf{X}^n + \mathbf{Y}^n)_{ia}\phi_i(r)\phi_a(r) \,. \tag{2.32}$$

Note that Eq. (2.32) can be obtained by assuming the definitions of Bouman and Hansen for ground and excited states (Eqs. (2.4) and (2.5)) and applying standard commutation rules, leading to the given definition of Eq. (2.32) for the transition density.

Calculating the RPA ground-state correlation energy: the density matrix formulation, the dielectric matrix formulation and the plasmon formula

Solving the RPA eigenvalue equation given by Eq. (2.7) provides approximated excitation energies Ω_n, excitation vectors $\mathbf{X}^n$ and $\mathbf{Y}^n$ and the corresponding transition densities ρ_{0n}. Several expressions exist to obtain the thereon based RPA correlation energy, defined as the difference between the exact and the reference energy, $E_C^{\text{RPA}} = E_{\text{exact}} - E_{\text{ref}}$. A classification for the different formulations is for example given in Ref. [138]: Based on the type and ordering of integration over the frequency or the interaction strength, the correlation energy can be obtained within the "density matrix formulation" [7, 40, 139] , the "dielectric matrix formulation" [11, 65, 138] or via the "plasmon formula" [140]. Of course, all formulations yield within numerical accuracy an equivalent expression for the RPA correlation energy, as shown e.g. in the appendix of Ref. [138]. However, as the different ansätze are required in the following chapters, they are shortly summarized in the following. For the sake of convenience, the equations of the following section refer to open-shell references, spin variables $x = r\sigma$ and spin orbitals, indicated by capital letters $\{P, Q, \dots\}$.

The density matrix formulation

The starting point for the density matrix formulation is the adiabatic connection [22, 141, 142], which allows to formulate the correlation energy as an integral over the coupling-strength parameter ζ,

$$E_c = \int_0^1 d\zeta\, W_c^\zeta = \int_0^1 d\zeta \left(\langle \Psi_0^\zeta | \hat{V}_{\text{ee}} | \Psi_0^\zeta \rangle - \langle \Psi_0^0 | \hat{V}_{\text{ee}} | \Psi_0^0 \rangle \right) \tag{2.33}$$

with the electron-electron interaction energy operator $\hat{V}_{\text{ee}} = \frac{1}{2} \sum_{PQRS} g_{RS}^{PQ} \hat{a}_P^\dagger \hat{a}_Q^\dagger \hat{a}_S \hat{a}_R$, the ground state at coupling strength ζ and at zero coupling, $|\Psi_0^\zeta\rangle$ and $|\Psi_0^0\rangle$, respectively. For KS references, the adiabatic connection furthermore defines the density to be equal for different coupling-strength values, thus $\rho(x) = \langle \Psi_0^\zeta | \hat{\rho}(x) | \Psi_0^\zeta \rangle = \langle \Psi_0^0 | \hat{\rho}(x) | \Psi_0^0 \rangle$ with the one-particle density operator $\hat{\rho}(x)$. Note that this constraint holds only for KS references; for HF references the density changes with varying ζ. For the sake of convenience, the following discussion thus only refers to KS references. A detailed comparison and a derivation for HF references is given in Ref. [7].

The adiabatic-connection constraint for the density as well as standard commutation rules and the resolution of the identity formulation of the delta function $\delta(x_1 - x_2) = \sum_q \phi_q(x_1)\phi_q(x_2)$ allow to rewrite the coupling-strength kernel as

$$W_c^\zeta = \frac{1}{2} \sum_{PQRS} g_{RS}^{PQ} \left[\langle \Psi_0^\zeta | \hat{a}_P^\dagger \hat{a}_R \hat{a}_Q^\dagger \hat{a}_S - \delta_{QR} \hat{a}_P^\dagger \hat{a}_S | \Psi_0^\zeta \rangle - \langle \Psi_0^0 | \hat{a}_P^\dagger \hat{a}_R \hat{a}_Q^\dagger \hat{a}_S - \delta_{QR} \hat{a}_P^\dagger \hat{a}_S | \Psi_0^0 \rangle \right] ,$$

$$= \frac{1}{2} \sum_{PQRS} g_{RS}^{PQ} \left[\langle \Psi_0^\zeta | \hat{a}_P^\dagger \hat{a}_R \hat{a}_Q^\dagger \hat{a}_S | \Psi_0^\zeta \rangle - \langle \Psi_0^0 | \hat{a}_P^\dagger \hat{a}_R \hat{a}_Q^\dagger \hat{a}_S | \Psi_0^0 \rangle \right] . \tag{2.34}$$

Inserting the resolution of the identity, $\mathbf{1} = \sum_n |\Psi_n^\zeta\rangle\langle\Psi_n^\zeta|$, according to

$$\langle \Psi_0^\zeta | \hat{a}_P^\dagger \hat{a}_R \hat{a}_Q^\dagger \hat{a}_S | \Psi_0^\zeta \rangle = \sum_n \langle \Psi_0^\zeta | \hat{a}_P^\dagger \hat{a}_R | \Psi_n^\zeta \rangle \langle \Psi_n^\zeta | \hat{a}_Q^\dagger \hat{a}_S | \Psi_0^\zeta \rangle , \tag{2.35}$$

the correlation energy can be expressed in terms of transition densities $\rho_{0n}^\zeta(x)$,

$$E_c = \frac{1}{2} \int\int dx_1 dx_2 \int_0^1 d\zeta \left(\sum_{n \neq 0} \frac{\rho_{0n}^\zeta(x_1)\rho_{0n}^\zeta(x_2) - \rho_{0n}^0(x_1)\rho_{0n}^0(x_2)}{|r_1 - r_2|} \right) . \tag{2.36}$$

Finally, the random-phase approximation is introduced by approximating the transition densities according to Eq. (2.32) as obtained from the RPA eigenvalue problem (Eq. (2.7)), now depending on the coupling-strength parameter and therefore given as

$$\rho_{0n}^\zeta(x) = \sum_{IA} (\mathbf{X}^{n\zeta} + \mathbf{Y}^{n\zeta})_{IA} \phi_I(x)\phi_A(x) , \tag{2.37}$$

$$\begin{pmatrix} \mathbf{A}^\zeta & \mathbf{B}^\zeta \\ \mathbf{B}^\zeta & \mathbf{A}^\zeta \end{pmatrix} \begin{pmatrix} \mathbf{X}^{n\zeta} \\ \mathbf{Y}^{n\zeta} \end{pmatrix} = \Omega_n^\zeta \begin{pmatrix} 1 & 0 \\ 0 & -1 \end{pmatrix} \begin{pmatrix} \mathbf{X}^{n\zeta} \\ \mathbf{Y}^{n\zeta} \end{pmatrix} , \tag{2.38}$$

with the adapted definitions for matrices $\mathbf{A}^\zeta$ and $\mathbf{B}^\zeta$,

$$(\mathbf{A}^\zeta)_{IJ}^{AB} \overset{\text{RPAX}}{=} F_{AB}\delta_{IJ} - F_{JI}\delta_{AB} + \zeta(g_{IB}^{AJ} - g_{IB}^{JA}) \overset{\text{dRPA}}{=} F_{AB}\delta_{IJ} - F_{JI}\delta_{AB} + \zeta g_{IB}^{AJ}, \tag{2.39}$$

$$(\mathbf{B}^\zeta)_{IJ}^{AB} \overset{\text{RPAX}}{=} \zeta(g_{IJ}^{AB} - g_{JI}^{AB}) \overset{\text{dRPA}}{=} \zeta g_{IJ}^{AB}. \tag{2.40}$$

Insertion of Eq. (2.37) into Eq. (2.36) yields the RPA correlation energy within the density matrix formulation [140],

$$E_{\text{C}}^{\text{RPA}} = \tfrac{1}{2}\int_0^1 \sum_{IAJB} g_{IJ}^{AB} \left(\sum_{n\neq 0} (\mathbf{X}^{n\zeta} + \mathbf{Y}^{n\zeta})_{IA}(\mathbf{X}^{n\zeta} + \mathbf{Y}^{n\zeta})_{JB} - \delta_{IJ}\delta_{AB} \right) \mathrm{d}\zeta. \tag{2.41}$$

Eq. (2.41) is thus obtained by analytical integration over the frequency; integration over the coupling strength is performed numerically, e.g. by Gauss-Legendre quadrature, as described in Ref. [40] and implemented in the MPGRAD module of the TURBOMOLE program package [71], leading to an N^6 scaling with system size N. The implementation is thereby based on the following reformulation,

$$E_{\text{C}}^{\text{RPA}} = \tfrac{1}{2}\int_0^1 \sum_{IAJB} g_{IJ}^{AB}(\mathbf{P}^\zeta)_{IJ}^{AB}\, \mathrm{d}\zeta, \tag{2.42}$$

with matrices $\mathbf{P}^\zeta$ and $\mathbf{M}^\zeta$,

$$\mathbf{P}^\zeta = (\mathbf{A}^\zeta - \mathbf{B}^\zeta)^{1/2}(\mathbf{M}^\zeta)^{-1/2}(\mathbf{A}^\zeta - \mathbf{B}^\zeta)^{1/2} - \mathbf{1}, \tag{2.43}$$

$$\mathbf{M}^\zeta = (\mathbf{A}^\zeta - \mathbf{B}^\zeta)^{1/2}(\mathbf{A}^\zeta + \mathbf{B}^\zeta)(\mathbf{A}^\zeta - \mathbf{B}^\zeta)^{1/2}, \tag{2.44}$$

corresponding to the transformed eigenvalue problem

$$\mathbf{M}^\zeta \mathbf{Z}^\zeta = \mathbf{Z}^\zeta (\mathbf{\Omega}^\zeta)^2, \quad \mathbf{Z}^\zeta(\mathbf{Z}^\zeta)^{\text{T}} = \mathbf{1}. \tag{2.45}$$

Note that both $\mathbf{A}^\zeta - \mathbf{B}^\zeta$ and $\mathbf{A}^\zeta + \mathbf{B}^\zeta$ are positive definite for stable reference states [40] and that $\mathbf{Z}^\zeta$ is related to the excitation amplitudes $\mathbf{X}^\zeta$ and $\mathbf{Y}^\zeta$ via $\mathbf{Z}_n^\zeta = (\Omega_n^\zeta)^{1/2}(\mathbf{A} - \mathbf{B})^{-1/2}(\mathbf{X}^{n\zeta} + \mathbf{Y}^{n\zeta})$ (see e.g. Ref. [143]).

The plasmon formula

According to the Hellmann-Feynman theorem [144], the derivative of Ω_n^ζ with respect to the coupling strength ζ is given for dRPA as

$$\frac{\mathrm{d}\Omega_n^\zeta}{\mathrm{d}\zeta} = \langle \mathbf{X}^{n\zeta}, \mathbf{Y}^{n\zeta} | \frac{\mathrm{d}\mathbf{\Lambda}^\zeta}{\mathrm{d}\zeta} | \mathbf{X}^{n\zeta}, \mathbf{Y}^{n\zeta} \rangle \overset{\text{dRPA}}{=} \sum_{IAJB} (\mathbf{X}^{n\zeta} + \mathbf{Y}^{n\zeta})_{IA}\, g_{AB}^{IJ} (\mathbf{X}^{n\zeta} + \mathbf{Y}^{n\zeta})_{JB}, \tag{2.46}$$

where $\mathbf{\Lambda}^\zeta$ is defined in Eq. (2.21). Additional analytical integration over the coupling strength is therefore possible, yielding the so-called plasmon formula [140],

$$E_{\text{C}}^{\text{RPA}} = \tfrac{1}{2}\int_0^1 \mathrm{d}\zeta \sum_n \left(\frac{\mathrm{d}\Omega_n^\zeta}{\mathrm{d}\zeta} - \frac{\mathrm{d}\Omega_n^\zeta}{\mathrm{d}\zeta}\bigg|_{\zeta=0} \right) \overset{\text{dRPA}}{=} \tfrac{1}{2}\sum_n (\Omega_n^{\text{dRPA}} - \Omega_n^{\text{dTDA}}), \tag{2.47}$$

which reduces for dRPA to the difference of excitation energies within dRPA and dTDA at full coupling, Ω_n^{dRPA} and Ω_n^{dTDA}, respectively. The dTDA excitation energies $\Omega_n^{\text{dTDA}} = \text{tr}(\mathbf{A}^{\text{dTDA}}) = \sum_{IA}(\varepsilon_A - \varepsilon_I + g_{IA}^{AI})$ are obtained by solving the eigenvalue problem $\mathbf{A}^{\text{dTDA}}\mathbf{X}^{n\text{dTDA}} = \Omega_n^{\text{dTDA}}\mathbf{X}^{n\text{dTDA}}$ with $(A^{\text{dTDA}})_{IJ}^{AB} = (\varepsilon_A - \varepsilon_I)\delta_{IJ}\delta_{AB} + 2g_{IB}^{AJ}$.

It is interesting to note that the inclusion of exchange is not trivial [7, 145]: For unrestricted KS (UKS) references, the antisymmetrized interaction operator $\hat{V}_{ee} = \tfrac{1}{4}\sum_{PQRS} g_{RS}^{PQ}(\hat{a}_P^\dagger \hat{a}_Q^\dagger \hat{a}_R \hat{a}_S - \hat{a}_P^\dagger \hat{a}_Q^\dagger \hat{a}_S \hat{a}_R)$ leads to the coupling-strength integrand

$$W_{\text{C}}^\zeta(\text{UKS}) = \tfrac{1}{4}\sum_{PQRS} g_{RS}^{PQ} \left[\langle\Psi_0^\zeta|\hat{a}_P^\dagger \hat{a}_R|\Psi_n^\zeta\rangle\langle\Psi_n^\zeta|\hat{a}_Q^\dagger \hat{a}_S|\Psi_0^\zeta\rangle - \langle\Psi_0^\zeta|\hat{a}_P^\dagger \hat{a}_S|\Psi_n^\zeta\rangle\langle\Psi_n^\zeta|\hat{a}_Q^\dagger \hat{a}_R|\Psi_0^\zeta\rangle \right.$$

$$\left. - \langle\Psi_0^0|\hat{a}_P^\dagger \hat{a}_R|\Psi_n^0\rangle\langle\Psi_n^0|\hat{a}_Q^\dagger \hat{a}_S|\Psi_0^0\rangle + \langle\Psi_0^0|\hat{a}_P^\dagger \hat{a}_S|\Psi_n^0\rangle\langle\Psi_n^0|\hat{a}_Q^\dagger \hat{a}_R|\Psi_0^0\rangle \right]. \tag{2.48}$$

An analogous derivation for UHF references requires further correction terms, as outlined in Ref. [7]. However, for both UKS and UHF references, the final expression for the correlation energy can be summarized in terms of the transition densities $\rho_{0n}^{\zeta}(x)$ and transition density matrices $\gamma_{0n}^{\zeta}(x_1, x_2)$,

$$E_{\mathrm{C}}^{\mathrm{RPAX}}(\mathrm{UKS/UHF}) = \tfrac{1}{4} \int_0^1 \mathrm{d}\zeta \int \mathrm{d}x_1 \mathrm{d}x_2 \left(\sum_{n \neq 0} \frac{\rho_{0n}^{\zeta}(x_1)\rho_{0n}^{\zeta}(x_2) - \rho_{0n}^{0}(x_1)\rho_{0n}^{0}(x_2)}{|r_1 - r_2|} \right)$$
$$- \tfrac{1}{4} \int_0^1 \mathrm{d}\zeta \sum_{PQRS} g_{RS}^{PQ} \left(\sum_{n \neq 0} \gamma_{0nPS}^{\zeta} \gamma_{0nQR}^{\zeta} - \sum_{n \neq 0} \gamma_{0nPS}^{0} \gamma_{0nQR}^{0} \right), \qquad (2.49)$$

where the latter are defined as Ref. [145]

$$\gamma_{0nPR}^{\zeta} = \langle \Psi_0^{\zeta} | \hat{a}_P \hat{a}_R | \Psi_n^{\zeta} \rangle = X_{PR}^{n\zeta} v_P (1 - v_R) + Y_{PR}^{n\zeta} v_R (1 - v_P). \qquad (2.50)$$

v_P and v_R denote orbital occupation numbers, hence in order to get a non-zero contribution for γ_{0nPR}^{ζ}, P has to refer to an occupied orbital and R to an unoccupied,

$$g_{RS}^{PQ} \gamma_{0nPS}^{\zeta} \gamma_{0nQR}^{\zeta} \rightarrow g_{JB}^{IA} (X_{IA}^{n\zeta} X_{JB}^{n\zeta} + Y_{IA}^{n\zeta} Y_{JB}^{n\zeta}) + g_{BA}^{IJ} (X_{IA}^{n\zeta} Y_{JB}^{n\zeta} + Y_{IA}^{n\zeta} X_{JB}^{n\zeta}). \qquad (2.51)$$

The derivative of $\Omega_n^{\zeta\,\mathrm{RPAX}}$ is therefore given as

$$\frac{\mathrm{d}\Omega_n^{\zeta\,\mathrm{RPAX}}}{\mathrm{d}\zeta} = \sum_{IAJB} (\mathbf{X}^{n\zeta} + \mathbf{Y}^{n\zeta})_{IA} \, g_{AB}^{IJ} (\mathbf{X}^{n\zeta} + \mathbf{Y}^{n\zeta})_{JB}$$
$$- g_{BA}^{IJ} \left((\mathbf{X}^{n\zeta})_{IA} (\mathbf{Y}^{n\zeta})_{JB} + (\mathbf{Y}^{n\zeta})_{IA} (\mathbf{X}^{n\zeta})_{JB} \right) - g_{JB}^{IA} \left((\mathbf{X}^{n\zeta})_{IA} (\mathbf{X}^{n\zeta})_{JB} + (\mathbf{Y}^{n\zeta})_{IA} (\mathbf{Y}^{n\zeta})_{JB} \right) \qquad (2.52)$$

and the final expression for the correlation energy can be formulated in analogy to Eq. (2.47), including an additional factor of one half,

$$E_{\mathrm{C}}^{\mathrm{RPAX}}(\mathrm{UHF}) = \tfrac{1}{4} \sum_n \left(\Omega_n^{\mathrm{RPAX}} - \Omega_n^{\mathrm{TDAX}} \right). \qquad (2.53)$$

For closed-shell references (restricted HF (RHF)), the consideration of spin-flip excitations requires a partitioning into singlet (S) and triplet (T) contributions [146],

$$E_{\mathrm{C}}^{\mathrm{RPAX}}(\mathrm{RHF}) = \tfrac{1}{4} \sum_n \left(\Omega_{n\mathrm{S}}^{\mathrm{RPAX}} - \Omega_{n\mathrm{S}}^{\mathrm{TDAX}} \right) + \tfrac{3}{4} \sum_n \left(\Omega_{n\mathrm{T}}^{\mathrm{RPAX}} - \Omega_{n\mathrm{T}}^{\mathrm{TDAX}} \right). \qquad (2.54)$$

The dielectric matrix formulation

The most efficient formulation with a scaling of $N^4 \log N$ can be obtained within the dielectric matrix formulation, when integrating analytically over the coupling strength and numerically over the frequency [65]. According to the fluctuation-dissipation theorem [147, 148], Eq. (2.35) can be connected with the density response function [22, 141, 142],

$$\sum_{n \neq 0} \langle \Psi_0^{\zeta} | \hat{\rho}(x_1) | \Psi_n^{\zeta} \rangle \langle \Psi_n^{\zeta} | \hat{\rho}(x_2) | \Psi_0^{\zeta} \rangle = - \int_0^{\infty} \frac{\mathrm{d}\Omega}{\pi} \mathrm{Im}\, \chi^{\zeta}(\Omega, x_1, x_2), \qquad (2.55)$$

allowing to express the correlation energy as

$$E_{\mathrm{C}} = -\tfrac{1}{2} \int_0^1 \mathrm{d}\zeta \int_0^{\infty} \frac{\mathrm{d}\Omega}{\pi} \mathrm{Im} \int \mathrm{d}x_1 \mathrm{d}x_2 \frac{\chi^{\zeta}(\Omega, x_1, x_2) - \chi^0(\Omega, x_1, x_2)}{|r_1 - r_2|}. \qquad (2.56)$$

Inserting the response function of Eq. (2.31) yields the RPA correlation energy, which can be formulated for dRPA in an efficient way using resolution of the identity methods (for the explicit reformulation see Refs. [51, 65]),

$$E_{\mathrm{C}}^{\mathrm{dRPA}} = \int_{-\infty}^{\infty} \mathrm{d}\Omega \frac{1}{4\pi} \mathrm{tr} \left[\ln(\mathbf{1} + \mathbf{Q}(\Omega)) - \mathbf{Q}(\Omega) \right], \qquad (2.57)$$

with $\mathbf{Q}(\Omega) = 2\mathbf{S}^{\mathrm{T}}\Delta_{\mathrm{DIAG}}((\Delta_{\mathrm{DIAG}})^2 + \Omega^2\mathbf{1})^{-1}\mathbf{S}$ and the diagonal matrix $(\Delta_{\mathrm{DIAG}})^{AB}_{IJ} = (\varepsilon_A - \varepsilon_I)\delta_{IJ}\delta_{AB}$. The matrix elements $S_{IA,P'}$ are intermediates obtained when factorizing the two-electron integrals using the resolution of the identity, given in Mulliken notation as $g^{AB}_{IJ} = \sum_{P'} S_{IA,P'}S_{JB,P'} = \sum_{P'Q'}(IA|P')(P'|Q')^{-1}(Q'|JB)$. $\{P',Q',\ldots\}$ denote the auxiliary basis. Note that such a formulation in terms of matrix $\mathbf{Q}$ is only straightforward for dRPA — when including exchange, the two-electron integral contributions to matrices $\mathbf{A}$ and $\mathbf{B}$ are no longer equivalent, prohibiting an analogous treatment for RPAX.

2.2 From single excitations to double excitations: Working equations based on the equivalence of RPA and ring coupled-cluster theory

Already in early papers on the random-phase approximation [149–151], it was shown that both the dRPA and the RPAX eigenvalue problem can be formulated as a doubles amplitude equation,

$$\mathbf{B} + \mathbf{AT} + \mathbf{TA} + \mathbf{TBT} = 0\,, \tag{2.58}$$

based on the connection of doubles and singles amplitudes, see Eq. (2.10). In addition, the correlation energy, as defined within Eqs. (2.47) and (2.53), can be expressed in terms of the respective amplitudes $\mathbf{T}$, given for open-shell systems as

$$E^{\mathrm{dRPA}}_{\mathrm{C}} = \tfrac{1}{2}\mathrm{tr}[\mathbf{B}^{\mathrm{dRPA}}\mathbf{T}]\,, \tag{2.59}$$

$$E^{\mathrm{RPAX}}_{\mathrm{C}} = \tfrac{1}{4}\mathrm{tr}[\mathbf{B}^{\mathrm{RPAX}}\mathbf{T}]\,. \tag{2.60}$$

For the sake of convenience, the amplitudes are in the following not labeled according to the underlying method — a specification is only added in case of ambiguity. For dRPA, Scuseria *et al.* [43] furthermore proved that the matrix $\mathbf{X}$ is invertible and that the given Riccati equation can also be obtained when approximating the coupled-cluster doubles (CCD) approach by solely considering ring contributions and neglecting all ladder and cross terms [43, 44].

Within CCD theory (see e.g. Refs. [144, 152] and references therein), the wave function is parametrized through the double excitation operator $\hat{T}_2$,

$$|\Psi_{\mathrm{CCD}}\rangle = \exp(\hat{T}_2)|\Psi_0\rangle\,, \tag{2.61}$$

with $\hat{T}_2 = \tfrac{1}{4}\sum_{IJAB} t^{AB}_{IJ}\hat{a}^{\dagger}_A\hat{a}^{\dagger}_B\hat{a}_J\hat{a}_I$. Acting on the reference function $|\Psi_0\rangle$, $\hat{T}_2$ generates double excitations into the conventional virtual space weighted by the amplitudes t^{AB}_{IJ}. The amplitudes are determined by projecting the Schrödinger equation on the double excitation manifold,

$$\begin{aligned}(\mathbf{\Omega}^{\mathrm{CCD}})^{AB}_{IJ} &= \langle{}^{AB}_{IJ}|\exp(-\hat{T}_2)\hat{H}\exp(\hat{T}_2)|\mathrm{HF}\rangle \\ &= \langle{}^{AB}_{IJ}|[\hat{F},\hat{T}_2] + \hat{\phi} + [\hat{\phi},\hat{T}_2] + \tfrac{1}{2}[[\hat{\phi},\hat{T}_2],\hat{T}_2]|\mathrm{HF}\rangle\,,\end{aligned} \tag{2.62}$$

where the Hamiltonian is split into the zeroth-order Fock operator $\hat{F} = \sum_{PQ} F_{PQ}\hat{a}^{\dagger}_P\hat{a}_Q$ and the first-order fluctuation potential $\hat{\phi}$, $\hat{H} = \hat{F} + \hat{\phi}$. Note that the fluctuation potential is — in contrast to the earlier used two-electron interaction potential $\hat{V}_{\mathrm{ee}}$ — defined as $\hat{\phi} = \hat{V}_{\mathrm{ee}} - \hat{J} + \hat{K}$, where $\hat{J}$ and $\hat{K}$ are the Coulomb and non-local exchange operators. Furthermore, a HF (or KS) determinant is assumed as reference function $|\Psi_0\rangle$. For KS references, the KS orbitals are used to form a determinant and the succeeding CC treatment is identical to HF-based CC calculations. The correlation energy is therefore defined as the difference between the exact energy and the energy expectation value of the KS determinant,

$$E_{\mathrm{C}} = E_{\mathrm{exact}} - \langle\mathrm{KS}|\hat{H}|\mathrm{KS}\rangle\,. \tag{2.63}$$

See for example Refs. [153, 154] for a validation on the performance of KS references for CC methods and the connection to Brueckner CC schemes. More explicitly, the CCD correlation energy is defined through the double excitation amplitudes t^{AB}_{IJ} as,

$$E^{\mathrm{CCD}}_{\mathrm{C}} = \langle\mathrm{HF}|\hat{H}|\Psi_{\mathrm{CCD}}\rangle - \langle\mathrm{HF}|\hat{H}|\mathrm{HF}\rangle = \tfrac{1}{4}\sum_{IJAB}\left(g^{IJ}_{AB} - g^{IJ}_{BA}\right)t^{AB}_{IJ} = \tfrac{1}{4}\mathrm{tr}\left[\mathbf{B}^{\mathrm{RPAX}}\mathbf{T}\right]\,. \tag{2.64}$$
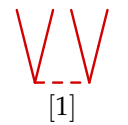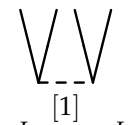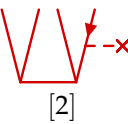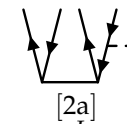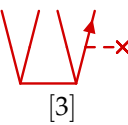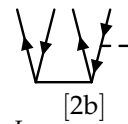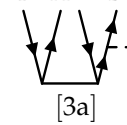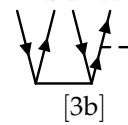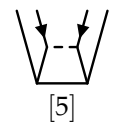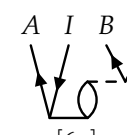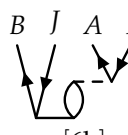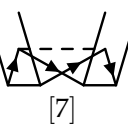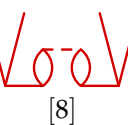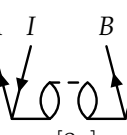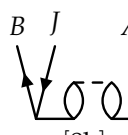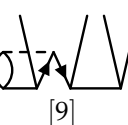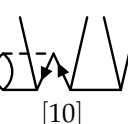
CCD		rCCD and drCCD	
[1]	$g_{IJ}^{AB} - g_{JI}^{AB}$	[1]	$g_{IJ}^{AB} - g_{JI}^{AB}$
[2]	$\hat{P}_{AB}^- t_{IJ}^{AC} F_{BC}$	[2a] [2b]	$t_{IJ}^{AC} F_{BC} + t_{IJ}^{CB} F_{AC}$
[3]	$-\hat{P}_{IJ}^- t_{IK}^{AB} F_{KJ}$	[3a] [3b]	$-t_{IK}^{AB} F_{KJ} - t_{KJ}^{AB} F_{KI}$
[4]	$\frac{1}{2}(g_{CD}^{AB} - g_{DC}^{AB}) t_{IJ}^{CD}$		
[5]	$\frac{1}{2}(g_{IJ}^{KL} - g_{JI}^{KL}) t_{KL}^{AB}$		
[6]	$(\hat{P}^-)_{IJ}^{AB} t_{IK}^{AC}(g_{CJ}^{KB} - g_{JC}^{KB})$	[6a] [6b]	$(g_{IC}^{AK} - g_{CI}^{AK}) t_{KJ}^{CB} + (g_{JC}^{BK} - g_{CJ}^{BK}) t_{KI}^{CA}$
[7]	$\frac{1}{4}(g_{CD}^{KL} - g_{DC}^{KL}) t_{IJ}^{CD} t_{KL}^{AB}$		
[8]	$\hat{P}_{IJ}^-(g_{CD}^{KL} - g_{DC}^{KL}) t_{IK}^{AC} t_{JL}^{BD}$	[8a] [8b]	$t_{IK}^{AC}(g_{KL}^{CD} - g_{LK}^{CD}) t_{LJ}^{DB}$
[9]	$-\frac{1}{2}\hat{P}_{IJ}^-(g_{CD}^{KL} - g_{DC}^{KL}) t_{IK}^{DC} t_{LJ}^{AB}$		
[10]	$-\frac{1}{2}\hat{P}_{AB}^-(g_{CD}^{KL} - g_{DC}^{KL}) t_{LK}^{AC} t_{IJ}^{DB}$		

Fig. 2.2: Antisymmetrized Goldstone diagrams representing spin orbitals for the CCD and rCCD residual equations. Ring diagrams are coloured in red. Exchange contributions which are omitted within drCCD are marked in blue; corresponding diagrams require a nomenclature where the dashed line refers to the non-antisymmetrized two-electron interaction operator. The permutation operators $\hat{P}_{AB}^-$, $\hat{P}_{IJ}^-$ and $(\hat{P}^-)_{IJ}^{AB}$ are defined as $\hat{P}_{AB}^- X_{IJ}^{AB} = X_{IJ}^{AB} - X_{IJ}^{BA}$, $\hat{P}_{IJ}^- X_{IJ}^{AB} = X_{IJ}^{AB} - X_{JI}^{AB}$ and $(\hat{P}^-)_{IJ}^{AB} = \hat{P}_{IJ}^- \hat{P}_{AB}^-$. For convenience, Einstein summation rules are assumed. The nomenclature for antisymmetrized Goldstone diagrams is explained in Appendix A.

In contrast to CCD, it is not possible to derive the rCCD residual equations algebraically, starting from an appropriate wave function expressed in terms of annihilation and creation operators and evaluating the projected equations by applying Wick's theorem [155]. However, based on the CCD equations, the rCCD approach can be derived graphically, as visualized in Figure 2.2. On the left, the CCD residual equations are explicitly given in terms of antisymmetrized Goldstone diagrams with the corresponding algebraic expressions [106]. The standardly used nomenclature for antisymmetrized Goldstone diagrams representing spin orbitals is explained in Appendix A. Ring terms, i.e. those contributions which solely represent particle-hole interactions, are represented by diagrams where the double amplitudes are contracted with the two-electron integrals in such a way that the particle and hole lines corresponding to one electron start and end pairwise at the same vertex. Graphically this corresponds to a closed loop (if fully contracted) which can be easily associated with a ring. The accordingly featured ring diagrams of Figure 2.2 are highlighted in red. It should however be noted that diagrams [1], [2], [3], [6] and [8] do so far not solely comprise the wanted subset of particle-hole contributions as it would be the case for non-antisymmetrized diagrams. Due to the chosen (standard) definition including antisymmetrization, the ring or particle-hole terms still need to be concretized by either changing the interpretation rules, as done in Ref. [156], or by adding labels and arrow directions to the present diagrams, as depicted on the right-hand side of Figure 2.2. Furthermore, the standard CC nomenclature, interpreting up- and down-going lines in terms of creation and annihilation operators and associating vertexes with one- and two-electron operators, is inappropriate as it assumes that these translation rules allow to derive the algebraic expressions by applying Wick's theorem. This is as already mentioned not possible for rCCD. However, simplified interpretation rules which are reduced to amplitude matrices and two-electron interaction integrals still hold for diagrams [1] to [8b]. The so-obtained rCCD residual equation is equivalent to the RPAX eigenvalue problem of Eq. (2.7) and thus corresponds to Eq. (2.58) assuming the same definitions for matrices $\mathbf{A}$ and $\mathbf{B}$ as defined within RPAX (see Eqs. (2.11) and (2.12)). The rCCD correlation energy then corresponds to Eq. (2.60),

$$E_C^{\text{rCCD}} = \tfrac{1}{4} \sum_{IJAB} (g_{AB}^{IJ} - g_{BA}^{IJ}) t_{IJ}^{AB} = \tfrac{1}{4} \text{tr} \left[\mathbf{B}^{\text{RPAX}} \mathbf{T} \right]. \tag{2.65}$$

Furthermore, the drCCD equations can be extracted from the rCCD equations when neglecting exchange. Exchange contributions are marked in blue on the right-hand side of Figure 2.2. The drCCD diagrams are obtained by assuming - in contrast to rCCD - a nomenclature with non-antisymmetrized two-electron interaction operator, yielding identically looking diagrams which simply differ in the algebraic expressions requiring an additional factor of two. Consistently, the drCCD correlation energy is, in contrast to Eq. (2.65), defined as

$$E_C^{\text{drCCD}} = \tfrac{1}{2} \sum_{IJAB} g_{AB}^{IJ} t_{IJ}^{AB} = \tfrac{1}{2} \text{tr} \left[\mathbf{B}^{\text{dRPA}} \mathbf{T} \right]. \tag{2.66}$$

The role of spin-flipped excitations: derivation of the closed-shell equations for rCCD and drCCD

Regarding the zeroth-order Fock (or KS) matrix contributions to the CCD and rCCD equations, it is important to note that the rCCD contributions, $t_{IJ}^{AC} F_{BC} + t_{IJ}^{CB} F_{AC}$ and $-t_{IK}^{AB} F_{KJ} - t_{KJ}^{AB} F_{KI}$ corresponding to diagrams [2a], [2b] as well as [3a] and [3b], cannot be formulated as for CCD by exploiting the permutation operators $\hat{P}_{AB}^-$ and $\hat{P}_{IJ}^-$, $\hat{P}_{AB}^- t_{IJ}^{AC} F_{BC} = t_{IJ}^{AC} F_{BC} - t_{IJ}^{BC} F_{AC}$ and $-\hat{P}_{IJ}^- t_{IK}^{AB} F_{KJ} = -t_{IK}^{AB} F_{KJ} + t_{JK}^{AB} F_{KI}$. This is due to the fact that the CCD amplitudes are symmetric with respect to the interchange of I and J and A and B,

$$t_{IJ}^{AB} = -t_{JI}^{AB} = -t_{IJ}^{BA} = t_{JI}^{BA}, \tag{2.67}$$

whereas the rCCD amplitudes are not. As a consequence, the CCD correlation energy can be expressed as

$$E_C^{\text{CCD}} = \tfrac{1}{2} \sum_{IJAB} t_{IJ}^{AB} g_{AB}^{IJ} = \tfrac{1}{2} \text{tr} \left[\mathbf{B}^{\text{dRPA}} \mathbf{T} \right], \tag{2.68}$$

while the rCCD correlation energy is restricted to the formulation of Eq. (2.64). The reduced symmetry of the rCCD amplitudes needs to be taken into account for the derivation of the corresponding closed-shell equations: For standard coupled-cluster schemes like CCD, spin integration over the two spin components $\sigma = \alpha, \beta$ can be performed in various ways yielding different residual equations for spatial orbitals [121, 157–159]. This ambiguity arises due to the fact that the number of independent variables (cluster amplitudes) is larger than the projection manifold. One standardly used adaptation scheme is to exclude spin-flipped amplitudes like $t_{i\alpha j\beta}^{a\beta b\alpha}$ from the projection manifold as the corresponding doubly excited singlet-spin eigenfunctions

would be linearly dependent on the eigenfunctions corresponding to $t_{i\alpha j\beta}^{a\alpha b\beta}$ and $t_{i\beta j\alpha}^{a\beta b\alpha}$. The redundancy becomes apparent when recalling the spin-expanded formulation of Eqs. (2.64) and (2.68),

$$E_C^{CCD} = \frac{1}{4} \sum_{abij} \left(t_{i\alpha j\alpha}^{a\alpha b\alpha} \left(g_{a\alpha b\alpha}^{i\alpha j\alpha} - g_{a\alpha b\alpha}^{j\alpha i\alpha} \right) + t_{i\beta j\beta}^{a\beta b\beta} \left(g_{a\beta b\beta}^{i\beta j\beta} - g_{a\beta b\beta}^{j\beta i\beta} \right) + t_{i\alpha j\beta}^{a\alpha b\beta} g_{a\alpha b\beta}^{i\alpha j\beta} + t_{i\beta j\alpha}^{a\beta b\alpha} g_{a\beta b\alpha}^{i\beta j\alpha} - t_{i\alpha j\beta}^{a\alpha b\beta} g_{b\alpha a\beta}^{i\alpha j\beta} - t_{i\beta j\alpha}^{a\alpha b\beta} g_{b\beta a\alpha}^{i\beta j\alpha} \right) ,$$

(2.69)

$$= \frac{1}{2} \sum_{abij} \left(t_{i\alpha j\alpha}^{a\alpha b\alpha} g_{a\alpha b\alpha}^{i\alpha j\alpha} + t_{i\beta j\beta}^{a\beta b\beta} g_{a\beta b\beta}^{i\beta j\beta} + t_{i\alpha j\beta}^{a\alpha b\beta} g_{a\alpha b\beta}^{i\alpha j\beta} + t_{i\beta j\alpha}^{a\beta b\alpha} g_{a\beta b\alpha}^{i\beta j\alpha} \right) .$$

(2.70)

The projection manifold can thus be restricted to

$$\Omega_{IJ}^{AB} = \Omega_{i\alpha j\alpha}^{a\alpha b\alpha} + \Omega_{i\beta j\beta}^{a\beta b\beta} + \Omega_{i\alpha j\beta}^{a\alpha b\beta} + \Omega_{i\beta j\alpha}^{a\beta b\alpha} .$$

(2.71)

The resulting residual equations for $t_{i\alpha j\alpha}^{a\alpha b\alpha}$, $t_{i\beta j\beta}^{a\beta b\beta}$, $t_{i\beta j\alpha}^{a\beta b\alpha}$ and $t_{i\alpha j\beta}^{a\alpha b\beta}$ show that the CCD amplitudes obey the following symmetry relations [160–162],

$$t_{i\alpha j\alpha}^{a\alpha b\alpha} = t_{i\beta j\beta}^{a\beta b\beta} = t_{i\alpha j\beta}^{a\alpha b\beta} - t_{j\alpha i\beta}^{a\alpha b\beta} ,$$

(2.72)

$$t_{i\alpha j\beta}^{a\alpha b\beta} = t_{i\beta j\alpha}^{a\beta b\alpha} ,$$

(2.73)

which allow to express all four residuals in terms of one amplitude, for example $t_{i\alpha j\beta}^{a\alpha b\beta} \to t_{ij}^{ab}$. t_{ij}^{ab} and t_{ji}^{ab} are independent, each related to the corresponding singlet-spin eigenfunction $\langle_{ij}^{ab}|$ and $\langle_{ji}^{ab}|$,

$$|_{ij}^{ab}\rangle = \hat{a}_{a\alpha}^{\dagger}\hat{a}_{b\alpha}^{\dagger}\hat{a}_{j\alpha}\hat{a}_{i\alpha}|HF\rangle + \hat{a}_{a\alpha}^{\dagger}\hat{a}_{b\beta}^{\dagger}\hat{a}_{j\beta}\hat{a}_{i\alpha}|HF\rangle + \hat{a}_{a\beta}^{\dagger}\hat{a}_{b\alpha}^{\dagger}\hat{a}_{j\alpha}\hat{a}_{i\beta}|HF\rangle + \hat{a}_{a\beta}^{\dagger}\hat{a}_{b\beta}^{\dagger}\hat{a}_{j\beta}\hat{a}_{i\beta}|HF\rangle ,$$

(2.74)

$$|_{ij}^{ba}\rangle = \hat{a}_{b\alpha}^{\dagger}\hat{a}_{a\alpha}^{\dagger}\hat{a}_{j\alpha}\hat{a}_{i\alpha}|HF\rangle + \hat{a}_{b\alpha}^{\dagger}\hat{a}_{a\beta}^{\dagger}\hat{a}_{j\beta}\hat{a}_{i\alpha}|HF\rangle + \hat{a}_{b\beta}^{\dagger}\hat{a}_{a\alpha}^{\dagger}\hat{a}_{j\alpha}\hat{a}_{i\beta}|HF\rangle + \hat{a}_{b\beta}^{\dagger}\hat{a}_{a\beta}^{\dagger}\hat{a}_{j\beta}\hat{a}_{i\beta}|HF\rangle ,$$

(2.75)

and not symmetric with respect to the exchange of indices i and j,

$$t_{ij}^{ab} = t_{ji}^{ba} \neq t_{ij}^{ba} = t_{ji}^{ab} .$$

(2.76)

To simplify the equations further, it is therefore common to combine both projection manifolds, yielding a biorthogonal basis as used in the beginning of this chapter and explained in Appendix A. In conclusion, spin integration for CCD allows to reduce computation time by condensing the open-shell equations into a single closed-shell residual equation (see also Figure 2.4), which defines the amplitudes t_{ij}^{ab} and therefore the CCD correlation energy,

$$E_C^{CCD} = \sum_{ijab} t_{ij}^{ab} \left(2g_{ab}^{ij} - g_{ba}^{ij} \right) = \text{tr} \left[\mathbf{B}^{RPAX} \mathbf{T} \right] .$$

(2.77)

This is not possible for rCCD: As solely ring diagrams are considered, requiring that the index pair (IA) can only be permuted as a unit with (JB), the amplitude t_{JI}^{AB} is neglected. In consequence, t_{ji}^{ab} and the corresponding eigenfunction $|_{ji}^{ab}\rangle$ are omitted for spatial orbitals. Hence, by definition, the rCCD spin amplitudes do not fulfill the symmetry relation of Eq. (2.72) and the rCCD correlation energy cannot be recast into an expression without exchange, but has to rely on the spin-expanded formulation of Eq. (2.69) depending on spin-flipped amplitudes of the type $t_{i\beta j\alpha}^{a\alpha b\beta}$. Starting from the rCCD residual equations for spin orbitals, given in Figure 2.2, the diagrams for the different spin cases can be derived taking into account that spin has to be conserved along each continuous path with the exception of spin-flipped excitations, as summarized in Figure 2.3. Spin-flipped amplitudes are marked at the vertex by an empty circle and the label $\alpha\beta$ indicates that spin is flipped from α spin to β spin or *vice versa*. Note that the equations are illustrated using antisymmetrized Goldstone diagrams, which would require a labeling of the paired indices (AI) and (BJ) to specify the particle-hole contributions, analogously to Figure 2.2. For the sake of convenience, such a labeling is omitted in Figure 2.3. The so-obtained rCCD diagrams for the spin-expanded open-shell case visualize that the residuals for same- and opposite-spin amplitudes are no longer redundant and that, in contrast to CCD, only those exchange terms contribute which arise from the antisymmetrization of the two-electron integrals. The rCCD amplitude equations can therefore not be merged into a single residual equation for closed-shell

—— $\Omega_{i\alpha j\alpha}^{a\alpha b\alpha}$ block ——

$$\Omega_{i\alpha j\alpha}^{a\alpha b\alpha} = g_{i\alpha j\alpha}^{a\alpha b\alpha} - g_{j\alpha i\alpha}^{a\alpha b\alpha} + \hat{P}_{i\alpha j\alpha}^{a\alpha b\alpha} \left[F_{b\alpha c\alpha} t_{i\alpha j\alpha}^{a\alpha c\alpha} - F_{k\alpha j\alpha} t_{i\alpha k\alpha}^{a\alpha b\alpha} + t_{i\alpha k\alpha}^{a\alpha c\alpha} \left(g_{c\alpha j\alpha}^{k\alpha b\alpha} - g_{j\alpha c\alpha}^{k\alpha b\alpha} \right) + t_{i\alpha k\beta}^{a\alpha c\beta} g_{c\beta j\alpha}^{k\beta b\alpha} \right.$$
$$\left. + g_{c\beta d\alpha}^{k\beta l\alpha} t_{j\alpha k\beta}^{b\alpha c\beta} t_{i\alpha l\alpha}^{a\alpha d\alpha} \right] + \left(g_{c\alpha d\alpha}^{k\alpha l\alpha} - g_{d\alpha c\alpha}^{k\alpha l\alpha} \right) t_{j\alpha k\alpha}^{b\alpha c\alpha} t_{i\alpha l\alpha}^{a\alpha d\alpha} + \left(g_{c\beta d\beta}^{k\beta l\beta} - g_{d\beta c\beta}^{k\beta l\beta} \right) t_{j\alpha k\beta}^{b\alpha c\beta} t_{i\alpha l\beta}^{a\alpha d\beta}$$

—— $\Omega_{i\alpha j\beta}^{a\alpha b\beta}$ block ——

$$\Omega_{i\alpha j\beta}^{a\alpha b\beta} = g_{i\alpha j\beta}^{a\alpha b\beta} + t_{i\alpha j\beta}^{a\alpha c\beta} F_{b\beta c\beta} + t_{i\alpha j\beta}^{c\alpha b\beta} F_{a\alpha c\alpha} - t_{k\alpha j\beta}^{a\alpha b\beta} F_{k\alpha i\alpha} - t_{i\alpha k\beta}^{a\alpha b\beta} F_{k\beta j\beta} + t_{k\alpha j\beta}^{c\alpha b\beta} \left(g_{i\alpha c\alpha}^{a\alpha k\alpha} - g_{c\alpha i\alpha}^{a\alpha k\alpha} \right)$$
$$+ t_{k\beta j\beta}^{c\beta b\beta} g_{i\alpha c\beta}^{a\alpha k\beta} + t_{k\beta i\alpha}^{c\beta a\alpha} \left(g_{j\beta c\beta}^{b\beta k\beta} - g_{c\beta j\beta}^{b\beta k\beta} \right) + t_{k\alpha i\alpha}^{c\alpha a\alpha} g_{j\beta c\alpha}^{b\beta k\alpha} + t_{i\alpha k\alpha}^{a\alpha c\alpha} \left(g_{k\alpha l\alpha}^{c\alpha d\alpha} - g_{l\alpha k\alpha}^{c\alpha d\alpha} \right) t_{l\alpha j\beta}^{d\alpha b\beta}$$
$$+ t_{i\alpha k\beta}^{a\alpha c\beta} \left(g_{k\beta l\beta}^{c\beta d\beta} - g_{l\beta k\beta}^{c\beta d\beta} \right) t_{l\beta j\beta}^{d\beta b\beta} + t_{i\alpha k\alpha}^{a\alpha c\alpha} g_{k\alpha l\beta}^{c\alpha d\beta} t_{l\beta j\beta}^{d\beta b\beta} + t_{i\alpha k\beta}^{a\alpha c\beta} g_{k\beta d\alpha}^{c\beta l\alpha} t_{l\alpha j\beta}^{d\alpha b\beta}$$

—— $\Omega_{i\beta j\alpha}^{a\alpha b\beta}$ block ——

$$\Omega_{i\beta j\alpha}^{a\alpha b\beta} = -g_{j\alpha i\beta}^{a\alpha b\beta} + t_{i\beta j\alpha}^{a\alpha c\beta} F_{b\beta c\beta} + t_{i\beta j\alpha}^{c\alpha b\beta} F_{a\alpha c\alpha} - t_{i\beta k\alpha}^{a\alpha b\beta} F_{j\alpha k\alpha} - t_{k\beta j\alpha}^{c\alpha b\beta} F_{k\beta i\beta}$$
$$+ t_{k\beta j\alpha}^{c\alpha b\beta} \left(-g_{c\alpha i\beta}^{a\alpha k\beta} \right) + t_{k\alpha i\beta}^{c\beta a\alpha} \left(-g_{c\beta j\alpha}^{b\beta k\alpha} \right) + t_{i\beta k\alpha}^{a\alpha c\beta} \left(-g_{l\beta k\alpha}^{c\beta d\alpha} \right) t_{l\beta j\alpha}^{d\alpha b\beta}$$
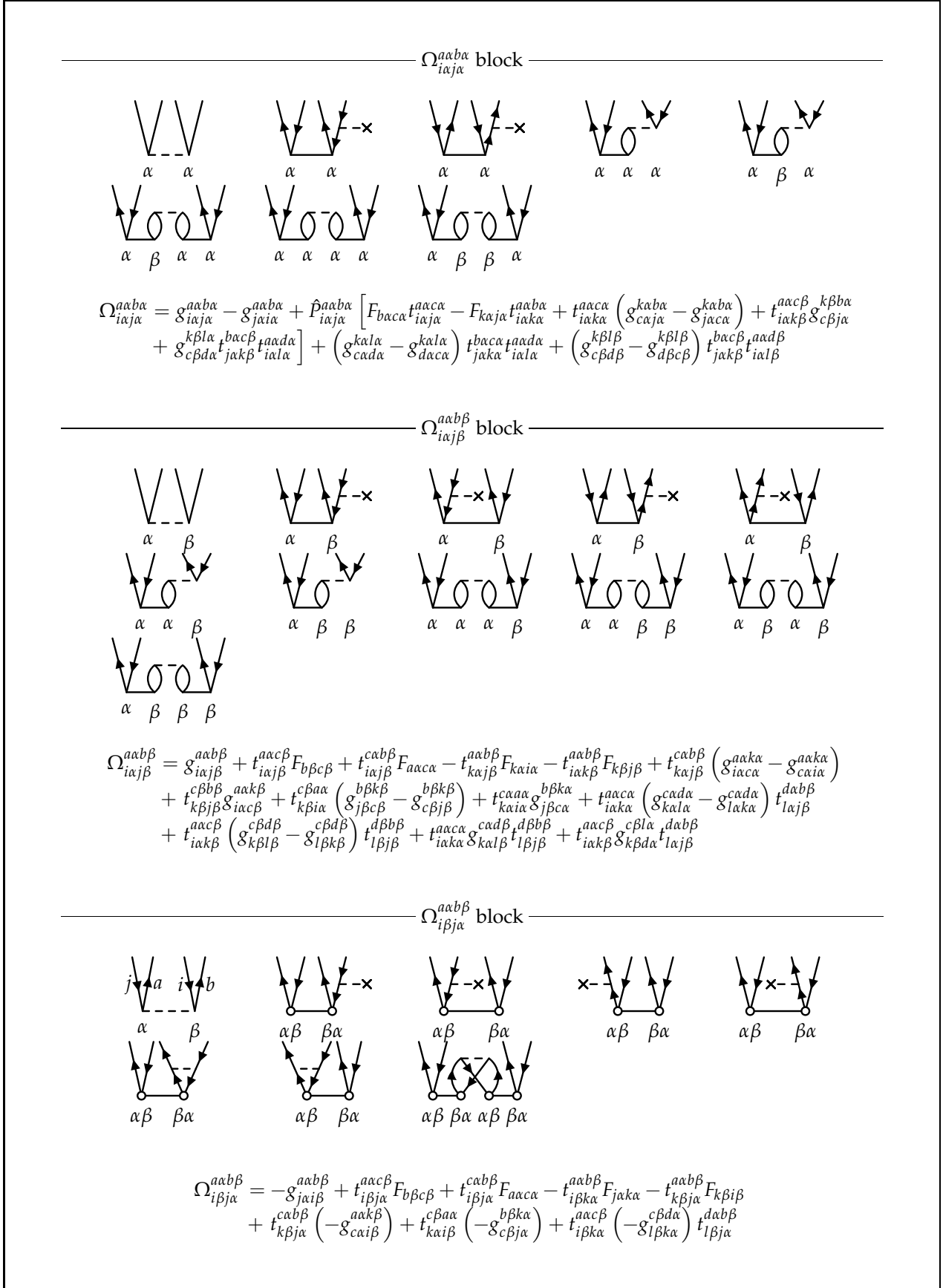
Fig. 2.3: Diagrammatic representation of the spin-expanded open-shell rCCD residual equations. A detailed diagrammatic treatment of spin summation is outlined in Ref. [121, 152]. Spin-flipped amplitudes are marked at the vertex by an empty circle. The Einstein summation convention is assumed.
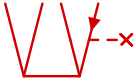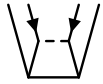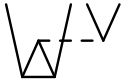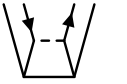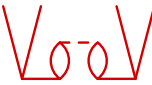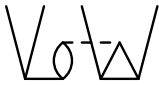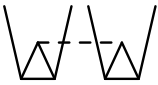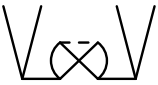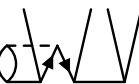
Coulomb	Exchange			Algebraic expression	
[1]				g_{ij}^{ab}	F
[2]				$-\hat{P}_{ij}^{ab}t_{ik}^{ab}F_{kj}$	E
[3]				$\hat{P}_{ij}^{ab}t_{ij}^{ac}F_{bc}$	E
[4]				$\frac{1}{2}\hat{P}_{ij}^{ab}t_{ij}^{cd}g_{cd}^{ab}$	B
[5]				$\frac{1}{2}\hat{P}_{ij}^{ab}t_{kl}^{ab}g_{ij}^{kl}$	A
[6]	[6ex_a]	[6ex_b]	[6ex_c]	$\hat{P}_{ij}^{ab}(2t_{ik}^{ac}g_{cj}^{kb} - t_{ik}^{ca}g_{cj}^{kb}$ $- t_{kj}^{ac}g_{ic}^{kb} - t_{ik}^{ac}g_{jc}^{kb})$	D+C
[7]				$\frac{1}{2}\hat{P}_{ij}^{ab}t_{ij}^{cd}t_{kl}^{ab}g_{cd}^{kl}$	A
[8]	[8ex_a]	[8ex_b]	[8ex_c]	$\hat{P}_{ij}^{ab}(2t_{ik}^{ac}t_{lj}^{db}g_{cd}^{kl} - 2t_{ik}^{ac}t_{jl}^{db}g_{cd}^{kl}$ $+ \frac{1}{2}t_{ik}^{ca}t_{jl}^{db}g_{cd}^{kl} - t_{ik}^{ac}t_{lj}^{db}g_{dc}^{kl})$	D+C
	[8ex_d]	[8ex_e]		$\hat{P}_{ij}^{ab}(t_{ki}^{ac}t_{lj}^{db}g_{dc}^{kl}$ $+ \frac{1}{2}t_{kj}^{ac}t_{il}^{db}g_{cd}^{lk})$	D+C
[9]	[9ex]			$\hat{P}_{ij}^{ab}(-2t_{ki}^{cd}t_{lj}^{ab}g_{cd}^{kl}$ $+ t_{ik}^{cd}t_{lj}^{ab}g_{cd}^{kl})$	E
[10]	[10ex]			$\hat{P}_{ij}^{ab}(-2t_{kl}^{ca}t_{ij}^{db}g_{cd}^{kl}$ $+ t_{kl}^{ac}t_{ij}^{db}g_{cd}^{kl})$	E

Fig. 2.4: Non-antisymmetrized Goldstone diagrams for the CCD and drCCD residual equations representing spatial orbitals. The labeling on the right-hand side, classifying the different terms as contributions A to F, refers to Appendix E explaining the implementation in the TURBOMOLE program package.

references and a representation in the biorthogonal basis analogously to CCD is also not possible. However, the spin-flipped residual $\Omega_{i\beta j\alpha}^{a\alpha b\beta}$ is decoupled from the other residual equations and can be evaluated separately. As noted and examined by Klopper *et al.*, the decoupling allows to completely neglect spin-flipped contributions [146] when aiming for an approximate rCCD method. In comparison to CCD, they find that the exclusion of spin-flipped excitations rises the rCCD correlation energy by about 30 %, while incorporation effects a lowering of about 40 %. Both approximations deviate in total by a factor of two.

In order to avoid the bottleneck of solving three residual equations for the same-spin, opposite-spin and spin-flip case in corresponding closed-shell implementations, the three spin cases can be furthermore connected by linear combination, exploiting the redundancy of the spin-flipped contributions and introducing singlet and triplet amplitudes $^1t_{ij}^{ab}$ and $^3t_{ij}^{ab}$ as,

$$^1t_{ij}^{ab} = t_{i\alpha j\alpha}^{a\alpha b\alpha} + t_{i\alpha j\beta}^{a\alpha b\beta} , \tag{2.78}$$

$$^3t_{ij}^{ab} = t_{i\alpha j\alpha}^{a\alpha b\alpha} - t_{i\alpha j\beta}^{a\alpha b\beta} = t_{i\beta j\alpha}^{a\alpha b\beta} . \tag{2.79}$$

Note that Eqs. (2.78) and (2.79) hold for both CCD and rCCD. For CCD, the symmetry relations allow to express the CCD correlation energy in multiple ways,

$$E_C^{CCD} = \frac{1}{4} \sum_{ijab} \left[^1t_{ij}^{ab} \left(2g_{ab}^{ij} - g_{ba}^{ij} \right) + 3\, ^3t_{ij}^{ab} \left(-g_{ba}^{ij} \right) \right] = \frac{1}{4}\text{tr} \left[^1\mathbf{T}\, ^1\mathbf{B}^{\text{RPAX}} + 3\, ^3\mathbf{T}\, ^3\mathbf{B}^{\text{RPAX}} \right] , \tag{2.80}$$

$$= \frac{1}{2} \sum_{ijab} {}^1t_{ij}^{ab} \left(2g_{ab}^{ij} \right) = \frac{1}{2}\text{tr} \left[^1\mathbf{T}\, ^1\mathbf{B}^{\text{dRPA}} \right] , \tag{2.81}$$

$$= \frac{1}{2} \sum_{ijab} \left(^1t_{ij}^{ab} - {}^3t_{ij}^{ab} \right) \left(2g_{ab}^{ij} - g_{ba}^{ij} \right) = \frac{1}{2}\text{tr} \left[^1\mathbf{T} - {}^3\mathbf{T} \right] {}^1\mathbf{B}^{\text{RPAX}} , \tag{2.82}$$

with the singlet and triplet matrices $(^1\mathbf{B}^{\text{RPAX}})_{ij}^{ab} = 2g_{ab}^{ij} - g_{ba}^{ij}$, $(^1\mathbf{B}^{\text{dRPA}})_{ij}^{ab} = 2g_{ab}^{ij}$ and $(^3\mathbf{B}^{\text{RPAX}})_{ij}^{ab} = -g_{ba}^{ij}$. In contrast, the rCCD correlation energy can only be represented by a single singlet-triplet-formulation [116],

$$E_C^{rCCD} = \frac{1}{4} \sum_{ijab} \left[^1t_{ij}^{ab} \left(2g_{ab}^{ij} - g_{ba}^{ij} \right) + 3\, ^3t_{ij}^{ab} \left(-g_{ba}^{ij} \right) \right] = \frac{1}{4}\text{tr} \left[^1\mathbf{B}^{\text{RPAX}}\, ^1\mathbf{T} + 3\, ^3\mathbf{B}^{\text{RPAX}}\, ^3\mathbf{T} \right] . \tag{2.83}$$

The corresponding residual equations for singlet and triplet amplitudes are given in terms of the analogously defined matrices $(^1\mathbf{A}^{\text{RPAX}})_{ij}^{ab} = 2g_{ib}^{aj} - g_{bi}^{aj}$ and $(^3\mathbf{A}^{\text{RPAX}})_{ij}^{ab} = -g_{bi}^{aj}$,

$$^s\mathbf{\Omega} = {}^s\mathbf{T}\mathbf{\Delta} + {}^s\mathbf{B}^{\text{RPAX}} + {}^s\mathbf{A}^{\text{RPAX}}\, {}^s\mathbf{T} + {}^s\mathbf{T}\, {}^s\mathbf{A}^{\text{RPAX}} + {}^s\mathbf{T}\, {}^s\mathbf{B}^{\text{RPAX}}\, {}^s\mathbf{T} , \tag{2.84}$$

with $s = 1$ for the singlet and $s = 3$ for the triplet quantities. $\mathbf{\Delta}$ summarizes the zeroth-order contributions, as already defined after Eq. (2.57).

Concerning spin adaptation, it is furthermore interesting to note that the reformulation in terms of singlet and triplet amplitudes corresponds to an orthogonal transformation (see Chapter 4 and e.g. Refs. [47, 145]). Moreover, it can be shown that the analogously defined singlet and triplet amplitudes $^s\mathbf{Y}$ and $^s\mathbf{X}$ are related by $^1\mathbf{Y}^1\mathbf{X}^{\text{T}} = -{}^3\mathbf{Y}^3\mathbf{X}^{\text{T}}$, a requirement from the condition that the wave function is an eigenfunction of the square of the spin operator with eigenvalue zero [163].

Even though Eq. (2.84) reduces the computational effort of closed-shell rCCD schemes, requiring solely the calculation of singlet and triplet amplitudes compared to the calculation of same-spin, opposite-spin and spin-flipped amplitudes, the efficiency of standard CC schemes like CCD cannot be achieved, because for the latter, closed-shell implementations only rely on one-type of spin-adapted, closed-shell amplitudes. Approximate and more cost-efficient rCCD schemes were however introduced by Szabo and Ostlund [21, 151], based on the CCD formulations of Eqs. (2.82) and (2.81),

$$E_C^{\text{rCCD-SO1}} = \frac{1}{2}\text{tr} \left[^1\mathbf{B}^{\text{RPAX}} \left(^1\mathbf{T} - {}^3\mathbf{T} \right) \right] , \tag{2.85}$$

$$E_C^{\text{rCCD-SO2}} = \frac{1}{2}\text{tr} \left[^1\mathbf{B}^{\text{dRPA}}\, ^1\mathbf{T} \right] . \tag{2.86}$$

The nomenclature, denoting the approaches "rCCD-SO1" and "rCCD-SO2", is taken from Ref. [86] and is adopted for the later discussions in Chapter 4. Both approximations were shown to be correct to second-order perturbation theory and to describe dispersion at the coupled HF level. In comparison, the rCCD-SO2 method

was proven to be the most accurate and practical approach [86, 164] as it solely involves singlet excitations, thus reducing computation time and avoiding triplet instabilities which are otherwise a serious bottleneck for rCCD schemes [146]. Furthermore, it is in contrast to rCCD-SO1 possible to recast the closed-shell equations into an open-shell analogon [164]. More precisely, the open-shell rCCD-SO2 correlation energy resembles the non-antisymmetrized formulation of open-shell CCD (Eq. (2.68)), now referring to the rCCD amplitudes,

$$E_C^{\text{rCCD-SO2}} = \frac{1}{2} \sum_{IJAB} (\mathbf{T}^{\text{rCCD}})_{IJ}^{AB} g_{AB}^{IJ} = \frac{1}{2} \text{tr} \left[\mathbf{B}^{\text{dRPA}} \mathbf{T}^{\text{rCCD}} \right] . \tag{2.87}$$

In contrast to the rCCD schemes including exchange, the direct rCCD approach allows straightforward spin integration: Even though the symmetry relation of Eq. (2.72) is also not fulfilled, spin integration yields a single closed-shell residual equation, exploiting that the amplitudes of same- and opposite-spin are connected by

$$t_{i\alpha j\alpha}^{a\alpha b\alpha} = t_{i\alpha j\beta}^{a\alpha b\beta} , \tag{2.88}$$

and that spin-flipped contributions are all of exchange type and therefore do not contribute to drCCD [146]. Thus, the closed-shell drCCD equations [145] can be derived starting from the CCD equations within the biorthogonal basis, as given in Figure 2.4. Exchange contributions are hereby visualized by expanding the antisymmetrized Goldstone diagrams of Figure 2.2 in terms of ordinary Goldstone diagrams, yielding additional contributions for diagrams [6],[8],[9] and [10] [121]. Those terms corresponding to the closed-shell dr-CCD residual equations are marked in red. Note that the highlighted diagrams are identical to the open-shell rCCD diagrams of Figure 2.2, deviating only by the underlying nomenclature and the algebraic expressions as the closed-shell drCCD analogues now correspond to the non-antisymmetrized two-electron interaction. Thus, they solely represent particle-hole contributions and require no additional labeling as introduced in Figure 2.2. The so-obtained drCCD amplitudes yield the drCCD correlation energy which is equivalent to the dRPA energy of Eq. (2.47),

$$E_C^{\text{drCCD}} = \sum_{abij} 2 g_{ab}^{ij} t_{ij}^{ab} = \text{tr} \left[\mathbf{B}^{\text{dRPA}} \mathbf{T}^{\text{drCCD}} \right] = E_C^{\text{dRPA}} . \tag{2.89}$$

Eq. (2.89) highlights once more the connection between RPA and ring coupled-cluster methods, showing that the coupled RPA eigenvalue problem can be rewritten as an amplitude equation and that the correlation energy can be expressed in terms of double excitation amplitudes. Despite the equivalency of the dRPA (RPAX) and drCCD (rCCD) correlation energies, it is however important to keep in mind that both approaches are based on a different formalism varying in the elementary working equations. Within RPA, for instance, the energy is given as the sum of excitation energies; rCCD theory expresses it in contrast in terms of pair interaction energy differences [140]. It is furthermore interesting to note that approximations to such differing formulations may also need to be distinguished: the Tamm-Dancoff Approximation (TDA) for example is only defined for rCCD correlation methods [165]. For RPA *correlation energies* based on the TDDFT eigenvalue problem (Eq. (2.7)) and the plasmon formula (Eq. (2.47)), it is however invalid, yielding by definition zero correlation energies [140].

2.3 F12 theory: Including geminals in the wave-function expansion

Modern F12 methods are based on Slater-type correlation factors depending exponentially on the interelectronic distance r_{12} [99],

$$f(r_{12}) = \gamma^{-1}(1 - \exp(-\gamma r_{12})) . \tag{2.90}$$

The prefactors γ are optimized according to the chosen orbital basis [166–169]. The corresponding geminal functions $w_{\overline{XY}}^{\mathbb{AB}}$,

$$w_{\overline{XY}}^{\mathbb{AB}} = \langle \mathbb{AB} | \hat{Q}_{12} f(r_{12}) | \widetilde{XY} \rangle , \tag{2.91}$$

are added to the conventional wave-function ansatz, parameterizing e.g. the configuration interaction doubles (CID) wavefunction as

$$|\text{CID-F12}\rangle = |\text{HF}\rangle + \sum_{I>J,A>B} c_{IJ}^{AB} |_{IJ}^{AB}\rangle + \sum_{I>J,X>Y,\mathbb{A}>\mathbb{B}} c_{IJ}^{XY} w_{\overline{XY}}^{\mathbb{AB}} |_{IJ}^{\mathbb{AB}}\rangle , \tag{2.92}$$

or the coupled-cluster doubles (CCD) approach according to

$$|\text{CCD-F12}\rangle = \exp(\hat{T}_2 + \hat{T}_{2'})|\text{HF}\rangle = \exp\left(\sum_{I>J,A>B} t_{IJ}^{AB}\tau_{IJ}^{AB} + \sum_{I>J,\mathbb{A}>\mathbb{B}} t_{IJ}^{\mathbb{A}\mathbb{B}}\tau_{IJ}^{\mathbb{A}\mathbb{B}}\right)|\text{HF}\rangle, \tag{2.93}$$

$$= \exp\left(\sum_{I>J,A>B} t_{IJ}^{AB}\tau_{IJ}^{AB} + \sum_{I>J,X>Y,\mathbb{A}>\mathbb{B}} c_{IJ}^{XY} w_{\widetilde{XY}}^{\mathbb{A}\mathbb{B}}\tau_{IJ}^{\mathbb{A}\mathbb{B}}\right)|\text{HF}\rangle. \tag{2.94}$$

c_{IJ}^{AB} and t_{IJ}^{AB} denote the corresponding conventional CI coefficients and CC amplitudes, weighting double excitations from the occupied to the virtual space. $\tau_{IJ}^{AB} = \hat{a}_A^\dagger \hat{a}_B^\dagger \hat{a}_J \hat{a}_I$ denote the double excitation operators. The explicitly correlated geminal amplitudes $t_{IJ}^{\mathbb{A}\mathbb{B}} = \sum_{X>Y} c_{IJ}^{XY} w_{\widetilde{XY}}^{\mathbb{A}\mathbb{B}}$ are defined analogously, now referring to an excitation from the occupied spin orbitals $\{I, J, \dots\}$ into the spin orbitals of the infinite virtual basis $\{\mathbb{A}, \mathbb{B}, \dots\}$. (Note that spatial orbitals of the infinite virtual space are in the following indicated as $\{\alpha, \beta, \dots\}$). $\{X, Y, \dots\}$ denote spin orbitals of the geminal space, which are standardly taken to be occupied orbitals.
While the CI formulation of Eq. (2.92) visualizes that the wave-function ansatz is linear in r_{12}, the CC ansatz of Eq. (2.94) highlights that the inclusion of geminals can also be interpreted as double excitations into an infinite virtual basis with subsequent reprojection onto the geminal space. The projection operator $\hat{Q}_{12}$ thereby ensures that the geminals are orthogonal to the conventional excitation manifold [112]. Different ansätze for $\hat{Q}_{12}$ were introduced [102, 170] and are summarized in Appendix B. The most common ansatz 2 is defined as

$$\hat{Q}_{12} = (1 - \hat{O}_1)(1 - \hat{O}_2) - \hat{V}_1\hat{V}_2, \tag{2.95}$$

with the projection operators onto the occupied and virtual orbital space, $\hat{O}$ and $\hat{V}$, respectively. Standardly, three-center integrals are avoided by introducing auxiliary basis sets and it is common to evaluate F12 integrals using a complementary auxiliary basis (CABS) [102]. Throughout the thesis, CABS orbitals are indicated as $\{P'', Q'', \dots\}$.
Evaluating the Schrödinger equation using the wave-function expansions of Eqs. (2.92) and (2.94) yields working equations for both conventional and geminal CI coefficients or CC amplitudes. For explicitly correlated coupled-cluster approaches, the so-obtained residual equations for the geminal amplitudes can be solved iteratively in analogy to the conventional counterparts (see Appendix B). However, it became common practice to keep the geminal amplitudes fixed according to the s- and p-wave cusp conditions [171], motivated by the fact that the ansatz is not only more efficient than an iterative procedure, but also avoids numerical instabilities. Furthermore, it is free from geminal BSSE and provides stable predictions for weak van der Waals interactions [172]. Keeping the geminal amplitudes fixed is often also called rational generator approach or SP ansatz [99], as the basic working equations can be expressed by introducing the rational generator $\hat{S}_{XY}$,

$$|\widetilde{XY}\rangle = \hat{S}_{XY}|XY\rangle = (\tfrac{3}{8} + \tfrac{1}{8}\hat{P}_{XY}^{\text{flip}})|XY\rangle. \tag{2.96}$$

The permutation operator $\hat{P}_{XY}^{\text{flip}}$ flips the spatial part of the orbitals X and Y keeping the spin functions σ_X and σ_Y the same,

$$\hat{P}_{XY}^{\text{flip}}\varphi_X\sigma_X\varphi_Y\sigma_Y = \varphi_Y\sigma_X\varphi_X\sigma_Y. \tag{2.97}$$

Eq. (2.97) can thus be interpreted as flipping from α to β spin or vice versa, justifying to call the open-shell approach "spin-flipped amplitudes". In contrast to other common choices for fixed amplitudes, the rational generator approach ensures basis-set convergence proportional to X^{-7} and has the advantage that open-shell equations can be directly transformed into the closed-shell analogues, just by applying spin summation rules and using identical orbitals for α and β spin. The presented F12 approaches in the following chapters therefore always refer to spin-flipped amplitudes. It should however be kept in mind that other choices for fixed amplitudes are possible which are more cost-efficient [103, 173, 174] (see Appendix B).

Towards explicitly correlated RPA: On the basis-set convergence of established F12 methods and its transferability to RPA approaches

Based on the original idea of Kutzelnigg, various explicitly correlated wave-function methods have been developed in the last decades. One of the first approaches was based on second-order Møller-Plesset perturbation theory [97] and further developments led to the nowadays established MP2-F12 approach [105].

MP2-F12 theory proved as convincingly efficient, accelerating basis-set convergence while solely requiring an additive F12 contribution with N^5 scaling,

$$E_{\mathrm{C}}^{\text{MP2-F12}} = \tfrac{1}{4}\mathrm{tr}[\mathbf{B}^{\text{RPAX}}\mathbf{T}] + \tfrac{1}{4}\mathrm{tr}[(\boldsymbol{\mathcal{V}} - \boldsymbol{\mathcal{V}}^{\text{X}})^{\dagger}\mathbf{D}] + \tfrac{1}{4}\mathrm{tr}[\boldsymbol{\Omega}^{\text{F12(MP2-F12)}}\mathbf{D}^{\text{LAG}}],$$

$$= \tfrac{1}{4}\sum_{ABIJ} t_{IJ}^{AB}\left(g_{AB}^{IJ} - g_{BA}^{IJ}\right) + \tfrac{1}{4}\sum_{XYIJ} d_{IJ}^{XY}\left(\left(\mathcal{V}^{\dagger}\right)_{\widetilde{XY}}^{IJ} - \left(\mathcal{V}^{\dagger}\right)_{\widetilde{YX}}^{IJ}\right) + \tfrac{1}{4}\sum_{XYIJ} d_{IJ}^{XY}\left(\Omega^{\text{F12(MP2-F12)}}\right)_{IJ}^{\widetilde{XY}}. \tag{2.98}$$

Keeping the geminal amplitudes fixed and assuming ansatz 2* for the projection operator $\hat{Q}_{12}$, the residual equation for the geminal amplitudes is reduced to a constant term, given as

$$\left(\Omega^{\text{F12(MP2-F12)}}\right)_{IJ}^{\widetilde{XY}} = \mathcal{V}_{IJ}^{\widetilde{XY}} - \mathcal{V}_{JI}^{\widetilde{XY}} + \sum_{VW} d_{IJ}^{VW}\mathcal{B}_{\widetilde{XY},\widetilde{VW}}^{(IJ)}. \tag{2.99}$$

Eq. (2.98) parameterizes the MP2-F12 correlation energy analogously to Eq. (2.65) referring to matrix $\mathbf{B}^{\text{RPAX}}$ which contains the antisymmetrized two-electron integrals as defined within Eq. (2.12). In contrast to Eq. (2.65), the first-order double excitation amplitudes are now given as $\mathbf{T} = \mathbf{B}^{\text{RPAX}}/\boldsymbol{\Delta}$ with $\Delta_{IJ}^{AB} = (\varepsilon_I + \varepsilon_J - \varepsilon_A - \varepsilon_B)$. Note that pure exchange contributions are in the following indicated by adding the superscript X, as already done in Eq. (2.98) for matrix $\boldsymbol{\mathcal{V}}$. The latter F12 intermediate and matrix $\boldsymbol{\mathcal{B}}$ are defined as

$$\mathcal{V}_{IJ}^{\widetilde{XY}} = \langle\widetilde{XY}|f_{12}\hat{Q}_{12}\hat{g}_{12}|IJ\rangle, \tag{2.100}$$

$$\mathcal{B}_{\widetilde{XY},\widetilde{VW}}^{(IJ)} = \langle\widetilde{XY}|f_{12}\hat{Q}_{12}(\hat{F}_1 + \hat{F}_2 - \varepsilon_I - \varepsilon_J)\hat{Q}_{12}f_{12}|\widetilde{VW}\rangle. \tag{2.101}$$

Details on the further evaluation of the matrices $\boldsymbol{\mathcal{V}}$ and $\boldsymbol{\mathcal{B}}$ are summarized in Appendix B, showing that the projection onto the infinite virtual basis is treated analytically enabling fast basis-set convergence. In Eq. (2.98), the geminal amplitudes are parameterized in terms of d_{IJ}^{XY} to highlight that the fixed ansatz requires antisymmetrized coefficients when including exchange, $d_{IJ}^{XY} = \delta_{IX}\delta_{JY} - \delta_{IY}\delta_{JX}$, with the corresponding matrix representation $\mathbf{D}$. Ten-no furthermore suggested to set the Lagrange multipliers equal to $\mathbf{D}^{\text{LAG}} = \mathbf{D}$ since this is true for optimized amplitudes [175, 176].

Neglecting all exchange contributions gives a corresponding direct MP2-F12 (dMP2-F12) approach, yielding the Lagrangian with the conventional dMP2 contribution [177] in analogy to Eq. (2.66) as well as the related explicitly correlated energy and residual term in analogy to Eq. (2.66),

$$E_{\mathrm{C}}^{\text{dMP2-F12}} = \tfrac{1}{2}\mathrm{tr}[\mathbf{B}^{\text{dRPA}}\mathbf{T}] + \tfrac{1}{2}\mathrm{tr}[\boldsymbol{\mathcal{V}}^{\dagger}\mathbf{C}] + \tfrac{1}{2}\mathrm{tr}[\boldsymbol{\Omega}^{\text{dMP2-F12}}\mathbf{C}^{\text{LAG}}],$$

$$= \tfrac{1}{2}\sum_{ABIJ} t_{IJ}^{AB}g_{AB}^{IJ} + \tfrac{1}{2}\sum_{XYIJ} c_{IJ}^{XY}\left(\mathcal{V}^{\dagger}\right)_{\widetilde{XY}}^{IJ} + \tfrac{1}{2}\sum_{XYIJ} c_{IJ}^{XY}\left(\Omega^{\text{F12(dMP2-F12)}}\right)_{IJ}^{\widetilde{XY}}, \tag{2.102}$$

with

$$\left(\Omega^{\text{F12(dMP2-F12)}}\right)_{IJ}^{\widetilde{XY}} = \mathcal{V}_{IJ}^{\widetilde{XY}} + \sum_{VW} c_{IJ}^{VW}\mathcal{B}_{\widetilde{XY},\widetilde{VW}}^{(IJ)}. \tag{2.103}$$

For dMP2, fixed amplitudes are chosen according to $c_{IJ}^{XY} = \delta_{IX}\delta_{JY}$ for all spin cases. The Lagrange multipliers are again given by the relation $\mathbf{C}^{\text{LAG}} = \mathbf{C}$. Even though this connection might appear trivial for open-shell systems, it should be noted that the strict identity between Lagrange multipliers and geminal amplitudes is lifted when introducing a biorthogonal basis for closed-shell equations. Taking the partial derivatives of the closed-shell analogues for Eq. (2.102) with respect to both coefficients and comparing the so-obtained equations shows that $\mathbf{C}^{\text{LAG}}$ and $\mathbf{C}$ differ by a factor of two (or analogously it is found for closed-shell counterpart of Eq. (2.98) that $\mathbf{C}^{\text{LAG}}$ has to be set equal to $2\mathbf{C} - \mathbf{C}^{\text{X}}$). Explicit working equations for the closed-shell case are given in Appendix C.

To visualize the three different contributions to the (d)MP2-F12 correlation energy, diagrams for the conventional and the explicitly correlated energy contributions are given in Figure 2.5. An overview on the nomenclature, summarizing all special vertices which are necessary to describe the additional F12 terms, is given in Appendix A. In short, contractions over the infinite virtual basis are indicated by double arrows and geminal amplitudes are represented by a double bar. The integral over the Slater geminal is drawn as a wiggly line. Also note that contributions which cancel due to the chosen ansatz and the corresponding projection operator $\hat{Q}_{12}$ are already neglected. Regarding the translation rules to obtain the algebraic expressions, it should be mentioned that these are identical to the standard rules for antisymmetrized Goldstone diagrams representing spin orbitals in the case of MP2-F12 theory including exchange. Moreover, analogously

to the two-electron interaction contribution (corresponding to the dashed line), the two-electron integral over the Slater geminal is assumed to be antisymmetrized. Based on the nomenclature of Figure A.1, the algebraic equations can be derived by applying Wick's theorem, as outlined in standard textbooks (see e.g. Ref. [121]). The dMP2-F12 diagrams however refer to non-antisymmetrized integrals introducing — in analogy to drCCD — an additional factor of 2. The dashed line thus corresponds to $\frac{1}{2} g_{QS}^{PR} \hat{a}_P^\dagger \hat{a}_R^\dagger \hat{a}_S \hat{a}_Q$ instead of the antisymmetrized definition $\frac{1}{4} \left(g_{QS}^{PR} - g_{SQ}^{PR} \right) \hat{a}_P^\dagger \hat{a}_R^\dagger \hat{a}_S \hat{a}_Q$.

It should furthermore be noted that the geminal amplitudes are not specified; the diagrams visualize not only fixed, but also optimized amplitudes. Matrix $\mathcal{B}$, as given in Eq. (2.101), is therefore depicted in terms of the two diagrams [4] and [5]. This general representation does however not provide any information on the further evaluation of the F12 intermediate. A short outline concerning the final working equations is given in Appendix B, following Refs. [105, 178, 179] and showing that diagram [4] cancels to zero for fixed amplitudes. When furthermore referring to KS references with local exchange-correlation functional, exchange contributions cancel and the two common approximations A and B turn out to be equivalent due to the fact that all local potentials commute with the correlation factor f_{12} [180]. Approximations to the kinetic energy term are also identical, elsewise standardly denoted as [T+V] and [F+K]. This conclusion holds for all F12 methods that are presented in the following chapters of the thesis and, in consequence, all further discussions thus only discriminate between ansatz 1, 2 and 2*. Assuming a KS reference with local exchange-correlation functionals and fixed amplitudes, the final working equations for intermediate $\mathcal{B}$ thus reduce to the single diagram no. [5]. Note that the diagrams for ansatz 1 and 2* are identical - the two approaches solely differ due to the corresponding definitions of $\hat{Q}_{12}$ which only effects the explicit evaluation of intermediates $\mathcal{V}$ and $\mathcal{B}$. Ansatz 2, however, leads not only to a second contribution to the F12 intermediate $\mathcal{B}$, but also to an additional term in the F12 residual, given in Eq. (E.8) and represented in terms of diagram [6] (see Appendix E). In contrast to ansatz 1 and 2*, ansatz 2 thus requires an iterative update of the conventional MP2 amplitudes.

To combine RPA with the explicitly correlated wave-function ansatz in analogy to the established MP2-F12 approaches, the connection to CC and many-body perturbation theory can be exploited: Based on the equivalence of drCCD/rCCD and dRPA/RPAX approaches, it can be shown that the dMP2/MP2 correlation energy is obtained when truncating the dRPA/RPAX energy after first-order perturbation theory,

$$E_C^{dMP2} = \frac{1}{2} \mathrm{tr} \left[\mathbf{B}^{dRPA} \mathbf{T}^{dRPA(1)} \right] , \tag{2.104}$$

$$E_C^{MP2} = \frac{1}{2} \mathrm{tr} \left[\mathbf{B}^{RPAX} \mathbf{T}^{RPAX(1)} \right] , \tag{2.105}$$

with the corresponding residual equations for the first-order amplitudes $\mathbf{T}^{(1)}$,

$$\mathbf{B}^{dRPA} + \mathbf{A}^{(0)} \mathbf{T}^{dRPA(1)} + \mathbf{T}^{dRPA(1)} \mathbf{A}^{(0)} = \mathbf{0}, \tag{2.106}$$

$$\mathbf{B}^{RPAX} + \mathbf{A}^{(0)} \mathbf{T}^{RPAX(1)} + \mathbf{T}^{RPAX(1)} \mathbf{A}^{(0)} = \mathbf{0} . \tag{2.107}$$

The zeroth-order contribution to matrix $\mathbf{A}$ is given for both dRPA and RPAX as $(\mathbf{A}^{(0)})_{IJ}^{AB} = (\varepsilon_A - \varepsilon_I) \delta_{IJ} \delta_{AB}$. Due to this connection, perturbative dRPA+F12 and RPA+F12 methods can be set up by taking into account the F12 contribution of the presented dMP2-F12 and MP2-F12 methods [181],

$$E_C^{dRPA+F12} = E_C^{dRPA} - E_C^{dMP2} + E_C^{dMP2-F12} , \tag{2.108}$$

$$E_C^{RPAX+F12} = E_C^{RPAX} - E_C^{MP2} + E_C^{MP2-F12} . \tag{2.109}$$

Explicit equations for closed- and open-shell references are given in Appendix C. Moreover, the "+F12" correction can be universally applied to beyond-RPA methods, which require — depending on the underlying method — either just the Coulomb or both Coulomb and exchange contributions. Of course, RPA variants whose second-order limits yield standard MP2 theory should be corrected by the F12 contribution of MP2-F12 while the analogous contribution from dMP2-F12 theory should be added to those methods which yield the dMP2 result to second order. As an example, the promising exchange methods ACSOSEX [145, 182] and AXK [8] can be corrected according to

$$E_C^{ACSOSEX+F12} = E_C^{dRPA} + E_C^{\Delta ACSOSEX} - E_C^{MP2} + E_C^{MP2-F12} , \tag{2.110}$$

$$E_C^{AXK+F12} = E_C^{dRPA} + E_C^{\Delta AXK} - E_C^{MP2} + E_C^{MP2-F12} . \tag{2.111}$$

Working equations for both correction terms ΔAXK and $\Delta ACSOSEX$ are summarized in Appendix C, emphasizing that the latter approach has to be distinguished from the CC-formulation of second-order screened exchange, standardly referred to as SOSEX [45, 52]. Furthermore, the equations of Appendix C reveal that both ACSOSEX and AXK contain exchange contributions to higher-order perturbation theory. In comparison, the perturbative F12 correction, as derived from MP2 theory, includes Coulomb and exchange contributions

only to second-order perturbation theory, lacking a consistent screening as included for the conventional counterparts.

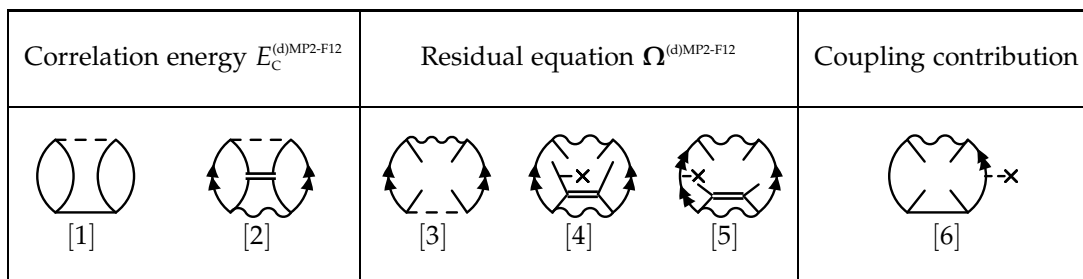| Correlation energy $E_{\mathrm{c}}^{\mathrm{(d)MP2\text{-}F12}}$	Residual equation $\Omega^{\mathrm{(d)MP2\text{-}F12}}$	Coupling contribution
[1] [2]	[3] [4] [5]	[6]

Fig. 2.5: Diagrams [1] to [5] represent the (d)MP2-F12 correlation energy and amplitude equations within ansatz 2*, referring to Eqs. (2.98) and (2.99) or Eqs. (2.102) and (2.103), respectively. For ansatz 2, an additional coupling contribution has to be considered, see Eq. (E.8). Algebraic expressions for the MP2-F12 approach can be obtained by applying the standard translation rules for antisymmetrized Goldstone diagrams representing spin orbitals. The dMP2-F12 ansatz however requires a non-antisymmetrized definition of the two-electron interaction operator, resulting in an additional factor of 2.

However, due to the fact that higher-order terms are small in magnitude, the perturbative +F12 correction is promising for all RPA and beyond-RPA methods: As depicted in Figure 2.6, basis-set convergence of the correlation contribution to the atomization energy is significantly accelerated for the aug-cc-pVXZ basis sets [183, 184]. Results are shown for 10 small molecules, namely CH_4, CN, CO, C_2H_2, C_2H_4, F_2, H_2, N_2, NH_3, O_2, as well as 3 dimers, the H_2O, CH_4 and NH_3 dimers. For the latter, the geometries were taken from the S22 test set [36]; all other geometries refer to Ref. [185]. Aug-cc-pVXZ basis sets [183, 184] were chosen together with the aug-cc-pwCV(X+1)Z [186, 187] and the aug-cc-pV(X+1)Z [188] basis sets as cbas and jkbas, respectively. In addition, the optimized aug-cc-pVXZ/OPTRI basis sets were used as CABS [189]. Basis-set convergence is investigated for double-zeta to quintuple-zeta size and the conventional results are extrapolated to the basis-set limit using the two-point formula of Helgaker *et al.* [190],

$$E_{\mathrm{c}}(XY) = \frac{X^3 E_{\mathrm{c}}(X) - Y^3 E_{\mathrm{c}}(Y)}{X^3 - Y^3} \,, \tag{2.112}$$

where $E_{\mathrm{c}}(X)$ and $E_{\mathrm{c}}(Y)$ denote correlation energies obtained in basis sets of cardinal numbers X and Y. The following discussion is restricted to mean errors per valence electron with the corresponding standard deviations as error bars in kJ/mol; explicit numbers and further statistical measures including mean absolute errors and root-mean-square errors are given in Table C.2. The errors were calculated with respect to the corresponding +F12 calculation performed within the aug-cc-pV5Z basis, in the following abbreviated as +F12/aug-cc-pV5Z. The deviations of the chosen reference from the extrapolated aug-cc-pV(Q5)Z result only amount up to 0.05 kJ/mol with a maximum standard deviation of 0.06 kJ/mol. All computations were performed using PBE orbitals, ansatz 2* was chosen for the F12 calculations and the geminal amplitudes were kept fixed. This choice enables a simple additive scheme; optimized amplitudes as well as the inclusion of coupling contributions would require an iterative update of the conventional amplitudes. It should be furthermore noted that hydrogen has a non-zero dRPA and dMP2 correlation energy and thus contributes to the depicted atomization energies.

The plot is split in two parts: on the left-hand side, the direct RPA and MP2 approaches are compared with the corresponding explicitly correlated schemes and on the right-hand side, the two different beyond-RPA variants AXK and ACSOSEX are assessed with respect to the related, conventional and explicitly correlated MP2 approaches. For all five conventional methods, the basis-set limit is reached from below. Mean errors are slowly decreasing, starting in the range of -9.2 to -6.2 kJ/mol and declining up to a deviation of -0.7 to -0.4 kJ/mol for the aug-cc-pV5Z basis. The extrapolated limits are as already mentioned in close agreement with the +F12/aug-cc-pV5Z results. The similar convergence behavior of MP2 and RPA is not astonishing as it was already shown by Furche [40] and Eshuis [80] that RPA correlation energies show an asymptotic X^{-3} basis-set dependence with respect to the cardinal number X, as standardly found for all orbital-dependent wave-function methods [190]. In comparison, the explicitly correlated approaches are converging much faster, even though the dMP2-F12 results within the aug-cc-pVDZ basis still show a mean error of -1.2 kJ/mol, which is only slightly smaller than the conventional aug-cc-pVTZ errors. However, convergence to within 99 % of the basis-set limit can already be achieved for the triple-zeta basis set, even outrivalling conventional aug-cc-pV6Z results. Comparable trends are found for MP2-F12 including exchange. The corresponding +F12

schemes for RPA and beyond-RPA approaches are corrected in the same manner, shifting the conventional results by the additive F12 contribution. Due to the slightly differing slopes of conventional MP2 and RPA, the double-zeta +F12 results are already converged to within 99 % of the basis-set limit for all three approaches dRPA+F12, ACSOSEX+F12 and AXK+F12. Convergence is however not smooth: the error increases when expanding the basis to triple-zeta quality and in the case of AXK and ACSOSEX, the aug-cc-pVQZ error is even larger in magnitude than the +F12/aug-cc-pVDZ result.

Next to atomization energies, it is interesting to take a look at interaction energies as geminals were shown to compensate the lack of diffuse basis functions [191]. Diffuse functions are of particular importance for an accurate description of binding energies [192], generally accelerating basis-set convergence when added in the important bonding regions [193, 194]. Conventional methods were furthermore shown to require basis sets of augmented quintuple-zeta quality to achieve accurate binding energies [195]. Moreover, wave-function methods suffer from the basis-set superposition error (BSSE), leading to an overestimation of the binding energy and requiring to be corrected for by the counterpoise (CP) approach [82]. The BSSE was however shown to be reduced due to the explicitly correlated wave-function ansatz, leading to much smaller counterpoise corrections [191]. CP corrections are in general of particular importance when regarding interactions between weakly bound dimers as the BSSE causes a stabilization of the dimer relative to the individual monomers, caused by the additional basis functions of the neighboring monomer.

Figures 2.7 and 2.8 show the mean errors per valence electron in the interaction energies of the water, the ammonia and the methane dimers, with and without counterpoise correction. For both graphs the counterpoise-corrected +F12/aug-cc-pV5Z result serves as reference which agrees with the extrapolated counterpoise-corrected aug-cc-pV(Q5)Z result to within 0.01 kJ/mol. Note that the interaction energies were calculated without considering optimized geometries for the isolated monomers. The examined monomer geometries were identical to the geometry that the monomer possesses in the dimer. Deformation energies were thus neglected and the calculated energies have to be referred to as interaction energies instead of binding energies. Conventional results without counterpoise correction converge for both direct and exchange methods smoothly from above, with mean errors of 0.31-0.61 kJ/mol for the aug-cc-pVDZ basis to 0.04-0.09 kJ/mol for the aug-cc-pV5Z basis. This systematic convergence is lost when including the perturbative F12 correction: double-zeta results overestimate the interaction energy by roughly -0.32 to -0.17 kJ/mol, while triple-zeta results overshoot the basis-set limit by a maximum of 0.10 kJ/mol. However, percentage errors show that triple-zeta basis sets are sufficient to achieve convergence to within 97.1 to 99.6 % of the basis-set limit, being comparable to the conventional auf-cc-pV5Z results with 95.2 to 98.6 %. Including the counterpoise correction, all conventional methods overestimate the interaction energy and the mean errors with respect to the basis-set limit are comparable to the non-corrected results, now approaching the reference value from below. Thus even though the counterpoise correction removes the basis-set *superposition* error, it does not diminish the basis-set *incompleteness* error. The magnitude of the CP correction for the conventional methods is in the range of 0.74 to 1.25 kJ/mol for the aug-cc-pVDZ basis. In comparison, the +F12 results are, as expected, much less sensitive to the BSSE: the CP correction only amounts up to a maximum value of 0.2 kJ/mol for dRPA+F12 within the aug-cc-pVDZ basis. Nevertheless, the inclusion of the CP correction has the advantage that the so-obtained results converge smoothly to the basis-set limit, a necessary requirement for basis-set extrapolation techniques [172]. Furthermore, the results suggest the hypotheses that it is more accurate to correct the BSSE by adding a perturbative F12 correction than applying the usual counterpoise correction scheme.

Regarding both results for atomization and interaction energies, it can be concluded that the perturbative +F12 approaches accelerate basis-set convergence in the same manner as for the well-established MP2-F12 method, achieving convergence to within 99% of the basis-set limit for aug-cc-pVDZ or aug-cc-pVQZ results, respectively. The gain is about more than three cardinal numbers for atomization energies; for interaction energies conventional aug-cc-pV5Z results are comparable to explicitly correlated aug-cc-pVTZ calculations, reducing the required cardinal number by two. However, convergence to the basis-set limit is not systematic and relies on fortuitous error cancellation, as shown in Figure 2.6 for atomization energies when expanding the basis set from double- to triple-zeta size. A comparable kink in the plotted error lines can also be observed for correlation energies, as depicted in Figure C.2 of Appendix C. Nevertheless, the +F12 schemes demonstrate that efficiency can be tuned and that the required basis-set size can be reduced by adding a perturbation correction to the conventional correlation energy. The F12 contribution is cost-efficient with a scaling of N^5, requiring — for fixed geminal amplitudes — solely the diagonal contributions of the F12 intermediates $\mathcal{V}$ and $\mathcal{B}$. It can thus be expected that more sophisticated explicitly correlated RPA approaches yield the same benefit in terms of efficiency while being more rigorous and robust, not suffering from the disadvantages of many-body perturbation theory.
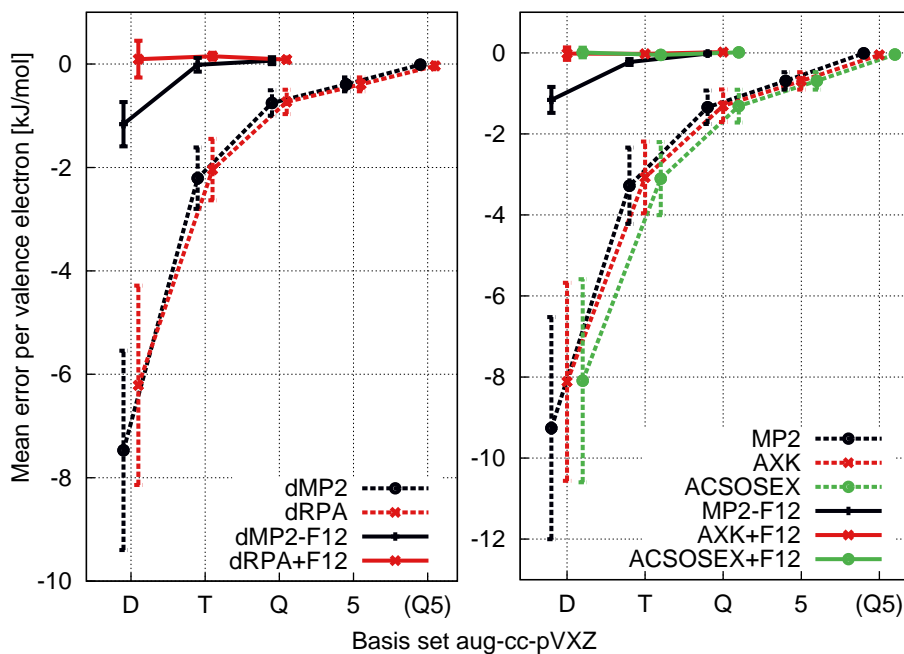
Fig. 2.6: Basis-set convergence of the correlation contribution to the atomization energies for selected +F12 approaches, the underlying dMP2-F12 and MP2-F12 methods as well as the corresponding conventional counterparts.
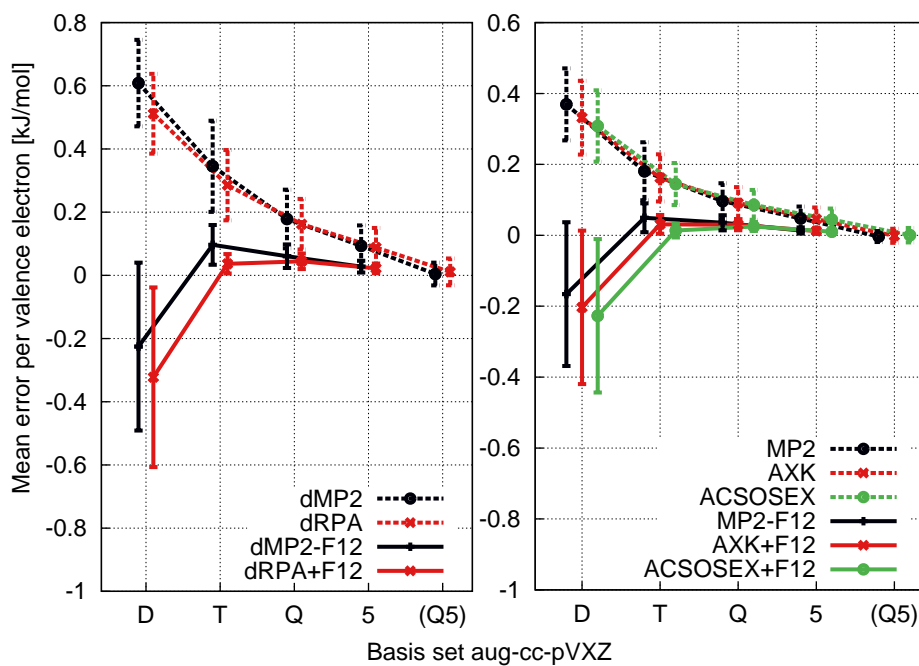

Fig. 2.7: Basis-set convergence of interaction energies (without counterpoise correction) for selected +F12 approaches as well as the underlying dMP2-F12 and MP2-F12 methods.
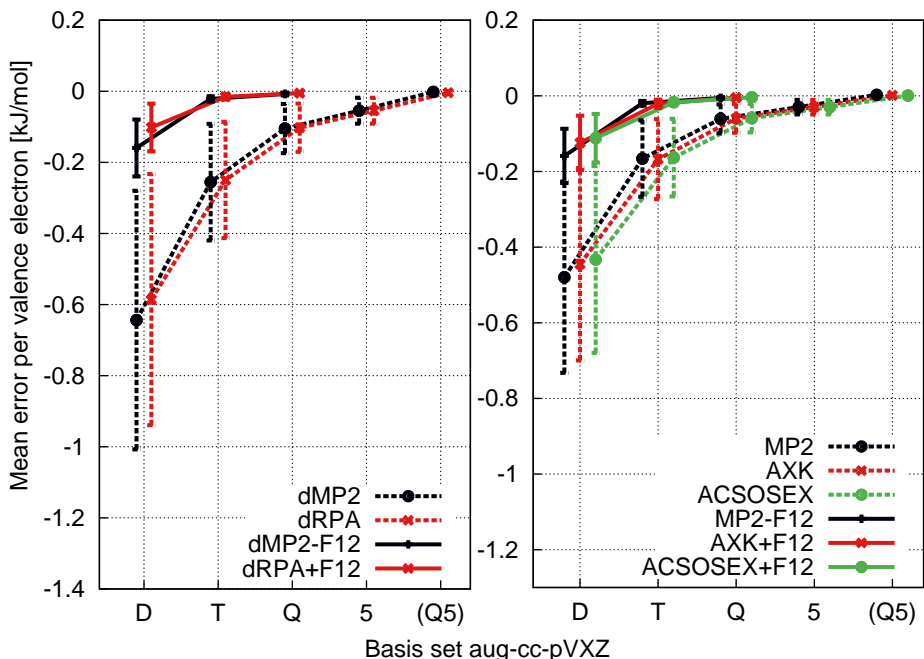
Fig. 2.8: Basis-set convergence of counterpoise-corrected interaction energies for selected +F12 approaches as well as the underlying dMP2-F12 and MP2-F12 methods.

Accelerating basis-set convergence of the Kohn-Sham reference determinant

When considering the convergence of total energies with respect to the size of the chosen basis set, it is important to distinguish between basis-set convergence of the correlation contribution and the underlying reference energy [190]. While it has been shown that the truncation error in the correlation energy converges as L^{-3} with L as the maximum angular momentum number [196–198], the convergence of the reference energy is significantly faster and can be well described by an exponential function [96, 199, 200]. Nevertheless, the basis-set incompleteness error in the reference energy is still significant for small basis sets and gains particular importance when the correlation energy is already converged to the basis-set limit, as in the case of F12 methods. Adding geminals in the wave-function expansion as done within F12 theory only accelerates convergence in the double-excitation space, omitting an equally extensive parameterization of the HF or KS orbitals in terms of single excitations. To reduce the basis-set error in the reference determinant, it was thus proposed to include single excitations into the CABS basis, yielding a perturbative second-order energy correction which is standardly abbreviated as "CABS-singles correction" [201, 202]. It was shown for HF references that the CABS-singles correction reduces the HF basis-set error by one order of magnitude, allowing to reach chemical accuracy with double-zeta basis sets for total reaction energies [203]. In general, the CABS-singles correction ensures that the error in the HF energy is smaller than the corresponding error in the correlation energy while the computation time is negligible, being comparable to a single HF iteration within the combined MO and CABS basis. Regarding the following Chapter 3, it is also interesting to note that the impact of the CABS-singles correction onto the singles correlation contribution is unimportant [202, 204]. Detailed equations for HF references are e.g. given in Refs. [105, 178]. For KS references, the singles residual equation is evaluated analogously, now based on the KS matrix $\mathbf{F}^{KS}$,

$$t_i^{a'}(\text{ansatz 2}) = -\sum_{b'}[F_{a'b'}^{KS} - \delta_{a'b'}\varepsilon_i^{KS}]^{-1}F_{b'i}^{KS}, \tag{2.113}$$

while the correction to the reference energy is calculated using the Fock matrix $\mathbf{F}^{HF}$ from HF theory,

$$E_{\Delta CABS}(\text{ansatz 2}) = 2\sum_{a'i} F_{a'i}^{HF} t_i^{a'}. \tag{2.114}$$

Still, the Fock matrix is built from KS orbitals, thus neither the extended nor the generalized Brioullin condition hold. Eqs. (2.113) and (2.114), which refer to ansatz 2 including excitations into the combined virtual and CABS basis $\{p', q', \dots\}$, thus consider coupling contributions of the virtual-virtual and the CABS-virtual

block. In contrast, ansatz 2* only accounts for singles excitations into the CABS space,

$$t_i^{a''}(\text{ansatz } 2^*) = -\sum_{b''}[F_{a''b''}^{\text{KS}} - \delta_{a''b''}\varepsilon_i^{\text{KS}}]^{-1}F_{b''i}^{\text{KS}}, \tag{2.115}$$

$$E_{\Delta\text{CABS}}(\text{ansatz } 2^*) = 2\sum_{a''i}F_{a''i}^{\text{HF}}t_i^{a''}. \tag{2.116}$$

The CABS-singles correction for Kohn-Sham references was implemented by Dr. David Tew from the University of Bristol in the program part RICCTOOLS of the TURBOMOLE program package [180]. Details on the required keywords are given in Appendix E. Note that the reference energy is calculated as defined within Eq. (2.63). Figure 2.9 visualizes the impact of the CABS-singles correction on the basis-set convergence of the reference energy, depicting mean errors in kJ/mol for the earlier presented test set of 10 molecules, 3 dimers as well as the corresponding atoms C, N, O, H, and F. HF and PBE references are examined for the Dunning aug-cc-pVXZ basis sets, revealing that the basis-set incompleteness error is most prominent for the double-zeta basis, amounting up to 2.0 and 2.2 kJ/mol, respectively. Including the CABS-singles correction, denoted as HF+CABS and PBE+CABS, reduces the error in the HF (PBE) reference energy to 0.2 (0.4) kJ/mol. The double-zeta +CABS result is thus comparable to conventional aug-cc-pVTZ errors, demonstrating that the required basis-set size is reduced by one cardinal number. Further benchmark studies for PBE references are published in Ref. [180].
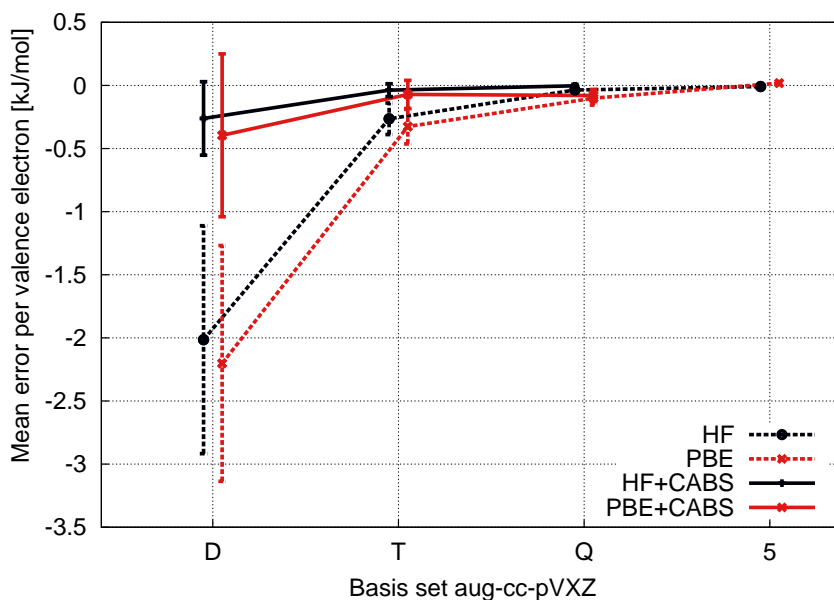

Fig. 2.9: Impact of the CABS-singles correction on the basis-set convergence of the reference energy.

3. RPA-F12 based on the hypervirial theorem

The promising performance of the perturbative RPA+F12 approach motivates to take further interest in other possible variants of explicitly correlated RPA. While some derivations of conventional RPA are based on the density, emphasizing the connection of the correlation method to (time-dependent) density-functional theory, a wave-function ansatz, as given by the equations of motion presented at the beginning of Chapter 2, is most suitable in order to enable a straightforward inclusion of F12 geminals, defined in Section 2.3. More precisely, the explicitly correlated dRPA approach as outlined in the following follows the ansatz of Bouman and Hansen, specifying the projection manifolds of ground and excited states in terms of single and double excitation amplitudes [117, 118]. To highlight the difference between the so introduced F12 contributions, the derivation of the corresponding eigenvalue problem is split in two parts, first adding geminals to the double excitation space and secondly including singles excitations into the CABS basis. Possible ansätze for the correlation energy are investigated, showing that the density matrix formulation still holds, requiring to compute the energy contribution via numerical integration over the frequency and implying a subsequent orthogonalization of the eigenvectors. Exemplary results demonstrate that the so-obtained explicitly correlated dRPA method, in the following denoted "dRPA-F12", can be interpreted or compared to a corresponding dual basis-set approach where the orbital basis is extended by the complementary auxiliary basis for the correlation treatment. This result is in line with the general idea of RPA which is to describe the correlation energy in terms of single excitations.

3.1 Adding geminals to the double excitation space

As geminals can be parameterized in terms of double excitations, it is straightforward to extend the double excitation space only, including geminals in the description of the ground state,

$$|0\rangle = N_0[|\text{HF}\rangle + \tfrac{1}{2}\sum_{aibj} t_{ij}^{ab}|_{ij}^{ab}\rangle + \tfrac{1}{2}\sum_{xyij}\sum_{\alpha\beta} c_{ij}^{xy}\langle\alpha\beta|\hat{Q}_{12}f_{12}|xy\rangle|_{ij}^{\alpha\beta}\rangle]\,, \tag{3.1}$$

and the resolution of the identity,

$$1 = |\text{HF}\rangle\langle\text{HF}| + \sum_{ai}|_i^a\rangle\langle_i^{\bar{a}}| + \tfrac{1}{2}\sum_{abij}|_{ij}^{ab}\rangle\langle_{ij}^{\overline{ab}}| + \tfrac{1}{2}\sum_{vwxyij}|_{ij}^{xy}\rangle(\boldsymbol{\mathcal{X}}^{-1})_{vw}^{xy}\langle_{ij}^{\overline{vw}}| + \dots. \tag{3.2}$$

To highlight that the manifold of excited states $|n\rangle$ is still restricted to the conventional orbital space and thus spans a dimension of $N_{\text{OCC}} \times N_{\text{VIR}}$, the subscript V is added to indicate the dimension of excited states, n_{V}. Throughout the chapter, N_{OCC} denotes the number of occupied orbitals, N_{VIR} the number of virtual orbitals, N_{GEM} the size of the geminal space and N_{CABS} the dimension of the CABS space. Normalization of the geminal part is conserved by the overlap matrix $\boldsymbol{\mathcal{X}}$,

$$\mathcal{X}_{vw}^{xy} = \langle xy|f_{12}\hat{Q}_{12}f_{12}|vw\rangle\,, \tag{3.3}$$

which is evaluated analogously to the F12 intermediate $\boldsymbol{\mathcal{V}}$ (see Appendix B). In the following, the projection operator $\hat{Q}_{12}$ is chosen as defined within ansatz 2 (see Appendix B), thus it ensures orthogonalization of the geminal space with respect to the conventional orbital basis, taking into account mixed double excitations into the CABS and virtual basis. To evaluate the right-hand side of the equations of motion, Eq. (2.3), the generalized Brillouin condition is assumed (see Appendix B), implying that $\langle\text{HF}|\hat{H}|_i^{a'}\rangle$ cancels to zero within

the entire combined virtual and CABS block, denoted as $\{a', b', \ldots\}$. Hence, three different contributions to the transition moment are obtained,

$$\sum_{ai} \langle \bar{0}|\hat{O}|_i^a \rangle t_{ai}^{n_V} = \sum_{ai} X_{ai}^{n_V} \langle \text{HF}|\hat{O}|_i^a \rangle + \sum_{ai} Y_{ai}^{n_V} \langle_i^{\bar{a}}|\hat{O}|\text{HF} \rangle + \sum_{p''i} (Y^{\text{F12}})_{p''i}^{n_V} \langle_i^{\overline{p''}}|\hat{O}|\text{HF} \rangle \,, \tag{3.4}$$

parametrized by the conventional amplitudes $X_{ai}^{n_V}$ and $Y_{ai}^{n_V}$, given in Eqs. (2.8) and (2.9), as well as the explicitly correlated excitation vector $(\mathbf{Y}^{\text{F12}})^{n_V}$,

$$(\mathbf{Y}^{\text{F12}})_{p''i}^{n_V} = \sum_{ckxy} N_0 t_{ck}^{n_V} c_{ki}^{xy} f_{cp''}^{xy} \,. \tag{3.5}$$

$(\mathbf{Y})_{p''i}^{n_V}$ is defined in analogy to the conventional amplitude $Y_{ai}^{n_V}$ as the contraction of single excitation amplitudes $t_{ck}^{n_V}$ with the explicitly correlated double excitation amplitudes, partitioned into geminal coefficients c_{kj}^{xy} and the corresponding integrals over the correlation factor $f_{cq''}^{xy}$. The dimension of the explicitly correlated excitation vector differs from its conventional counterpart, spanning the space $(N_{\text{OCC}} \times (N_{\text{VIR}} + N_{\text{CABS}}))$. A second label is therefore added whenever the specific orbital indices are omitted, referring to $(\mathbf{Y}^{\text{F12}})_{n_C}^{n_V}$ where n_C indicates the dimension $(N_{\text{OCC}} \times N_{\text{CABS}})$. Evaluating the commutator on the left-hand side of the hyperviri-altheorem (Eq. (2.3)) and partitioning the equations subsequently according to the three transition moments $\langle \text{HF}|\hat{O}|_i^a \rangle$, $\langle_j^{\bar{b}}|\hat{O}|\text{HF} \rangle$ and $\langle_j^{\overline{p''}}|\hat{O}|\text{HF} \rangle$ gives a set of coupled eigenvalue equations, which can be summarized in matrix form as

$$\begin{pmatrix} \mathbf{A} & \mathbf{B} & \mathbf{B}_{n_V,n_C}^{\text{F12}} \\ \mathbf{A}_{n_C,n_V} & \mathbf{B}_{n_C,n_V}^{\text{F12}} & \mathbf{B}_{n_C,n_C}^{\text{F12}} \\ \mathbf{B} & \mathbf{A} & \mathbf{A}_{n_V,n_C} \\ \left(\mathbf{B}_{n_C,n_V}^{\text{F12}}\right)^{\dagger} & \mathbf{A}_{n_C,n_V} & \mathbf{A}_{n_C,n_C} \end{pmatrix} \begin{pmatrix} \mathbf{X}^{n_V} \\ \mathbf{Y}^{n_V} \\ (\mathbf{Y}^{\text{F12}})_{n_C}^{n_V} \end{pmatrix} = \Omega_{n_V} \begin{pmatrix} \mathbf{1}_{n_V,n_V} & \mathbf{0} & \mathbf{0} \\ \mathbf{0} & \mathbf{0} & \mathbf{0} \\ \mathbf{0} & -\mathbf{1}_{n_V,n_V} & \mathbf{0} \\ \mathbf{0} & \mathbf{0} & -\mathbf{1}_{n_C,n_C} \end{pmatrix} \begin{pmatrix} \mathbf{X}^{n_V} \\ \mathbf{Y}^{n_V} \\ (\mathbf{Y}^{\text{F12}})_{n_C}^{n_V} \end{pmatrix} \,, \tag{3.6}$$

depending on the generalized definition of matrix $\mathbf{A}$,

$$A_{ij}^{a'b'} = F_{a'b'}\delta_{ij} - F_{ij}\delta_{a'b'} + 2g_{ib'}^{a'j} \,, \tag{3.7}$$

and including the intermediate $\mathbf{B}^{\text{F12}}$,

$$(\mathbf{B}^{\text{F12}})_{ij}^{a'b'} = \sum_{xyvw} 2f_{xy}^{a'b'} (\boldsymbol{\mathcal{X}}^{-1})_{vw}^{xy} \mathcal{V}_{ij}^{vw} \,, \tag{3.8}$$

$$((\mathbf{B}^{\text{F12}})^{\dagger})_{a'b'}^{ij} = \sum_{xyvw} 2(\mathcal{V}^{\dagger})_{xy}^{ij} (\boldsymbol{\mathcal{X}}^{-1})_{vw}^{xy} f_{a'b'}^{vw} \,. \tag{3.9}$$

Analogously to the explicitly correlated amplitude $\mathbf{Y}^{\text{F12}}$, the dimensions of matrices $\mathbf{A}$ and $\mathbf{B}^{\text{F12}}$ are specified by adding pairs of indices corresponding to the different subblocks. For the sake of convenience, superscripts are in the following omitted for the conventional contributions $\mathbf{A}$ and $\mathbf{B}$, referring to the dRPA variant of Eqs. (2.11) and (2.12). Introducing geminals in the RI and the definition of the ground-state thus increases the size of the matrix eigenvalue problem, yielding $(N_{\text{OCC}} \times N_{\text{VIR}})$ positive and negative excitation energies which are parameterized in an orbital space of dimension $(N_{\text{OCC}} \times (N_{\text{VIR}} + N_{\text{CABS}}))$. The matrices are however not symmetric, highlighting that the evaluation of the commutator on the left-hand side of Eq. (2.3) gives terms including a fourth transition moment, $\langle \text{HF}|\hat{O}|_i^{p''} \rangle$, while analogous contributions are lacking on the right-hand side of the hypervirial theorem. Furthermore, it should be stressed that an explicitly correlated analog to $\mathbf{X}^{n_V}$ does not occur, emphasizing that the amplitude parameterizes single excitations only. Detailed equations are given in Appendix D.

3.2 Expanding the excitation manifold to the CABS basis

Aiming for a more symmetric eigenvalue problem, it is thus necessary to describe the excited states in terms of the combined orbital and CABS basis,

$$|n\rangle = \sum_{bj} t_{bj}^{n_V}|_j^b \rangle + \sum_{q''j} t_{q''j}^{n_C}|_j^{q''} \rangle \,, \tag{3.10}$$

and to further include single excitations into the CABS basis within the resolution of the identity,

$$1 = |\text{HF}\rangle\langle\text{HF}| + \sum_{ai} |_i^a\rangle\langle_i^{\bar{a}}| + \sum_{p''i} |_i^{p''}\rangle\langle_i^{\overline{p''}}| + \dots . \tag{3.11}$$

The corresponding transition moment,

$$\sum_{ai} \langle\bar{0}|\hat{O}|_i^a\rangle t_{ai}^{n_V} + \sum_{p''i} \langle\bar{0}|\hat{O}|_i^{p''}\rangle t_{p''i}^{n_C} = \sum_{ai} X_{ai}^{n_V}\langle\text{HF}|\hat{O}|_i^a\rangle + \sum_{p''i} X_{p''i}^{n_C}\langle\text{HF}|\hat{O}|_i^{p''}\rangle$$

$$+ \sum_{ai} \left(Y_{ai}^{n_V} + (\mathbf{Y}^{\text{F12}})_{ai}^{n_C}\right)\langle_i^{\bar{a}}|\hat{O}|\text{HF}\rangle + \sum_{p''i} \left((\mathbf{Y}^{\text{F12}})_{p''i}^{n_V} + (\mathbf{Y}^{\text{F12}})_{p''i}^{n_C}\right)\langle_i^{\overline{p''}}|\hat{O}|\text{HF}\rangle , \tag{3.12}$$

comprises all contributions of Eq. (3.4) and three further terms, parameterized by the amplitudes $\mathbf{X}^{n_C}$, $(\mathbf{Y}^{\text{F12}})_{n_V}^{n_C}$ and $(\mathbf{Y}^{\text{F12}})_{n_C}^{n_C}$. It should be noted that both $(\mathbf{Y}^{\text{F12}})_{n_V}^{n_C}$ and $(\mathbf{Y}^{\text{F12}})_{n_C}^{n_C}$ imply an inner contraction over the CABS basis,

$$(\mathbf{Y}^{\text{F12}})_{a'i}^{n_C} = \sum_{r''kxy} N_0 t_{r''k}^{n_C} c_{ki}^{xy} f_{r''a'}^{xy} , \tag{3.13}$$

while $(\mathbf{Y}^{\text{F12}})_{n_C}^{n_V}$ is obtained by an analogous summation over the virtual orbital space, see Eq. (3.5). Finally, the four coupled eigenvalue equations can be summarized in terms of a single matrix equation,

$$\begin{pmatrix} \mathbf{A} & \mathbf{A}_{n_V,n_C} & \mathbf{B} & \mathbf{B}_{n_V,n_C}^{\text{F12}} \\ \mathbf{A}_{n_C,n_V} & \mathbf{A}_{n_C,n_C} & \mathbf{B}_{n_C,n_V}^{\text{F12}} & \mathbf{B}_{n_C,n_C}^{\text{F12}} \\ \mathbf{B} & \left(\mathbf{B}_{n_V,n_C}^{\text{F12}}\right)^\dagger & \mathbf{A} & \mathbf{A}_{n_V,n_C} \\ \left(\mathbf{B}_{n_C,n_V}^{\text{F12}}\right)^\dagger & \left(\mathbf{B}_{n_C,n_C}^{\text{F12}}\right)^\dagger & \mathbf{A}_{n_C,n_V} & \mathbf{A}_{n_C,n_C} \end{pmatrix} \begin{pmatrix} \mathbf{X}^{n_V} \\ \mathbf{X}^{n_C} \\ \left(\mathbf{Y}+\mathbf{Y}_{n_C}^{\text{F12}}\right)^{n_V} \\ \left(\mathbf{Y}_{n_V}^{\text{F12}}+\mathbf{Y}_{n_C}^{\text{F12}}\right)^{n_C} \end{pmatrix}$$

$$= \Omega_n \begin{pmatrix} \mathbf{1}_{n_V,n_V} & 0 & 0 & 0 \\ 0 & \mathbf{1}_{n_C,n_C} & 0 & 0 \\ 0 & 0 & -\mathbf{1}_{n_V,n_V} & 0 \\ 0 & 0 & 0 & -\mathbf{1}_{n_C,n_C} \end{pmatrix} \begin{pmatrix} \mathbf{X}^{n_V} \\ \mathbf{X}^{n_C} \\ \left(\mathbf{Y}+\mathbf{Y}_{n_C}^{\text{F12}}\right)^{n_V} \\ \left(\mathbf{Y}_{n_V}^{\text{F12}}+\mathbf{Y}_{n_C}^{\text{F12}}\right)^{n_C} \end{pmatrix} . \tag{3.14}$$

As for standard dRPA, the normalization condition

$$\begin{pmatrix} \mathbf{X}^{n_V} \\ \mathbf{X}^{n_C} \\ \left(\mathbf{Y}+\mathbf{Y}_{n_C}^{\text{F12}}\right)^{n_V} \\ \left(\mathbf{Y}_{n_V}^{\text{F12}}+\mathbf{Y}_{n_C}^{\text{F12}}\right)^{n_C} \end{pmatrix}^\dagger \begin{pmatrix} \mathbf{1}_{n_V,n_V} & 0 & 0 & 0 \\ 0 & \mathbf{1}_{n_C,n_C} & 0 & 0 \\ 0 & 0 & -\mathbf{1}_{n_V,n_V} & 0 \\ 0 & 0 & 0 & -\mathbf{1}_{n_C,n_C} \end{pmatrix} \begin{pmatrix} \mathbf{X}^{m_V} \\ \mathbf{X}^{m_C} \\ \left(\mathbf{Y}+\mathbf{Y}_{m_C}^{\text{F12}}\right)^{m_V} \\ \left(\mathbf{Y}_{m_V}^{\text{F12}}+\mathbf{Y}_{m_C}^{\text{F12}}\right)^{m_C} \end{pmatrix} = \delta_{nm} \tag{3.15}$$

is an additional constraint. Given that Eqs. (3.14) and (3.15) rely on the conventional dRPA eigenvalue problem and imply no approximations regarding the treatment of explicitly correlated terms, the approach is in the following denoted dRPA-F12.

3.3 Calculating the correlation energy based on single-particle transition densities

When dividing the supermatrices of Eq. (3.14) into four blocks of dimension $(N_{\text{OCC}} \times (N_{\text{VIR}} + N_{\text{CABS}}))$, e.g. according to

$$\mathbf{A}^{\text{dRPA-F12}} = \begin{pmatrix} \mathbf{A} & \mathbf{A}_{n_V,n_C} \\ \mathbf{A}_{n_C,n_V} & \mathbf{A}_{n_C,n_C} \end{pmatrix} \text{ and } \mathbf{B}^{\text{dRPA-F12}} = \begin{pmatrix} \mathbf{B} & \mathbf{B}_{n_V,n_C}^{\text{F12}} \\ \mathbf{B}_{n_C,n_V}^{\text{F12}} & \mathbf{B}_{n_C,n_C}^{\text{F12}} \end{pmatrix} , \tag{3.16}$$

it becomes apparent that the so-obtained dRPA-F12 eigenvalue problem with the supermatrix $\begin{pmatrix} \mathbf{A}^{\text{dRPA-F12}} & \mathbf{B}^{\text{dRPA-F12}} \\ \left(\mathbf{B}^{\text{dRPA-F12}}\right)^\dagger & \mathbf{A}^{\text{dRPA-F12}} \end{pmatrix}$ has the same structure as conventional dRPA, enlarging the dimension of each matrix by the size of the CABS basis. However, in contrast to the conventional scheme, only the full matrix $\mathbf{A}^{\text{dRPA-F12}}$ is still symmetric for real orbitals, while the matrix $\mathbf{B}^{\text{dRPA-F12}}$ is neither symmetric nor Hermitian due to the additional F12 contributions. Hence, both $\mathbf{B}^{\text{F12}}$ and the adjoint $(\mathbf{B}^{\text{F12}})^\dagger$ need to be calculated. The structure

of $\mathbf{B}^{\text{dRPA-F12}}$ has to be taken into account when aiming for the dRPA-F12 correlation energy: Standardly, the derivation of the plasmon formula, summarized in Eqs. (2.46) and (2.47), starts from the conventional dRPA eigenvalue problem and exploits the equality of the two-electron integral contributions to the matrices $\mathbf{A}$ and $\mathbf{B}$. In the case of dRPA-F12, however, $\mathbf{A}^{\text{dRPA-F12}}$ and $\mathbf{B}^{\text{dRPA-F12}}$ differ in the first-order terms and it is therefore not possible to derive an equivalent plasmon formula for dRPA-F12. Moreover, the density-matrix formulation based on the matrix $\mathbf{P}^{\zeta}$, as defined within Eqs. (2.42) and (2.43), is no longer possible, requiring that the two-electron integral contributions to $\mathbf{A}^{\zeta} - \mathbf{B}^{\zeta}$ cancel, reducing to a positive definite diagonal matrix which solely contains the zeroth-order Fock (or KS) matrix elements. This is again not the case for dRPA-F12 due to the non-diagonal and asymmetric structure of the difference matrix $\mathbf{A}^{\text{dRPA-F12}} - \mathbf{B}^{\text{dRPA-F12}}$. However, a density-matrix formulation based on one-particle transition densities ρ_{0n}^{ζ} and the related excitation vectors $\mathbf{X}$ and $\mathbf{Y}$ can be set up in analogy to Eqs. (2.32) and (2.41): The conventional formula is derived starting from the coupling-strength integral as defined within the adiabatic connection, introducing the electron-electron interaction through the coupling-strength parameter ζ and expressing the correlation energy in terms of one-particle transition densities. As such an ansatz implies no symmetry constraints, it is possible to derive the dRPA-F12 equivalent using the already introduced definitions for the ground and excited states, (Eqs. (3.1) and (3.10)), yielding

$$\rho_{0n}^{\zeta}(r) = \langle \Psi_0^{\zeta} | \hat{\rho}(r) | \Psi_n^{\zeta} \rangle = \sum_{a'i} (\mathbf{X}^{\text{dRPA-F12}} + \mathbf{Y}^{\text{dRPA-F12}})_{ia'}^{n\zeta} \phi_i(r) \phi_{a'}(r) . \tag{3.17}$$

The density operator $\hat{\rho}(r)$ is defined in Eq. (2.32). Inserting the dRPA-F12 transition density into the coupling-strength integral of Eq. (2.36) gives the final expression for the correlation energy, analoguously to Eq. (2.41),

$$E_{\text{C}}^{\text{dRPA-F12}} = \frac{1}{2} \int_0^1 d\zeta \sum_{ia'jb'} g_{ij}^{a'b'} \left(\sum_{n \neq 0} (\mathbf{X}^{\text{dRPA-F12}} + \mathbf{Y}^{\text{dRPA-F12}})_{ia'}^{n\zeta} (\mathbf{X}^{\text{dRPA-F12}} + \mathbf{Y}^{\text{dRPA-F12}})_{jb'}^{n\zeta} - \delta_{ij}\delta_{a'b'} \right) , \tag{3.18}$$

with the dRPA-F12 eigenvectors

$$(\mathbf{X}^{\text{dRPA-F12}})^{n\zeta} = \begin{pmatrix} \mathbf{X}^{n_{\text{V}}\zeta} \\ \mathbf{X}^{n_{\text{C}}\zeta} \end{pmatrix} \text{ and } (\mathbf{Y}^{\text{dRPA-F12}})^{n\zeta} = \begin{pmatrix} (\mathbf{Y} + \mathbf{Y}_{n_{\text{C}}}^{\text{F12}})^{n_{\text{V}}\zeta} \\ (\mathbf{Y}_{n_{\text{V}}}^{\text{F12}} + \mathbf{Y}_{n_{\text{C}}}^{\text{F12}})^{n_{\text{C}}\zeta} \end{pmatrix} . \tag{3.19}$$

Assuming the adiabatic connection Hamiltonian, the dRPA-F12 eigenvalue problem and the therein obtained matrices depend on the coupling-strength parameter ζ according to

$$(\mathbf{A}^{\zeta})_{ij}^{a'b'} = F_{a'b'}\delta_{ij} - F_{ij}\delta_{a'b'} + 2\zeta g_{ib'}^{a'j} , \tag{3.20}$$

$$(\mathbf{B}^{\zeta})_{ij}^{ab} = 2\zeta g_{ij}^{ab} , \tag{3.21}$$

$$(\mathbf{B}^{\text{F12}\zeta})_{ij}^{a'b'} = \sum_{xyvw} 2\zeta f_{xy}^{a'b'} (\boldsymbol{\mathcal{X}}^{-1})_{vw}^{xy} \mathcal{V}_{ij}^{vw} . \tag{3.22}$$

3.4 Evaluation of the dRPA-F12 approach

The dRPA-F12 method, based on the coupled eigenvalue problem of Eq. (3.14) and the presented density-matrix formulation for the correlation energy, given in Eq. (3.18), was implemented in the KOALA program package [205]. The Fock matrix in the combined orbital and CABS basis is constructed and the CABS-CABS block is diagonalized in order to obtain canonical CABS orbitals. F12 intermediates $\mathcal{V}$ and $\mathcal{X}$ are calculated within ansatz 2 (see Appendix B). The coupling-strength integration is performed numerically using a seven point Gauss-Legendre quadrature. For each quadrature step, the dRPA-F12 eigenvalue problem (Eq. (3.14)) is solved and to ensure normalization for degenerate orbitals (Eq. (3.15)), the eigenvectors $\mathbf{X}^{\text{dRPA-F12}}$ and $\mathbf{Y}^{\text{dRPA-F12}}$ are subsequently orthogonalized. It should be noted that only the subspace of positive eigenvalues is taken into account (see Appendix D). All integrals are evaluated using resolution of the identity techniques. For comparison, the implementation also enables to compute the dRPA eigenvalue problem in the combined orbital and CABS basis, based on a HF calculation which is still restricted to the conventional orbital basis. The so-obtained correlation energy is denoted "dRPA+CABS". If both the reference and the correlation energy are obtained within the combined basis, the results are labeled as "dRPA/basis+CABS".

Performance of the dRPA-F12 approach is assessed regarding a test set of 20 small molecules taken from Ref. [206], which includes small molecules of the first and second period (see Appendix D). The number of valence electrons ranges from 2 (H_2) to 18 (O_2), with a mean value of 10 electrons. All calculations were

performed using a HF reference and the hierarchy of def2-SVP, def2-TZVPP and def2-QZVPP basis sets of Ahlrichs and co-workers [207]. For convenience, the acronym def2- is neglected in the following discussion and RPA calculations performed within a def2-SVP basis are abbreviated as dRPA/SVP. Core orbitals were kept frozen for the correlation treatment. Given that no optimized CABS basis sets are available for the def2-basis sets, they are chosen identically to the auxiliary basis for density fitting (cbas). An optimization could of course improve results and remains to be investigated.
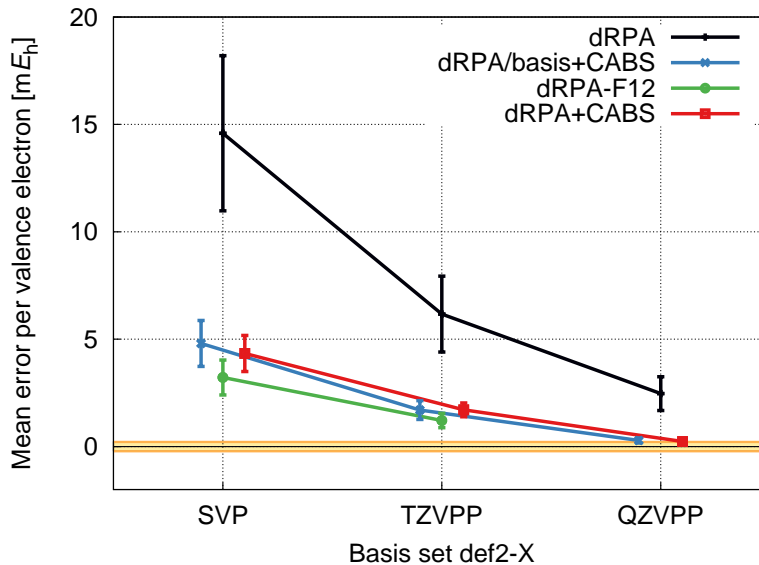
Basis-set convergence of correlation energies

Fig. 3.1: Basis-set convergence of the dRPA-F12 correlation energy for a testset of 20 molecules.

Figure 3.1 depicts the mean error per valence electron in the correlation energy with the corresponding standard deviations as error bars for the hierarchy of def2-basis sets. The corresponding statistical measures are given in Appendix D. Errors are calculated with respect to the dRPA-F12/QZVPP results assuming that the presented dRPA-F12 approach is most accurate and close to the basis-set limit. The accuracy of the dRPA-F12/QZVPP reference is validated by extrapolation, as proposed by Schwenke [208] and applied in Ref. [180]: First, extrapolation factors F_{XY} are calculated for all test molecules by inverting the general two-point extrapolation formula between subsequent basis sets of cardinal numbers X and Y,

$$E_c(\infty) = [E_c(Y) - E_c(X)]F_{XY} + E_c(X). \tag{3.23}$$

dRPA-F12/QZVPP results are taken as reference for the basis-set limit $E_c(\infty)$, while conventional dRPA calculations obtained within the def2-TZVPP and the def2-QZVPP basis were used as data points for the correlation energies $E_c(Y)$ and $E_c(X)$. The mean average of all F_{XY} factors is calculated by linear regression and, in a second step, used to extrapolate the basis-set limit $E_c(\infty)$ according to Eq. (3.23) taking the same reference values for $E_c(X)$ and $E_c(Y)$. As noted in Ref. [180], the deviation of the extrapolated $E_c(\infty)$ limit with respect to the dRPA-F12/QZVPP result reflects the inherent error of the extrapolation scheme and should thus allow to assess the accuracy of the chosen dRPA-F12/QZVPP reference. The corresponding standard deviation σ amounts up to 0.217 mE_h per valence electron and is depicted as a yellow bar in Figure (3.1), indicating the range from $-\sigma$ to σ.

Figure 3.1 illustrates the slow basis-set convergence of dRPA, with mean errors decreasing from 14.6 over 6.2 to 2.5 mE_h when going from SVP to QZVPP basis-set size. Enlarging the basis set by the corresponding CABS basis pushes results closer to the basis-set limit, however, dRPA/SVP+CABS results cannot reach the dRPA/QZVPP mark, still showing an error of 4.8 mE_h. Nevertheless, the deviation of the corresponding dRPA/QZVPP+CABS calculations lies within the accuracy of the dRPA-F12/QZVPP basis-set limit. Comparable basis-set convergence is found for the dual basis-set approach dRPA+CABS, which differs only for the SVP basis by 0.5 mE_h from the dRPA/basis+CABS result. For the two larger basis sets, deviations are still one magnitude smaller and the close-lying results coincide for both TZVPP and QZVPP calculations. Further improvement by 1.6 (0.5) mE_h for the SVP (TZVPP) basis sets can be achieved when taking into account explicit correlation. The mean error for dRPA-F12/SVP still lies 0.8 mE_h above the conventional dRPA/QZVPP

result and it is thus necessary to enlarge the basis to triple-zeta size to converge to the conventional QZVPP limit.

Dependence on the correlation factor γ

Up to now, basis-set convergence was investigated keeping the exponent of the Slater-type geminals fixed at $\gamma = 1.4\, a_0^{-1}$ for all basis-set sizes. However, Höfener *et al.* showed that optimal γ values can lie around $0.7\, a_0^{-1}$ for CCS(F12) and that the correlation energy depends strongly on the correlation coefficient, at least for fixed amplitudes [206]. Within CCS(F12), the conventional correlation energy is captured via singles excitations; explicit correlation is introduced through geminals which are parameterized by double excitations into the infinite basis. dRPA-F12 can be interpreted in a similar way: the conventional dRPA correlation energy is also described by single excitations only (Eq. (2.15)) and explicit correlation is taken into account by adding geminals to the wave-function expansion of the ground state. In analogy to CCS(F12), an optimization of the correlation factor could thus improve the explicitly correlated dRPA ansatz.

In Figure 3.2, exemplary results for the molecules HF (left-hand side) and CH_2 (right-hand side) are depicted, showing the correlation energy in dependence of the correlation factor γ for the series of def2-basis sets. Optimal γ values are marked in red, ranging with increasing basis-set size from $2.6\, a_0^{-1}$ to $3.9\, a_0^{-1}$ for HF and from $1.7\, a_0^{-1}$ to $2.7\, a_0^{-1}$ for CH_2, respectively. Thus, the optimal γ exponent is shifted towards larger values which can be, as shown for the two tested molecules, approximately twice as large as the standardly used exponent of $1.4\, a_0^{-1}$. Furthermore, the dependence on the correlation factor decreases when enlarging the basis set from def2-SVP to def2-QZVPP size, resulting in flatened curves with constantly declining slopes. This is in line with earlier findings of Tew and Klopper [166]. In comparison to Ref. [206], it is moreover important to note that the dependence on the correlation factor is much less pronounced for dRPA-F12 than for CCS(F12): the change in the correlation energy with varying γ is about one magnitude smaller, indicating the relatively small impact of the F12 correction on the dRPA correlation energy.
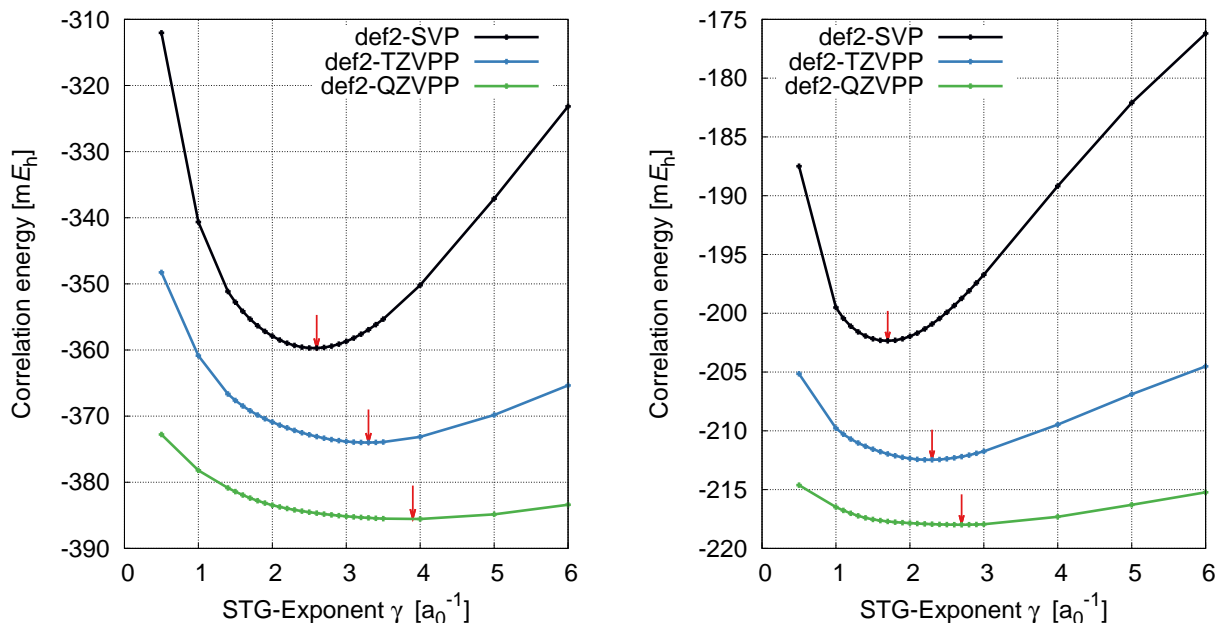

Fig. 3.2: Dependence of the correlation energy on the correlation factor γ for hydrogen fluoride (left-hand side) and methylene (right-hand side). The optimal γ values for HF amount up to 2.6 (SVP), 3.3 (TZVPP) and 3.9 (QZVPP) a_0^{-1}; for CH_2, an exponent of 1.7 (SVP), 2.3 (TZVPP) and 2.7 (QZVPP) a_0^{-1} was found.

Basis-set convergence of excitation energies

Calculating the dRPA ground-state correlation energy according to Eqs. (2.7) and (2.47) requires the explicit computation of all excited states, characterized by the eigenvectors $\mathbf{X}$ and $\mathbf{Y}$ as well as the eigenvalues $\mathbf{\Omega}$. This connection is highlighted for conventional dRPA by the plasmon formula (Eq. (2.47)), which directly relates the excitation energies of the correlated and uncorrelated system with the ground-state energy. Regarding dRPA-F12, one might therefore not only assume an improved basis-set convergence for the ground state, but

also for the excited states. A thorough investigation of this hypothesis would of course require a detailed analysis of the excited states allowing to assign each excitation energy to a specified transition between occupied and virtual orbitals. Only such a precise assignment allows to compare all excitation energies for different basis sets as not only the number but also the energetic ordering of states changes with basis-set size. The following investigation can however not rely on a robust classification and, when comparing different basis sets, the discussion is therefore restricted to the lowest lying excited states which are well separated in energy. Within a given basis set, it is furthermore possible to match excited states for the three different approaches dRPA, dRPA-F12 and dRPA+CABS. Each excitation n is therefore characterized by a conventional and an explicitly correlated weight, w_{conv} and w_{f12}, which are defined based on the corresponding eigenvectors,

$$
\begin{aligned}
1 &= w_{\text{conv}} + w_{\text{f12}} \\
&= (\mathbf{X}^{n_V})^{\dagger}\mathbf{X}^{n_V} - ((\mathbf{Y} + \mathbf{Y}_{n_C}^{\text{F12}})^{n_V})^{\dagger}(\mathbf{Y} + \mathbf{Y}_{n_C}^{\text{F12}})^{n_V} + (\mathbf{X}^{n_C})^{\dagger}\mathbf{X}^{n_C} - ((\mathbf{Y}_{n_V}^{\text{F12}} + \mathbf{Y}_{n_C}^{\text{F12}})^{n_C})^{\dagger}(\mathbf{Y}_{n_V}^{\text{F12}} + \mathbf{Y}_{n_C}^{\text{F12}})^{n_C} .
\end{aligned}
\tag{3.24}
$$

Those excitations with dominating w_{conv} can be assigned as transitions between the occupied and the conventional virtual orbital basis and hence be compared with corresponding dRPA calculations - enduring the assumption that the mixing between orbital and CABS basis is negligible.

Regarding the five lowest excited states of HF, as depicted in Figure 3.3, falsifies the hypothesis of equally fast convergence for ground and excited states: Independent of the basis-set size, the states are well separated in energy with the first and the third one being doubly degenerate. Assuming thus a comparison between the different basis sets as justified, it can be concluded that the excitation energies decrease equally fast with increasing cardinal number for both dRPA, dRPA+CABS and dRPA-F12. The total energies differ only by a maximum of 1 mE_{h} when comparing the three different methods, while the basis-set incompleteness error for the SVP basis amounts up to 0.5 E_{h}. The corresponding conventional weights are in the range of 99.7 to 99.9%, supporting the conclusion that the influence of the CABS basis and the effect of explicit correlation is negligible. This analysis is of course restricted to the lowest excitation energies and might not be transferable to higher lying states.
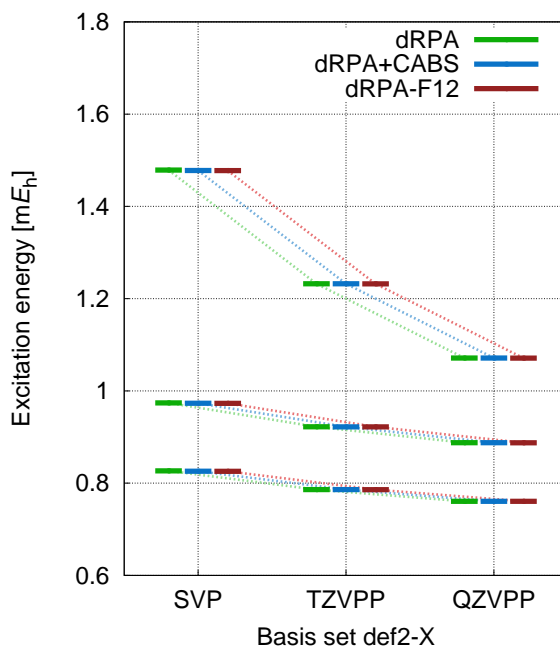

Fig. 3.3: Basis-set convergence of the five lowest lying excited states for hydrogen fluoride.

3.5 Conclusions

The presented dRPA-F12 approach improves basis-set convergence of the correlation energy in comparison to conventional dRPA, in particular, the gain is about one cardinal number for the def2-basis sets. Convergence to within 97% of the basis-set limit is achieved for the def2-TZVPP basis, corresponding to a mean error of 1 mE_{h} per valence electron. Results could still be improved when optimizing the CABS basis as well as the correlation factor. Explicit correlation is included in the virtual-CABS, CABS-virtual and CABS-CABS block of the orbital rotation Hessian $\mathbf{B}^{\text{dRPA-F12}}$. As visualized in Figure 3.4, the calculation of the intermediate $\mathbf{B}^{\text{dRPA-F12}}$

implies an inner contraction over four geminal indices, resulting in a matrix of dimension $(N_{\text{OCC}} \times (N_{\text{VIR}} + N_{\text{CABS}}))^2$. $\mathbf{A}^{\text{dRPA-F12}}$, in contrast, comprises no F12 intermediates and is a generalization of the conventional matrix $\mathbf{A}$, now considering excitations into the conventional virtual as well as the CABS basis. In consequence, the dimension of the total eigenvalue problem is analogously enlarged to the combined orbital and CABS space, increasing the computation time and therefore limiting the applications to moderately sized (CABS) basis sets. Equally large matrices are obtained for the dual basis-set approach dRPA+CABS as well as for corresponding calculations in the combined basis, dRPA/basis+CABS. The overall gain of all three methods, dRPA-F12, dRPA+CABS and dRPA/basis+CABS is comparable in magnitude, with mean errors deviating by at most 1.5 mE_{h}. Even though dRPA-F12 shows a slightly faster convergence then dRPA+CABS, it requires the additional calculation of the F12 intermediate $\mathbf{B}^{\text{dRPA-F12}}$. The ratio between accuracy and computational cost can thus regarded as equal for both dRPA-F12 and dRPA+CABS. Contrary results are obtained for other wave-function methods: In the case of MP2, for example, dual basis-set approaches [209–211] are standardly discarded due to the more efficient, explicitly correlated alternative MP2-F12. It is furthermore interesting to note that Köhn and Tew found for CC methods that the improvement of the singles correlation energy by adding single excitations into the CABS basis is negligible, at least when considering single-reference closed-shell molecules [204]. However, in the context of response theory, the contribution of single excitations to the correlation energy gains in importance, demanding for iterative CABS singles approaches [212, 213]. In case of dRPA-F12 correlation energies, the presented results show that the expansion of the excitation manifold to the CABS basis is more effective than adding geminals to the double excitation space. This is however not astonishing as RPA is standardly interpreted as a single excitation approach, which is, as outlined in Chapter 2, related to TDHF and CIS.
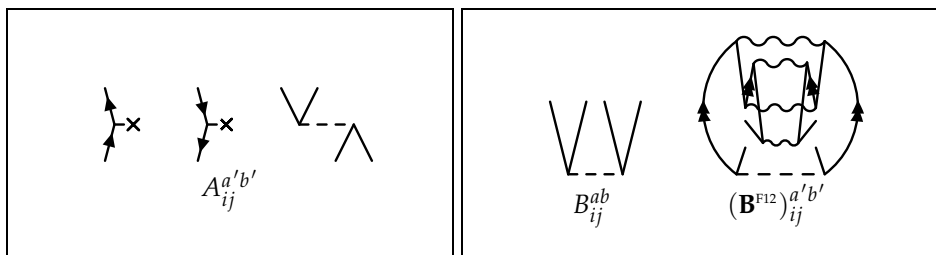

Fig. 3.4: Contributions to matrices $\mathbf{A}^{\text{dRPA-F12}}$ and $\mathbf{B}^{\text{dRPA-F12}}$, referring to Eqs. (3.7) and (3.8).

4. Explicitly correlated ring coupled-cluster doubles theory

The hypervirial theorem allows to combine RPA and F12 by introducing geminals in the description of the ground state and the resolution of the identity. The resulting equations are however expressed in terms of single excitation amplitudes, which follows the original idea and interpretation of RPA, but hinders, as shown in Chapter 3, an efficient incorporation of two-particle quantities as needed for a corresponding F12 approach. This bottleneck can be circumvented when exploiting the connection between RPA and CC theory: As outlined in Section 2.2, the coupled RPA eigenvalue problem can be rewritten as an amplitude equation and the correlation energy can be expressed in terms of the so-defined double excitation amplitudes. The ring coupled-cluster doubles (rCCD) ansatz reproduces the RPA correlation energy, even though it is based on a different formalism [140].

The connection to coupled-cluster theory was already exploited to construct range-separated DFT functionals, describing the long-range part of the electron-electron interaction within density-functional theory and incorporating the drCCD correlation energy for the short-range part [86–89]. Range-separated RPA approaches correct the poor description of correlation energies inherent to standard RPA and can accurately describe van der Waals systems, mending an important shortcoming of density-functional theory [214]. Toulouse *et al.* for example demonstrated that the interaction energy curve of Be_2 shows an unphysical bump within RPA [40, 215], but is correctly described when applying range separation due to the short-range functional [214]. In comparison to standard wave-function methods, range-separated RPA approaches were furthermore proven to exhibit fast basis-set convergence with exponential asymptotics for both the short- and the long-range part [90]. The reduced basis-set dependence also entails a smaller basis-set superposition error. However, it has to be kept in mind that the improvement comes with a change of the basis-set limit due to the range-separated definition of the Hamiltonian.

In contrast, F12 theory allows to set up an explicitly correlated rCCD approach which converges to the conventional RPA basis-set limit by including geminals in the wave-function expansion. Both the direct variant as well as the RPAX approach including exact exchange can be formulated based on the corresponding drCCD or rCCD schemes. The approaches are in the following denoted (d)rCCD(F12) in order to distinguish them from the dRPA-F12 ansatz of Chapter 3 and to indicate the underlying ring coupled-cluster formalism. The close relation and similarity to already established explicitly correlated coupled-cluster approaches enables to exploit earlier implementations in the TURBOMOLE program package (see e.g. Refs. [91, 216]). The results of the following chapter were published in Refs. [156, 180, 217]. Figures 4.5 and 4.10 are taken from Ref. [180]; Figure 4.9 is adapted from Ref. [156]. The following sections summarize briefly the results reported therein, detailed information and explicit numbers can be found in the references as well as the corresponding supplementary information. Statistical measures which are not published in the cited references are given in Appendix E.

4.1 From CCD(F12) to (direct) rCCD(F12) — a diagrammatic approach

In analogy to conventional drCCD and rCCD, the derivation of the corresponding drCCD(F12) and rCCD(F12) equations requires to start with explicitly correlated coupled-cluster doubles theory, given that the ring coupled-cluster amplitudes do not correspond to an appropriate wave function and cannot be derived from a similarity transformed Hamiltonian [155]. The equations can however be obtained when starting from the underlying CCD-F12 approach [106, 144, 218, 219]: For the latter, the wave-function is well-defined, given as the sum of the conventional expansion of doubly excited determinants and the additional manifold of geminals, which can be parameterized by the double excitation operator $\hat{T}_{2'}$,

$$|\Psi_{\text{CCD-F12}}\rangle = \exp(\hat{T}_2 + \hat{T}_{2'})|\Psi_0\rangle .$$

(4.1)

As outlined in Eqs. (2.61) and (2.94) of Section 2.2, the excitation operators $\hat{T}_2$ and $\hat{T}_{2'}$ are defined in terms of the conventional and the geminal amplitude t_{IJ}^{AB} and d_{IJ}^{XY}, which are both required to determine the correlation energy according to

$$E_{\mathrm{C}}^{\mathrm{CCD\text{-}F12}} = \langle \mathrm{HF}|\hat{H}|\Psi_{\mathrm{CCD\text{-}F12}}\rangle = \tfrac{1}{4}\mathrm{tr}\left[\mathbf{B}^{\mathrm{RPAX}}\mathbf{T}^{\mathrm{CCD\text{-}F12}}\right] + \tfrac{1}{4}\mathrm{tr}\left[(\boldsymbol{\mathcal{V}} - \boldsymbol{\mathcal{V}}^{\mathrm{x}})^{\dagger}\mathbf{D}\right]. \tag{4.2}$$

The diagrammatic representation of the conventional and the explicitly correlated energy contributions is given in terms of antisymmetrized Goldstone diagrams in Figure 4.9. Analogously to MP2-F12 theory, the energy expression can be formulated as a Lagrangian including the geminal residual when using fixed amplitudes.

The geminal residual as well as the conventional amplitude equations are obtained by projecting the Schrödinger equation on the double excitation manifold of the conventional orbital and the geminal space,

$$(\boldsymbol{\Omega}^{\mathrm{CCD\text{-}F12}})_{IJ}^{AB} = \langle_{IJ}^{AB}| \exp\left(-\hat{T}_2 - \hat{T}_{2'}\right)\hat{H}\exp\left(\hat{T}_2 + \hat{T}_{2'}\right)|\mathrm{HF}\rangle = 0, \tag{4.3}$$

$$(\boldsymbol{\Omega}^{\mathrm{F12(CCD\text{-}F12)}})_{IJ}^{XY} = \langle_{IJ}^{XY}| \exp\left(-\hat{T}_2 - \hat{T}_{2'}\right)\hat{H}\exp\left(\hat{T}_2 + \hat{T}_{2'}\right)|\mathrm{HF}\rangle = 0. \tag{4.4}$$

Due to the projection technique, the amplitude equations are truncated, but comprise nevertheless a series of higher-order terms, as illustrated in Figure 4.2. The depicted antisymmetrized Goldstone diagrams represent spin orbitals and the subset of conventional CCD diagrams from [1] to [10] on the left-hand side is identical to Figure 2.2. Explicitly correlated contributions can be derived from the conventional terms by substituting the double excitation amplitude $\mathbf{T}$ with its explicitly correlated counterpart $\mathbf{T}'$, for instance according to

Moreover, the projection onto the geminal space has to be taken into account for the geminal residual,
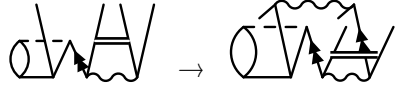
Drawing all possible combinations according to the different commutator contributions of Eqs. (4.3) and (4.4) and taking into account standard contraction rules leads to the depicted diagrams. As for conventional CC, it is important to bear in mind that some terms can be represented by more than one diagram which differ in shape, but are nevertheless identical: In analogy to the equality of $\frac{1}{2}[[\hat{\phi},\hat{T}_2],\hat{T}_{2'}] = \frac{1}{2}[[\hat{\phi},\hat{T}_{2'}],\hat{T}_2]$,
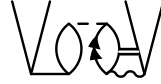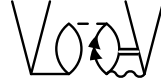
diagram [8f12t_a] can e.g. be equally depicted as . In addition, it should be noted that the orthogonality of the conventional virtual and the CABS space is ensured by the projection operator $\hat{Q}_{12}$, implying $\hat{Q}_{12}|ab\rangle = 0$. This explains for example why the series of diagrams in row [9] do not comprise a contribution to the geminal residual which still includes two conventional doubles amplitudes and which

would look like . For the same reason, the conventional diagram [10] leads to three F12 contributions in the conventional amplitudes equation, [10f12t_a], [10f12t_b] and [10f12t_c], whereas diagram [9] only has one explicitly correlated counterpart. Following these rules yields 38 diagrams in addition to the conventional CCD contributions. Incorporating all terms in the residual equations is however tedious and unneccessary since it was shown that the impact of higher-order contributions on the correlation energy is negligible [220, 221]. It is thus justified to introduce the so-called "(F12)" approximation [112, 222, 223]: All terms that are higher than second order in perturbation theory are neglected within the conventional and the F12 residual. Splitting the Hamiltonian into the zeroth-order Fock operator $\hat{F}$ and the first-order fluctuation potential $\hat{\phi}$, considering all possible contractions with the zeroth-order $\hat{T}_2$ and the first-order $\hat{T}_{2'}$ amplitudes and projecting onto the zeroth-order $\langle_{IJ}^{AB}|$ and the first-order $\langle_{IJ}^{XY}|$ double-excitation manifold, the CCD(F12) residual equations are obtained as

$$(\boldsymbol{\Omega}^{\mathrm{CCD(F12)}})_{IJ}^{AB} = \langle_{IJ}^{AB}|[\hat{F},\hat{T}_2 + \hat{T}_{2'}] + \hat{\phi} + [\hat{\phi},\hat{T}_2 + \hat{T}_{2'}] + [[\hat{\phi},\hat{T}_2],\hat{T}_{2'}] + \tfrac{1}{2}[[\hat{\phi},\hat{T}_2],\hat{T}_2]|\mathrm{HF}\rangle, \tag{4.5}$$

$$(\boldsymbol{\Omega}^{\mathrm{F12(CCD(F12))}})_{IJ}^{XY} = \langle_{IJ}^{XY}|[\hat{F},\hat{T}_2 + \hat{T}_{2'}] + \hat{\phi} + [\hat{\phi},\hat{T}_2]|\mathrm{HF}\rangle. \tag{4.6}$$

Those diagrams of Figure 4.2, which are neglected within the (F12) approximation, are marked in blue, illustrating that the number of higher-order terms is drastically reduced, especially for the geminal residual. Equations are simplified even further for the desired rCCD(F12) variant, which solely incorporates ring diagrams corresponding to particle-hole interactions. Ring diagrams are highlighted in red, comprising the zeroth- and first-order driver contributions of row [1] to [3] as well as the higher-order terms of row [6] and

[8] containing the characteristic closed loops. Diagrams [6f12c_b], [8f12t_b], [8f12c_a] and [8f12c_b] thus represent ring terms, which would contribute to a rCCD-F12 approach, but are in the following neglected due to the (F12) approximation. Concerning rCCD approaches, it is important to keep in mind that the red-colored ring diagrams correspond to particle-hole terms only if labels are added to the relevant diagrams, analogously to the conventional counterpart depicted in Figure 2.2. Alternatively, interpretation rules can be modified, as explained in Section 2.2 and Appendix A. Furthermore, a specific nomenclature is required when aiming for drCCD(F12) neglecting all exchange contributions. In terms of diagrams, this can be achieved analogously to dMP2-F12 by assuming that the dashed line now corresponds to non-antisymmetrized two-electron integrals. Also note that ordinary Goldstone diagrams for closed-shell drCCD(F12) are identical in shape to the set of antisymmetrized diagrams depicted in Figure 4.2, solely referring to different algebraic expressions. However, in contrast to the open-shell case, the closed-shell diagrams require no further labeling and stick to the standard interpretation rules. For both rCCD(F12) and drCCD(F12) diagrams, closed- and open-shell, it should be kept in mind that common translation rules based on creation and annihilation operators are inappropriate. Instead, a direct assignment of amplitude matrix elements and two-electron integrals is required. Taking a closer look, the F12 contributions to the conventional and the geminal residual of (d)rCCD(F12) can be classified according to the three different ansätze for the projection operator $\hat{Q}_{12}$: when choosing fixed amplitudes, the simplest ansatz 1 is represented by the two second-order contributions [1f12c] and [3f12_b]. If the geminal amplitudes are optimized, diagram [2f12c] yields an additional contribution to the F12 intermediate $\mathcal{B}$, as explained in Section 2.3 and Appendix B for the MP2-F12 residual. (d)rCCD(F12) within ansatz 2^* furthermore takes into account mixed excitations into the virtual and CABS basis, resulting in diagrams [6f12t], [8f12t_a] and [6f12c_a]. Coupling between conventional and geminal amplitudes is considered within ansatz 2, represented by diagrams [3f12t] and [3f12c_a]. In comparison to the perturbative RPA+F12 approach, which comprises diagrams [1f12c] and [3f12c_b], (d)rCCD(F12) thus includes three additional higher-order terms and, depending on the chosen ansatz, further coupling contributions.

A variety of other related F12 approaches [201, 203, 224] next to the presented (F12) approximation can be constructed in terms of the given diagrams. As discussed in Ref. [180], the two approaches (d)rCCD[F12] and (d)rCCD(F12*) are identical within ring coupled-cluster theory and can be obtained by neglecting diagram [8f12t_a]. The more simplified approximations (d)rCCD-F12a and (d)rCCD-F12b also reduce to equivalent formulations, both omitting the higher-order contributions [6f12t], [8f12t_a] and [6f12c_a]. It is furthermore interesting to note that diagrams [4], [5] and [7] comprise the so-called ladder contributions, yielding — in addition to the corresponding F12 contributions [4f12t], [4f12c_a] and [7f12t] as well as the driver diagrams of the entire row [1], [2] and [3] — a particle-particle RPA(F12) approach [44, 225]. An analogous third RPA(F12) variant without clear physical meaning can be identified when taking into account all of the so-called crossed-ring terms.
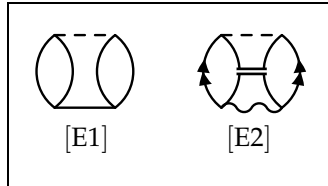

Fig. 4.1: Antisymmetrized Goldstone diagrams representing the conventional and the explicitly correlated contribution to the CCD-F12 correlation energy.

4.1.1 Explicit working equations for the direct rCCD(F12) approach

As shown in Figure 4.2, the inclusion of F12 geminals in the wave-function expansion leads to additional contributions to the amplitude and energy equations, which bare close analogy to the conventional counterparts. Also the algebraic equations can be formulated similarly to the drCCD Riccati equation, Eq. (2.58), summarizing the supplementary F12 terms of the conventional drCCD(F12) residual according to

$$\mathbf{\Omega}^{\mathrm{drCCD(F12)}} \leftarrow \mathbf{A}^{\mathrm{dRPA}}\mathbf{T}' + \mathbf{T}'\mathbf{A}^{\mathrm{dRPA}} + \mathbf{T}\mathbf{B}^{\mathrm{dRPA}}\mathbf{T}' + \mathbf{T}'\mathbf{B}^{\mathrm{dRPA}}\mathbf{T}. \tag{4.7}$$

The amplitude matrix $\mathbf{T}'$ refers to the double excitation operator $\hat{T}_{2'}$, describing excitations into the infinite virtual basis as defined within Eq. (2.94). The F12 contribution to the drCCD(F12) correlation energy, corresponding to the non-antisymmetrized version of diagram [E2] of Figure 4.9, can be traced back to the conventional expression of Eq. (2.59),

$$E_{\mathrm{C}}^{\mathrm{drCCD(F12)}} = E_{\mathrm{C}}^{\mathrm{drCCD}} + \tfrac{1}{2}\mathrm{tr}\left[\mathbf{B}^{\mathrm{dRPA}}\mathbf{T}'\right] = E_{\mathrm{C}}^{\mathrm{drCCD}} + \tfrac{1}{2}\mathrm{tr}\left[\mathcal{V}^{\dagger}\mathbf{C}\right]. \tag{4.8}$$
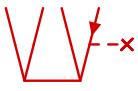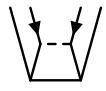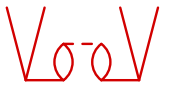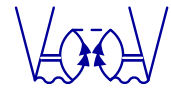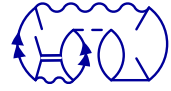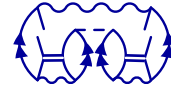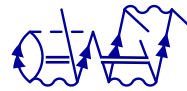
Residual for conventional amplitudes		Residual for geminal amplitudes
Conventional	F12	

[1]

[1f12c]

[2]

[2f12c]

[3] [3f12t] [3f12c_a] [3f12c_b]

[4] [4f12t] [4f12c_a] [4f12c_b]

[5] [5f12c]

[6] [6f12t] [6f12c_a] [6f12c_b]

[7] [7f12t] [7f12c_a] [7f12c_b]

[8] [8f12t_a] [8f12t_b] [8f12c_a] [8f12c_b]

[9] [9f12t_a] [9f12c_c] [9f12c_d]

[10] [10f12t_a] [10f12t_b] [10f12c_a] [10f12c_b]

[10f12t_c] [10f12c_c]

Fig. 4.2: (*On page 42:*) Antisymmetrized Goldstone diagrams representing spin orbitals for the CCD-F12 residual equation. Neglecting all blue diagrams yields the CCD(F12) approach. Diagrams contributing to rCCD(F12) and drCCD(F12) are highlighted in red. For the direct approach, a non-antisymmetrized definition of the two-electron integrals over r_{12}^{-1} and f_{12} is required, introducing an additional factor of two.

Open-shell equations implying $c_{IJ}^{XY} = \delta_{IX}\delta_{JY}$:

$$E_{\mathrm{C}}^{\mathrm{drCCD(F12)}} = \tfrac{1}{2}\sum_{ABIJ} t_{IJ}^{AB} g_{AB}^{IJ} + \tfrac{1}{2}\sum_{XYIJ} c_{IJ}^{XY}\left(\boldsymbol{\mathcal{V}}^\dagger\right)_{\widetilde{XY}}^{IJ} + \tfrac{1}{2}\sum_{XYIJ} c_{IJ}^{XY}(\boldsymbol{\Omega}^{\mathrm{F12(drCCD(F12))}})_{IJ}^{\widetilde{XY}},\tag{4.9}$$

$$(\boldsymbol{\Omega}^{\mathrm{drCCD(F12)}})_{IJ}^{AB} = g_{IJ}^{AB} + \hat{P}_{IJ}^{AB}\left[\sum_C t_{IJ}^{AC} F_{BC} - \sum_K t_{IK}^{AB} F_{KJ} + \sum_{CK} t_{JK}^{BC}\left(g_{CI}^{KA} + \tfrac{1}{2}\sum_{DL} t_{IL}^{AD} g_{CD}^{KL}\right)\right.$$
$$\left. + \sum_{P''KXY} c_{JK}^{XY} f_{\widetilde{XY}}^{BP''}\left(g_{P''I}^{KA} + \sum_{DL} t_{IL}^{AD} g_{P''D}^{KL}\right)\right] + \sum_{XY}\mathcal{C}_{AB,\widetilde{XY}}^{(IJ)} c_{IJ}^{XY},\tag{4.10}$$

$$(\boldsymbol{\Omega}^{\mathrm{F12(drCCD(F12))}})_{IJ}^{\widetilde{XY}} = \sum_{VW}\mathcal{B}_{\widetilde{XY},\widetilde{VW}}^{(IJ)} c_{IJ}^{VW} + \mathcal{V}_{IJ}^{\widetilde{XY}} + \hat{P}_{IJ}^{XY}\sum_{P''B} f_{P''B}^{\widetilde{XY}}\left(\sum_{CK} t_{JK}^{BC} g_{CI}^{KP''}\right) + \sum_{AB}\mathcal{C}_{\widetilde{XY},AB}^{(IJ)} t_{IJ}^{AB}.\tag{4.11}$$

with $\hat{P}_{IJ}^{XY} A_{IJ}^{XY} = A_{IJ}^{XY} + A_{JI}^{YX}$.

Closed-shell equations implying $c_{ij}^{xy} = \delta_{ix}\delta_{jy}$:

$$E_{\mathrm{C}}^{\mathrm{drCCD(F12)}} = 2\sum_{aibj} t_{ij}^{ab} g_{ab}^{ij} + 2\sum_{xiyj} c_{ij}^{xy}(\boldsymbol{\mathcal{V}}^\dagger)_{\widetilde{xy}}^{ij} + 2\sum_{xiyj} c_{ij}^{xy}(\boldsymbol{\Omega}^{\mathrm{F12(drCCD(F12))}})_{ij}^{\widetilde{xy}},\tag{4.12}$$

$$(\boldsymbol{\Omega}^{\mathrm{drCCD(F12)}})_{ij}^{ab} = g_{ij}^{ab} + \hat{P}_{ij}^{ab}\left[\sum_c t_{ij}^{ac} F_{bc} - \sum_k t_{ik}^{ab} F_{kj} + 2\sum_{ck} t_{jk}^{bc}\left(g_{ic}^{ak} + \sum_{dl} t_{il}^{ad} g_{dc}^{lk}\right)\right.$$
$$\left. + 2\sum_{p''kxy} c_{jk}^{xy} f_{\widetilde{xy}}^{bp''}\left(g_{p''i}^{ka} + 2\sum_{dl} t_{il}^{ad} g_{p''d}^{kl}\right)\right] + \sum_{xy}\mathcal{C}_{ab,\widetilde{xy}}^{(ij)} c_{ij}^{xy},\tag{4.13}$$

$$(\boldsymbol{\Omega}^{\mathrm{F12(drCCD(F12))}})_{ij}^{\widetilde{xy}} = \sum_{vw}\mathcal{B}_{\widetilde{xy},\widetilde{vw}}^{(ij)} c_{ij}^{vw} + \mathcal{V}_{ij}^{\widetilde{xy}} + 2\hat{P}_{ij}^{xy}\sum_{p''b} f_{p''b}^{\widetilde{xy}}\sum_{ck} t_{jk}^{bc} g_{ci}^{kp''} + \sum_{ab}\mathcal{C}_{\widetilde{xy},ab}^{(ij)} t_{ij}^{ab}.\tag{4.14}$$

with $\hat{P}_{ij}^{ab} A_{ij}^{ab} = A_{ij}^{ab} + A_{ji}^{ba}$.

Fig. 4.3: Explicit equations for drCCD(F12) within ansatz 2.

Assuming fixed geminal amplitudes, the residual $\mathbf{\Omega}^{\text{F12(drCCD(F12))}}$ is furthermore added as a constraint to the Lagrangian formulation of the correlation energy,

$$E_{\text{C}}^{\text{drCCD(F12)}} \longleftarrow \tfrac{1}{2}\text{tr}\left[\mathbf{\Omega}^{\text{F12(drCCD(F12))}}\mathbf{C}^{\text{LAG}}\right] , \qquad (4.15)$$

with

$$\mathbf{\Omega}^{\text{F12(drCCD(F12))}} = \mathcal{B}\mathbf{C} + \mathcal{V} + \mathbf{f}\mathbf{TA} + \mathbf{ATf} . \qquad (4.16)$$

$\mathbf{f}$ denotes the bare integrals over the Slater-type correlation factor f_{12}. Analogously to dMP2-F12, the geminal amplitude equations are calculated only once and added to the correlation energy as a constant term at the end of the iterative CC procedure [176]. Furthermore, the Lagrange multipliers $\mathbf{C}^{\text{MP2-F12}}$ are chosen as for dMP2-F12, keeping them fixed according to $\mathbf{C}^{\text{LAG}} = \mathbf{C} = \delta_{IX}\delta_{JY}$ [178]. It is interesting to note that, in contrast to MP2-F12 theory, a similar procedure, deriving the connection by solving a set of linear equations, would break orbital invariance [176]. Note that Eqs. (4.7) and (4.16) refer to ansatz 2^*, neglecting coupling contributions between conventional and geminal amplitudes. The complete working equations for drCCD(F12) within ansatz 2 are given for closed- and open-shell systems in Figure 4.3. Notes on the corresponding implementation in the CCSDF12 module of the TURBOMOLE program package [71] are summarized in Appendix E.

4.2 Assessment of the drCCD(F12) approach

As shown in Ref. [80], basis-set convergence of the dRPA approach differs significantly for non-covalent and covalent interactions. More precisely, quadruple-zeta basis sets were found to be sufficiently accurate for medium- and short-range correlation, while basis sets of quintuple-zeta size are required to obtain reliable results for binding energies. Additionally to the slow basis-set convergence, calculations on long-range interactions are most affected by the BSSE, influencing the basis-set dependence and often hindering a systematic convergence to the basis-set limit [226]. The drCCD(F12) approach is therefore validated regarding both atomization and interaction energies: Atomization energies are examined for a test set of 106 molecules, that was set up in Ref. [227] in order to assess F12 methods. It contains small molecules which represent a wide range of bonding situations, comprising the first- and second-row elements H, C, N, O, and F. Calculations are performed using the augmented correlation-consistent aug-cc-pVXZ basis sets [183, 184] with the aug-cc-pwCV(X+1)Z [186, 187] and aug-cc-pV(X+1)Z [188] basis sets as cbas and jkbas, respectively. Aug-cc-pVXZ/OPTRI basis sets [189] are taken as CABS basis for the F12 integrals and the CABS-singles correction. Interaction energies are in contrast evaluated for the S22 test set [36], a benchmark database including hydrogen-bonded, dispersion-dominated and mixed complexes. Due to the scaling of the drCCD(F12) approach, the tests were limited to the 10 smallest dimers, which nevertheless still cover all different bonding motifs in a balanced ratio. Furthermore, the comparatively small seasonal basis sets jun-cc-pV(X+d)Z are used [228, 229] and auxiliary basis sets are chosen as for the aug-cc-pVXZ basis-set series. The calculations for both the test set of 106 molecules and the S22 test set are performed using a PBE reference and excluding core orbitals from the correlation treatment. Convergence is examined regarding the error relative to the drCCD(F12) result within ansatz 2 and the largest basis set, i.e. for the aug-cc-pV5Z or the jun-cc-pV(Q+d)Z basis. As for the dRPA-F12 approach of Chapter 2, the chosen basis-set limits are validated by applying the two-point extrapolation scheme of Schwenke [208]. Details on the estimated trust region and the so determined scaling factors are reported in Ref. [180]. The corresponding standard deviations σ are indicated in Figures 4.4 and 4.5 as a yellow bar around the basis-set limit, ranging from $-\sigma$ to σ. The deviation amounts up to 0.02 kJ/mol per valence electron for the test set of 106 molecules while a threshold of 0.005 kJ/mol per valence electron is obtained for the 10 molecules of the S22 test set. The following discussion is restricted to mean errors, mean percentage errors and the corresponding standard deviations, all reported per valence electron to eliminate the dependence on the basis-set size. For the test set of 106 molecules, the number of valence electrons ranges between 2 and 36 with a mean value of 18; the complexes of the S22 test set comprehend 16 to 38 valence electrons, in average 28.

Correlation and atomization energies

Figure 4.4 is split in two parts: On the left-hand side, the mean error in the correlation energy is plotted with respect to the cardinal number of the basis set. Conventional drCCD results are shown to converge slowly, yielding errors of -46.2, -19.2 and -8.9 kJ/mol for double-, triple- and quadruple-zeta basis sets. Even the aug-cc-pV5Z and aug-cc-pV6Z calculations are still off by -4.7 and -2.7 kJ/mol, respectively. drCCD(F12) within ansatz 1 only achieves a minor improvement, reducing the error by about a factor of two and thus gain-
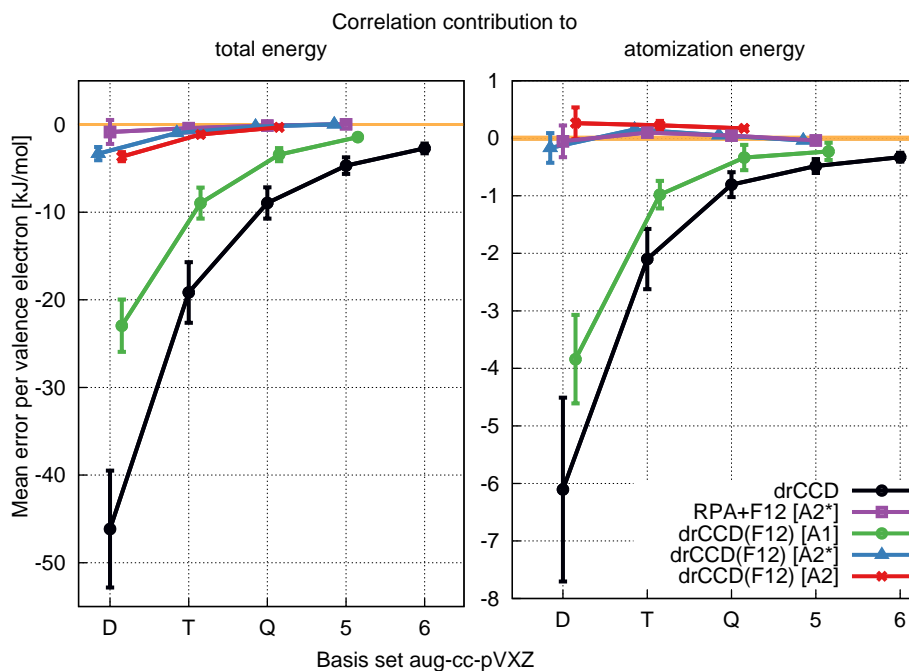
Fig. 4.4: **Test set of 106 molecules:** Basis-set convergence of the correlation energy contribution to the total and atomization energies for the aug-cc-pVXZ basis sets.

ing approximately one cardinal number. More effective is ansatz 2*, for which the double-zeta results already outpace the conventional aug-cc-pV5Z calculations, reducing the error to −3.4 kJ/mol. Calculations within the medium-sized aug-cc-pVTZ basis yield the desired 99 % of the reference limit with a mean error of less than 1 kJ/mol. Even though the result is compelling, it should be noted that including coupling between conventional and geminal amplitudes, as defined within ansatz 2, slightly increases the error, revealing that the performance of ansatz 2* relies to a small percentage on spurious error cancellation. The effect is however small and coupling between conventional and geminal amplitudes can be regarded as negliglible, given that the maximum deviation between ansatz 2 and 2* does not exceed 0.3 kJ/mol. The perturbative RPA+F12 ansatz performs surprisingly well, yielding double-zeta results which show even smaller errors than corresponding drCCD(F12) calculations within the larger aug-cc-pVTZ basis. Basis-set convergence is smooth as demonstrated by the gradually declining mean errors of −0.8, −0.4 and −0.1 kJ/mol for double-, triple- and quadruple-zeta basis sets. However, it should be kept in mind that the good performance of RPA+F12 relies on fortuitous error cancellation, as mentioned in Chapter 2.3.

The presented conclusions for correlation energies can be transferred to atomization energies, as shown on the right-hand side of Figure 4.4. Again, conventional results bear the slowest convergence, reaching errors of −6.1 to −2.1 kJ/mol for the aug-cc-pVDZ and aug-cc-pVTZ basis sets. Even the largest aug-cc-pV6Z basis still deviates by 0.3 kJ/mol from the aspired reference value. While ansatz 1 is again insufficient, the more sophisticated ansätze 2* and 2 are converged to within 99% of the basis-set limit for double-zeta basis sets, deviating solely by −0.2 and 0.3 kJ/mol. However, in contrast to correlation energies, convergence is not smooth for ansatz 2*: the error changes sign and increases to 0.2 kJ/mol when enlarging the basis to triple-zeta size. An analogous unsystematic behavior can be found for RPA+F12, where the aug-cc-pVDZ result is 0.5 kJ/mol below the reference limit while triple-zeta calculations overshoot by 0.1 kJ/mol. Only the inclusion of coupling contributions ensures smooth convergence, yielding steadily decreasing errors of 0.26, 0.22 and 0.17 kJ/mol for aug-cc-pVDZ, aug-cc-pVTZ and aug-cc-pVQZ calculations, respectively. For both correlation and atomization energies it should be furthermore mentioned that standard deviations are drastically reduced for drCCD(F12), not only in comparison to conventional drCCD, but also with respect to the perturbative RPA+F12 approach. Error distributions are thus both narrower and closer to zero, as shown in detail in Ref. [180].

Interaction energies

Since RPA is known to describe dispersion accurately, it is worth testing the benefit of explicitly correlated drCCD regarding long-range forces. In Figure 4.5, interaction energies for 10 molecules of the S22 test set are depicted analyzing the mean error per valence electron with increasing cardinal number for the jun-cc-pV(X+d)Z basis sets. More precisely, the plot shows the bare total interaction energies on the left, opposed to
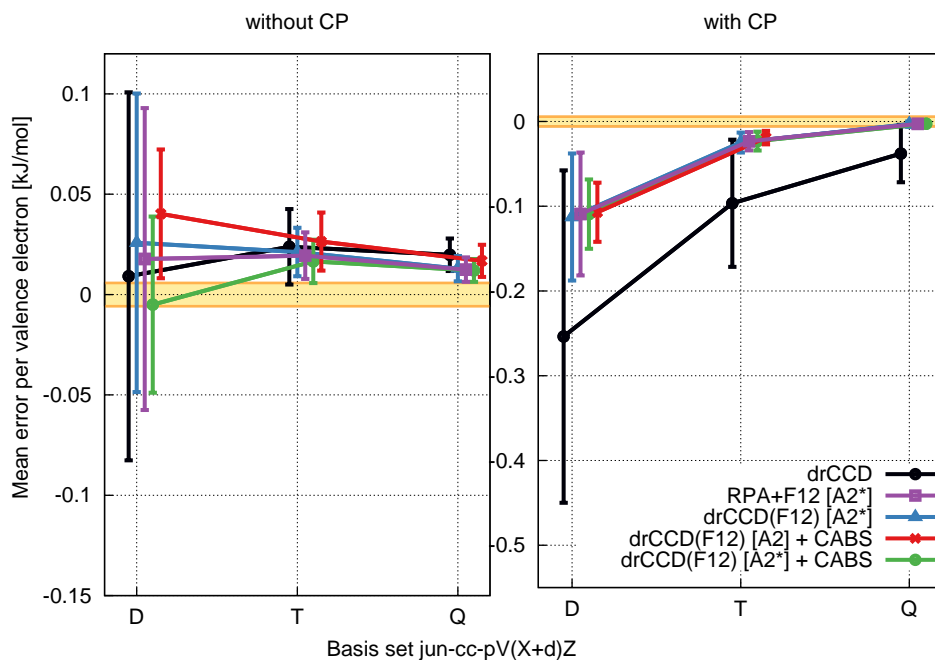
Fig. 4.5: **10 molecules of the S22 test set:** Basis-set convergence of interaction energies with and without counterpoise correction for the jun-cc-pV(X+d)Z basis sets.

the graph on the right where the energies include the CP correction to cure the BSSE. For both plots, the CP-corrected drCCD(F12) result within ansatz 2, including the CABS-singles correction for the reference energy and using the jun-cc-pV(Q+d) basis, is taken as reference. No systematic convergence is found for the non-corrected interaction energies: all methods are within the same error range of -0.005 to 0.04 kJ/mol for the smallest jun-cc-pV(D+d)Z basis. Triple-zeta results are comparable in magnitude, but the deviation between the different methods is reduced and the range of values is limited to 0.03 to 0.02 kJ/mol. However, even the largest jun-cc-pVQZ basis is not sufficient to reach the basis-set limit. The results are thus in agreement with earlier findings, indicating that the CP correction is crucial to secure a monotonic convergence behavior [230]. The conclusion is also confirmed by the plot on the right-hand side of Figure 4.5: Here, the CP-corrected results approach the basis-set limit smoothly from below. Errors of the conventional drCCD approach reduce e.g. stepwise when enlarging the basis set from double- to quadruple-zeta size, starting at -0.25 kJ/mol, followed by -0.10 kJ/mol for the medium-sized basis and ending with a deviation of -0.04 kJ/mol for the jun-cc-pVQZ results. In comparison, all explicitly correlated approaches improve the basis-set convergence even though the gain of about one cardinal number is much less pronounced than for correlation and atomization energies. Deviations between the different F12 approaches are of at most 0.006 kJ/mol, emphasizing that both the CABS-singles correction for the reference energy (indicated by the additional acronym "+CABS") as well as the coupling contributions of ansatz 2 are negligible. Solely the standard deviations for the double-zeta basis are in comparison reduced by a factor of two for the drCCD(F12)[A2]+CABS and drCCD(F12)[A2*]+CABS approaches, resulting in tighter normal distributions, as shown in detail in Ref. [180]. All approaches finally reach the basis-set limit within the trust region of 0.005 kJ/mol for the jun-cc-pVQZ basis. It should be furthermore stated that the CP correction for all explicitly correlated approaches is about a factor of 2 smaller than for the corresponding conventional methods, indicating that F12 analogues are less sensible to the BSSE, reflecting their reduced basis-set dependence.

4.3 Including exchange: explicitly correlated rCCD, rCCD-SO1 and rCCD-SO2

The deficiencies of dRPA or drCCD are well known: Due to the insufficient description of short-range interactions [231, 232], correlation energies are in general overestimated resulting in a poor description of total energies which are far too negative [233, 234]. Furthermore, atomization energies were found to be too low [28, 40], sometimes referred to as the RPA atomization puzzle [235]. Even binding energies of van-der-Waals systems are often underestimated. Most strikingly, the dissociation curves of several diatomics, like e.g. the

Be$_2$ dimer, show an erroneous bump at intermediate distances [236]. A self-consistent treament helps in lowering the energy, but cannot reduce the unphysical maximum in the interaction curve [237, 238]. Finally, energies are flawed by the self-interaction error, which becomes most apparent in the non-zero correlation energy of the hydrogen atom, see Ref. [7] for example.

Even though RPA can be considered as a promising post-KS approach, the specified shortcomings point out the need for corrections. As outlined in the introduction, a range of beyond-RPA methods have been proposed in the last decades. One ansatz is to include exact exchange (in different flavours), shown to improve correlation and total energies [239, 240] as well as dissociation curves and the related delocalisation error [241], even though it should be noted that the improvement comes hand in hand with an inferior description of static correlation. The repulsive bump in the interaction curve of diatomics is reduced or even cured [64]. Moreover, the one-electron self-interaction error is eliminated for several approaches, as e.g. demonstrated in the case of SOSEX [64] and AXK [8].

Aiming for analogous improvements, the concept of including exchange can be transferred to ring coupled-cluster schemes: as already introduced in Chapter 2 and outlined in the previous sections, the rCCD approach can be set up as an equivalent formulation to RPAX, including exchange in the residual equations and the correlation energy. Such an ansatz requires spin adaptation for closed-shell equations, partitioning the correlation energy into singlet and triplet contributions according to Eq. (2.83). While Eq. (2.83) is exact, it leads to severe triplet instabilities, as shown by Klopper *et al.* [146]. As a remedy, Toulouse and Mussard *et al.* [86, 164] revived an initial idea of Szabo and Ostlund [21, 151], setting up two approximate schemes called rCCD-SO1 and rCCD-SO2 in order to develop the corresponding range-separated approaches [86, 164]. Their tests on rare-gas dimers and the S22 set showed that the approaches give the most accurate interaction energies when compared to direct and exact rCCD including exchange. rCCD-SO2 was pointed out to be most promising since it solely relies on singlet excitations and thus avoids triplet instabilities. Furthermore, Mussard *et al.* proved that open-shell equations can only be formulated for rCCD-SO2 and not for the related rCCD-SO1 approach [164]. Open-shell rCCD-SO2 avoids both triplet and spin-flipped amplitudes, improving not only the stability but also reducing the computation times in comparison to exact rCCD. These results motivate the development of analogous explicitly correlated rCCD approaches as presented in the following.

4.3.1 Working equations for explicitly correlated ring coupled-cluster doubles approaches including exchange

Following Ref. [86], three different rCCD(F12) approaches are summarized in Table 4.6, labeled accordingly as rCCD(F12)-SO2, rCCD(F12)-SO1 and rCCD(F12). Only rCCD(F12) and rCCD(F12)-SO2 are defined for open-shell systems: both approaches rely on the same residual equation for the conventional amplitudes $\mathbf{T}$, which depends — in contrast to drCCD(F12) — on the antisymmetrized matrices $\mathbf{A}^{\text{RPAX}}$ and $\mathbf{B}^{\text{RPAX}}$. The additional F12 terms can hence be summarized as

$$\mathbf{\Omega}^{\text{rCCD(F12)}} \leftarrow \mathbf{A}^{\text{RPAX}}\mathbf{T}' + \mathbf{T}'\mathbf{A}^{\text{RPAX}} + \mathbf{T}\mathbf{B}^{\text{RPAX}}\mathbf{T}' + \mathbf{T}'\mathbf{B}^{\text{RPAX}}\mathbf{T}. \tag{4.17}$$

The correlation energy is obtained in analogy to Eqs. (2.65) and (2.87), incorporating an additional F12 and the constant geminal residual term,

$$E_{\text{C}}^{\text{rCCD(F12)}} = \tfrac{1}{4}\text{tr}\left[\mathbf{B}^{\text{RPAX}}\mathbf{T}^{\text{rCCD(F12)}}\right] + \tfrac{1}{4}\text{tr}\left[(\mathbf{\mathcal{V}} - \mathbf{\mathcal{V}}^{\text{X}})^{\dagger}\mathbf{D}\right] + \tfrac{1}{4}\text{tr}\left[\mathbf{\Omega}^{\text{F12(rCCD(F12))}}\mathbf{D}^{\text{LAG}}\right], \tag{4.18}$$

$$E_{\text{C}}^{\text{rCCD(F12)-SO2}} = \tfrac{1}{2}\text{tr}\left[\mathbf{B}^{\text{dRPA}}\mathbf{T}^{\text{rCCD(F12)}}\right] + \tfrac{1}{2}\text{tr}\left[\mathbf{\mathcal{V}}^{\dagger}\mathbf{D}\right] + \tfrac{1}{2}\text{tr}\left[\mathbf{\Omega}^{\text{F12(rCCD(F12)-SO2)}}\mathbf{D}^{\text{LAG}}\right], \tag{4.19}$$

where $\mathbf{\mathcal{V}}^{\text{X}}$ denotes the exchange contribution to the F12 intermediate $\mathbf{\mathcal{V}}$ and the geminal residuals are given as

$$\mathbf{\Omega}^{\text{F12(rCCD(F12))}} = \mathbf{\mathcal{B}}\mathbf{D} + \mathbf{\mathcal{V}} - \mathbf{\mathcal{V}}^{\text{X}} + \mathbf{f}\mathbf{T}\mathbf{A}^{\text{RPAX}} + \mathbf{A}^{\text{RPAX}}\mathbf{T}\mathbf{f}, \tag{4.20}$$

$$\mathbf{\Omega}^{\text{F12(rCCD(F12)-SO2)}} = \mathbf{\mathcal{B}}\mathbf{C} + \mathbf{\mathcal{V}} + \mathbf{f}\mathbf{T}\mathbf{A}^{\text{dRPA}} + \mathbf{A}^{\text{dRPA}}\mathbf{T}\mathbf{f}. \tag{4.21}$$

Analogously to the conventional schemes, the F12 variants are constructed in such a way that they reproduce the MP2-F12 correlation energy if truncated at second-order perturbation theory. Including exchange, the coalescence conditions imply antisymmetrized geminal amplitudes. Thus, in contrast to drCCD(F12), where the geminal amplitudes are chosen according to $c_{IJ}^{XY} = \delta_{IX}\delta_{JY}$ for both same and opposite spin, the rCCD amplitudes are kept fixed at $d_{IJ}^{XY} = \delta_{IX}\delta_{JY} - \delta_{IY}\delta_{JX}$. Again, the Lagrange multipliers are defined by the relation $\mathbf{D}^{\text{LAG}} = \mathbf{D}$. Note that the rCCD(F12)-SO2 approach assumes antisymmetrized amplitudes in combination with non-antisymmetrized integrals. Consistently, a non-antisymmetrized geminal residual is required and

the method thus implies both geminal amplitudes $\mathbf{D}$ and $\mathbf{C}$.

For closed-shell systems, spin-adapted rCCD equations can be obtained by applying the orthogonal transformation $\mathbf{M'} = \mathbf{U}^T\mathbf{M}\mathbf{U}$ [86], assuming the following spin block structure for the symbolic matrix $\mathbf{M}$,

$$
\mathbf{M} = \begin{pmatrix} \mathbf{M}^{\alpha\alpha}_{\alpha\alpha} & \mathbf{M}^{\alpha\beta}_{\alpha\beta} & \mathbf{0} & \mathbf{0} \\ \mathbf{M}^{\beta\alpha}_{\beta\alpha} & \mathbf{M}^{\beta\beta}_{\beta\beta} & \mathbf{0} & \mathbf{0} \\ \mathbf{0} & \mathbf{0} & \mathbf{M}^{\beta\beta}_{\alpha\alpha} & \mathbf{M}^{\beta\alpha}_{\alpha\beta} \\ \mathbf{0} & \mathbf{0} & \mathbf{M}^{\alpha\beta}_{\beta\alpha} & \mathbf{M}^{\alpha\alpha}_{\beta\beta} \end{pmatrix} , \tag{4.22}
$$

and defining the transformation matrix $\mathbf{U}$ as

$$
\mathbf{U} = \frac{1}{\sqrt{2}} \begin{pmatrix} 1 & 1 & 0 & 0 \\ 1 & -1 & 0 & 0 \\ 0 & 0 & 1 & 1 \\ 0 & 0 & 1 & -1 \end{pmatrix} . \tag{4.23}
$$

The transformation leads to a decomposition into singlet and triplet contributions; the transformed anti- and non-antisymmetrized geminal amplitude matrices $\mathbf{D'}$ and $\mathbf{C'}$ are e.g. given as

$$
\mathbf{D'} = \begin{pmatrix} {}^1\mathbf{D} & \mathbf{0} & \mathbf{0} & \mathbf{0} \\ \mathbf{0} & {}^3\mathbf{D} & \mathbf{0} & \mathbf{0} \\ \mathbf{0} & \mathbf{0} & {}^3\mathbf{D} & \mathbf{0} \\ \mathbf{0} & \mathbf{0} & \mathbf{0} & -{}^3\mathbf{D} \end{pmatrix} , \quad \mathbf{C'} = \begin{pmatrix} {}^1\mathbf{C} & \mathbf{0} & \mathbf{0} & \mathbf{0} \\ \mathbf{0} & \mathbf{0} & \mathbf{0} & \mathbf{0} \\ \mathbf{0} & \mathbf{0} & \mathbf{0} & \mathbf{0} \\ \mathbf{0} & \mathbf{0} & \mathbf{0} & \mathbf{0} \end{pmatrix} , \tag{4.24}
$$

with the singlet and triplet amplitudes ${}^1d_{ij}^{xy} = 2\delta_{ix}\delta_{jy} - \delta_{iy}\delta_{jx}$, ${}^3d_{ij}^{xy} = -\delta_{iy}\delta_{jx}$ and ${}^1c_{ij}^{xy} = 2\delta_{ix}\delta_{jy}$. Accordingly, all other antisymmetrized matrices can be decomposed into singlet and triplet blocks, while the non-antisymmetrized counterparts only lead to a contribution from singlet excitations.

The structure of the so-obtained closed-shell rCCD(F12), rCCD(F12)-SO2 and rCCD(F12)-SO1 variants resembles the conventional approaches of Eqs. (2.80), (2.81) and (2.82): While rCCD(F12) and rCCD(F12)-SO1 require the calculation of singlet and triplet amplitudes,

$$
\begin{aligned}
E_C^{\text{rCCD(F12)}} = {} & \tfrac{1}{4}\text{tr}\left[{}^1\mathbf{T}^{\text{rCCD(F12)}}\,{}^1\mathbf{B}^{\text{RPAX}} + 3\,{}^3\mathbf{T}^{\text{rCCD(F12)}}\,{}^3\mathbf{B}^{\text{RPAX}}\right] + \tfrac{1}{4}\text{tr}\left[{}^1\mathbf{D}\,{}^1\boldsymbol{\mathcal{V}}^\dagger + 3\,{}^3\mathbf{D}\,{}^3\boldsymbol{\mathcal{V}}^\dagger\right] \\
& + \tfrac{1}{4}\text{tr}\left[{}^1\mathbf{D}\,{}^1\boldsymbol{\Omega}^{\text{F12(rCCD(F12))}} + 3\,{}^3\mathbf{D}\,{}^3\boldsymbol{\Omega}^{\text{F12(rCCD(F12))}}\right] ,
\end{aligned} \tag{4.25}
$$

$$
\begin{aligned}
E_C^{\text{rCCD(F12)-SO1}} = {} & \tfrac{1}{2}\text{tr}\left[{}^1\mathbf{B}^{\text{RPAX}}\left({}^1\mathbf{T}^{\text{rCCD(F12)}} - {}^3\mathbf{T}^{\text{rCCD(F12)}}\right)\right] + \tfrac{1}{2}\text{tr}\left[{}^1\boldsymbol{\mathcal{V}}^\dagger\left({}^1\mathbf{D} - {}^3\mathbf{D}\right)\right] \\
& + \tfrac{1}{2}\text{tr}\left[{}^1\boldsymbol{\Omega}^{\text{F12(rCCD(F12))}}\left({}^1\mathbf{D} - {}^3\mathbf{D}\right)\right] ,
\end{aligned} \tag{4.26}
$$

the rCCD(F12)-SO2 approach is solely based on singlet contributions,

$$
E_C^{\text{rCCD(F12)-SO2}} = \tfrac{1}{2}\text{tr}\left[{}^1\mathbf{B}^{\text{dRPA}}\,{}^1\mathbf{T}^{\text{rCCD(F12)}}\right] + \tfrac{1}{2}\text{tr}\left[\left(2\boldsymbol{\mathcal{V}}^\dagger\right)\,{}^1\mathbf{D}\right] + \tfrac{1}{2}\text{tr}\left[{}^1\boldsymbol{\Omega}^{\text{F12(rCCD(F12)-SO2)}}\,{}^1\mathbf{D}\right] . \tag{4.27}
$$

Note that for both open- and closed-shell systems the conventional amplitude equations are identical for all rCCD(F12) variants, differing only in the formulation of the correlation energy. This aspect can be highlighted e.g. for the open-shell variants of rCCD(F12) and rCCD(F12)-SO2 when drawing the corresponding antisymmetrized Goldstone diagrams, depicted in Figure 4.7. As for conventional rCCD, the diagrams either require a specific labeling of all non-contracted external lines or a redefinition of standard interpretation rules. More precisely, an additional factor of 2 has to be associated with non-antisymmetrized integrals or geminal amplitudes and all distinct permutations of inequivalent external lines have to be considered by including the permutation operator $\hat{P}^{AB}_{IJ}M^{AB}_{IJ} = M^{AB}_{IJ} + M^{BA}_{JI}$ (instead of the often employed $\hat{P}^-_{IJ}$ and $\hat{P}^-_{AB}$ operators with $\hat{P}^-_{IJ}M^{AB}_{IJ} = M^{AB}_{IJ} - M^{AB}_{JI}$). Furthermore, in order to summarize both rCCD(F12) and rCCD(F12)-SO2 in terms of a single set of diagrams, it is necessary to redefine two symbols introducing a twofold nomenclature which discriminates between the two approaches, see Figure 4.8. By doing so, the connection between rCCD(F12), rCCD(F12)-SO2 and drCCD(F12) becomes apparent: rCCD(F12) can be described by solely assuming antisymmetrized integrals and geminal amplitudes. drCCD(F12) diagrams look identical, reqiring however non-antisymmetrized definitions for both integrals and amplitudes. rCCD(F12)-SO2 is a mixed variant: while the residual equation for the conventional doubles amplitudes refers to antisymmetrized quantities, the geminal residual requires non-antisymmetrized two-electron integrals and geminal coefficients. The final expression for the correlation energy, depicted in terms of diagrams [E1] to [E5], thus assumes antisymmetrized amplitudes, but non-antisymmetrized integrals and consistently a non-antisymmetrized geminal residual. Analogously to Eq. (4.21), diagram [E4] thus implies both $\mathbf{D}$ and $\mathbf{C}$.

Open-shell equations implying $c_{IJ}^{XY} = \delta_{IX}\delta_{JY}$ **and** $d_{IJ}^{XY} = \delta_{IX}\delta_{JY} - \delta_{IY}\delta_{JX}$:

$$E_{\rm C}^{\rm rCCD(F12)} = \frac{1}{4}\sum_{ABIJ} t_{IJ}^{AB}\left(g_{AB}^{IJ} - g_{BA}^{IJ}\right) + \frac{1}{4}\sum_{XYIJ} d_{IJ}^{XY}\left(\left(\boldsymbol{\mathcal{V}}^\dagger\right)_{\widetilde{XY}}^{IJ} - \left(\boldsymbol{\mathcal{V}}^\dagger\right)_{\widetilde{XY}}^{JI}\right) + \frac{1}{4}\sum_{XYIJ} d_{IJ}^{XY}\left(\boldsymbol{\Omega}^{\rm F12(rCCD(F12))}\right)_{IJ}^{\widetilde{XY}},$$

(4.28)

$$E_{\rm C}^{\rm rCCD(F12)\text{-}SO2} = \frac{1}{2}\sum_{ABIJ} t_{IJ}^{AB} g_{AB}^{IJ} + \frac{1}{2}\sum_{XYIJ} d_{IJ}^{XY}\left(\boldsymbol{\mathcal{V}}^\dagger\right)_{\widetilde{XY}}^{IJ} + \frac{1}{2}\sum_{XYIJ} d_{IJ}^{XY}\left(\boldsymbol{\Omega}^{\rm F12(rCCD(F12)\text{-}SO2)}\right)_{IJ}^{\widetilde{XY}},$$

(4.29)

$$\left(\boldsymbol{\Omega}^{\rm rCCD(F12)}\right)_{IJ}^{AB} = g_{IJ}^{AB} - g_{JI}^{AB} + \hat{P}_{IJ}^{AB}\left[\sum_C t_{IJ}^{AC}F_{BC} - \sum_K t_{IK}^{AB}F_{KJ} + \sum_{CK} t_{JK}^{BC}\left(g_{IC}^{AK} - g_{CI}^{AK}\right)\right.$$
$$\left. + \frac{1}{2}\sum_{DLCK} t_{IL}^{AD}t_{JK}^{BC}\left(g_{DC}^{LK} - g_{CD}^{LK}\right) + \sum_{P''KXY} d_{JK}^{XY}f_{\widetilde{XY}}^{BP''}\left(g_{P''I}^{KA} - g_{IP''}^{KA} + \sum_{DL} t_{IL}^{AD}\left(g_{P''D}^{KL} - g_{DP''}^{KL}\right)\right)\right],$$

(4.30)

$$\left(\boldsymbol{\Omega}^{\rm F12(rCCD(F12))}\right)_{IJ}^{\widetilde{XY}} = \sum_{VW} \mathcal{B}_{\widetilde{XY},\widetilde{VW}}^{(IJ)} d_{IJ}^{VW} + \mathcal{V}_{IJ}^{\widetilde{XY}} - \mathcal{V}_{JI}^{\widetilde{XY}} + \hat{P}_{IJ}^{XY}\sum_{P''B} f_{P''B}^{\widetilde{XY}}\sum_{CK} t_{JK}^{BC}\left(g_{CI}^{KP''} - g_{IC}^{KP''}\right),$$

(4.31)

$$\left(\boldsymbol{\Omega}^{\rm F12(rCCD(F12)\text{-}SO2)}\right)_{IJ}^{\widetilde{XY}} = \sum_{VW} \mathcal{B}_{\widetilde{XY},\widetilde{VW}}^{(IJ)} c_{IJ}^{VW} + \mathcal{V}_{IJ}^{\widetilde{XY}} + \hat{P}_{IJ}^{XY}\sum_{P''B} f_{P''B}^{\widetilde{XY}}\sum_{CK} t_{JK}^{BC} g_{CI}^{KP''},$$

(4.32)

with $\hat{P}_{IJ}^{AB}M_{IJ}^{AB} = M_{IJ}^{AB} + M_{JI}^{BA}$.

Closed-shell equations implying $^1d_{ij}^{xy} = 2\delta_{ix}\delta_{jy} - \delta_{iy}\delta_{jx}$, $^3d_{ij}^{xy} = -\delta_{jx}\delta_{iy}$ **and** $^1c_{ij}^{xy} = 2\delta_{ix}\delta_{jy}$:

$$E_{\rm C}^{\rm rCCD(F12)} = \frac{1}{4}\sum_{abij}\left(^1t_{ij}^{ab}\,^1g_{ab}^{ij} + 3\,^3t_{ij}^{ab}\,^3g_{ab}^{ji}\right) + \frac{1}{4}\sum_{xyij}\left(^1d_{ij}^{xy}\left(^1\boldsymbol{\mathcal{V}}^\dagger\right)_{\widetilde{xy}}^{ij} + 3\,^3d_{ij}^{xy}\left(^3\boldsymbol{\mathcal{V}}^\dagger\right)_{\widetilde{xy}}^{ji}\right)$$
$$+ \frac{1}{4}\sum_{xyij}\left(^1d_{ij}^{xy}\left(^1\boldsymbol{\Omega}^{\rm F12(rCCD(F12))}\right)_{ij}^{\widetilde{xy}} + 3\,^3d_{ij}^{xy}\left(^3\boldsymbol{\Omega}^{\rm F12(rCCD(F12))}\right)_{ij}^{\widetilde{xy}}\right)$$

(4.33)

$$E_{\rm C}^{\rm rCCD(F12)\text{-}SO2} = \frac{1}{2}\sum_{aibj}\,^1t_{ij}^{ab}\left(2g_{ab}^{ij}\right) + \frac{1}{2}\sum_{xiyj}\,^1d_{ij}^{xy}\left(2(\boldsymbol{\mathcal{V}}^\dagger)_{\widetilde{xy}}^{ij}\right) + \frac{1}{2}\sum_{xiyj}\,^1d_{ij}^{xy}\left(^1\boldsymbol{\Omega}^{\rm F12(rCCD(F12)\text{-}SO2)}\right)_{ij}^{\widetilde{xy}}$$

(4.34)

$$E_{\rm C}^{\rm rCCD(F12)\text{-}SO1} = \frac{1}{2}\sum_{abij}\left(^1t_{ij}^{ab} - \,^3t_{ij}^{ab}\right)\,^1g_{ab}^{ij} + \frac{1}{2}\sum_{xiyj}\left(^1d_{ij}^{xy} - \,^3d_{ij}^{xy}\right)(^1\boldsymbol{\mathcal{V}}^\dagger)_{\widetilde{xy}}^{ij}$$
$$+ \frac{1}{2}\sum_{xiyj}\left(^1d_{ij}^{xy} - \,^3d_{ij}^{xy}\right)\left(^1\boldsymbol{\Omega}^{\rm F12(rCCD(F12))}\right)_{ij}^{\widetilde{xy}}$$

(4.35)

$$\left(^s\boldsymbol{\Omega}^{\rm rCCD(F12)}\right)_{ij}^{ab} = \,^sg_{ij}^{ab} + \hat{P}_{ij}^{ab}\left[\sum_c \,^st_{ij}^{ac}F_{bc} - \sum_k \,^st_{ik}^{ab}F_{kj} + \sum_{ck} \,^st_{jk}^{bc}\left(^sg_{ic}^{ak} + \frac{1}{2}\sum_{dl} \,^st_{il}^{ad}\,^sg_{dc}^{lk}\right)\right.$$
$$\left. + \sum_{p''kxy} \,^sd_{jk}^{xy}f_{\widetilde{xy}}^{bp''}\left(^sg_{p''i}^{ka} + \sum_{dl} \,^st_{il}^{ad}\,^sg_{p''d}^{kl}\right)\right]$$

(4.36)

$$\left(^s\boldsymbol{\Omega}^{\rm F12(rCCD(F12))}\right)_{ij}^{\widetilde{xy}} = \sum_{vw} \mathcal{B}_{\widetilde{xy},\widetilde{vw}}^{(ij)}\,^sd_{ij}^{vw} + \,^s\mathcal{V}_{ij}^{\widetilde{xy}} + \hat{P}_{ij}^{xy}\sum_{p''b} f_{p''b}^{\widetilde{xy}}\sum_{ck} \,^st_{jk}^{bc}\,^sg_{ci}^{kp''}$$

(4.37)

$$\left(^s\boldsymbol{\Omega}^{\rm F12(rCCD(F12)\text{-}SO2)}\right)_{ij}^{\widetilde{xy}} = \sum_{vw} \mathcal{B}_{\widetilde{xy},\widetilde{vw}}^{(ij)}\,^1c_{ij}^{vw} + 2\mathcal{V}_{ij}^{\widetilde{xy}} + \hat{P}_{ij}^{xy}\sum_{p''b} f_{p''b}^{\widetilde{xy}}\sum_{ck} \,^1t_{jk}^{bc}\left(2g_{ci}^{kp''}\right)$$

(4.38)

with $s = 1,3$ indicating singlet and triplet intermediates, defined as $^1M_{ij}^{ab} = 2M_{ij}^{ab} - M_{ij}^{ba}$ and $^3M_{ij}^{ab} = -M_{ij}^{ba}$.

Fig. 4.6: Working equations for rCCD(F12), rCCD(F12)-SO1 and rCCD(F12)-SO2 within ansatz 2*.
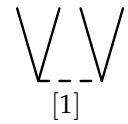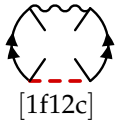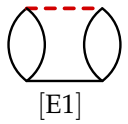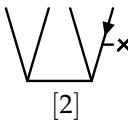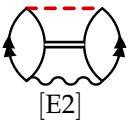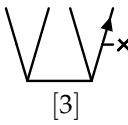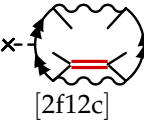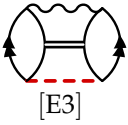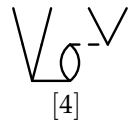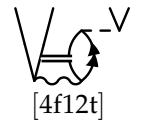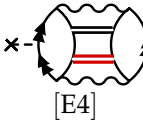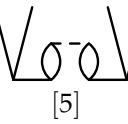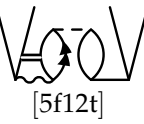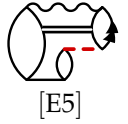
Residual for conventional amplitudes		Residual for geminal ampl.	Correlation energy
Conventional	F12		
[1]		[1f12c]	[E1]
[2]			[E2]
[3]		[2f12c]	[E3]
[4]	[4f12t]	[3f12c]	[E4]
[5]	[5f12t]		[E5]

Fig. 4.7: Antisymmetrized Goldstone diagrams visualizing open-shell rCCD(F12) variants within ansatz 2^* using fixed geminal amplitudes. The conventional residual equations comprise diagrams [1] to [5] as well as the two F12 contributions [4f12t] and [5f12t]. The geminal residual, represented by diagrams [1f12c] to [3f12c], requires a specific nomenclature for the non-antisymmetrized two-electron integrals and geminal amplitudes, given in Figure 4.8. Due to the fixed-amplitude approach, it contributes as a constant term to the correlation energy, depicted in terms of diagrams [E1] to [E5].

	$\langle \mathbb{KL}|\mathbb{MN}\rangle$	for drCCD and rCCD-SO2
	$\langle \mathbb{KL}\|\mathbb{MN}\rangle$	for rCCD
	$c_{IJ}^{XY} = \delta_{IX}\delta_{JY}$	for drCCD and rCCD-SO2
	$d_{IJ}^{XY} = \delta_{IX}\delta_{JY} - \delta_{IY}\delta_{JX}$	for rCCD

Fig. 4.8: Specific nomenclature for the rCCD diagrams of Figure 4.7. In addition to the standard interpretation rules for antisymmetrized Goldstone diagrams representing spin orbitals (see Appendix A), an additional factor of 2 has to be associated with non-antisymmetrized two-electron integrals or geminals amplitudes and distinct permutations of inequivalent external lines are accounted for by including the permutation operator $\hat{P}_{IJ}^{AB}$ with $\hat{P}_{IJ}^{AB} M_{IJ}^{AB} = M_{IJ}^{AB} + M_{JI}^{BA}$. $\{\mathbb{K}, \mathbb{L}, \dots\}$ denote spin orbitals of the complete infinite basis, comprising the complete virtual as well as the occupied basis.

4.4 Validation of the different rCCD(F12) approaches

The presented rCCD(F12) variants were implemented in the KOALA program package [205] and validated for a small test set of 18 closed-shell molecules containing elements of the first and second row of the periodic table. Geometries were taken from Ref. [206]. For the sake of convenience, basis-set convergence is investigated for the relatively small def2-basis sets of Ahlrichs and co-workers, ranging from double-zeta to quadruple-zeta quality [207]. As no optimized CABS basis is available for the def2-series, it is chosen identically to the auxiliary basis for density fitting (cbas). Core orbitals are excluded from the correlation treatment. HF, PBE and PBE0 references were tested, however, convergence could in general not be achieved for the latter two Kohn-Sham determinants, regardless of the employed rCCD(F12) approach. Using HF references instead, improves the performance even though triplet instabilities still hampered rCCD(F12) and rCCD(F12)-SO1 calculations for the molecules BN, C_2, C_2H_4, CH_2, CN^+, and O_3, even when modifying the DIIS algorithm or adding a shift to the quasi-Newton update. Furthermore, convergence could not be achieved for atomic oxygen and fluorine in the case of all three rCCD(F12) approaches. Thus, the following statistical measures comprise different sets of molecules depending on the chosen method: rCCD(F12)-SO2 correlation energies include the full test set of 18 molecules, while the corresponding results for rCCD(F12) and rCCD(F12)-SO1 are restricted to a total sum of 12 test cases. Atomization energies refer to C_2H_2, $C_2H_3^+$, CH_4, H_2 and N_2 in the case of rCCD(F12); the molecules BN, C_2H_4, CH_2 and CN^+ are additionally included for rCCD(F12)-SO2. Nevertheless, the comparison between the different rCCD(F12) approaches is considered to be reliable since the remaining test molecules all showed analogous convergence behavior with similar statistical measures. Detailed results and explicit statistical data including mean errors, mean absolute deviations, root-mean-square errors, standard deviations and percentage errors are published in Ref. [156]. For the following validation, it is however sufficient to restrict the discussion to mean errors and corresponding standard deviations, as depicted in Figure 4.9.

On the left-hand side of Figure 4.9, basis-set convergence of the correlation energy is depicted for the three closed-shell methods, rCCD, rCCD-SO1 and rCCD-SO2 as well as the corresponding explicitly correlated (F12) and +F12 schemes. Mean errors are calculated with respect to the corresponding (F12) result using the def2-QZVPP basis. Hence, rCCD(F12)-SO1/def2-QZVPP calculations serve e.g. as reference for conventional rCCD-SO1 and the perturbative rCCD+F12-SO1 approach. Analogously to Chapter 3.4, the trust region of the chosen reference is estimated by the outlined two-step procedure based on Schwenke's extrapolation formula of Eq. (3.23). The so-obtained standard deviations σ amount up to a maximum value of 0.36 kJ/mol per valence electron for the rCCD(F12)-SO2/def2-QZVPP limit. This accuracy limit is indicated in Figure 4.9 as a yellow bar around the basis-set limit, ranging from $-\sigma$ to σ.

All three conventional methods — rCCD, rCCD-SO1 and rCCD-SO2 — converge slowly to the basis-set limit, manifesting mean errors of -35.8 to -29.5 kJ/mol for the def2-SVP basis which decrease gradually by about 20 and then by another 7 kJ/mol when enlarging the basis-set size to triple- and quadruple-zeta quality. Extrapolation is required to reach the basis-set limit with a remaining deviation of 0.1-0.3 kJ/mol for the def2-(TQ)ZVPP result. In comparison, the explicitly correlated approaches accelerate convergence: the error of the def2-SVP basis set is reduced to -7.4 to -4.3 kJ/mol, lying in the range of the conventional def2-QZVPP result. Triple-zeta calculations are already converged to within 99% of the basis-set limit, even though the errors of -0.8 to -1.3 kJ/mol are still out of the trust region of the (F12)/def2-QZVPP reference. The performance of the perturbative +F12 ansatz is comparable to the corresponding (F12) approaches, showing either slightly smaller (rCCD+F12-SO1 and rCCD+F12-SO2) or larger (rCCD+F12) mean errors. When opposing the different (F12) schemes, the results of Figure 4.9 might give the impression that all SO2 variants possess the fastest convergence. However, mean percentage errors indicate a different ranking, relating the smallest deviations to the rCCD approach, followed by the SO1 ansatz.

On the right-hand side of Figure 4.9, convergence of the correlation contribution to the atomization energy is illustrated for both rCCD and rCCD-SO2, the two variants which provide open-shell equations. In accordance with the findings for correlation energies, rCCD-SO2 and rCCD approaches show similar convergence behavior, differing by at most 1.3 kJ/mol. Both conventional schemes approach the basis-set limit slowly, with mean errors of -9.8 to -8.5 kJ/mol for the def2-SVP basis and of -4.3 to -3.8 kJ/mol for the def2-TZVPP basis. Def2-QZVPP results are still off by -1.7 kJ/mol; the expolated def2-(TQ)ZVPP limit finally coincides with the chosen reference, showing a maximum deviation of -0.2 kJ/mol. As expected, all explicitly correlated approaches outperform the conventional counterparts, however, in contrast to correlation energies, convergence is not smooth: for rCCD(F12), double-zeta results overshoot the basis-set limit by about 0.2 kJ/mol while triple-zeta results lie nearly equally far below the reference value with a mean error of -0.3 kJ/mol. +F12 and (F12) variants are again comparable, deviating by at most 0.7 kJ/mol. For both schemes, convergence to within 99% of the basis-set limit is reached for triple-zeta basis sets.

Further benchmark studies on rCCD(F12)-SO2 within the larger aug-cc-pVXZ [183, 184] and cc-pVXZ-F12

[242] basis sets are summarized in Ref. [156], based on the rCCD(F12)-SO2 implementation in the TURBO-MOLE program package by Christof Holzer. In summary, the therein reported calculations indicate that the findings from above can be transferred to the correlation consistent basis sets, proving that triple-zeta results recover 99% of the basis-set limit and can thus be considered as reliable, independent of the chosen basis set.
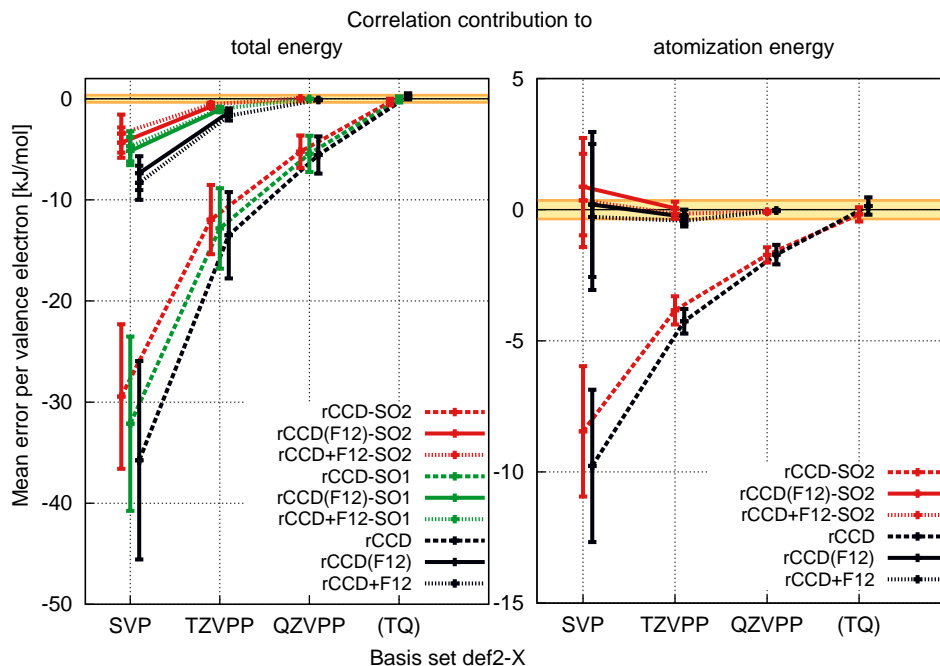
Fig. 4.9: Basis-set convergence of the correlation contribution to total and atomization energies for conventional and explicitly correlated rCCD(F12) variants.

4.5 Conclusions

The connection between RPA and ring coupled-cluster theory was exploited to set up explicitly correlated ring coupled-cluster approaches which accelerate basis-set convergence and allow to reach the RPA basis-set limit with medium-sized basis sets. Mean percentage errors, as depicted in Figure 4.10 and 4.11, demonstrate that atomization energies are converged to within 99% of the basis-set limit for both drCCD(F12) and the selected rCCD(F12) approaches including exchange when using triple-zeta basis sets. This corresponds to a gain of about 4 cardinal numbers for the aug-cc-pVXZ basis sets and of about 2 cardinal numbers for the def2-basis sets, respectively. The result is in line with other established explicitly correlated CC methods, yielding in general quintuple-zeta quality for triple-zeta basis sets [112, 223]. Interaction energies in contrast require basis sets of quadruple-zeta size, as shown on the right-hand side of Figure 4.10, reflecting the fact that the F12 wave-function ansatz was not designed to capture long-range phenomena like dispersion [172, 243]: The more efficient description of the monomers relative to the dimer leads to large errors in the binding energy. The scaling of the drCCD(F12) implementation in TURBOMOLE is proportional to N^6, however, is should be noted that computation times can be reduced to N^5 for the direct scheme when applying Cholesky decomposition and using fixed geminal amplitudes [43]. rCCD(F12) approaches including exchange are less efficient from the computational point of view, requiring the calculation of both singlet and triplet amplitudes in case of closed-shell references and the determination of spin-flipped amplitudes for open-shell systems. Efficiency can be increased when approximating the exact rCCD formalism according to the SO2 ansatz: rCCD(F12)-SO2 only relies on either same- and opposite-spin or singlet amplitudes in case of UHF or RHF references. Instabilities which occur in rCCD theory due to the calculation of triplet or spin-flipped amplitudes are thus avoided, improving convergence and expanding the applicability. In general, the perturbative +F12 correction is recommended for both drCCD and rCCD as a cost-efficient alternative to the corresponding (F12) variant, given the fact that deviations between the two approaches are negligible for both atomization and interaction energies. Higher-order terms can thus be considered as unimportant when regarding the effective basis-set dependence. However, the contributions are necessary to ensure smooth convergence and to avoid spurious error cancellation. The results of the preceding sections thus prove once more that the additive second-order correction, which was introduced in Chapter 2, is promising, accelerating convergence while the computation

times are insignificant in comparison to the otherwise required self-consistent HF or KS calculation within the larger basis set. To ensure that the basis-set error in the reference energy is of the same order of magnitude than the error in the correlation energy, the +F12 schemes should furthermore be applied in combination with the CABS-singles correction, see Section 2.3.
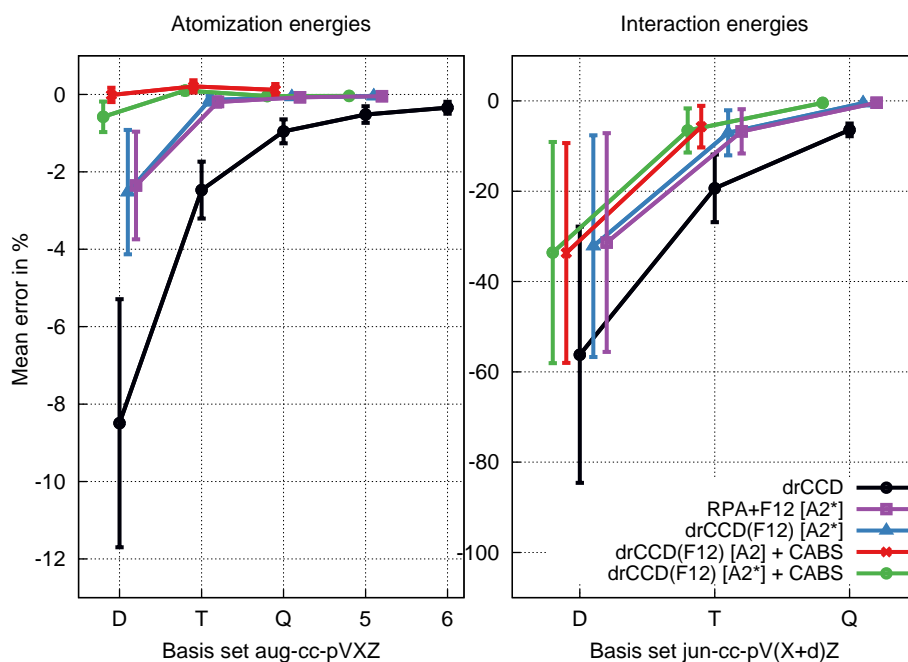
Fig. 4.10: drCCD approaches: Mean errors in percent for total atomization energies and counterpoise-corrected interaction energies.
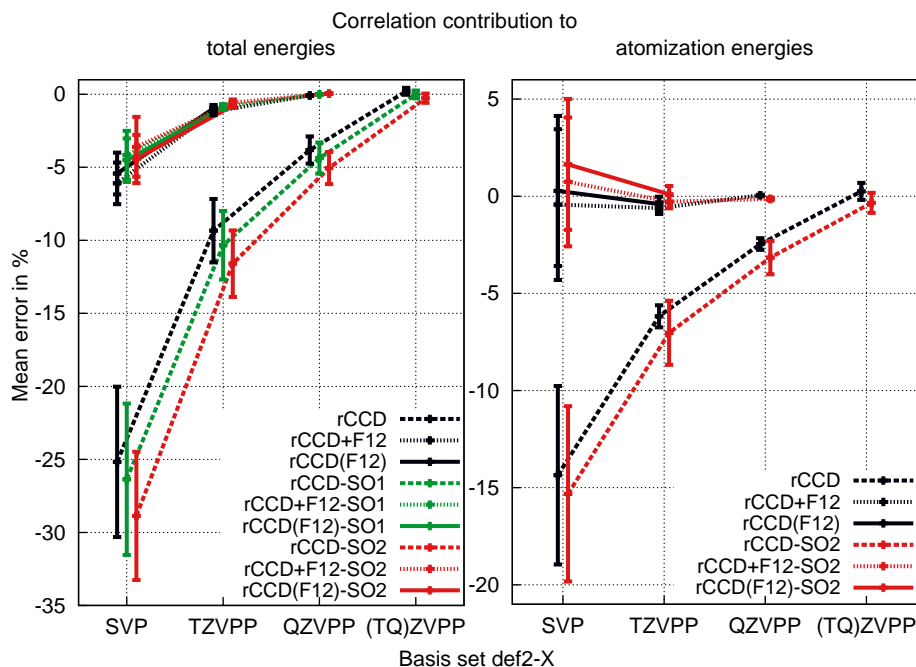
Fig. 4.11: rCCD approaches: Mean errors in percent for correlation energies and the correlation contribution to atomization energies.

5. Diagnostics for random-phase approximation methods

It is well-known that single-reference methods, which are designed to capture dynamic correlation, fail for systems where static correlation plays a significant role, leaving the field to multireference approaches. The latter are however restricted to applications on small systems due to the larger computational costs. It is therefore desirable to set up robust diagnostic schemes which allow to quantify the multireference character of the examined system and thus falsify the applicability of single-reference schemes. Several approaches have been developed in the last decades, which range from density-functional theory [244, 245] to wave-function methods including Møller-Plesset perturbation [246], coupled-cluster [247–249] or configuration interaction approaches [250]. The strategies of the various diagnostics are versatile:

Some approaches rely on characteristic features of the examined single-reference method. The T_1 and D_1 diagnostics e.g. are based on different norms of the single excitation amplitudes [247, 249, 251]; analogous T_2 and D_2 diagnostics refer to the corresponding double excitation vectors [248, 252]. Closely related is the $\%T_1$ measure for the contribution of single excitations to the norm of the excitation amplitudes [253] and the energy-based %TAE diagnostics, analyzing the importance of triple, quadruple or quintuple excitations [254, 255]. To quantify static correlation within density-functional theory, the B_1 diagnostics was proposed to ascertain the multireference character in a bond, taking the difference between two binding energies, one calculated with a GGA functional, the other with a hybrid functional [256]. It is thus assumed that the impact of exact exchange in hybrid functionals indicates multireference character, based on the knowledge that HF exchange is inaccurate for multi-configurational systems. A similar diagnostic for density-functional approaches regarding total atomization energies was suggested by Martin *et al.* [244].

A second ansatz for diagnostic schemes is to base the examination not on a single-reference, but rather a multiconfigurational approach as only the latter can capture static correlation and therefore help to gauge other quantities or methods. A common diagnostic is the square of the leading CI coefficient in CISD or CASSCF calculations [257, 258]. Apart from the mentioned diagnostics, a variety of other popular schemes exist, based e.g. on natural orbital occupation numbers [259–262] or orbital entanglement [263–265]. The spectrum of mentioned diagnostics indicates that none of the approaches is sufficient to detect and quantitatively predict static correlation. As shown e.g. by Wilson *et al.*, a composite scheme comprising several diagnostics is required to enable a robust classification [266, 267]. Several recommendations on how to combine or complement the existing analysis schemes can be found in the literature, see e.g. Refs. [248, 268]. The aim of the following chapter is thus not to set up a new diagnostics which can be regarded as sufficiently accurate, but to investigate if the diagnostic tools of coupled-cluster theory can be transferred to random-phase approximation methods. The focus is on the D_1 and D_2 diagnostics as suggested by Nielsen and Janssen [247, 248]. The scheme is implemented in the CCSDF12 module of TURBOMOLE and in the KOALA program package to allow first benchmark calculations on the original test set of Nielsen and Janssen.

5.1 D_1 and D_2 diagnostics based on dRPA excitation amplitudes

The motivation for taking the singly-excited amplitudes as central quantity in D_1 diagnostics is based on the fact that the amplitudes describe orbital relaxation [269] and therefore the appropriateness of the utilized molecular orbitals. As this concept assumes that multireference character can be associated with the choice of molecular orbitals (in contrast to other definitions of static correlation which define this characteristic feature as an intrinsic trait of multireference systems that cannot be cured by orbital relaxation), the diagnostics schemes cannot yield, by definition, a sufficiently extensive analysis to capture and detect all problematic systems. The D_1 diagnostics would, e.g., fail if not singly but higher excited determinants are required to describe the wave function. Nielsen and Janssen therefore suggested a complementary D_2 diagnostics [248], based on the double-excitation amplitudes as provided within the underlying CCD or CCSD method. The

density matrix of the single or double excitation amplitudes, t_i^a or t_{ij}^{ab}, is constructed and diagonalized to obtain the root of the largest eigenvalue $\lambda_{\max}$,

$$D_1 = \sqrt{\max\left(\lambda_{\max}\left[\sum_i t_i^a t_i^b\right], \lambda_{\max}\left[\sum_a t_i^a t_j^a\right]\right)}, \tag{5.1}$$

$$D_2 = \sqrt{\max\left(\lambda_{\max}\left[\sum_{ijc} t_{ij}^{ac} t_{ij}^{bc}\right], \lambda_{\max}\left[\sum_{kab} t_{ik}^{ab} t_{jk}^{ab}\right]\right)}. \tag{5.2}$$

Due to the connection of dRPA and CC theory, the single excitation amplitudes $\mathbf{X}$ and $\mathbf{Y}$ can be related to the doubles amplitude matrix $\mathbf{T}$, see Eq. (2.10) of Chapter 2. Since Eq. (5.2) is not restricted to a specific CC approach, it can be applied using the drCCD amplitudes. Analogously, D_1 diagnostics can be based on matrix $\mathbf{Y}$,

$$D_1(\mathrm{dRPA}) = \sqrt{\max\left(\sum_n \lambda_{\max}\left[\sum_i Y_{ai}^n Y_{bi}^n\right], \lambda_{\max}\left[\sum_a Y_{ai}^n Y_{aj}^n\right]\right)}. \tag{5.3}$$

Note that ground-state correlation is standardly related to the contribution of $\mathbf{Y}$, as $\mathbf{Y}$ cancels to zero within the Tamm-Dancoff approximation, but not within dRPA. From a conceptual point of view, it is thus more well-founded to use the eigenvector $\mathbf{Y}$ instead of $\mathbf{X}$. Nevertheless, a corresponding diagnostics based on matrix $\mathbf{X}$ was tested and proven to yield meaningless values. Results for $\mathbf{X}$ are thus not reported in the following and $D_1(\mathrm{dRPA})$ always refers to $\mathbf{Y}$.

Evaluation for main-group compounds and comparison with standard CC diagnostics

To validate the performance of the proposed D_1 and D_2 analysis, Nielsen and Janssen performed test calculations on a set of 34 closed-shell molecules, selected to represent both dynamical and non-dynamical correlation effects. A list of the examined compounds comprising the main-group elements C, O, N, F, Cl, H, P, S, and Si is given in Appendix F. Both bond distances and harmonic vibrational frequencies at the level of MP2 and CCSD theory were compared to CCSD(T) results, premising that the latter agree with experiment and thus exploiting that errors due to basis-set deficiency, neglect of core correlation or anharmonicity are abstracted. It was shown that the percentage error for bond lengths and vibrational frequencies in comparison to CCSD(T) results corresponds to the so-obtained D_1 and D_2 values. More precisely, large errors were only encountered for large diagnostics, not excluding large diagnostics for test cases with small errors. The thresholds of $D_1(\mathrm{MP2}) < 0.015$, $D_1(\mathrm{CCSD}) < 0.020$, $D_2(\mathrm{MP2}) < 0.15$ and $D_2(\mathrm{CCSD}) < 0.15$ are proposed as limits which guarantee a reliable performance, ensuring errors of less than 0.6% (0.7% for MP2 (CCSD) bondlengths and of less than 3.0% (1.3%) for MP2 (CCSD) vibrational frequencies. Inadequate values were found for $D_1(\mathrm{MP2}) > 0.040$, $D_1(\mathrm{CCSD}) > 0.050$, $D_2(\mathrm{MP2}) > 0.17$ and $D_2(\mathrm{CCSD}) > 0.18$, respectively. In summary, the authors of Refs. [247, 248] also note that a stronger correlation between performance and the size of the diagnostic can be assigned to CCSD than to MP2 theory.

To assess the performance of the proposed dRPA diagnostics, Eqs. (5.3) and (5.2) were implemented in the KOALA program package [205] and in the CCSDF12 and MPGRAD module of the TURBOMOLE program package [71]. To enable highly accurate KS calculations using the KOALA program, numerical integration grids were extended to the finest grid 7 [270]. Apart from efficiency, both implementations in TURBOMOLE and KOALA only differ slightly when comparing D1 diagnostic resuls obtained with KOALA and the MP-GRAD module, given that the latter does not exploit resolution of the identity approximations. For the sake of consistency, the presented D_2 values were therefore obtained with the implementation in TURBOMOLE, while D_1 values were calculated with KOALA. CCSD, CCSD(T) and CCSDT geometry optimizations as well as the corresponding analytical frequency calculations were performed with the CFOUR program package [271, 272] using tight convergence criteria for both geometry optimizations as well as SCF and CC calculations. dRPA geometries were obtained with the RIRPA gradient module of TURBOMOLE [273]. Due to the restriction of the RIRPA gradient code, core correlation had to be taken into account and, consistently, the cc-pwCVTZ basis set [274] was chosen for the presented benchmark study. Harmonic vibrational frequencies were calculated from finite differences of the analytical dRPA gradients using the NUMFORCE module [275, 276]. HF, PBE and PBE0 references were tested as input for the dRPA correlation treatment; the so-obtained results are indicated as dRPA/PBE and dRPA/PBE0, respectively. Detailed results are summarized in Tables F.1 to F.3 of Appendix F, reporting bond distances and vibrational frequencies as well as the corresponding D_1 and D_2 measures.

Figure 5.1 shows the correlation of D_2(dRPA) diagnostics with respect to the percentage error of bond lengths and vibrational frequencies using a HF reference determinant. Results corresponding to molecules containing elements of the 2nd row of the periodic table are coloured in light red in order to distinguish them from the 3rd row analogues, indicated with black crosses. The plot highlights that small D_2 values up to a threshold of 0.09 ensure a percentage error of less than 0.2% for bond lengths. Comparatively large errors are found for the same threshold when regarding vibrational frequencies, on the right-hand side of Figure 5.1. Here, an error of 7.3% is found for ammonia already for the relatively small D_2 reference of 0.09. Furthermore, the error increases quickly, reaching a hight of 9.9% for BeO at $D_2 = 0.10$ and maximum errors of up to 23.5 % for flourine. The latter result even exceeds the plotted error range. These huge values might appear questionable, however, it is already stated in Ref. [247] that the halogens show relatively large errors in the analogous D_2(CCSD) study. Off-scale values are also equally found for some test cases, amounting e.g. up to an error of 94% for O_3 when regarding harmonic frequencies. Of course, the data of Ref. [247] refers to the cc-pVTZ basis and a straight comparison of D_2(CCSD) and D_2(dRPA) diagnostics should be based on the same basis set. CCSD results within the cc-pwCVTZ basis are therefore reported in Table F.4 of Appendix F; the corresponding plots are given in Figure F.1. In comparison, the D_2(CCSD) diagnostics are shifted to larger values in the range of $0.12 < D_2(\text{CCSD}) < 0.37$, while D_2(dRPA) lies between 0.08 and 0.14, indicating that new trust regions have to be defined for the dRPA variant. The scattering of the data points however is comparable for both methods, lacking indeed a straight, linear correlation between D_2 values and percentage errors, but allowing to define D_2 limits which guarantee a reliable performance. Indeed, a nearly linear dependence between D_2(CCSD) and D_2(dRPA) diagnostics is found, as shown on the right-hand side of Figure 5.3.

The analysis of the D_1 diagnostics appears more biased: In Figure 5.2, the D_1(dRPA) results are plotted against the already discussed percentage errors in bond lengths (left-hand side) and vibrational frequencies (right-hand side). While the error in the bond distance appears to be correlated with the D_1(dRPA) values, the plot for harmonic frequencies gives the impression of randomly scattered data points. Nevertheless, the agreement between D_1(dRPA) and D_2(dRPA) diagnostics is reasonable, as shown by the scattering plot of Figure 5.4. The corresponding graphs for D_1(CCSD), given in Figure F.2 of Appendix F, show a better correlation between D_1(CCSD) and the magnitude of the corresponding percentage errors. A scattering plot contrasting D_1(dRPA) with D_1(CCSD) is furthermore flawed by two outliers, coloured in green. Based on the presented results, which indicate on the one side an arbitrary scattering and on the other side a clear correlation between D_1(dRPA) and D_2(dRPA), the appropriateness of the D_1(dRPA) diagnostics cannot be falsified for harmonic frequencies and thus remains to be investigated. For bond lengths, however, it seems to be reasonable to define a D_1(dRPA) threshold of 0.03 corresponding to percentage errors of less than 2%.

Since dRPA is standardly applied using KS references, a short discussion of an analogous study using PBE and PBE0 references suggests itself. The corresponding data is depicted in Figures F.3, F.4, F.5, and F.6 in Appendix F. In summary, PBE references perform best, allowing to set up D_2(dRPA) and D_1(dRPA) thresholds for both bond lengths and vibrational frequencies. PBE0 results are comparable to the corresponding HF values: while the error in the bond lengths seems to be reflected by the D_1 and D_2 diagnostics, no clear correlation can be found for vibrational frequencies. In general, D_1(dRPA) and D_2(dRPA) values increase in magnitude when going from HF over PBE0 to PBE.
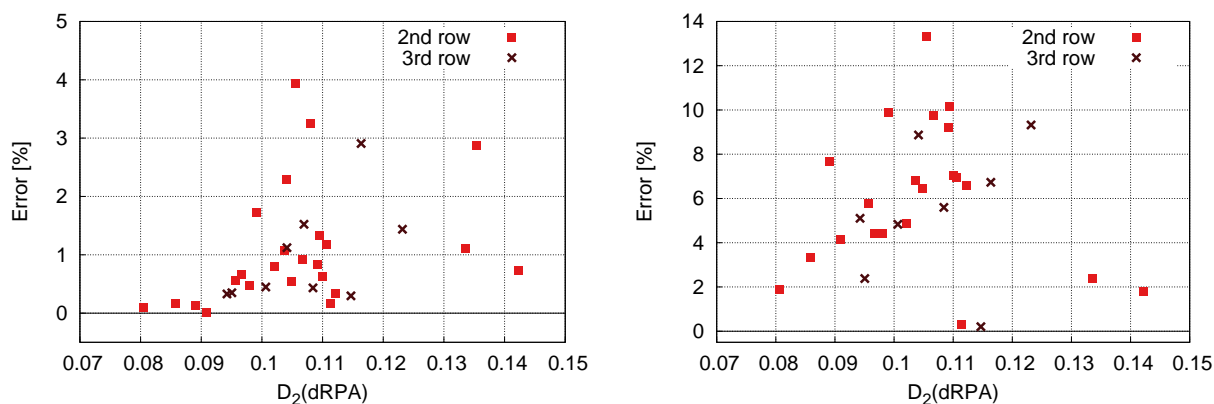
Fig. 5.1: D_2 diagnostics for bond lengths (left-hand side) and vibrational frequencies (right-hand side) using a HF reference, corresponding to Table F.1 of Appendix F. Due to the large error range for vibrational frequences, the following test cases with [Error(%)/D2(dRPA)] are not included in the plot on the right-hand side: O_3 with [18.0%/0.14], F_2 with [23.5%/0.11], FOH with [15.7%/0.10] and Cl_2O with [19.2%/0.10].
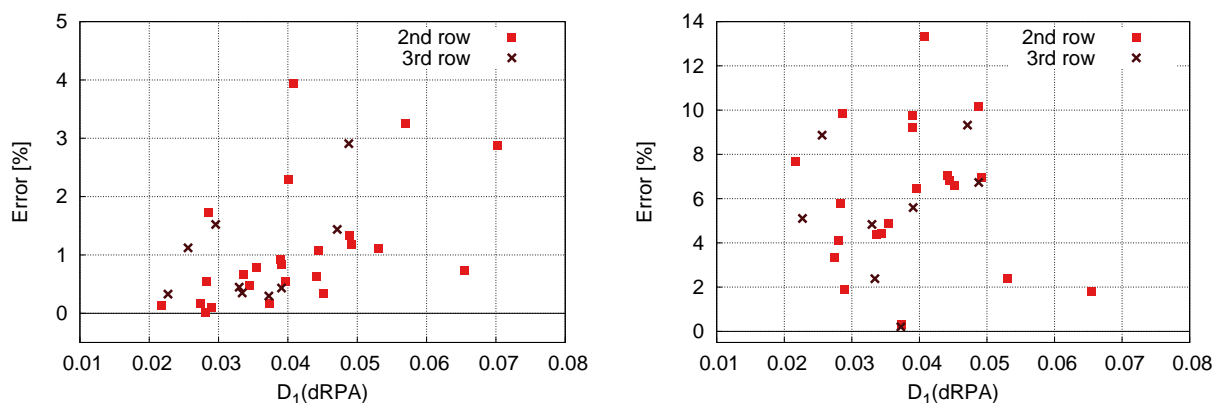
Fig. 5.2: D_1 diagnostics for bond lengths (left-hand side) and vibrational frequencies (right-hand side) using a HF reference, corresponding to Table F.1 of Appendix F. Analogously to Figure 5.1, the following test cases are omitted in the plot on the right-hand side: O_3 with [18.8%/0.07], F_2 with [23.5%/0.06], FOH with [15.7%/0.04] and Cl_2O with [19.2%/0.03].
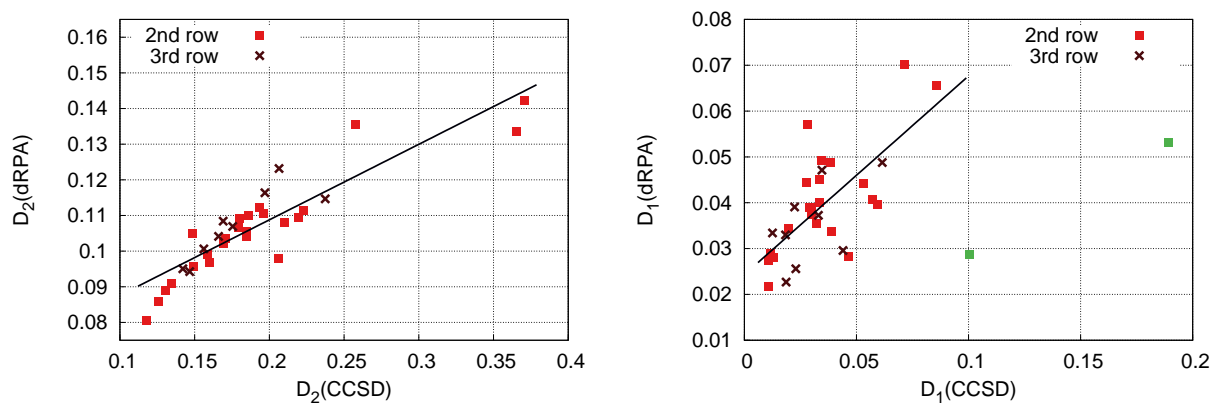
Fig. 5.3: Scattering plot of D_2(dRPA) versus D_2(CCSD) and D_1(dRPA) versus D_1(CCSD) diagnostics. The slope of the trendline for the comparison of D_2 (D_1) diagnostics is 0.21 (0.43) with an intercept of 0.066 (0.024). The trendline on the left-hand side is obtained without considering the green-coloured data points.
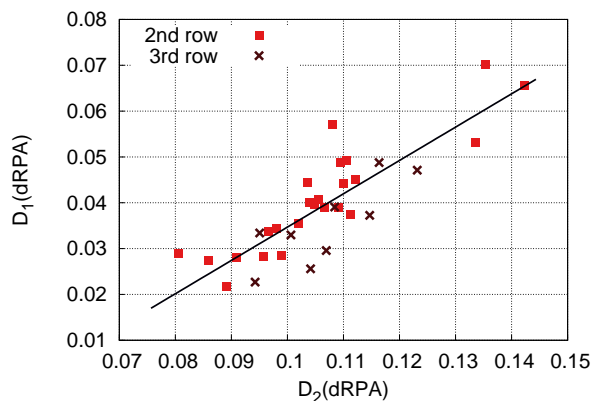
Fig. 5.4: Scattering plot contrasting the D_1(dRPA) and D_2(dRPA) diagnostics. The slope of the trendline is 0.73 with an intercept of -0.038.

5.2 Conclusions

Based on the presented results, it is possible to define thresholds for the D_2(dRPA) and D_1(dRPA) diagnostics, as summarized in Table 5.1. To allow a straightforward comparison with the established diagnostic limits of MP2 and CCSD theory, the MP2 and CCSD error ranges as well as the corresponding D_2 or D_1 thresholds are reported as well, taken from Refs. [247, 248]. Nielsen and Janssen assigned a trust region for each diagnostic scheme by specifying minimum and maximum D_1 or D_2 measures. However, for dRPA diagnostics, it seems in most cases more appropriate to define one threshold only, given that the corresponding percentage errors do not rise gradually but rather abruptly with increasing D_2 and D_1 values. Regarding the limits in detail, it can be concluded that D_2(dRPA) and D_1(dRPA) diagnostics do not seem to be redundant and moreover that a stronger correlation between performance and the size of the diagnostics is found when treating double excitations as done within D_2(dRPA). The results for PBE references are most convincing, allowing to set up tresholds for both D_1(dRPA) and D_2(dRPA) contemplating bond lengths as well as vibrational frequencies. In particular, a final trust region of $< 0.16 / 0.6\%$ and $> 0.18 / 1.5\%$ is obtained when regarding bond distances; thr error in vibrational frequencies is less than 3.0% for diagnostic measures smaller than 0.15. The latter can thus be defined as general threshold for D_2(dRPA) when using PBE references. For the related D_1(dRPA) diagnostics, a limiting value of 0.050 ensures errors that differ less than 0.6% or 2.5% from the reference value for bond lengths or harmonic frequencies, respectively. However, given that only a relatively small test set of main-group compounds was investigated, it is necessary to perform more extensive studies regarding for instance diradicals and bond dissociation to allow for a more robust and well-founded calibration. It also remains to be investigated if it is sufficient to base the analysis on correlation energies and if a reliable prediction based on dRPA diagnostics is possible when treating geometries within density-functional theory and solely performing a subsequent dRPA single-point calculation. If that were the case, the diagnostics could help to validate and establish RPA applications on small-gap systems over the entire periodic table.

Tab. 5.1: Percentage errors and corresponding D_2 and D_1 thresholds, calibrated for main-group compounds based on the test set of Refs. [247, 248].

Diagnostics	Percentage error
	Bond lengths
D_2(MP2)[a]	$< 0.15 / 0.6\%$ and $> 0.17 / 2.0\%$
D_2(CCSD)[a]	$< 0.15 / 0.7\%$ and $> 0.18 / 1.2\%$
D_2(dRPA)/HF	$< 0.09 / 0.2\%$
D_2(dRPA)/PBE	$< 0.16 / 0.6\%$ and $> 0.18 / 1.5\%$
D_2(dRPA)/PBE0	$< 0.13 / 1.0\%$
D_1(MP2)[b]	$< 0.015 / 0.6\%$ and $> 0.040 / 1.3\%$
D_1(CCSD)[b]	$< 0.020 / 0.3\%$ and $> 0.050 / 1.5\%$
D_1(dRPA)/HF	$> 0.030 / 2.0\%$
D_1(dRPA)/PBE	$< 0.050 / 0.6\%$ and $> 0.080 / 1.5\%$
D_1(dRPA)/PBE0	$> 0.060 / 1.5\%$
	Vibrational frequencies
D_2(MP2)[a]	$< 0.15 / 3.0\%$ and $> 0.17 / 8.0\%$
D_2(CCSD)[a]	$< 0.15 / 1.0\%$ and $> 0.18 / 7.0\%$
D_2(dRPA)/HF	$< 0.04 / 2.0\%$
D_2(dRPA)/PBE	$< 0.15 / 3.0\%$
D_2(dRPA)/PBE0	—
D_1(MP2)[b]	$< 0.015 / 2.9\%$ and $> 0.040 / *$
D_1(CCSD)[b]	$< 0.020 / 1.3\%$ and $> 0.050 / *$
D_1(dRPA)/HF	—
D_1(dRPA)/PBE	$< 0.050 / 2.5\%$
D_1(dRPA)/PBE0	—

[a] taken from Ref. [248]; [b] taken from Ref. [247].

*The corresponding error threshold is not specified in Ref. [247].

6. Summary

The aim of this thesis was to tackle an important drawback of a wave-function method called random-phase approximation (RPA): RPA suffers as all orbital-based methods from the slow convergence of the correlation energy with respect to the size of the basis set. The unfavorable basis-set dependence implicates the need for large basis sets with high angular momentum quantum numbers in order to ensure reliable results. Furthermore, the basis-set superposition error can become dominant, in particular when regarding weakly interacting systems, a research field for which RPA is known to perform best. Applications on larger systems throughout the periodic table are thus hindered even though the method was proven to be a promising post-Kohn Sham approach capturing long-range dynamic as well as static correlation. The topic of the presented thesis was therefore focused on overcoming these shortcomings by combining RPA with the explicitly correlated wave-function ansatz of F12 theory.

In Chapter 2, perturbative +F12 approaches [180, 181, 217] were presented based on the well-established MP2-F12 method. The additive correction proved to be efficient, exhibiting a scaling proportional to N^5 with respect to the system size N. It can be combined with various beyond-RPA approaches, as demonstrated for the exchange methods AXK+F12 and ACSOSEX+F12. The additive scheme was implemented in the RICC2 and CCSDF12 modules of the TURBOMOLE program package. Test calculations regarding correlation, atomization and interaction energies demonstrated that explicitly correlated triple- or quadruple-zeta results outperform conventional quintuple-zeta calculations, being comparable to extrapolated limits obtained from basis sets of quadruple- and quintuple-zeta quality. Furthermore, it was shown that the error in the Kohn-Sham reference energy can be reduced by one order of magnitude when taking into account singles excitations into the complementary auxiliary basis (CABS), standardly referred to as CABS-singles correction [180].

A disadvantage of the perturbative +F12 correction can be seen in the unsteady basis-set convergence of the correlation energy reflecting that the convincing performance of the +F12 ansatz relies on error cancellation. To overcome such shortcomings, more sophisticated explicitly correlated RPA variants were investigated:

In Chapter 3, the RPA-F12 method was derived starting from the equations of motion and explicit correlation was introduced by incorporating the geminal excitation manifold in the chosen reference state. It was shown that single excitations into the CABS basis are required to obtain a symmetric eigenvalue problem. The ansatz was validated based on a pilot implementation in the KOALA program package for a small test set of closed-shell main-group compounds, indicating that an overall gain of about one cardinal number can be achieved for the def2-basis sets. The ansatz was thus shown to be comparable to a dual basis-set approach, if the latter implies a Hartree-Fock calculation within the conventional orbital basis and a correlation treatment within the combined orbital and CABS basis.

Various explicitly correlated ring coupled-cluster (rCC) approaches were outlined in Chapter 4 [156, 180]. The presented ansätze exploit the fact that the RPA eigenvalue problem can be recast into a residual equation for double excitation amplitudes and that the so-defined ring coupled-cluster doubles (rCCD) approach yields an equivalent expression for the RPA correlation energy. A diagrammatic interpretation of the rCC approximation enables a consistent derivation of the working equations for both direct rCCD(F12) and the corresponding rCCD(F12) ansatz including exchange. The drCCD(F12) implementation in the CCSDF12 module of the TURBOMOLE program package was based on the already available explicitly correlated coupled-cluster singles doubles (CCSD(F12)) code. Benchmark calculations for a test set of 106 molecules and the S22 database on weakly interacting dimers showed that triple-zeta basis sets are sufficient to achieve convergence to within 99% of the basis-set limit for atomization energies, while quadruple-zeta basis sets are required when investigating long-range forces. The (F12) method proved to be more robust than the perturbative +F12 correction, demonstrating smooth convergence to the basis-set limit when coupling between conventional and geminal amplitudes is taken into account. In addition to drCCD(F12), three different rCCD(F12) methods were set up to investigate the impact of exchange: Whereas the inclusion of exchange is straight-forward for open-shell references, it necessitates spin adaptation in terms of singlet and triplet amplitudes for an analogous closed-shell formulation. The exact rCCD(F12) variant as well as two approximate schemes, rCCD(F12)-SO1 and rCCD(F12)-SO2, were derived and implemented in the KOALA program package for both open- and

closed-shell systems supporting Hartree-Fock as well as Kohn-Sham references. Results for correlation and atomization energies demonstrated that rCCD(F12)-SO2 outperforms both rCCD(F12) and rCCD(F12)-SO1, showing equally fast basis-set convergence while being at the same time insensible to triplet instabilities and most efficient in terms of computation times. In analogy to drCCD(F12), all three explicitly correlated rCCD(F12) approaches accelerate basis-set convergence in comparison to the conventional schemes, reaching 99% of the basis-set limit for triple-zeta basis sets.

To assess the applicability of RPA methods and to outline possible applications of the developed rCCD(F12) approaches, two wave-function diagnostic schemes were presented in Chapter 5. It was shown that established diagnostic tools, which are standardly used within coupled-cluster theory to validate the performance of truncated wave-function approaches like MP2 or CC2, are transferable to direct RPA. D_2 and D_1 diagnostics were implemented and the reliability was proven for direct RPA based on a small test set of closed-shell molecules, representing both dynamic and static correlation effects. Regarding the accordance between the diagnostic measures and the percentage errors in bond lengths and vibrational frequencies allowed to calibrate threshold values for Hartree-Fock, PBE and PBE0 references.

The developed wave-function approaches outline possible strategies on how to improve the efficiency and to clarify the applicability of RPA, an approximation which combines three ambitious qualities of the ideal wave-function method — efficiency, accuracy and applicability — in a favorable ratio. As the research field of beyond-RPA approaches is growing rapidly, the presented explicitly correlated RPA ansätze might be of further use, e.g. in combination with local correlation methods or symmetry-adapted perturbation theory.

7. Zusammenfassung

Das Ziel dieser Arbeit war es, ein wesentliches Problem einer Wellenfunktionsmethode namens Random-Phase-Approximation (RPA) zu bearbeiten: Wie alle Methoden, die auf Orbitalen basieren, leidet auch RPA unter der langsamen Konvergenz der Korrelationsenergie hinsichtlich der Größe des Basissatzes. Durch diese unvorteilhafte Basissatzabhängigkeit bedarf es großer Basissätze mit hohen Drehimpulsquantenzahlen um zuverlässliche Ergebnisse zu gewährleisten. Zudem kann der Fehler durch die Überlagerung von Basissätzen an Bedeutung gewinnen, insbesondere wenn schwach wechselwirkende Systeme betrachtet werden — ein Forschungsgebiet, für das RPA bekanntlich am besten geeignet ist. Anwendungen an größeren Systemen innerhalb des gesamten Periodensystems werden dadurch erschwert, obwohl sich die Methode als vielversprechender Post-Kohn-Sham-Ansatz erwiesen hat, der langreichweitige dynamische als auch statische Korrelation beschreibt. Gegenstand der vorgestellten Arbeit war es daher, diese Nachteile durch die Kombination von RPA mit dem explizit korrelierten Wellenfunktionsansatz der F12-Theorie zu überwinden. In Kapitel 2 wurden störungstheoretische +F12-Ansätze [180, 181, 217] vorgestellt, welche auf der bewährten MP2-F12-Methode basieren. Die additive Korrektur erweist sich als effizient und skaliert proportional zu N^5 mit zunehmender Systemgröße N. Sie kann mit verschiedenen, auf RPA aufbauenden Ansätzen kombiniert werden, wie für die Austauschmethoden AXK+F12 und ACSOSEX+F12 gezeigt wurde. Der additive Ansatz wurde in die Module RICC2 und CCSDF12 des TURBOMOLE-Programmpakets implementiert. Testrechnungen zu Korrelations-, Atomisierungs- and Wechselwirkungsenergien zeigten, dass explizit korrelierte triple-zeta- und quadruple-zeta-Ergebnisse die konventionellen quintuple-zeta-Berechnungen übertreffen und vergleichbar sind mit extrapolierten Grenzwerten, welche mit Basissätzen von quadruple- und quintuple-zeta-Qualität erhalten wurden. Zudem wurde gezeigt, dass der Fehler in der Kohn-Sham-Referenzenergie um eine Größenordnung reduziert werden kann, wenn Einfachanregungen in die komplementäre Hilfsbasis (*complementary auxiliary basis*, CABS) berücksichtigt werden. Dieses Verfahren wird standardmäßig als CABS-Singles-Korrektur bezeichnet [180].

Ein Nachteil der störungstheoretischen +F12-Korrektur kann in der unsteten Basissatzkonvergenz der Korrelationsenergie gesehen werden, welche verdeutlicht, dass die überzeugenden Ergebnisse des +F12-Ansatzes auf Fehlerkompensation beruhen. Um diese Defizite zu überwinden, wurden technisch aufwändigere explizit korrelierte RPA-Varianten untersucht:

In Kapitel 3 wurde die RPA-F12-Methode ausgehend von den Bewegungsgleichungen hergeleitet und explizite Korrelation eingeführt, indem Anregungen in den Geminalraum in der Beschreibung des gewählten Referenzzustandes berücksichtigt wurden. Es wurde gezeigt, dass Einfachanregungen in die CABS-Basis erforderlich sind um ein symmetrisches Eigenwertproblem zu erhalten. Der Ansatz wurde anhand einer Pilot-Implementierung im KOALA-Programmpaket für einen kleinen Testsatz von geschlossenschaligen Verbindungen der Hauptgruppenelemente getestet. Es zeigte sich, dass im Falle der def2-Basissätze ein Gewinn von einer Kardinalzahl erzielt werden kann. Der Ansatz erwies sich damit als vergleichbar mit einem Dual-Basis-Set-Ansatz (Ansatz unter Verwendung zweier Basissätze), wenn letzterer eine Hartree-Fock-Rechnung mit konventioneller Orbitalbasis und eine Korrelationsrechnung mit kombinierter Orbital- und CABS-Basis umfasst.

In Kapitel 4 wurden mehrere explizit korrelierte Ring-Coupled-Cluster-Verfahren (rCC-Verfahren) behandelt [156, 180]. Die vorgestellten Ansätze machen von der Tatsache Gebrauch, dass das RPA-Eigenwertproblem in eine Residuengleichung für Zweifachanregungsamplituden umformuliert werden kann und dass die so definierte Ring-Coupled-Cluster-Doubles-Methode (rCCD-Methode) einen äquivalenten Ausdruck für die RPA-Korrelationsenergie liefert. Eine Darstellung der rCC-Näherung in Form von Diagrammen ermöglicht hierbei eine konsistente Herleitung der Arbeitsgleichungen für sowohl direktes rCCD(F12) als auch die entsprechenden rCCD(F12)-Ansätze unter Berücksichtigung der Austauschwechselwirkung. Die drCCD(F12)-Implementierung in das CCSDF12-Modul des TURBOMOLE-Programmpakets wurde aufgebaut auf den bereits vorhandenen, explizit korrelierten Coupled-Cluster-Singles-Doubles-Code (CCSD(F12)). Benchmark-Rechnungen für einen Testsatz von 106 Molekülen und für die S22-Datenbank über schwach wechselwirkende Dimere zeigten, dass triple-zeta-Basissätze ausreichen, um Atomisierungsenergien bis zu 99% des

Basissatzlimits zu konvergieren. Für die Betrachtung von langreichweitigen Kräften werden dahingegen quadruple-zeta-Basissätze benötigt. Im Vergleich zur störungstheoretischen +F12-Korrektur erwies sich die (F12)-Methode als robuster, da sie, bei Berücksichtigung der Kopplung zwischen konventionellen und Geminal-Amplituden, eine regelmäßige Konvergenz zum Basissatzlimit aufweist. Zusätzlich zu drCCD(F12) wurden drei verschiedene rCCD(F12)-Methoden entwickelt um den Einfluss der Austauschwechselwirkung zu untersuchen: Während für offenschalige Referenzen der Austausch ohne weitreichende Änderungen berücksichtigt werden kann, benötigt man für eine analoge geschlossenschalige Formulierung eine Spin-Adaptierung in Form von Singlet- und Triplet-Amplituden. Die exakte rCCD(F12)-Variante als auch zwei Näherungen, rCCD(F12)-SO1 und rCCD(F12)-SO2, wurden hergeleitet und im KOALA-Programmpaket implementiert, für offen- als auch geschlossenschalige Systeme sowie Hartree-Fock und Kohn-Sham-Referenzen. Ergebnisse für Korrelations- und Atomisierungsenergien zeigten, dass rCCD(F12)-SO2 sowohl rCCD(F12) als auch rCCD(F12)-SO1 übertrifft, da der Ansatz eine vergleichbar schnelle Basissatzkonvergenz aufzeigt, gleichzeitig aber auch unanfällig für Triplett-Instabilitäten und am effizientesten hinsichtlich der Rechenzeiten ist. Wie im Falle von drCCD(F12) beschleunigen alle drei explizit korrelierten rCCD(F12)-Ansätze die Basissatzkonvergenz im Vergleich mit den konventionellen Varianten und erreichen 99% des Basissatzlimits für triple-zeta-Basissätze.

Um die Anwendbarkeit der RPA-Methoden zu überprüfen und mögliche Anwendungen der entwickelten rCCD(F12)-Verfahren aufzuzeigen, wurden in Kapitel 5 zwei Wellenfunktionsdiagnostiken vorgestellt. Es wurde gezeigt, dass etablierte Diagnostik-Verfahren, welche standardmäßig im Rahmen der Coupled-Cluster-Theorie verwendet werden um genäherte Wellenfunktionsansätze wie MP2 oder CC2 zu überprüfen, auch auf direktes RPA angewendet werden können. D_2- und D_1-Diagnostiken wurden implementiert und die Zuverlässigkeit für direktes RPA anhand eines kleinen Testsatzes für geschlossenschalige Moleküle bewiesen. Die Testsysteme beschrieben dabei sowohl dynamische als auch statische Korrelationseffekte. Anhand der Übereinstimmung der Diagnostik-Werte mit den prozentualen Fehlern in Bindungslängen und Schwingungsfrequenzen konnten Grenzwerte für Hartree-Fock-, PBE- und PBE0-Referenzen festgelegt werden.

Die entwickelten Methoden skizzieren mögliche Strategien zur Steigerung der Effizienz und Untersuchung der Anwendbarkeit von RPA, einer Näherung, welche drei anspruchsvolle Eigenschaften der idealen Wellenfunktionsmethode — Effizienz, Genauigkeit und Anwendbarkeit — vorteilhaft vereint. Da das Forschungsgebiet der auf RPA aufbauenden Methoden rasch an Bedeutung gewinnt, könnten die vorgestellten explizit korrelierten RPA-Ansätze von weiterem Nutzen sein, zum Beispiel in Kombination mit lokalen Korrelationsmethoden oder symmetrieadaptierter Störungstheorie.

Appendix

A. Notation

Symbols and Intermediates

$\{i, j, k, l, \ldots\}$ and $\{a, b, c, d, \ldots\}$ indicate occupied and virtual orbitals, respectively. $\{x, y, v, w, \ldots\}$ denote the geminal basis, $\{p, q, r, s, \ldots\}$ the complete MO basis, $\{p'', q'', r'', s'', \ldots\}$ the CABS basis and $\{p', q', r', s', \ldots\}$ the combined MO and CABS basis. $\{a', b', c', d', \ldots\}$ correspond to orbitals of the combined virtual and CABS basis. The complete virtual space is indicated as $\{\alpha, \beta, \gamma, \delta, \ldots\}$ when referring to spatial orbitals and as $\{\mathbb{A}, \mathbb{B}, \mathbb{C}, \mathbb{D}, \ldots\}$ when referring to spin orbitals. Accordingly, $\{\mathbb{K}, \mathbb{L}, \mathbb{M}, \mathbb{N}, \ldots\}$ denote spin orbitals of the complete infinite basis and $\{\kappa, \lambda, \mu, \nu, \ldots\}$ the corresponding spatial orbitals. In general, spatial orbitals are indicated by lower case letters, $\{i, j, a, b, \ldots\}$, spin orbitals by capital letters $\{I, J, A, B, \ldots\}$.
The biorthogonal basis is chosen as defined in Ref. [144],

$$\langle \bar{{}^a_i}| = \frac{1}{2} \langle {}^a_i| \,, \tag{A.1}$$

$$\langle \overline{{}^{ab}_{ij}}| = \frac{1}{3} \langle {}^{ab}_{ij}| + \frac{1}{6} \langle {}^{ab}_{ji}| \,, \tag{A.2}$$

ensuring normalization of the overlap integrals,

$$\langle \bar{{}^a_i}|{}^c_k \rangle = \delta_{ac}\delta_{ik} \,, \tag{A.3}$$

$$\langle \overline{{}^{ab}_{ij}}|{}^{cd}_{kl} \rangle = \delta_{ac}\delta_{bd}\delta_{jl}\delta_{ik} + \delta_{bc}\delta_{ad}\delta_{il}\delta_{jk} \,. \tag{A.4}$$

$|{}^a_i\rangle$ and $|{}^{ab}_{ij}\rangle$ assign singly and doubly excited determinants, which are obtained by applying the corresponding excitation operators $\hat{E}_{pq}$ on the chosen reference state $|\Psi_0\rangle$,

$$|{}^a_i\rangle = \hat{E}_{ai}|\Psi_0\rangle \,, \tag{A.5}$$

$$|{}^{ab}_{ij}\rangle = \hat{E}_{ai}\hat{E}_{bj}|\Psi_0\rangle \,. \tag{A.6}$$

The excitation operators $\hat{E}_{pq}$ are defined as a linear combination of creation and annihilation operators, $\hat{a}^\dagger_p$ and $\hat{a}_p$, allowing a short notation for closed-shell references by summing over the two spin cases α and β,

$$\hat{E}_{pq} = \hat{a}^\dagger_{p\alpha}\hat{a}_{q\alpha} + \hat{a}^\dagger_{p\beta}\hat{a}_{q\beta} \,. \tag{A.7}$$

In accordance, the two-electron excitation operator is defined as $\hat{e}_{pqrs} = \hat{E}_{pq}\hat{E}_{rs} - \delta_{rq}\hat{E}_{ps}$. Throughout the thesis, this notation is restricted to the spin-free representation of closed-shell references; $\hat{a}^\dagger_P$ and $\hat{a}_P$ are used when referring to spin orbitals and open-shell references. Based on these definitions, the Hamiltonian operator can be written in the form

$$\hat{H} \stackrel{\text{UHF}}{=} \sum_{PQ} h_{PQ}\hat{a}^\dagger_P\hat{a}_Q + \frac{1}{2}\sum_{PQRS} g^{PR}_{QS}\hat{a}^\dagger_P\hat{a}^\dagger_R\hat{a}_S\hat{a}_Q + h_{\text{nuc}} \,, \tag{A.8}$$

$$\stackrel{\text{RHF}}{=} \sum_{pq} h_{pq}\hat{E}_{pq} + \frac{1}{2}\sum_{pqrs} g^{pr}_{qs}\hat{e}_{pqrs} + h_{\text{nuc}} \,, \tag{A.9}$$

when referring to open- and closed-shell references, respectively. h_{nuc} denotes the constant nuclear-nuclear contribution, h_{pq} and g^{pr}_{qs} the molecular one- and two-electron integrals.
The latter are defined as

$$g^{pr}_{qs} = \int\int \phi^*_p(r_1)\phi^*_r(r_2)\hat{g}_{12}\phi_q(r_1)\phi_s(r_2)dr_1 dr_2 = \langle pr|qs \rangle \,, \tag{A.10}$$

with the two-electron operator $\hat{g}_{12} = r^{-1}_{12}$.
f_{12} is the correlation factor; the integral over the Slater function is denoted $f^{xy}_{pq} = \langle xy|f_{12}|pq \rangle$. Spin-flipped functions are defined in terms of the rational generator $\hat{S}_{xy}$,

$$|\widetilde{xy}\rangle = \hat{S}_{xy}|xy\rangle = \tfrac{3}{8}|xy\rangle + \tfrac{1}{8}\hat{P}^{\text{flip}}_{xy}|xy\rangle \,, \tag{A.11}$$

where the permutation operator $\hat{P}^{\text{flip}}_{xy}$ flips the spatial part of the geminal while keeping the spin functions the same,

$$\hat{P}^{\text{flip}}_{xy}|x\sigma y\sigma'\rangle = |x\sigma y\sigma'\rangle + |y\sigma x\sigma'\rangle \,. \tag{A.12}$$

Throughout the thesis, F12 integrals are summarized in terms of the following intermediates,

$$\mathcal{V}_{ij}^{xy} = \langle xy|f_{12}\hat{Q}_{12}\hat{g}_{12}|ij\rangle \,, \tag{A.13}$$

$$(\mathcal{V}^{\dagger})_{xy}^{ij} = \langle ij|\hat{g}_{12}\hat{Q}_{12}f_{12}|xy\rangle \,, \tag{A.14}$$

$$\mathcal{X}_{vw}^{xy} = \langle xy|f_{12}\hat{Q}_{12}f_{12}|vw\rangle \,, \tag{A.15}$$

$$\mathcal{B}_{xy,vw}^{(ij)} = \langle xy|f_{12}\hat{Q}_{12}(\hat{F}_1 + \hat{F}_2 - \varepsilon_i - \varepsilon_j)\hat{Q}_{12}f_{12}|vw\rangle \,, \tag{A.16}$$

$$\mathcal{C}_{ab,xy}^{(ij)} = \langle ab|(\hat{F}_1 + \hat{F}_2 - \varepsilon_i - \varepsilon_j)\hat{Q}_{12}f_{12}|xy\rangle \,, \tag{A.17}$$

$$w_{xy}^{\alpha\beta} = \langle \alpha\beta|\hat{Q}_{12}f_{12}|xy\rangle \,, \tag{A.18}$$

$$(w^{\dagger})_{\alpha\beta}^{xy} = \langle xy|f_{12}\hat{Q}_{12}|\alpha\beta\rangle \,, \tag{A.19}$$

with the Fock or KS operator $\hat{F}$ and the projection operator $\hat{Q}_{12}$.

Diagrams

For a basic introduction into diagrammatics, the reader is referred to Refs. [121], [152] and [106] as well as the therein cited references. The notation and the algebraic assignment used for the diagrams of this thesis is chosen accordingly, explained in Figure A.1 for both ordinary and antisymmetrized Goldstone diagrams. Note that the reference state is not drawn explicitly. An incoming line is associated with an annihilation operator and an outgoing line with a creation operator, so that the two-electron integrals and double amplitudes are given as

$$g_{\text{left-in right-in}}^{\text{left-out right-out}} \,; \, t_{\text{left-in right-in}}^{\text{left-out right-out}} \,. \tag{A.20}$$

Standardly, closed-shell equations based on RHF references are represented by ordinary Goldstone diagrams referring to non-antisymmetrized two-electron integrals and depicting all exchange contributions separately (see for example Figure 2.4). However, in analogy to the identity

$$\tfrac{1}{2}g_{qs}^{pr}\hat{e}_{pqrs} = \tfrac{1}{4}(g_{qs}^{pr} - g_{sq}^{pr})\hat{e}_{pqrs} \,, \tag{A.21}$$

it is also possible and often more convenient to work with antisymmetrized Goldstone diagrams, representing the corresponding antisymmetrized two-electron integrals (see for example Figure 2.2). The rules to obtain the algebraic expressions for these two types of diagrams differ. For ordinary Goldstone diagrams, they can be summarized in four bullet points:

1. There is a weight factor 2 for each closed loop.

2. There is a weight factor $\frac{1}{2}$ for diagrams with left-right symmetry.

3. The phase factor is defined by the total number of holes (h) and loops (l), given as $(-1)^{h-l}$.

4. The permutation operator $\hat{P}_{ij}^{ab}$ accounts for the symmetry of spin-free amplitudes t_{ij}^{ab}.

For antisymmetrized Goldstone diagrams representing spin orbitals, the phase factor is obtained analogously by rule 3. Furthermore, the following rules hold:

1. A weight factor of $\frac{1}{2}$ is assigned for each pair of equivalent lines as well as for each pair of equivalent operators.

2. All distinct permutations of open lines are considered by introducing permutation operators.

It should be noted that the drCCD and rCCD diagrams require special interpretation rules due to the fact that the energy and amplitude equations cannot be derived starting from an appropriate wave function and applying Wick's theorem [155]. Therefore, standard notations which assign operators to graphical features, as done in Figure A.1, are unsuitable. However, a direct assignment relating lines and vertices to the corresponding integrals and amplitudes is possible, as done in Refs. [156, 180]. Furthermore, standard interpretation rules for antisymmetrized Goldstone diagrams referring to open-shell systems can only be applied when a) associating an additional factor of 2 with non-antisymmetrized integrals or geminal amplitudes and b) considering all distinct permutations of inequivalent external lines by including the permutation operator $\hat{P}_{IJ}^{AB} M_{IJ}^{AB} = M_{IJ}^{AB} + M_{JI}^{BA}$ instead of the standardly used $\hat{P}_{IJ}^{-}$ and $\hat{P}_{AB}^{-}$ operators with $\hat{P}_{IJ}^{-} M_{IJ}^{AB} = M_{IJ}^{AB} - M_{JI}^{AB}$

and $\hat{P}_{AB}^{-} M_{IJ}^{AB} = M_{IJ}^{AB} - M_{IJ}^{BA}$. For closed-shell systems, the interpretation rules of ordinary Goldstone diagrams can be used to extract the algebraic expressions for the drCCD energy and amplitude equations without requiring any further changes.
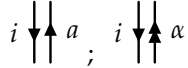
Feature	Algebraic expression	
	ordinary	antisymmetrized
$i \,\downarrow\!\!\uparrow\, a$; $i \,\downarrow\!\!\uparrow\, \alpha$	$\lvert^{a}_{i}\rangle, \langle^{a}_{i}\rvert \,;\, \lvert^{\alpha}_{i}\rangle, \langle^{\alpha}_{i}\rvert$	$\lvert^{A}_{I}\rangle, \langle^{A}_{I}\rvert \,;\, \lvert^{\mathbb{A}}_{I}\rangle, \langle^{\mathbb{A}}_{I}\rvert$
$\vdash\!\!-\!\!\times$	$F_{pq}\hat{E}_{pq}$	$F_{PQ}\hat{a}_{P}^{\dagger}\hat{a}_{Q}$
$\vdash\!\!-\!\!-\!\!\dashv$	$\frac{1}{2}g_{qs}^{pr}\hat{e}_{pqrs}$	$\frac{1}{4}(g_{QS}^{PR} - g_{SQ}^{PR})\hat{a}_{P}^{\dagger}\hat{a}_{R}^{\dagger}\hat{a}_{S}\hat{a}_{Q}$
$\bigvee\bigvee$	$\frac{1}{2}t_{ij}^{ab}\hat{E}_{ai}\hat{E}_{bj}$	$\frac{1}{4}t_{IJ}^{AB}\hat{a}_{A}^{\dagger}\hat{a}_{B}^{\dagger}\hat{a}_{J}\hat{a}_{I}$
$\bigwedge\!\!\bigwedge$	$f_{\alpha\beta}^{xy}\langle^{\alpha\beta}_{ij}\rvert$	$\frac{1}{2}(f_{\mathbb{A}\mathbb{B}}^{XY} - f_{\mathbb{B}\mathbb{A}}^{XY})\langle^{\mathbb{A}\mathbb{B}}_{IJ}\rvert$
$\bigvee\!\!\!\!\!\!\bigvee$	$\frac{1}{2}c_{ij}^{xy}f_{xy}^{\alpha\beta}\hat{E}_{\alpha x}\hat{E}_{\beta y}$	$\frac{1}{4}c_{IJ}^{XY}(f_{XY}^{\mathbb{A}\mathbb{B}} - f_{YX}^{\mathbb{A}\mathbb{B}})\hat{a}_{\mathbb{A}}^{\dagger}\hat{a}_{\mathbb{B}}^{\dagger}\hat{a}_{Y}\hat{a}_{X}$

Fig. A.1: Nomenclature for ordinary and antisymmetrized Goldstone diagrams representing spatial and spin orbitals, respectively.

B. Commonly used approximations within F12

Ansatz 1, 2* and 2: Projection operators and Brillouin conditions

The projection operators $\hat{Q}_{12}$ within ansatz 1 and ansatz 2 are defined as

$$
\begin{aligned}
\hat{Q}_{12}(\text{Ansatz 1}) &= (1-\hat{P}_1)(1-\hat{P}_2) \\
&\overset{\text{CABS}}{=} 1 - \hat{P}_1\hat{P}_2'' - \hat{P}_1''\hat{P}_2 - \hat{P}_1\hat{P}_2 = \hat{P}_1''\hat{P}_2'' \,,
\end{aligned}
\tag{B.1}
$$

$$
\begin{aligned}
\hat{Q}_{12}(\text{Ansatz 2}) &= (1-\hat{O}_1)(1-\hat{O}_2) - \hat{V}_1\hat{V}_2 \\
&\overset{\text{CABS}}{=} 1 - \hat{O}_1\hat{P}_2'' - \hat{P}_1''\hat{O}_2 - \hat{P}_1\hat{P}_2 = \hat{P}_1''\hat{V}_2 + \hat{V}_1\hat{P}_2'' + \hat{P}_1''\hat{P}_2'' \,,
\end{aligned}
\tag{B.2}
$$

where $\hat{V}$ is the projector onto the finite virtual space, $\hat{O}$ the projector onto the occupied space, $\hat{P}$ the projector onto the finite basis and $\hat{P}''$ the projector onto the CABS basis. In contrast to ansatz 1, ansatz 2 thus considers mixed double excitations into the CABS and virtual basis. Eqs. (B.1) and (B.2) imply that the projection onto the occupied space includes both inactive and active orbitals within the frozen-core approximation. Regarding the evaluation of matrix elements, it should be kept in mind that $\hat{Q}_{12}|ab\rangle$ is zero for both ansatz 1 and 2 because the CABS basis is chosen to be orthogonal to the orbital basis, $\langle p''|a\rangle = 0$.

Concerning the evaluation of Fock or KS matrix elements, it is furthermore common to distinguish between ansatz 2 and ansatz 2*, relying on the definition of the generalized and the extended Brillouin condition. The generalized Brillouin condition (GBC) [277] implies that the off-diagonal elements of the occupied-complete virtual space vanish and that the occupied orbitals are eigenfunctions of the Fock or KS operator in the combined MO and CABS basis (in case of canonical orbitals),

$$
F_{ip''} \approx 0 \;;\; F_{ip'} = \delta_{p'i}\varepsilon_i \,.
\tag{B.3}
$$

Ansatz 2* additionally avoids coupling terms between the virtual and the CABS basis, based on the extended Brillouin condition (EBC),

$$
F_{pp''} \approx 0 \;;\; F_{pp'} = \delta_{p'p}\varepsilon_p \,.
\tag{B.4}
$$

It should be furthermore noted that ansatz 2 is often dubbed ansatz 3 in the literature, see e.g. Ref. [278], reserving the first acronym for the projection onto $(1-\hat{O}_1)(1-\hat{O}_2)$.

Approximations for matrix $\mathcal{B}$ - implications for KS references

As explained in Refs. [105, 178, 179] for HF references, the F12 intermediate $\mathcal{B}$, as given in Eq. (A.16), has to be evaluated approximately in order to avoid numerical instabilities. Common approaches are denoted as ansätze A, A′, and B, specifying the treatment of exchange contributions, as well as approximations [T+V] and [J+K], labelling the different transformations for the kinetic energy term [92, 277]. It should be noted that ansatz C is also a common acronym in the literature, see e.g. Refs. [278, 279], however as it only differs from ansatz B in the treatment of RI and GBC, it is not discussed in particular. All other approximations are in the following briefly explained in order to highlight the differences for KS references.

Applying commutator rules (see Ref. [179]), matrix $\mathcal{B}$ can be partitioned into three contributions,

$$
\begin{aligned}
\mathcal{B}^{(ij)}_{xy,vw} = &\langle xy|\tfrac{1}{2}f_{12}\hat{Q}_{12}[\hat{F}_{12},f_{12}]|vw\rangle + \langle xy|\tfrac{1}{2}f_{12}\hat{Q}_{12}[\hat{F}_{12},\hat{Q}_{12}]f_{12}|vw\rangle \\
&+ \langle xy|\tfrac{1}{2}\left[f_{12}\hat{Q}_{12}f_{12}(\hat{F}_{12}-\varepsilon_{ij}) + (\hat{F}_{12}-\varepsilon_{ij})f_{12}\hat{Q}_{12}f_{12}\right]|vw\rangle \,.
\end{aligned}
\tag{B.5}
$$

For local KS references where the KS operator is given as the sum of the kinetic energy, the electron-core, the Coulomb and the exchange-correlation potential, $\hat{F}^{\text{KS}} = \hat{T} + \hat{V} + \hat{J} + \hat{V}_{\text{xc}}^{\text{local}}$, the first term of Eq. (B.5) simplifies due to the fact that both $\hat{J}$, $\hat{V}$ and $\hat{V}_{\text{xc}}^{\text{local}}$ are local and therefore commute with the correlation factor f_{12}. Solely the commutator over the kinetic energy operator $\hat{T}_{12}$ remains,

$$
\langle xy|\tfrac{1}{2}f_{12}\hat{Q}_{12}[\hat{F}_{12},f_{12}]|vw\rangle \overset{\text{local KS}}{=} \langle xy|\tfrac{1}{2}f_{12}\hat{Q}_{12}[\hat{T}_{12},f_{12}]|vw\rangle = T^{xy}_{vw} \,.
\tag{B.6}
$$

Approximations A′ and B are therefore identical, being originally defined for HF references in order to discriminate between the neglect (approximation A′) and the inclusion (approximation B) of the non-local exchange potential. The remaining kinetic energy term of Eq. (B.6) is evaluated analytically by inserting the chosen definition for the projection operator $\hat{Q}_{12}$ and by approximating the integral over the commutator

$[\hat{T}_{12}, f_{12}]$ introducing an additional resolution of the identity, as explained in Ref. [178]. The so-obtained one-electron integrals over $\hat{T}$ are numerically instable, and the kinetic energy operator $\hat{T}$ is therefore either replaced by $\hat{T} + \hat{V}$ or $\hat{T} + \hat{V} + \hat{J} = \hat{F} + \hat{K}$, two approximations which are accordingly denoted [T+V] and [F+K]. For local exchange-correlation functionals, both treatments are however identical as

$$[\hat{F} + \hat{K}, f_{12}] = [\hat{T} + \hat{V} + \hat{J} + \hat{V}_{xc}^{local}, f_{12}] = [\hat{T} + \hat{V}, f_{12}]. \tag{B.7}$$

Thus, for KS references with local exchange-correlation potentials, the discrimination between approximation A' and B as well as [T+V] and [F+K] is obsolete.

Within ansatz 2 assuming the GBC, the projection manifold of occupied orbitals represents eigenfunctions of the Fock or KS operator, reducing the second and the third term of Eq. (B.5) for both HF and KS references to

$$\langle xy| \tfrac{1}{2} \left[f_{12}\hat{Q}_{12}f_{12}(\hat{F}_{12} - \varepsilon_{ij}) + (\hat{F}_{12} - \varepsilon_{ij})f_{12}\hat{Q}_{12}f_{12} \right] |vw\rangle \overset{\text{GBC}}{=} \tfrac{1}{2}(\varepsilon_v + \varepsilon_w + \varepsilon_x + \varepsilon_y - 2\varepsilon_i - 2\varepsilon_j)\mathcal{X}_{vw}^{xy}, \tag{B.8}$$

$$\langle xy| \tfrac{1}{2} f_{12}\hat{Q}_{12}[\hat{F}_{12}, \hat{Q}_{12}]f_{12}|vw\rangle \overset{\text{GBC}}{=} (\mathcal{C}\mathbf{f})_{vw}^{xy}, \tag{B.9}$$

where matrices $\mathcal{X}$ and $\mathcal{C}$ are defined as in Eqs. (A.15) and (A.17). $\mathbf{f}$ denotes the integral matrix over the correlation factor; $\mathcal{C}\mathbf{f}$ is the corresponding contracted matrix over $\mathcal{C}$ and $\mathbf{f}$. In comparison to the already presented variant A', the third approximation A omits not only the exchange contributions in the kinetic energy term, but also the commutator term of Eq. (B.8). This contribution however cancels anyway — despite the underlying reference determinant — when implying fixed geminal amplitudes as defined in Eq. (B.24). Eq. (B.5) can be even more simplified by choosing ansatz 2^* for the projection operator, which assumes the EBC and therefore neglects the coupling contribution of Eq. (B.9).

Working equations for matrices $\mathcal{B}$, $\mathcal{V}$ and $\mathcal{X}$

As outlined in the last section, the three different ansätze A, A' and B and the approximations [T+V] and [F+K] turn out to be identical when assuming local KS references and fixed amplitudes. Within ansatz 2^*, coupling contributions are furthermore neglected and matrix $\mathcal{B}$ is given by the kinetic energy term of Eq. (B.6). The final working equations — for local KS references and fixed geminal amplitudes within ansatz 2^* — are thus given as

$$\mathcal{B}_{\widetilde{xy},\widetilde{vw}} = \tfrac{1}{2} \left[(f^2 r^2)_{\widetilde{vw}}^{\widetilde{xy}} - \sum_{pq} f_{pq}^{\widetilde{xy}} t_{\widetilde{vw}}^{pq} - \sum_{p''i} f_{p''i}^{\widetilde{xy}} t_{\widetilde{vw}}^{p''i} - \sum_{p''i} f_{ip''}^{\widetilde{xy}} t_{\widetilde{vw}}^{ip''} \right], \tag{B.10}$$

with the integrals

$$(f^2 r^2)_{\widetilde{vw}}^{\widetilde{xy}} = \langle \widetilde{xy}| \tfrac{1}{2}[f_{12}, [\hat{T}_{12}, f_{12}]] |\widetilde{vw}\rangle, \tag{B.11}$$

$$t_{xy}^{pq} = f_{xr'}^{pq} T_y^{r'} - T_{r'}^q f_{xy}^{pr'} + f_{r'y}^{pq} T_x^{r'} - T_{r'}^p f_{xy}^{r'q}, \tag{B.12}$$

$$T_l^{r'} = \langle r'|\hat{T} + \hat{V}|l\rangle. \tag{B.13}$$

Note that the Einstein summation convention is implied. Working equations for the F12 intermediates $\mathcal{V}$ and $\mathcal{X}$ within ansatz 2 (and 2^*) are obtained by inserting the corresponding projection operator in Eqs. (A.13) and (A.15),

$$\mathcal{V}_{ij}^{\widetilde{xy}} = (fg)_{ij}^{\widetilde{xy}} - \sum_{pq} f_{pq}^{\widetilde{xy}} g_{ij}^{pq} - \sum_{p''k} f_{p''k}^{\widetilde{xy}} g_{ij}^{p''k} - \sum_{p''k} f_{kp''}^{\widetilde{xy}} g_{ij}^{kp''}, \tag{B.14}$$

$$\mathcal{X}_{\widetilde{vw}}^{\widetilde{xy}} = (f^2)_{\widetilde{vw}}^{\widetilde{xy}} - \sum_{pq} f_{pq}^{\widetilde{xy}} f_{\widetilde{vw}}^{pq} - \sum_{p''i} f_{p''i}^{\widetilde{xy}} f_{\widetilde{vw}}^{p''i} - \sum_{p''i} f_{ip''}^{\widetilde{xy}} f_{\widetilde{vw}}^{ip''}, \tag{B.15}$$

with the integrals

$$(fg)_{ij}^{\widetilde{xy}} = \langle \widetilde{xy}|f_{12}\hat{g}_{12}|ij\rangle, \tag{B.16}$$

$$(f^2)_{\widetilde{vw}}^{\widetilde{xy}} = \langle \widetilde{xy}|f_{12}^2|\widetilde{vw}\rangle. \tag{B.17}$$

It should be noted that the projection on the occupied orbital space includes within the frozen-core approximation both active and frozen occupied orbitals.

Optimized, fixed and spin-flipped geminal amplitudes

Two main strategies to determine the geminal amplitudes exist: they are either optimized iteratively (invariant ansatz) [277] or kept fixed according to the s- and p-wave cusp conditions (rational generator approach

or SP ansatz) [99].

For closed-shell systems, where the pair functions are parametrized as

$$u_{ij} = \sum_{ab} t_{ij}^{ab}|ab\rangle + \sum_{xy} c_{ij}^{xy}\hat{Q}_{12}f(r_{12})|xy\rangle\,, \tag{B.18}$$

the optimization of the amplitudes requires the calculation of the corresponding residual equation $(\mathbf{\Omega}^{\text{F12}})_{ij}^{xy}$ (see e.g. the drCCD(F12) residual of Eq. (4.16)) as well as an update of the so-defined amplitudes c_{ij}^{xy}, given as

$$c_{ij}^{xy(\text{new})} = c_{ij}^{xy(\text{old})} + \sum_{vw}[\mathbf{\mathcal{B}}^{-1}]_{xy,vw}^{(ij)}(\mathbf{\Omega}^{\text{F12}})_{ij}^{vw}\,. \tag{B.19}$$

(Note that optimized MP2-F12 geminal amplitudes for ansatz 2^* are simply given as $c_{ij}^{xy} = \sum_{vw}[\mathbf{\mathcal{B}}^{-1}]_{xy,vw}^{(ij)}\mathcal{V}_{ij}^{vw}$, representing the exact solution which minimizes the Hylleraas functional [105, 178]. For other approaches, the preconditioner $\mathbf{\mathcal{B}}^{-1}$ for the iterative update can be chosen freely; standardly not the full matrix $\mathbf{\mathcal{B}}$ as defined in Eq. (A.16) is taken into account.) Alternatively, fixed amplitudes can be chosen according to the coalescence conditions [171, 280],

$$c_{ij}^{xy} = \frac{3}{8}\delta_{ix}\delta_{jy} + \frac{1}{8}\delta_{iy}\delta_{jx}\,. \tag{B.20}$$

For open-shell systems, it was shown that spin-flipped geminals have to be included in the wave-function manifold in order to fulfill the cusp conditions, to accelerate basis-set convergence from X^{-3} to X^{-7} and to give a balanced treatment of closed- and open-shell molecules [173, 174]. In the case of optimized amplitudes, this can be achieved by introducing contracted geminals [103],

$$u_{IJ} = \sum_{A<B} t_{IJ}^{AB}|AB\rangle + \sum_{X<Y} c_{IJ}^{XY}\hat{Q}_{12}f(r_{12})(c|XY\rangle + \bar{c}|\widetilde{XY}\rangle)\,, \tag{B.21}$$

with the contraction coefficients

$$c = \tfrac{1}{4}, \bar{c} = 0 \ \text{ for the same-spin case and} \tag{B.22}$$

$$c = \tfrac{3}{8}, \bar{c} = \tfrac{1}{8} \ \text{ for the opposite-spin case}\,. \tag{B.23}$$

Fixed open-shell amplitudes are in contrast obtained by generalizing Eq. (B.20), implying

$$c_{IJ}^{XY} = \delta_{IX}\delta_{JY} \ \text{ or } \ d_{IJ}^{XY} = \delta_{IX}\delta_{JY} - \delta_{IY}\delta_{JX}\,, \tag{B.24}$$

and introducing the rational generator $\hat{S}_{XY}$ [99],

$$|\widetilde{XY}\rangle = \hat{S}_{XY}|XY\rangle = (\frac{3}{8} + \frac{1}{8}\hat{P}_{XY}^{\text{flip}})|XY\rangle\,. \tag{B.25}$$

The permutation operator $\hat{P}_{XY}^{\text{flip}}$ flips the spatial part of the orbitals X and Y keeping the spin functions σ_X and σ_Y the same, $\hat{P}_{XY}^{\text{flip}}\varphi_X\sigma_X\varphi_Y\sigma_Y = \varphi_Y\sigma_X\varphi_X\sigma_Y$. Concerning fixed open-shell amplitudes, it should be noted that various other approaches exist which exclude the manifold of spin-flipped functions, setting up constraints for the different spin cases to fit the cusp conditions (see e.g. Ref. [202]). It was for instance shown that variationally optimized amplitudes tend in the limit of a large basis to

$$c_{IJ}^{XY} = \tfrac{1}{4}\delta_{IX}\delta_{JY} \ \text{ for the same-spin case}\,, \tag{B.26}$$

$$c_{IJ}^{XY} = \tfrac{3}{8}\delta_{IX}\delta_{JY} + \tfrac{1}{8}\delta_{IY}\delta_{JX} \ \text{ for the opposite-spin case and doubly occupied orbitals}\,, \tag{B.27}$$

$$c_{IJ}^{XY} = \tfrac{1}{2}\delta_{IX}\delta_{JY} \ \text{ for the opposite-spin case and singly occupied orbitals}\,. \tag{B.28}$$

These limits allow to assess or even set up alternative, fixed formulations, e.g. by defining the geminal coefficients depending on the MO overlap matrix $S_{XY} = \langle\phi_X|\phi_Y\rangle$ [103],

$$c_{IJ}^{XY} = \tfrac{1}{4}\delta_{IX}\delta_{JY} \ \text{ for the same-spin case}\,, \tag{B.29}$$

$$c_{IJ}^{XY} = \tfrac{1}{2}\delta_{IX}\delta_{JY} - \tfrac{1}{8}\sum_{MN} S_{IN}S_{XN}S_{MJ}S_{MY} + \tfrac{1}{8}S_{IY}S_{XJ} \ \text{ for the opposite-spin case}\,. \tag{B.30}$$

The latter, computationally less demanding approach is also implemented in TURBOMOLE, obtained when choosing fixed, non-spin-flipped amplitudes for open-shell molecules.

However, in summary, spin-flipped amplitudes as defined within Eqs. (B.24) and (B.25) are the most rigorous ansatz: they fulfill the cusp conditions exactly in contrast to other approaches and accelerate basis-set convergence to X^{-7}. Comparing optimized to fixed amplitudes, the latter are standardly preferred being computationally less demanding, numerically more stable and free from geminal BSSE [172] while the loss of accuracy is slight [103]. It should be noted that direct methods require a non-antisymmetrized definition of the geminal amplitudes, $c_{IJ}^{XY} = \delta_{IX}\delta_{JY}$, reflecting that the coalescence conditions are equal for both same and opposite spin, while correlation methods including exchange have to refer to $d_{IJ}^{XY} = \delta_{IX}\delta_{JY} - \delta_{JX}\delta_{IY}$, as already indicated in Eq. (B.24).

C. Perturbative +F12 methods and RPA approaches including exchange

Open-shell equations implying $c_{IJ}^{XY} = \delta_{IX}\delta_{JY}$ and $d_{IJ}^{XY} = \delta_{IX}\delta_{JY} - \delta_{IY}\delta_{JX}$:

$$E_{\mathrm{C}}^{\mathrm{F12(dMP2\text{-}F12)}} = \tfrac{1}{2}\sum_{XYIJ} c_{IJ}^{XY}\left(\boldsymbol{\mathcal{V}}^{\dagger}\right)_{\widetilde{XY}}^{IJ} + \tfrac{1}{2}\sum_{XYIJ}(\mathbf{C}^{\mathrm{LAG}})_{IJ}^{XY}\,(\boldsymbol{\Omega}^{\mathrm{F12(dMP2\text{-}F12)}})_{IJ}^{\widetilde{XY}}\,,\tag{C.1}$$

$$E_{\mathrm{C}}^{\mathrm{F12(MP2\text{-}F12)}} = \tfrac{1}{4}\sum_{XYIJ} d_{IJ}^{XY}\left(\left(\boldsymbol{\mathcal{V}}^{\dagger}\right)_{\widetilde{XY}}^{IJ} - \left(\boldsymbol{\mathcal{V}}^{\dagger}\right)_{\widetilde{YX}}^{IJ}\right) + \tfrac{1}{4}\sum_{XYIJ}(\mathbf{D}^{\mathrm{LAG}})_{IJ}^{XY}\,(\boldsymbol{\Omega}^{\mathrm{F12(MP2\text{-}F12)}})_{IJ}^{\widetilde{XY}}\,,\tag{C.2}$$

$$= \tfrac{1}{2}\sum_{XYIJ} d_{IJ}^{XY}\left(\boldsymbol{\mathcal{V}}^{\dagger}\right)_{\widetilde{XY}}^{IJ} + \tfrac{1}{2}\sum_{XYIJ}(\mathbf{D}^{\mathrm{LAG}})_{IJ}^{XY}\,(\boldsymbol{\Omega}^{\mathrm{F12(dMP2\text{-}F12)}})_{IJ}^{\widetilde{XY}}\,,$$

$$(\boldsymbol{\Omega}^{\mathrm{F12(dMP2\text{-}F12)}})_{IJ}^{\widetilde{XY}} = \mathcal{V}_{IJ}^{\widetilde{XY}} + \sum_{VW}\mathcal{B}_{\widetilde{XY},\widetilde{VW}}^{(IJ)}c_{IJ}^{VW}\,,\tag{C.3}$$

$$(\boldsymbol{\Omega}^{\mathrm{F12(MP2\text{-}F12)}})_{IJ}^{\widetilde{XY}} = \mathcal{V}_{IJ}^{\widetilde{XY}} - \mathcal{V}_{JI}^{\widetilde{XY}} + \sum_{VW}\mathcal{B}_{\widetilde{XY},\widetilde{VW}}^{(IJ)}d_{IJ}^{VW}\,,\tag{C.4}$$

with the Lagrangian multipliers $(\mathbf{C}^{\mathrm{LAG}})_{IJ}^{XY} = c_{IJ}^{XY}$ and $(\mathbf{D}^{\mathrm{LAG}})_{IJ}^{XY} = d_{IJ}^{XY}$.

Closed-shell equations implying $c_{ij}^{xy} = \delta_{ix}\delta_{jy}$, $^{1}d_{ij}^{xy} = 2\delta_{ix}\delta_{jy} - \delta_{iy}\delta_{jx}$ and $^{3}d_{ij}^{xy} = -\delta_{iy}\delta_{jx}$:

$$E_{\mathrm{C}}^{\mathrm{F12(dMP2\text{-}F12)}} = \sum_{xyij} c_{ij}^{xy}\left(2\boldsymbol{\mathcal{V}}^{\dagger}\right)_{\widetilde{xy}}^{ij} + \sum_{xyij}(\mathbf{C}^{\mathrm{LAG}})_{ij}^{xy}\,(\boldsymbol{\Omega}^{\mathrm{F12((d)MP2\text{-}F12)}})_{ij}^{\widetilde{xy}}\,,\tag{C.5}$$

$$E_{\mathrm{C}}^{\mathrm{F12(MP2\text{-}F12)}} = \tfrac{1}{4}\sum_{xyij}\left(^{1}d_{ij}^{xy}\left(^{1}\boldsymbol{\mathcal{V}}^{\dagger}\right)_{\widetilde{xy}}^{ij} + 3\,^{3}d_{ij}^{xy}\left(^{3}\boldsymbol{\mathcal{V}}^{\dagger}\right)_{\widetilde{xy}}^{ij}\right)$$

$$+ \tfrac{1}{4}\sum_{xyij}\left(\left(^{1}\mathbf{D}^{\mathrm{LAG}}\right)_{ij}^{xy}\left(^{1}\boldsymbol{\Omega}^{\mathrm{F12(MP2\text{-}F12)}}\right)_{ij}^{\widetilde{xy}} + 3\left(^{3}\mathbf{D}^{\mathrm{LAG}}\right)_{ij}^{xy}\left(^{3}\boldsymbol{\Omega}^{\mathrm{F12(MP2\text{-}F12)}}\right)_{ij}^{\widetilde{xy}}\right),\tag{C.6}$$

$$= \sum_{xyij} c_{ij}^{xy}\left(2\left(\boldsymbol{\mathcal{V}}^{\dagger}\right)_{\widetilde{xy}}^{ij} - \left(\boldsymbol{\mathcal{V}}^{\dagger}\right)_{\widetilde{yx}}^{ij}\right) + \sum_{xyij}(\mathbf{D}^{\mathrm{LAG}})_{ij}^{xy}\,(\boldsymbol{\Omega}^{\mathrm{F12((d)MP2\text{-}F12})})_{ij}^{\widetilde{xy}}\,,\tag{C.7}$$

$$(^{s}\boldsymbol{\Omega}^{\mathrm{F12(MP2\text{-}F12)}})_{ij}^{\widetilde{xy}} = \,^{s}\mathcal{V}_{ij}^{\widetilde{xy}} + \sum_{vw}\mathcal{B}_{\widetilde{xy},\widetilde{vw}}^{(ij)}\,^{s}d_{ij}^{vw}\,,\tag{C.8}$$

$$(\boldsymbol{\Omega}^{\mathrm{F12((d)MP2\text{-}F12)}})_{ij}^{\widetilde{xy}} = \mathcal{V}_{ij}^{\widetilde{xy}} + \sum_{vw}\mathcal{B}_{\widetilde{xy},\widetilde{vw}}^{(ij)}c_{ij}^{vw}\,,\tag{C.9}$$

with the Lagrangian multipliers $(\mathbf{C}^{\mathrm{LAG}})_{ij}^{xy} = 2c_{ij}^{xy}$, $(\mathbf{D}^{\mathrm{LAG}})_{ij}^{xy} = 2c_{ij}^{xy} - c_{ji}^{xy}$, $\left(^{1}\mathbf{D}^{\mathrm{LAG}}\right)_{ij}^{xy} = \,^{1}d_{ij}^{xy}$ and $\left(^{3}\mathbf{D}^{\mathrm{LAG}}\right)_{ij}^{xy} = \,^{3}d_{ji}^{xy}$.

Fig. C.1: Perturbative second-order F12 correction for ansatz 2*, neglecting coupling between conventional and explicitly correlated amplitudes. Note that the lengthy formulations might appear cumbersome, but are especially chosen to highlight that Eq. (C.6) for the closed-shell case is derived by implying antisymmetrized integrals and non-antisymmetrized coefficients in analogy to Eq. (2.98). This explains why the geminal coefficients c_{ij}^{xy} in Eq. (C.9) differ by a factor of two from the Lagrangian multipliers $\mathbf{C}^{\mathrm{LAG}}$ of Eq. (C.5). The derivation of the Lagrangian multipliers $\mathbf{C}^{\mathrm{LAG}}$ and $\mathbf{D}^{\mathrm{LAG}}$ is explained in detail in Ref. [178].

The idea of the +F12 schemes is to add a perturbative F12 correction to the RPA or beyond-RPA correlation energy which is obtained by truncating the explicitly correlated rCCD approach at second-order perturbation

theory. Analogously to the conventional methods, where the truncation of drCCD/rCCD amplitudes yields the dMP2/MP2 result (Eqs. (2.104) to (2.107)), the explicitly correlated approaches drCCD(F12)/rCCD(F12) lead to the corresponding dMP2-F12/MP2-F12 methods. Working equations for closed- and open-shell systems are given in Figure C.1, according to Ref. [105]. Note that the closed-shell formulation of the explicitly correlated contribution from MP2-F12 theory, as given in Eqs. (C.6) and (C.7), can be parametrized either in terms of singlet and triplet amplitudes or based on the non-antisymmetrized and antisymmetrized coefficients $\mathbf{C}$ and $\mathbf{D}^{\text{LAG}} = \mathbf{D}$. Both formulations are equivalent, representing first-order contributions to the rCCD correlation energy. A closed-shell rCCD scheme analogous to Eq. (C.7) is not possible due to the reduced symmetry of the rCCD amplitudes. Open-shell rCCD equations thus have to rely on a singlet-triplet formulation analogously to Eq. (C.6), including higher-order contributions.

The different +F12 schemes are defined in Eqs. (2.108), (2.109), (2.111), and (2.110), correcting both conventional dRPA and RPA as well as the beyond-RPA approaches SOSEX and AXK. The second-order screened exchange (SOSEX) can be based on the rCC formulation of the correlation energy (see Eq. (2.64)) [45, 52],

$$E_{\text{C}}^{\Delta\text{SOSEX}} = -\tfrac{1}{2}\text{tr}\left[\mathbf{B}^{\text{X}}\mathbf{T}^{\text{dRPA}}\right],\tag{C.10}$$

or it can be defined in the framework of the adiabatic connection [182] according to

$$E_{\text{C}}^{\Delta\text{ACSOSEX}} = -\tfrac{1}{2}\int_0^1 \text{tr}\left(\mathbf{B}^{\text{X}}\mathbf{P}_{\text{dRPA}}^{\zeta}\right)\mathrm{d}\zeta.\tag{C.11}$$

$\mathbf{P}_{\text{dRPA}}^{\zeta}$ is given in Eq. (2.43) and $\mathbf{B}^{\text{X}}$ indicates the pure exchange contribution to the standard RPAX matrix $\mathbf{B}^{\text{RPAX}}$, $\mathbf{B}^{\text{X}} = g_{JI}^{AB}$. Working equations for the approximate exchange kernel (AXK) are derived in Refs. [8, 51] and can be summarized as

$$E_{\text{C}}^{\Delta\text{AXK}} = -\int_0^1 \text{tr}\left(\mathbf{B}^{\text{X}}\mathbf{P}_{\text{dRPA}}^{\zeta(2)}\right)\mathrm{d}\zeta,\tag{C.12}$$

with the second-order pair density

$$\mathbf{P}_{\text{dRPA}}^{\zeta(2)} = \frac{\zeta}{\Omega_n^{\zeta\text{dRPA}} + \Omega_m^{\zeta\text{dRPA}}} \sum_{nm}\left(\left(\mathbf{X}_{\text{dRPA}}^{n\zeta} + \mathbf{Y}_{\text{dRPA}}^{n\zeta}\right)\left(\mathbf{X}_{\text{dRPA}}^{n\zeta} + \mathbf{Y}_{\text{dRPA}}^{n\zeta}\right)^{\text{T}}\mathbf{B}^{\text{dRPA}}\left(\mathbf{X}_{\text{dRPA}}^{m\zeta} + \mathbf{Y}_{\text{dRPA}}^{m\zeta}\right)\left(\mathbf{X}_{\text{dRPA}}^{m\zeta} + \mathbf{Y}_{\text{dRPA}}^{m\zeta}\right)^{\text{T}}\right).\tag{C.13}$$

Both approaches outperform the SOX variant, which simply adds second-order exchange to the dRPA correlation energy, overcorrecting the self-interaction error and inheriting the problems of MP2 theory for small-gap systems [233, 281],

$$E_{\text{C}}^{\Delta\text{SOX}} = -\tfrac{1}{2}\text{tr}[\mathbf{B}^{\text{X}}\mathbf{T}^{\text{MP2}}] = -\tfrac{1}{2}\sum_{ABIJ}\frac{g_{IJ}^{AB}g_{BA}^{IJ}}{\varepsilon_A + \varepsilon_B - \varepsilon_I - \varepsilon_J}.\tag{C.14}$$

SOSEX and ACSOSEX remove the self-interaction error, but still suffer from numerical instabilities for small-gap systems. AXK in contrast is fully screened, removing most of the self-interaction while capturing strong static correlation. However, SOSEX is computationally more efficient. Note that ACSOSEX and SOSEX correlation energies differ only slightly due to the inaccurateness of the numerical integration (for a comparison see Ref. [51]), even though the perturbation expansions reveal subtle differences [145, 182]. Refs. [63], [46] and [51] summarize a comparison of all four methods, SOX, ACSOSEX, SOSEX, and AXK, in terms of Goldstone diagrams. A detailed description on how to derive diagrammatic representations of perturbation expansions is given in Refs. [121, 282]. SOX is thereby represented by all second-order diagrams, which are identical for AXK, SOSEX and ACSOSEX. The latter three methods contain further higher-order contributions, which differ already at third order perturbation theory.

Basis-set convergence of +F12 schemes

To validate the proposed +F12 schemes, basis-set convergence with respect to the +F12/aug-cc-pV5Z limit is depicted in Figures 2.6, 2.7, 2.8, and 2.9 of Chapter 2.3 for the Dunning basis sets aug-cc-pVXZ. The corresponding statistical measures, including mean errors (ME), mean absolute deviations (MAD), root-mean-square errors (RMS), standard deviations (STD) and mean percentage errors (MPE), are given in Table C.1, C.2, C.3, and C.4 regarding correlation, atomization, interaction, and reference energies, respectively.

Tab. C.1: Valence-shell correlation energies: Statistical measures for the basis-set error per valence electron with respect to the +F12/aug-cc-pV5Z result (in mE_h).

Basis set	ME	MAD	RMS	STD	MPE
dMP2					
aug-cc-pVDZ	16.04	16.04	16.54	4.02	−22.90
aug-cc-pVTZ	6.64	6.64	6.92	1.97	−8.73
aug-cc-pVQZ	3.11	3.11	3.27	1.01	−3.93
aug-cc-pV5Z	1.62	1.62	1.71	0.53	−2.00
aug-cc-pV(Q5)Z	0.06	0.06	0.07	0.04	−0.02
dMP2-F12					
aug-cc-pVDZ	−0.40	0.44	0.58	0.41	−2.30
aug-cc-pVTZ	0.17	0.17	0.21	0.12	0.70
aug-cc-pVQZ	0.06	0.06	0.07	0.03	0.17
dRPA					
aug-cc-pVDZ	16.04	16.04	16.54	4.02	−28.74
aug-cc-pVTZ	6.64	6.64	6.92	1.97	−11.79
aug-cc-pVQZ	3.11	3.11	3.27	1.01	−5.50
aug-cc-pV5Z	1.62	1.62	1.71	0.53	−2.86
aug-cc-pV(Q5)Z	0.06	0.06	0.07	0.04	−0.10
dRPA+F12					
aug-cc-pVDZ	−0.40	0.44	0.58	0.41	0.62
aug-cc-pVTZ	0.17	0.17	0.21	0.12	−0.32
aug-cc-pVQZ	0.06	0.06	0.07	0.03	−0.12
MP2					
aug-cc-pVDZ	11.08	11.08	11.34	2.42	−21.59
aug-cc-pVTZ	3.91	3.91	4.05	1.03	−7.58
aug-cc-pVQZ	1.70	1.70	1.77	0.49	−3.28
aug-cc-pV5Z	0.84	0.84	0.88	0.24	−1.62
aug-cc-pV(Q5)Z	−0.06	0.06	0.06	0.02	0.12
MP2-F12					
aug-cc-pVDZ	1.38	1.38	1.40	0.23	−2.71
aug-cc-pVTZ	0.33	0.33	0.35	0.12	−0.64
aug-cc-pVQZ	0.08	0.08	0.08	0.03	−0.15
ACSOSEX					
aug-cc-pVDZ	9.49	9.49	9.71	2.06	−27.85
aug-cc-pVTZ	3.68	3.68	3.80	0.96	−10.74
aug-cc-pVQZ	1.66	1.66	1.72	0.48	−4.83
aug-cc-pV5Z	0.84	0.84	0.88	0.24	−2.45
aug-cc-pV(Q5)Z	−0.02	0.02	0.02	0.01	0.05
ACSOSEX+F12					
aug-cc-pVDZ	−0.20	0.26	0.35	0.28	0.54
aug-cc-pVTZ	0.09	0.09	0.11	0.06	−0.27
aug-cc-pVQZ	0.04	0.04	0.04	0.02	0.11
AXK					
aug-cc-pVDZ	10.08	10.08	10.30	2.11	−26.09
aug-cc-pVTZ	3.82	3.82	3.94	0.90	−9.83
aug-cc-pVQZ	1.68	1.68	1.75	0.48	−4.32
aug-cc-pV5Z	0.84	0.84	0.88	0.24	−2.16
aug-cc-pV(Q5)Z	−0.04	0.04	0.04	0.02	0.11
AXK+F12					
aug-cc-pVDZ	0.38	0.40	0.45	0.24	1.07
aug-cc-pVTZ	0.23	0.23	0.25	0.09	−0.61
aug-cc-pVQZ	0.06	0.06	0.06	0.02	0.16

Tab. C.2: Correlation contribution to the atomization energy: Statistical measures for the basis-set error per valence electron with respect to the +F12/aug-cc-pV5Z result (in kJ/mol).

Basis set	ME	MAD	RMS	STD	MPE
		dMP2			
aug-cc-pVDZ	−7.471	7.471	7.716	1.927	−10.40
aug-cc-pVTZ	−2.207	2.207	2.286	0.594	−3.02
aug-cc-pVQZ	−0.754	0.754	0.793	0.246	−1.00
aug-cc-pV5Z	−0.393	0.393	0.415	0.135	−0.52
aug-cc-pV(Q5)Z	−0.013	0.041	0.046	0.044	−0.02
		dMP2-F12			
aug-cc-pVDZ	−1.163	1.163	1.240	0.428	−1.53
aug-cc-pVTZ	−0.014	0.118	0.134	0.133	0.00
aug-cc-pVQZ	0.065	0.077	0.094	0.068	0.10
		dRPA			
aug-cc-pVDZ	−6.213	6.213	6.505	1.928	−6.21
aug-cc-pVTZ	−2.042	2.042	2.127	0.595	−2.04
aug-cc-pVQZ	−0.732	0.732	0.769	0.236	−0.73
aug-cc-pV5Z	−0.393	0.393	0.415	0.135	−0.39
aug-cc-pV(Q5)Z	−0.036	0.062	0.073	0.063	−0.04
		dRPA+F12			
aug-cc-pVDZ	0.095	0.328	0.369	0.357	0.09
aug-cc-pVTZ	0.151	0.151	0.165	0.067	0.15
aug-cc-pVQZ	0.087	0.087	0.096	0.041	0.09
		MP2			
aug-cc-pVDZ	−9.260	9.260	9.657	2.740	−12.22
aug-cc-pVTZ	−3.279	3.279	3.411	0.940	−4.28
aug-cc-pVQZ	−1.343	1.343	1.405	0.413	−1.74
aug-cc-pV5Z	−0.692	0.692	0.725	0.216	−0.90
aug-cc-pV(Q5)Z	−0.010	0.019	0.025	0.023	−0.01
		MP2-F12			
aug-cc-pVDZ	−1.161	1.161	1.204	0.319	−1.51
aug-cc-pVTZ	−0.227	0.227	0.238	0.073	−0.29
aug-cc-pVQZ	−0.018	0.024	0.033	0.028	−0.02
		ACSOSEX			
aug-cc-pVDZ	−8.091	8.091	8.470	2.506	−19.08
aug-cc-pVTZ	−3.104	3.104	3.232	0.903	−7.38
aug-cc-pVQZ	−1.314	1.314	1.375	0.404	−3.14
aug-cc-pV5Z	−0.692	0.692	0.725	0.216	−1.66
aug-cc-pV(Q5)Z	−0.040	0.044	0.058	0.042	−0.11
		ACSOSEX+F12			
aug-cc-pVDZ	0.008	0.086	0.119	0.119	0.05
aug-cc-pVTZ	−0.052	0.052	0.054	0.017	−0.13
aug-cc-pVQZ	0.011	0.011	0.014	0.009	0.02
		AXK			
aug-cc-pVDZ	−8.118	8.118	8.478	2.443	−18.96
aug-cc-pVTZ	−3.075	3.075	3.200	0.885	−7.21
aug-cc-pVQZ	−1.305	1.305	1.365	0.401	−3.06
aug-cc-pV5Z	−0.692	0.692	0.725	0.216	−1.63
aug-cc-pV(Q5)Z	−0.049	0.050	0.063	0.038	−0.12
		AXK+F12			
aug-cc-pVDZ	−0.019	0.112	0.154	0.153	−0.08
aug-cc-pVTZ	−0.023	0.028	0.035	0.027	−0.07
aug-cc-pVQZ	0.020	0.020	0.024	0.013	0.04

Tab. C.3: Interaction energies with and without counterpoise correction: Statistical measures for the basis-set error per valence electron with respect to the +F12/aug-cc-pV5Z result (in kJ/mol).

Basis set	without CP					with CP				
	ME	MAD	RMS	STD	MPE	ME	MAD	RMS	STD	MPE
dMP2										
aug-cc-pVDZ	0.609	0.609	0.624	0.137	30.55	−0.644	0.644	0.739	0.364	−18.41
aug-cc-pVTZ	0.345	0.345	0.374	0.144	12.79	−0.255	0.255	0.304	0.164	−7.06
aug-cc-pVQZ	0.178	0.178	0.201	0.093	6.08	−0.105	0.105	0.126	0.069	−2.84
aug-cc-pV5Z	0.093	0.093	0.114	0.065	2.94	−0.055	0.055	0.066	0.036	−1.47
aug-cc-pV(Q5)Z	0.004	0.032	0.036	0.036	−0.35	−0.002	0.002	0.003	0.002	−0.03
dMP2-F12										
aug-cc-pVDZ	−0.225	0.259	0.348	0.266	−4.26	−0.160	0.160	0.178	0.080	−4.76
aug-cc-pVTZ	0.096	0.096	0.115	0.063	2.91	−0.021	0.021	0.023	0.007	−0.76
aug-cc-pVQZ	0.061	0.061	0.071	0.037	1.88	−0.008	0.008	0.009	0.004	−0.23
aug-cc-pV5Z	0.027	0.027	0.033	0.019	0.81	—	—	—	—	—
dRPA										
aug-cc-pVDZ	0.511	0.511	0.527	0.126	63.55	−0.586	0.586	0.684	0.353	−24.41
aug-cc-pVTZ	0.285	0.285	0.306	0.111	21.74	−0.250	0.250	0.299	0.164	−10.07
aug-cc-pVQZ	0.162	0.162	0.181	0.080	10.63	−0.102	0.102	0.123	0.068	−3.99
aug-cc-pV5Z	0.088	0.088	0.108	0.062	4.81	−0.055	0.055	0.066	0.036	−2.11
aug-cc-pV(Q5)Z	0.011	0.036	0.044	0.042	−1.30	−0.004	0.004	0.006	0.004	−0.13
dRPA+F12										
aug-cc-pVDZ	−0.322	0.322	0.430	0.284	−12.20	−0.102	0.102	0.122	0.067	−3.44
aug-cc-pVTZ	0.037	0.037	0.048	0.031	0.98	−0.015	0.015	0.017	0.008	−1.05
aug-cc-pVQZ	0.044	0.044	0.051	0.025	2.46	−0.005	0.005	0.006	0.003	−0.27
aug-cc-pV5Z	0.022	0.022	0.027	0.015	1.06	—	—	—	—	—
MP2										
aug-cc-pVDZ	0.369	0.369	0.383	0.102	19.39	−0.480	0.480	0.542	0.253	−13.17
aug-cc-pVTZ	0.181	0.181	0.198	0.082	6.31	−0.166	0.166	0.194	0.101	−4.35
aug-cc-pVQZ	0.096	0.096	0.109	0.051	3.10	−0.061	0.061	0.072	0.038	−1.54
aug-cc-pV5Z	0.048	0.048	0.058	0.033	1.38	−0.030	0.030	0.036	0.019	−0.75
aug-cc-pV(Q5)Z	−0.003	0.016	0.016	0.016	−0.42	0.002	0.002	0.003	0.001	0.08
MP2-F12										
aug-cc-pVDZ	−0.166	0.200	0.262	0.203	−2.14	−0.159	0.159	0.174	0.072	−4.69
aug-cc-pVTZ	0.050	0.050	0.064	0.041	1.15	−0.020	0.020	0.021	0.006	−0.71
aug-cc-pVQZ	0.035	0.035	0.041	0.021	1.02	−0.006	0.006	0.006	0.002	−0.17
aug-cc-pV5Z	0.014	0.014	0.016	0.009	0.39	—	—	—	—	—
ACSOSEX										
aug-cc-pVDZ	0.308	0.308	0.324	0.101	40.13	−0.433	0.433	0.498	0.247	−18.50
aug-cc-pVTZ	0.145	0.145	0.156	0.059	10.58	−0.163	0.163	0.193	0.103	−6.78
aug-cc-pVQZ	0.086	0.086	0.096	0.042	5.57	−0.059	0.059	0.070	0.038	−2.35
aug-cc-pV5Z	0.044	0.044	0.054	0.031	2.30	−0.030	0.030	0.036	0.019	−1.17
aug-cc-pV(Q5)Z	0.000	0.019	0.020	0.020	−1.12	0.001	0.001	0.001	0.001	0.07
ACSOSEX+F12										
aug-cc-pVDZ	−0.227	0.227	0.314	0.216	−6.35	−0.112	0.112	0.129	0.064	−4.56
aug-cc-pVTZ	0.014	0.021	0.024	0.019	−0.44	−0.017	0.017	0.019	0.008	−1.15
aug-cc-pVQZ	0.025	0.025	0.028	0.013	1.42	−0.004	0.004	0.004	0.002	−0.22
aug-cc-pV5Z	0.010	0.010	0.012	0.007	0.51	—	—	—	—	—
AXK										
aug-cc-pVDZ	0.332	0.332	0.348	0.104	41.32	−0.445	0.445	0.513	0.254	−18.96
aug-cc-pVTZ	0.162	0.162	0.175	0.066	11.53	−0.167	0.167	0.198	0.106	−6.92
aug-cc-pVQZ	0.091	0.091	0.101	0.045	5.72	−0.060	0.060	0.071	0.038	−2.38
aug-cc-pV5Z	0.046	0.046	0.056	0.033	2.35	−0.030	0.030	0.036	0.019	−1.18
aug-cc-pV(Q5)Z	−0.001	0.019	0.020	0.020	−1.19	0.001	0.001	0.002	0.001	0.09
AXK+F12										
aug-cc-pVDZ	−0.203	0.214	0.297	0.216	−3.90	−0.124	0.124	0.144	0.072	−5.02
aug-cc-pVTZ	0.031	0.031	0.041	0.026	0.80	−0.021	0.021	0.024	0.011	−1.25
aug-cc-pVQZ	0.030	0.030	0.034	0.016	1.66	−0.005	0.005	0.005	0.002	−0.24
aug-cc-pV5Z	0.012	0.012	0.014	0.008	0.58	—	—	—	—	—

Tab. C.4: Reference energies and CABS-singles correction: Statistical measures for the basis-set error per valence electron with respect to the +F12/aug-cc-pV5Z result (in kJ/mol).

| Basis set	ME	MAD	RMS	STD
HF				
aug-cc-pVDZ	−2.014	2.014	2.207	0.903
aug-cc-pVTZ	−0.264	0.269	0.292	0.125
aug-cc-pVQZ	−0.037	0.037	0.043	0.023
aug-cc-pV5Z	−0.009	0.009	0.009	0.003
HF+CABS				
aug-cc-pVDZ	−0.262	0.309	0.392	0.291
aug-cc-pVTZ	−0.037	0.052	0.063	0.051
aug-cc-pVQZ	−0.003	0.010	0.012	0.012
PBE				
aug-cc-pVDZ	−2.202	2.202	2.392	0.934
aug-cc-pVTZ	−0.326	0.329	0.354	0.137
aug-cc-pVQZ	−0.101	0.101	0.115	0.054
aug-cc-pV5Z	0.019	0.019	0.022	0.012
PBE+CABS				
aug-cc-pVDZ	−0.395	0.617	0.756	0.645
aug-cc-pVTZ	−0.071	0.094	0.132	0.111
aug-cc-pVQZ	−0.079	0.079	0.093	0.048
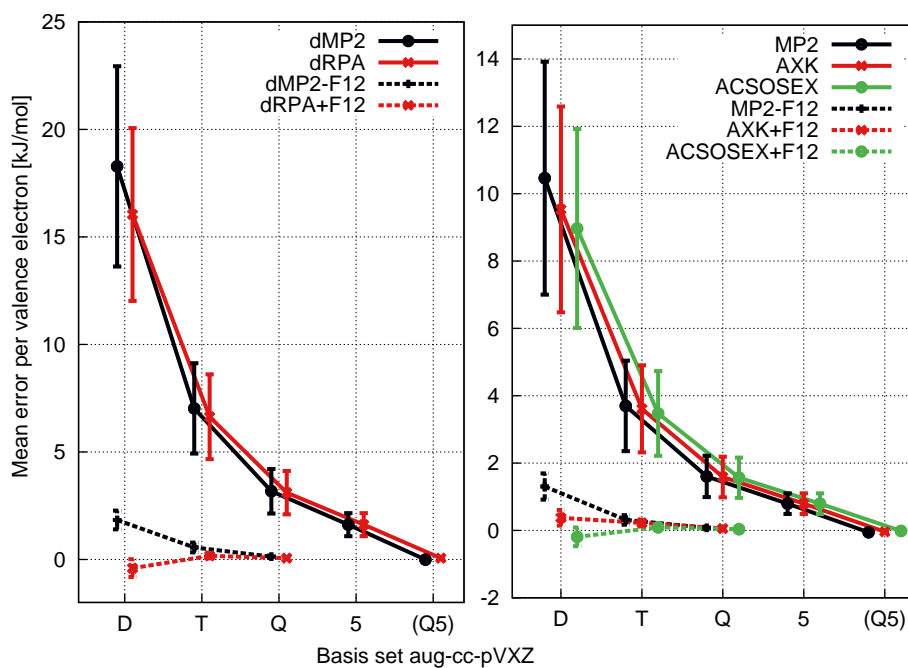
Fig. C.2: Basis-set convergence of the correlation energies, referring to Table C.1.

D. Derivation of dRPA-F12 based on the hypervirial theorem

Regarding the derivation of the conventional dRPA eigenvalue problem, it should be mentioned that the algebraic evaluation of Eq. (2.16) results in an additional factor of 2 for RHF references in comparison to the corresponding UHF formulation,

$$\langle \mathrm{HF}|[\hat{Q}_n, \hat{Q}_m^\dagger]|\mathrm{HF}\rangle = \langle \mathrm{HF}| \left[\sum_{ai} (X^\dagger)^n_{ia} \hat{E}_{ia} + \sum_{ai} (Y^\dagger)^n_{ia} \hat{E}_{ai}, \sum_{bj} X^m_{bj} \hat{E}_{bj} + \sum_{bj} Y^m_{bj} \hat{E}_{jb} \right] |\mathrm{HF}\rangle$$

$$= 2 \sum_{abij} \delta_{ab}\delta_{ij}((X^\dagger)^n_{ia} X^m_{bj} - Y^m_{bj}(Y^\dagger)^n_{ia}),$$
(D.1)

as spin summation implies

$$\langle \mathrm{HF}|[\hat{E}_{ia}, \hat{E}_{bj}]|\mathrm{HF}\rangle = \langle \mathrm{HF}|\hat{E}_{ij}\delta_{ab}|\mathrm{HF}\rangle = 2\delta_{ij}\delta_{ab}.$$
(D.2)

Normalization to unity (Eq. (2.16)) can however be conserved when introducing a metric (see Refs. [41, 42]) or by rewriting the equations in terms of the biorthogonal basis where the projection manifolds $\{\langle \bar{a}_i |, \langle \overline{ab}_{ij} |, ... \}$ are defined according to Eqs. (A.1) and (A.2).

Derivation of conventional dRPA according to Bouman and Hansen [117, 118]

Starting from the hypervirial theorem (Eq. (2.3)) and assuming the projection manifold for ground and excited state as proposed in Eqs. (2.4) and (2.5), the transition moment of the one-electron operator $\hat{O}$ can be summarized as

$$\langle \bar{0}|\hat{O}|n\rangle = N_0 \left[\langle \mathrm{HF}|\hat{O}|_i^a\rangle t^n_{ai} + \tfrac{1}{2} t^{ab}_{ij} \langle \overline{ab}_{ij}|\hat{O}|_k^c\rangle t^n_{ck} \right]$$

$$= N_0 \left[t^n_{ai}\langle \mathrm{HF}|\hat{O}|_i^a\rangle + \tfrac{1}{2} t^{ab}_{ij} t^n_{ck} \left[\langle \bar{a}_i|\hat{O}|\mathrm{HF}\rangle \delta_{bc}\delta_{jk} + \langle \bar{b}_j|\hat{O}|\mathrm{HF}\rangle \delta_{ac}\delta_{ik} \right] \right]$$

$$= X^n_{ai}\langle \mathrm{HF}|\hat{O}|_i^a\rangle + Y^n_{ai}\langle \bar{a}_i|\hat{O}|\mathrm{HF}\rangle,$$
(D.3)

depending on the amplitudes $\mathbf{X}^n$ and $\mathbf{Y}^n$ as defined within Eqs. (2.8) and (2.9). For the sake of convenience, the Einstein summation convention is assumed in Eq. (D.3) and in the following. Introducing the resolution of the identity,

$$1 = |\mathrm{HF}\rangle\langle \mathrm{HF}| + |_i^a\rangle\langle \bar{a}_i| + \tfrac{1}{2}|_{ij}^{ab}\rangle\langle \overline{ab}_{ij}| + \dots,$$
(D.4)

on the left-hand side of the hypervirial theorem gives

$$\langle \bar{0}|[\hat{O}, \hat{H}]|n\rangle = X^n_{ai}\langle \mathrm{HF}|[\hat{O}, \hat{H}]|_i^a\rangle + Y^n_{ai}\langle \bar{a}_i|[\hat{O}, \hat{H}]|\mathrm{HF}\rangle$$

$$= X^n_{ai} \left[\langle \mathrm{HF}|\hat{O}|_j^b\rangle \langle \bar{b}_j|\hat{H}|_i^a\rangle \right] - X^n_{ai} \left[\langle \mathrm{HF}|\hat{H}|\mathrm{HF}\rangle \langle \mathrm{HF}|\hat{O}|_i^a\rangle + \tfrac{1}{2}\langle \mathrm{HF}|\hat{H}|_{jk}^{bc}\rangle \langle \overline{bc}_{jk}|\hat{O}|_i^a\rangle \right]$$

$$+ Y^n_{ai} \left[\langle \bar{a}_i|\hat{O}|\mathrm{HF}\rangle \langle \mathrm{HF}|\hat{H}|\mathrm{HF}\rangle + \tfrac{1}{2}\langle \bar{a}_i|\hat{O}|_{jk}^{bc}\rangle \langle \overline{bc}_{jk}|\hat{H}|\mathrm{HF}\rangle \right] - Y^n_{ai} \left[\langle \bar{a}_i|\hat{H}|_j^b\rangle \langle \bar{b}_j|\hat{O}|\mathrm{HF}\rangle \right].$$
(D.5)

Note that the matrix elements $\langle \mathrm{HF}|\hat{H}|_i^a\rangle$ vanish due to Brillouin's theorem and that the projection onto the doubly excited determinants $\langle \mathrm{HF}|\hat{O}|_{ij}^{ab}\rangle$ equally cancels to zero as $\hat{O}$ represents a one-electron operator. Based on the dRPA definitions for matrices $\mathbf{A}$ (Eq. (2.11)) and $\mathbf{B}$ (Eq. (2.12)), Eq. (D.5) can be reformulated, exploiting the fact that both $\mathbf{A}$ and $\mathbf{B}$ are symmetric when assuming real orbitals,

$$\langle \bar{0}|[\hat{O}, \hat{H}]|n\rangle = X^n_{ai}\langle \mathrm{HF}|\hat{O}|_j^b\rangle A^{ab}_{ij} - X^n_{ai}\langle \bar{b}_j|\hat{O}|\mathrm{HF}\rangle B^{ab}_{ij}$$

$$- Y^n_{ai}\langle \bar{b}_j|\hat{O}|\mathrm{HF}\rangle A^{ab}_{ij} + Y^n_{ai}\langle \mathrm{HF}|\hat{O}|_j^b\rangle B^{ab}_{ij}.$$
(D.6)

For the sake of convenience, the superscript "dRPA" is omitted in the following when referring to matrices $\mathbf{A}$ and $\mathbf{B}$. As $\hat{O}$ was defined to be an arbitrary Hermitian operator, Eq. (D.6) can be split into two parts corresponding to the transition moments $\langle \mathrm{HF}|\hat{O}|_i^a\rangle$ and $\langle \bar{a}_i|\hat{O}|\mathrm{HF}\rangle$,

$$\langle \mathrm{HF}|\hat{O}|_i^a\rangle \rightarrow A^{ab}_{ij} X^n_{bj} + B^{ab}_{ij} Y^n_{bj} = \Omega_n X^n_{ai}$$
(D.7)

$$\langle \bar{a}_i|\hat{O}|\mathrm{HF}\rangle \rightarrow A^{ab}_{ij} Y^n_{bj} + B^{ab}_{ij} X^n_{bj} = -\Omega_n Y^n_{ai},$$
(D.8)

yielding the requested matrix eigenvalue problem of Eq. (2.7).

Evaluation of dRPA-F12 matrix elements

When adding geminals to the double excitation space and expanding the singles excitation manifold by means of the CABS basis, the transition moment is given as

$$
\begin{aligned}
\langle\bar{0}|\hat{O}|n\rangle = N_0 &\left[t_{ai}^{n_{\mathrm{V}}}\langle\mathrm{HF}|\hat{O}|_i^a\rangle + t_{p''i}^{n_{\mathrm{C}}}\langle\mathrm{HF}|\hat{O}|_i^{p''}\rangle + \tfrac{1}{2}t_{ai}^{n_{\mathrm{V}}}t_{kl}^{cd}\langle\overline{cd}|\hat{O}|_i^a\rangle + \tfrac{1}{2}t_{ai}^{n_{\mathrm{V}}}c_{kl}^{xy}(w^\dagger)_{\alpha\beta}^{xy}\langle\overline{\tfrac{\alpha\beta}{kl}}|\hat{O}|_i^a\rangle \right.\\
&\left. + \tfrac{1}{2}t_{p''i}^{n_{\mathrm{C}}}c_{kl}^{xy}(w^\dagger)_{\alpha\beta}^{xy}\langle\overline{\tfrac{\alpha\beta}{kl}}|\hat{O}|_i^{p''}\rangle \right]\\
= & \; X_{ai}^{n_{\mathrm{V}}}\langle\mathrm{HF}|\hat{O}|_i^a\rangle + X_{p''i}^{n_{\mathrm{C}}}\langle\mathrm{HF}|\hat{O}|_i^{p''}\rangle + Y_{ai}^{n_{\mathrm{V}}}\langle_i^{\bar{a}}|\hat{O}|\mathrm{HF}\rangle + (\mathbf{Y}^{\text{F12}})_{p''i}^{n_{\mathrm{V}}}\langle_i^{\overline{p''}}|\hat{O}|\mathrm{HF}\rangle\\
& + (\mathbf{Y}^{\text{F12}})_{ai}^{n_{\mathrm{C}}}\langle_i^{\bar{a}}|\hat{O}|\mathrm{HF}\rangle + (\mathbf{Y}^{\text{F12}})_{p''i}^{n_{\mathrm{C}}}\langle_i^{\overline{p''}}|\hat{O}|\mathrm{HF}\rangle .
\end{aligned}
\tag{D.9}
$$

n_{v} indicates the dimension ($N_{\mathrm{OCC}} \times N_{\mathrm{VIR}}$) and n_{c} the dimension ($N_{\mathrm{OCC}} \times N_{\mathrm{CABS}}$), respectively. Four commutators corresponding to the four different contributions to the transition moment $\langle\bar{0}|\hat{O}|n\rangle$ have to be evaluated,

$$
\begin{aligned}
\langle\mathrm{HF}|[\hat{O},\hat{H}]|_i^a\rangle = & \langle\mathrm{HF}|\hat{O}|_j^b\rangle\langle_j^{\bar{b}}|\hat{H}|_i^a\rangle + \langle\mathrm{HF}|\hat{O}|_j^{q''}\rangle\langle_j^{\overline{q''}}|\hat{H}|_i^a\rangle - \langle\mathrm{HF}|\hat{H}|\mathrm{HF}\rangle\langle\mathrm{HF}|\hat{O}|_i^a\rangle\\
& - \tfrac{1}{2}\langle\mathrm{HF}|\hat{H}|_{kl}^{cd}\rangle\langle\overline{cd}\langle|\hat{O}|_i^a\rangle - \tfrac{1}{2}\langle\mathrm{HF}|\hat{H}|_{kl}^{xy}\rangle(\boldsymbol{\mathcal{X}}^{-1})_{vw}^{xy}\langle\overline{\tfrac{vw}{kl}}|\hat{O}|_i^a\rangle\\
= & \; A_{ji}^{ba}\langle\mathrm{HF}|\hat{O}|_j^b\rangle + A_{ji}^{q''a}\langle\mathrm{HF}|\hat{O}|_j^{q''}\rangle - B_{ba}^{ji}\langle_j^{\bar{b}}|\hat{O}|\mathrm{HF}\rangle - ((\mathbf{B}^{\text{F12}})^\dagger)_{q''a}^{ji}\langle_j^{\overline{q''}}|\hat{O}|\mathrm{HF}\rangle ,
\end{aligned}
\tag{D.10}
$$

$$
\begin{aligned}
\langle\mathrm{HF}|[\hat{O},\hat{H}]|_i^{p''}\rangle = & \langle\mathrm{HF}|\hat{O}|_k^{q''}\rangle\langle_k^{\overline{q''}}|\hat{H}|_i^{p''}\rangle + \langle\mathrm{HF}|\hat{O}|_j^b\rangle\langle_j^{\bar{b}}|\hat{H}|_i^{p''}\rangle\\
& - \langle\mathrm{HF}|\hat{H}|\mathrm{HF}\rangle\langle\mathrm{HF}|\hat{O}|_i^{p''}\rangle - \tfrac{1}{2}\langle\mathrm{HF}|\hat{H}|_{kl}^{xy}\rangle(\boldsymbol{\mathcal{X}}^{-1})_{vw}^{xy}\langle\overline{\tfrac{vw}{kl}}|\hat{O}|_i^{p''}\rangle\\
= & \; A_{ji}^{bp''}\langle\mathrm{HF}|\hat{O}|_j^b\rangle + A_{ji}^{q''p''}\langle\mathrm{HF}|\hat{O}|_j^{q''}\rangle - ((\mathbf{B}^{\text{F12}})^\dagger)_{bp''}^{ji}\langle_j^{\bar{b}}|\hat{O}|\mathrm{HF}\rangle - ((\mathbf{B}^{\text{F12}})^\dagger)_{q''p''}^{ji}\langle_j^{\overline{q''}}|\hat{O}|\mathrm{HF}\rangle ,
\end{aligned}
\tag{D.11}
$$

$$
\begin{aligned}
\langle_i^{\bar{a}}|[\hat{O},\hat{H}]|\mathrm{HF}\rangle = & \langle_i^{\bar{a}}|\hat{O}|\mathrm{HF}\rangle\langle\mathrm{HF}|\hat{H}|\mathrm{HF}\rangle + \tfrac{1}{2}\langle_i^{\bar{a}}|\hat{O}|_{kl}^{cd}\rangle\langle\overline{cd}|\hat{H}|\mathrm{HF}\rangle\\
& + \tfrac{1}{2}\langle_i^{\bar{a}}|\hat{O}|_{kl}^{xy}\rangle(\boldsymbol{\mathcal{X}}^{-1})_{vw}^{xy}\langle\overline{\tfrac{vw}{kl}}|\hat{H}|\mathrm{HF}\rangle - \langle_i^{\bar{a}}|\hat{H}|_j^b\rangle\langle_j^{\bar{b}}|\hat{O}|\mathrm{HF}\rangle - \langle_i^{\bar{a}}|\hat{H}|_j^{q''}\rangle\langle_j^{\overline{q''}}|\hat{O}|\mathrm{HF}\rangle\\
= & \; B_{ji}^{ba}\langle\mathrm{HF}|\hat{O}|_j^b\rangle + (\mathbf{B}^{\text{F12}})_{ji}^{q''a}\langle\mathrm{HF}|\hat{O}|_j^{q''}\rangle - A_{ji}^{ba}\langle_j^{\bar{b}}|\hat{O}|\mathrm{HF}\rangle - A_{ji}^{q''a}\langle_j^{\overline{q''}}|\hat{O}|\mathrm{HF}\rangle ,
\end{aligned}
\tag{D.12}
$$

$$
\begin{aligned}
\langle_i^{\overline{p''}}|[\hat{O},\hat{H}]|\mathrm{HF}\rangle = & \langle_i^{\overline{p''}}|\hat{O}|\mathrm{HF}\rangle\langle\mathrm{HF}|\hat{H}|\mathrm{HF}\rangle + \tfrac{1}{2}\langle_i^{\overline{p''}}|\hat{O}|_{kl}^{xy}\rangle(\boldsymbol{\mathcal{X}}^{-1})_{vw}^{xy}\langle\overline{\tfrac{vw}{kl}}|\hat{H}|\mathrm{HF}\rangle\\
& - \langle_i^{\overline{p''}}|\hat{H}|_j^b\rangle\langle_j^{\bar{b}}|\hat{O}|\mathrm{HF}\rangle - \langle_i^{\overline{p''}}|\hat{H}|_j^{q''}\rangle\langle_j^{\overline{q''}}|\hat{O}|\mathrm{HF}\rangle\\
= & -A_{ji}^{bp''}\langle_j^{\bar{b}}|\hat{O}|\mathrm{HF}\rangle - A_{ji}^{q''p''}\langle_j^{\overline{q''}}|\hat{O}|\mathrm{HF}\rangle + (\mathbf{B}^{\text{F12}})_{ji}^{bp''}\langle\mathrm{HF}|\hat{O}|_j^b\rangle + (\mathbf{B}^{\text{F12}})_{ji}^{q''p''}\langle\mathrm{HF}|\hat{O}|_j^{q''}\rangle .
\end{aligned}
\tag{D.13}
$$

It should be noted that matrix $\mathbf{B}^{\text{F12}}$ is neither symmetric nor Hermitian, $\mathbf{B}^{\text{F12}} \neq (\mathbf{B}^{\text{F12}})^\dagger$. Moreover, the equation for $\langle\mathrm{HF}|\hat{O}|\mathrm{HF}\rangle$ is *a priori* fulfilled by assuming the GBC. Arranging Eqs. (D.10) to (D.13) according to the therein obtained left and right transition moments, $\langle\mathrm{HF}|\hat{O}|_i^a\rangle$, $\langle\mathrm{HF}|\hat{O}|_i^{p''}\rangle$, $\langle_i^{\bar{a}}|\hat{O}|\mathrm{HF}\rangle$ and $\langle_i^{\overline{p''}}|\hat{O}|\mathrm{HF}\rangle$, gives the extended dRPA-F12 eigenvalue problem of Eq. (3.14).

Orthogonalization of the eigenvectors

To ensure normalization, the eigenvectors $(\mathbf{X}^{\text{F12}})^n$ and $(\mathbf{Y}^{\text{F12}})^n$ are orthogonalized in the subspace of positive eigenvalues. First, the metric $\mathbf{U}$ of dimension ($N_{\mathrm{OCC}} \times (N_{\mathrm{VIR}} + N_{\mathrm{CABS}}), N_{\mathrm{OCC}} \times (N_{\mathrm{VIR}} + N_{\mathrm{CABS}})$),

$$
\mathbf{U} = \begin{pmatrix} \mathbf{1} & \mathbf{0} \\ \mathbf{0} & -\mathbf{1} \end{pmatrix} ,
\tag{D.14}
$$

is transformed with that part of the eigenvectors that corresponds to the subspace of positive eigenvalues, being of dimension $n/2$,

$$
\mathbf{U}' = \left(\mathbf{W}^{n/2}\right)^{\mathrm{T}} \mathbf{U}\mathbf{W}^{n/2} \quad\text{with}\quad \mathbf{W}^{n/2} = \begin{pmatrix} (\mathbf{X}^{\text{F12}})^{n/2} \\ (\mathbf{Y}^{\text{F12}})^{n/2} \end{pmatrix} .
\tag{D.15}
$$

Subsequently, the orthogonalized vectors $((\mathbf{X}^{F12})^{n/2})'$ and $((\mathbf{Y}^{F12})^{n/2})'$ of dimension $(N_{OCC} \times (N_{VIR} + N_{CABS})/2,$ $N_{OCC} \times (N_{VIR} + N_{CABS}))$ are obtained according to

$$\mathbf{W}^{n/2}(\mathbf{U}')^{-1/2} = \begin{pmatrix} ((\mathbf{X}^{F12})^{n/2})' \\ ((\mathbf{Y}^{F12})^{n/2})' \end{pmatrix}. \tag{D.16}$$

Test results

The investigated test set contains 20 closed-shell molecules, namely BeH_2, CH_2, HF, F_2, N_2, CO, $C_2H_3^+$, NO^+, BeO, C_2, O_3, CN^+, BN, C_2H_2, C_2H_4, CH_4, CO_2, H_2, H_2O, H_2O_2. Detailed information on the chosen geometries can be found in Ref. [178]. Energies were converged up to 1 nHartree, except for the dRPA/QZVPP+CABS calculations of molecules N_2 and BeH_2 where convergence could only be achieved up to 0.1 mHartree. A summary of mean (ME), mean absolute (MAD), root mean square (RMS) and percentage errors (PE) as well as the corresponding standard deviations (STD) is given in Table D.1. All errors are reported with respect to the dRPA-F12/def2-QZVPP result and are given per valence electron; the number of valence electrons ranges from 2 to 18 with a mean value of 10 electrons. To estimate the accuracy of the chosen dRPA-F12/def2-QZVPP reference, a trust region was extrapolated as described in Section 3.4. For the correlation energy contribution, an extrapolation factor of $F_{TQ} = 1.6520$ with a standard deviation of 0.217 mE_h per valence electron is obtained when performing the extrapolation based on the def2-TZVPP and def2-QZVPP results.

Tab. D.1: Statistical measures for the basis-set error per valence electron in the correlation energy for dRPA-F12 within ansatz 2, dRPA, dRPA/basis+CABS, and dRPA+CABS. Errors are calculated with respect to the dRPA-F12/def2-QZVPP result and are given in mE_h.

Basis set	ME	MAD	RMS	STD	MPE (STD)
dRPA					
def2-SVP	14.589	14.589	15.030	3.612	−32.740 (4.823)
def2-TZVPP	6.169	6.169	6.417	1.766	−13.704 (2.541)
def2-QZVPP	2.468	2.468	2.590	0.786	−5.430 (1.207)
dRPA/basis+CABS					
def2-SVP	4.803	4.803	4.920	1.069	−10.82 (1.348)
def2-TZVPP	1.700	1.700	1.755	0.437	−3.79 (0.589)
def2-QZVPP	0.285	0.285	0.308	0.117	−0.63 (0.252)
dRPA-F12					
def2-SVP	3.217	3.217	3.318	0.814	−7.31 (1.969)
def2-TZVPP	1.215	1.215	1.261	0.335	−2.83 (0.991)
dRPA+CABS					
def2-SVP	4.336	4.336	4.417	0.841	−9.87 (1.773)
def2-TZVPP	1.710	1.710	1.740	0.321	−3.94 (0.941)
def2-QZVPP	0.234	0.234	0.251	0.091	−0.54 (0.215)

E. Notes on the drCCD(F12) implementation in TURBOMOLE and validation of the drCCD(F12) and rCCD(F12) approaches
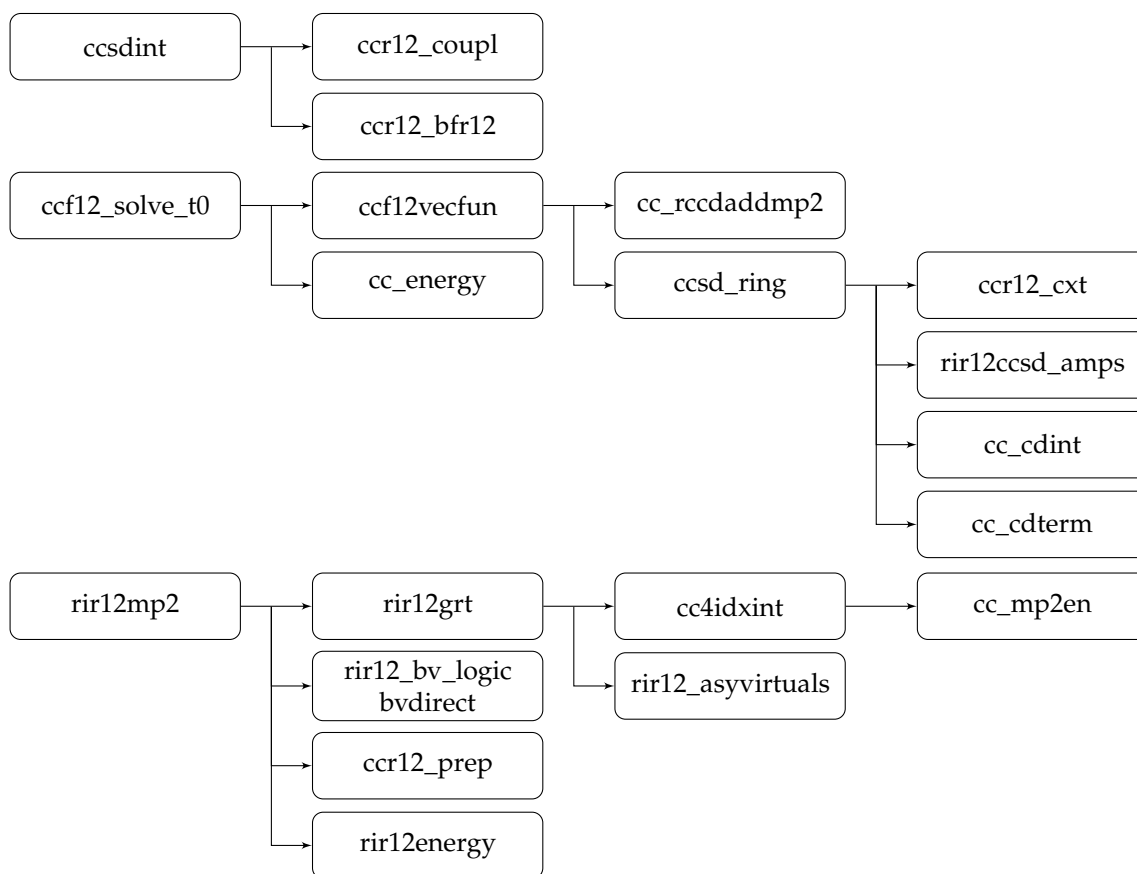
Fig. E.1: Program sketch summarizing the modified routines of the CCSDF12 module in the TURBOMOLE program package.

The drCCD(F12) method was implemented in the CCSDF12 program part of the TURBOMOLE program package for closed- and open-shell systems supporting ansatz 1, 2* and 2. The underlying CCSD(F12) implementation is documented in Refs. [216, 283]. In Figure E.1, a sketch of the CCSDF12 module in TURBOMOLE is given, including the most important subroutines that were changed for the drCCD(F12) implementation. Starting from CCD(F12), drCCD(F12) is obtained when neglecting all ladder terms and exchange contributions. The conventional ladder terms can be identified as explained in Figure 2.4, where all ring contributions to CCD are highlighted in red and labeled according to Ref. [216] as E, F, and D intermediates. The E and F terms are calculated in the especially for drCCD written routines `cc_rccdaddmp2` and `cc_addt2e`; for the D term the routine `ccsd_ring` of the already available CCSD(F12) implementation is used and modified accordingly. As exchange is neglected for the direct approach, all antisymmetrization steps are skipped. In the case of closed-shell systems, where antisymmetrization yields the typical "2 × Coulomb - Exchange" combination for amplitudes and integrals, an additional prefactor is introduced to account for the thus neglected, but still required double counting of the Coulomb contribution. It should be further noted that exchange contributions are sometimes included by exploiting the symmetry of the amplitudes. For spin orbitals,

$$t_{IJ}^{BA} = -t_{IJ}^{AB},$$ (E.1)

and, therefore, the calculation of the conventional CCD correlation energy can be rewritten as

$$E_C^{\text{CCD}} \overset{\text{UHF}}{=} \sum_{A>B,I>J} t_{IJ}^{AB}(g_{AB}^{IJ} - g_{BA}^{IJ}) = \tfrac{1}{4}\sum_{ABIJ} t_{IJ}^{AB}(g_{AB}^{IJ} - g_{BA}^{IJ}) \tag{E.2}$$

$$= \tfrac{1}{4}\sum_{ABIJ} t_{IJ}^{AB}g_{AB}^{IJ} + \tfrac{1}{4}\sum_{ABIJ} t_{IJ}^{BA}g_{BA}^{IJ} = \tfrac{1}{2}\sum_{ABIJ} t_{IJ}^{AB}g_{AB}^{IJ}$$

$$= \sum_{a>b,ij} t_{i\alpha j\alpha}^{a\alpha b\alpha}g_{a\alpha b\alpha}^{i\alpha j\alpha} + \sum_{a>b,ij} t_{i\beta j\beta}^{a\beta b\beta}g_{a\beta b\beta}^{i\beta j\beta} + \sum_{abij} t_{i\alpha j\beta}^{a\alpha b\beta}g_{a\alpha b\beta}^{i\alpha j\beta} \tag{E.3}$$

$$\overset{\text{RHF}}{=} \sum_{a>b,ij} t_{ij}^{ab}(g_{ab}^{ij} - g_{ba}^{ij}) + \sum_{a>b,ij} t_{ij}^{ab}(g_{ab}^{ij} - g_{ba}^{ij}) + \sum_{abij} t_{ij}^{ab}g_{ab}^{ij}$$

$$= \sum_{a>b,ij} 2t_{ij}^{ab}(2g_{ab}^{ij} - g_{ba}^{ij}) + \sum_{aij} t_{ij}^{aa}(g_{aa}^{ij}) . \tag{E.4}$$

The UHF CCD implementation in TURBOMOLE is based on Eq. (E.3), while the RHF implementation refers to Eq. (E.4). For drCCD, Eq. (E.1) does not hold, exclusion-principle violating terms do not vanish and both the drCCD amplitudes and the drCCD energy expression are not symmetric with respect to the permutation of indices A and B and I and J. Thus, an antisymmetrized reformulation as given in Eq. (E.2) is not possible, instead the drCCD energy is formulated as

$$E_C^{\text{drCCD}} \overset{\text{UHF}}{=} \tfrac{1}{2}\sum_{AIBJ} t_{IJ}^{AB}g_{AB}^{IJ}$$

$$= \tfrac{1}{2}\sum_{abij} t_{i\alpha j\alpha}^{a\alpha b\alpha}g_{a\alpha b\alpha}^{i\alpha j\alpha} + \tfrac{1}{2}\sum_{abij} t_{i\beta j\beta}^{a\beta b\beta}g_{a\beta b\beta}^{i\beta j\beta} + \sum_{abij} t_{i\alpha j\beta}^{a\alpha b\beta}g_{a\alpha b\beta}^{i\alpha j\beta} \tag{E.5}$$

$$\overset{\text{RHF}}{=} 2\sum_{abij} t_{ij}^{ab}g_{ab}^{ij} . \tag{E.6}$$

In consequence, the summations do not run over the triangle, but the complete matrices. This is also true for the implementation of the F12 part, especially for the calculation of the F12 intermediates $\mathcal{B}$ and $\mathcal{V}$. It should be furthermore noted that the original MP2-F12 implementation partitions all intermediates into singlet and triplet contributions, which is not possible for dMP2(F12) and drCCD(F12).

Coupling terms and KS Fock matrix

The drCCD(F12) method was implemented for ansatz 1, 2* and 2. While ansatz 1 and 2* assume the EBC and thus neglect coupling between conventional and geminal amplitudes, two additional coupling terms have to be considered within ansatz 2, contributing to the conventional and the geminal residuals,

$$(\mathbf{\Omega}^{\text{drCCD(F12)}})_{ij}^{ab} \leftarrow \langle \overline{ab}_{ij} |[\hat{F}, \hat{T}_{2'}]|\text{HF}\rangle = \sum_{xy} \mathcal{C}_{ab,xy}^{(ij)} c_{ij}^{xy} , \tag{E.7}$$

$$(\mathbf{\Omega}^{\text{F12(drCCD(F12))}})_{ij}^{xy} \leftarrow \langle \overline{xy}_{ij} |[\hat{F}, \hat{T}_2]|\text{HF}\rangle = \sum_{ab} \mathcal{C}_{xy,ab}^{(ij)} t_{ij}^{ab} . \tag{E.8}$$

Furthermore, a third coupling contribution needs to be added to the F12 intermediate $\mathcal{B}$, as outlined in Appendix B. The intermediate $\mathcal{C}$ is calculated in the routine ccr12_cxt using the Fock or KS matrix $\mathbf{F}$,

$$\mathcal{C}_{xy,ab} = \sum_{q''} f_{xy}^{aq''} F_{q''b} + \sum_{p''} f_{xy}^{p''b} F_{ap''} . \tag{E.9}$$

In TURBOMOLE, the KS matrix for the combined basis is generated in the program part RICCTOOLS, as implemented by David Tew [180]. For the CABS-singles correction, the CABS-CABS block of the KS matrix is required when assuming ansatz 2*, while further coupling contributions of the virtual-virtual and CABS-virtual block need to be considered within ansatz 2. Note, that for HF references, the virtual-virtual block of the Fock matrix is calculated without RI approximation while all other blocks are evaluated including RI. For KS references, in contrast, all blocks are calculated without RI.
Note that Eqs. (E.7) and (E.8) refer to diagrams [3f12t] and [3f12c_a] of Figure 4.2.

Performing drCCD(F12) calculations with TURBOMOLE

The keywords needed to perform a drCCD(F12) calculation are listed in Table E.1. In analogy to other CC methods, the $ricc2 keyword has to be added to the control file when requesting an (explicitly correlated or conventional) CC calculation and the desired CC approach has to be specified beneath. The F12 input section starts with the keyword $rir12. Open-shell drCCD(F12) calculations require spin-flipped amplitudes, which can be selected by choosing examp fixed flip. Furthermore, the keyword cofock needs to be added when using a KS reference and omitting the optional CABS-singles correction with cabssingles off. It should be noted that choosing ansatz 2 as an option in the $rir12 keyword section yields drCCD(F12) within ansatz 2^*, consistent with the underlying CCSD(F12) implementation. Performing a drCCD(F12) calculation also yields the dMP2(F12) result that is needed e.g. to set up the additive dRPA+F12 scheme. Note that it is often necessary to apply a shift to the quasi-Newton update and to modify the DIIS algorithn (direct inversion of the iterative subspace) in order to accelerate convergence to the ground state.

Tab. E.1: Required keywords to run a drCCD(F12) calculation.

keyword		description
$non-canonical MOs		calculation of KS Fock matrix without assuming GBC or EBC, necessary for KS references
$ricc2		keyword for conventional drCCD calculation
drccd		
$rir12		additional keyword for drCCD(F12)
ansatz	1/2	chosen ansatz for $\hat{Q}_{12}$, possible options: 1,2
ccsdapprox	rccd(f12)	ring approximation to CCSD(F12)
examp	fixed noflip/flip	chosen approximation for geminal amplitudes
cabssingles	off/ks	CABS-singles correction with KS Fock matrix
cofock		needed in case of cabssingles off

Validation of the drCCD(F12) approach

Statistical measures, which are needed for the discussion on drCCD(F12) and rCCD(F12) in Chapter 4 but not given in the supplementary material of Refs. [156, 180], are summarized in the following Tables E.2 to E.8.

Tab. E.2: Ten molecules of the S22 test set: Statistical measures for the basis-set error per valence electron with respect to drCCD(F12)/jun-cc-pV(Q+d)Z results for the correlation energy (in kJ/mol).

Basis set	ME	MAD	RMS	STD	MPE (STD)
		drCCD			
jun-cc-pV(D+d)Z	−43.970	43.970	44.338	5.697	−29.41 (2.18)
jun-cc-pV(T+d)Z	−17.287	17.287	17.500	2.727	−11.54 (1.15)
jun-cc-pV(Q+d)Z	−7.653	7.653	7.774	1.367	−5.10 (0.61)
		drCCD(F12) — Ansatz 2^*			
jun-cc-pV(D+d)Z	−5.346	5.346	5.349	0.187	−3.60 (0.21)
jun-cc-pV(T+d)Z	−1.013	1.013	1.019	0.102	−0.68 (0.03)
jun-cc-pV(Q+d)Z	−0.007	0.017	0.021	0.020	−0.00 (0.01)
		drCCD(F12) — Ansatz 2			
jun-cc-pV(D+d)Z	−5.994	5.994	5.999	0.244	−4.04 (0.34)
jun-cc-pV(T+d)Z	−1.080	1.080	1.084	0.094	−0.72 (0.04)
		RPA+F12 — Ansatz 2^*			
jun-cc-pV(D+d)Z	−3.412	3.412	3.444	0.467	−2.31 (0.42)
jun-cc-pV(T+d)Z	−0.575	0.575	0.576	0.024	−0.39 (0.03)
jun-cc-pV(Q+d)Z	0.078	0.078	0.082	0.027	0.05 (0.02)

Tab. E.3: Test set of 106 molecules: Statistical measures for the basis-set error per valence electron of the correlation contribution to the atomization energy for the drCCD(F12) approach within ansatz 1. Errors are calculated with respect to the drCCD(F12)[A2]+CABS/aug-cc-pV5Z result and are given in kJ/mol.

Basis set	ME	MAD	RMS	STD	MPE (STD)
aug-cc-pVDZ	−3.843	3.843	3.919	0.768	−10.29 (2.08)
aug-cc-pVTZ	−0.976	0.976	1.005	0.236	−2.62 (0.68)
aug-cc-pVQZ	−0.335	0.335	0.348	0.094	−0.89 (0.22)
aug-cc-pV5Z	−0.228	0.228	0.235	0.055	−0.61 (0.15)

Tab. E.4: Test set of 106 molecules: Statistical measures for the basis-set error per valence electron of the correlation energy. Errors are calculated with respect to the drCCD(F12)[A2]+CABS/aug-cc-pV5Z result and are given in kJ/mol.

Basis set	ME	MAD	RMS	STD	MPE (STD)
		drCCD			
aug-cc-pVDZ	−46.161	46.161	46.640	6.664	−28.39 (2.46)
aug-cc-pVTZ	−19.157	19.157	19.467	3.461	−11.75 (1.46)
aug-cc-pVQZ	−8.945	8.945	9.121	1.785	−5.48 (0.78)
aug-cc-pV5Z	−4.686	4.686	4.781	0.948	−2.87 (0.42)
aug-cc-pV6Z	−2.723	2.723	2.778	0.554	−1.67 (0.25)
		drCCD(F12) — Ansatz 1			
aug-cc-pVDZ	−22.956	22.956	23.151	2.991	−14.13 (1.05)
aug-cc-pVTZ	−8.966	8.966	9.139	1.769	−5.49 (0.79)
aug-cc-pVQZ	−3.433	3.433	3.512	0.743	−2.10 (0.34)
aug-cc-pV5Z	−1.434	1.434	1.466	0.309	−0.88 (0.14)
		drCCD(F12) — Ansatz 2*			
aug-cc-pVDZ	−3.320	3.320	3.405	0.758	−2.08 (0.56)
aug-cc-pVTZ	−0.959	0.959	0.983	0.217	−0.59 (0.10)
aug-cc-pVQZ	−0.227	0.227	0.240	0.078	−0.14 (0.04)
aug-cc-pV5Z	0.019	0.021	0.025	0.016	0.01 (0.01)
		drCCD(F12) — Ansatz 2			
aug-cc-pVDZ	−3.661	3.661	3.699	0.524	−2.29 (0.46)
aug-cc-pVTZ	−1.133	1.133	1.156	0.229	−0.70 (0.10)
aug-cc-pVQZ	−0.313	0.313	0.325	0.087	−0.19 (0.04)
		RPA+F12 — Ansatz 2*			
aug-cc-pVDZ	−0.846	1.343	1.611	1.371	−0.57 (0.88)
aug-cc-pVTZ	−0.410	0.410	0.420	0.092	−0.25 (0.05)
aug-cc-pVQZ	−0.114	0.114	0.122	0.044	−0.07 (0.02)
aug-cc-pV5Z	0.040	0.041	0.045	0.020	0.02 (0.01)

Tab. E.5: Mean percentage errors and corresponding standard deviations for the total atomization energies of the test set of 106 molecules, calculated for the aug-cc-pVXZ basis sets and given in kJ/mol.

	D	T	Q	5	6
drCCD	−8.49 (3.20)	−2.47 (0.74)	−0.95 (0.31)	−0.52 (0.22)	−0.34 (0.15)
dRPA+F12 [A2*]	−2.35 (1.39)	−0.19 (0.12)	−0.07 (0.03)	−0.04 (0.03)	—
drCCD(F12) [A1]	−6.37 (3.00)	−1.32 (0.41)	−0.50 (0.12)	−0.25 (0.10)	—
drCCD(F12) [A2*]	−2.52 (1.61)	−0.15 (0.12)	−0.07 (0.03)	−0.04 (0.03)	—
drCCD(F12) [A2*] + CABS	−0.58 (0.39)	0.10 (0.10)	−0.04 (0.04)	−0.04 (0.02)	—
drCCD(F12) [A2] + CABS	−0.01 (0.18)	0.21 (0.16)	0.12 (0.15)	—	—

Tab. E.6: Mean percentage errors and corresponding standard deviations for the CP-corrected interaction energies of the S22 test set, calculated for the jun-cc-pV(X+d)Z basis sets and given in kJ/mol.

	D	T	Q
drCCD	−56.21 (28.37)	−19.37 (7.48)	−6.42 (1.41)
dRPA+F12 [A2*]	−31.36 (24.22)	−6.75 (4.91)	−0.40 (0.14)
drCCD(F12) [A2*]	−32.17 (24.55)	−7.06 (5.00)	−0.48 (0.16)
drCCD(F12) [A2*] + CABS	−33.58 (24.49)	−6.54 (4.89)	−0.44 (0.13)
drCCD(F12) [A2] + CABS	−33.68 (24.34)	−5.70 (4.61)	—

Tab. E.7: Mean percentage errors and corresponding standard deviations for the correlation energies of the test set given in Appendix E, calculated for the def2-X basis sets and given in kJ/mol.

	SVP	TZVPP	QZVPP	(TQ)ZVPP
rCCD	−25.17 (5.15)	−9.34 (2.17)	−3.82 (0.93)	0.20 (0.24)
rCCD+F12 [A2*]	−6.10 (1.43)	−1.19 (0.25)	−0.08 (0.02)	—
rCCD(F12) [A2*]	−5.43 (1.43)	−0.96 (0.23)	—	—
rCCD-SO2	−28.87 (4.39)	−11.60 (2.28)	−5.05 (1.10)	−0.27 (0.32)
rCCD+F12-SO2 [A2*]	−3.60 (2.05)	−0.58 (0.22)	0.05 (0.03)	—
rCCD(F12)-SO2 [A2*]	−4.44 (1.65)	−0.78 (0.15)	—	—
rCCD-SO1	−26.36 (5.18)	−10.34 (2.35)	−4.37 (1.07)	−0.01 (0.27)
rCCD+F12-SO1 [A2*]	−4.17 (1.67)	−0.85 (0.17)	−0.01 (0.01)	—
rCCD(F12)-SO1 [A2*]	−4.51 (1.49)	−0.90 (0.17)	—	—

Tab. E.8: Mean percentage errors and corresponding standard deviations for the correlation contribution to the atomization energies of the test set given in Appendix E, calculated for the def2-X basis sets and given in kJ/mol.

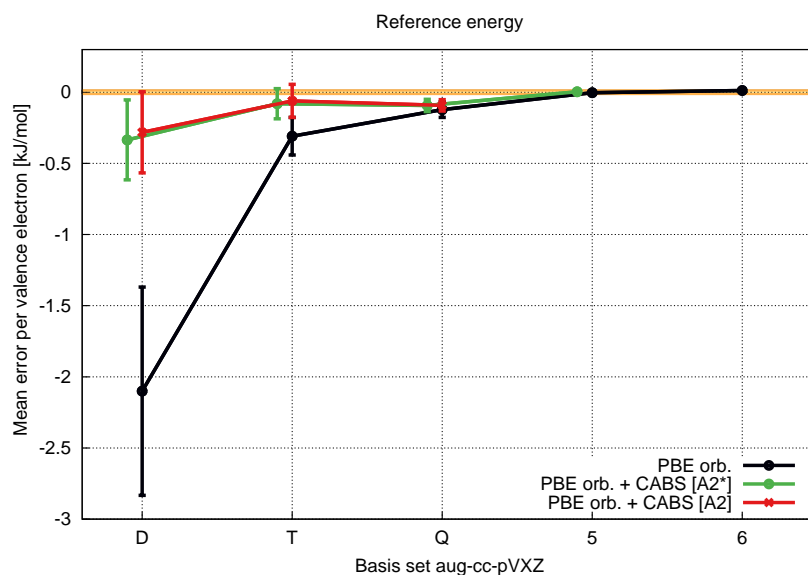|	SVP	TZVPP	QZVPP	(TQ)ZVPP
rCCD	−14.36 (4.59)	−6.18 (0.57)	−2.46 (0.30)	0.25 (0.44)
rCCD+F12 [A2*]	−0.43 (3.88)	−0.61 (0.30)	0.05 (0.03)	—
rCCD(F12) [A2*]	0.27 (3.86)	−0.40 (0.38)	—	—
rCCD-SO2	−15.32 (4.51)	−7.03 (1.65)	−3.16 (0.86)	−0.34 (0.52)
rCCD+F12-SO2 [A2*]	0.74 (3.32)	−0.28 (0.34)	−0.14 (0.06)	—
rCCD(F12)-SO2 [A2*]	1.64 (3.37)	0.10 (0.43)	—	—

Fig. E.2: Basis-set convergence of the reference energy for the test set of 106 molecules.
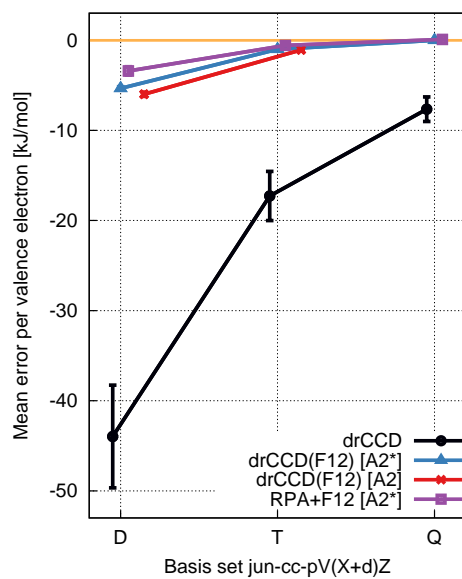
Fig. E.3: Basis-set convergence of the correlation energy for 10 molecules of the S22 test set.

F. D_1 and D_2 diagnostics

Evaluation for main-group compounds

Nielsen and Janssen tested their proposed D_1 and D_2 diagnostics on 34 small closed-shell molecules, comprising the molecules HF, H_2O, NH_3, CH_4, HCl, SiH_4, CO_2 H_2S, BeO, CO, HNC, N_2, ClOH, Cl_2, HCN, CH_2O, Cl_2O, C_2H_2, FOH, FNO, CH_2NH, C_2H_4, H_2N_2, ClNO, HNO, CH_2, F_2, P_2, BF, BCl, O_3, CN^+, C_2, and C_3. In Chapter 5, an analogous diagnostic scheme is set up using dRPA excitation amplitudes. HF, PBE and PBE0 references were tested as input for the dRPA correlation treatment; corresponding results are listed in Tables F.1 to F.3. Standardly, the test set includes the C_3 molecule in its linear geometry. However, for dRPA using a PBE reference, geometry optimization yields a non-linear alignment as ground-state structure prohibiting a reliable comparison. As also HF and PBE0 results yield errors which are one magnitude larger than the errors for the other test molecules (in accordance with Refs. [247, 248]), the C_3 molecule was excluded from the benchmark set. Furthermore, PBE reference calculations for the CN^+ and the C_2 molecule yielded negative HOMO-LUMO gaps, favoring the triplet instead of the singlet ground state and prohibiting further geometry optimizations at the RPA level. Results are therefore excluded in the corresponding Table F.2. To allow a straightforward comparison with Refs. [247, 248], CCSD diagnostic data using the cc-pwCVTZ basis is provided in Table F.4.

Tab. F.1: D_1 and D_2 diagnostics for HF references: dRPA bond distances r and harmonic vibrational frequencies ω are compared to the corresponding CCSD(T) reference values. Only the frequency with the largest percentage error is reported.

Molecule	D_2(dRPA)	D_1(dRPA)	r [Å]			ω [cm^{-1}]		
			dRPA	CCSD(T)	Error [%]	dRPA	CCSD(T)	Error [%]
HF	0.080551	0.028927	0.916	0.917	−0.10	4257.21	4178.09	1.89
H_2O	0.085831	0.027375	0.957	0.958	−0.17	1723.23	1667.66	3.33
NH_3	0.089069	0.021718	1.011	1.012	−0.13	1186.06	1105.10	7.33
CH_4	0.090898	0.028039	1.087	1.087	−0.01	1403.35	1347.69	4.13
HCl	0.095041	0.033404	1.268	1.272	−0.35	3085.41	3013.67	2.38
SiH_4	0.094243	0.022688	1.469	1.474	−0.33	984.30	936.50	5.10
CO_2	0.095663	0.028249	1.156	1.163	−0.55	706.88	668.29	5.77
H_2S	0.100631	0.032979	1.329	1.335	−0.45	1272.69	1214.00	4.83
BeO	0.099022	0.028598	1.315	1.338	−1.72	1612.64	1467.79	9.87
CO	0.096690	0.033651	1.124	1.131	−0.66	2258.92	2163.72	4.40
HNC	0.102053	0.035423	1.162, 0.989	1.171, 0.996	−0.79	2156.89	2056.97	4.86
N_2	0.103671	0.044452	1.088	1.100	−1.07	2518.05	2357.28	6.82
ClOH	0.104131	0.025597	1.677, 0.959	1.696, 0.964	−1.12	801.30	736.03	8.87
Cl_2	0.108418	0.039078	1.993	2.002	−0.43	583.40	552.49	5.59
HCN	0.106693	0.038920	1.145, 1.062	1.145, 1.066	−0.92	795.46	724.83	9.74
CH_2O	0.104856	0.039627	1.200, 1.098	1.206, 1.102	−0.54	1272.03	1194.97	6.45
Cl_2O	0.106933	0.029576	1.677	1.703	−1.52	843.98	708.00	19.21
C_2H_2	0.109138	0.039013	1.196, 1.058	1.206, 1.063	−0.83	644.15	589.84	9.21
FOH	0.104017	0.040038	1.402, 0.962	1.435, 0.966	−2.29	1073.80	928.45	15.65
FNO	0.105566	0.040759	1.437, 1.135	1.496, 1.138	−3.93	623.61	550.25	13.33
CH_2NH	0.109969	0.044138	1.265, 1.088	1.273, 1.091	−0.62	1160.66	1084.22	7.05
			1.084, 1.015	1.087, 1.020				
C_2H_4	0.112178	0.045161	1.079, 1.328	1.082, 1.333	−0.33	1033.43	969.37	6.61
H_2N_2	0.110614	0.049127	1.024, 1.235	1.029, 1.250	−1.17	1673.23	1564.38	6.96
ClNO	0.116359	0.048779	1.132, 1.914	1.139, 1.971	−2.91	654.52	613.24	6.73
HNO	0.109424	0.048822	1.195, 1.043	1.211, 1.054	−1.33	1762.52	1600.20	10.14
CH_2 ($\tilde{a}^1A_1$)	0.097978	0.034400	1.103	1.108	−0.47	1469.15	1407.06	4.41
F_2	0.108085	0.057004	1.367	1.413	−3.25	1142.66	925.43	23.47
P_2	0.123169	0.047117	1.874	1.901	−1.44	850.85	778.29	9.32
BF	0.111334	0.037384	1.267	1.265	0.17	1418.36	1413.89	0.32
BCl	0.114675	0.037257	1.723	1.718	0.30	848.61	846.87	0.21
O_3	0.135416	0.070177	1.236	1.273	−2.88	1252.49	1061.60	17.98
CN^+ ($\tilde{a}^1\Sigma^+$)	0.133582	0.053080	1.175	1.162	1.11	2029.34	1982.08	2.38
C_2	0.142254	0.065515	1.254	1.245	0.73	1825.94	1859.20	−1.79

Tab. F.2: D_1 and D_2 diagnostics for PBE references: dRPA bond distances r and harmonic vibrational frequencies ω are compared to the corresponding CCSD(T) reference values. Only the frequency with the largest percentage error is reported.

Molecule	D_2(dRPA)	D_1(dRPA)	r [Å]	Error [%]	ω [cm^{-1}]	Error [%]
HF	0.111317	0.038990	0.922	0.59	4093.08	−2.03
H_2O	0.118778	0.035127	0.964	0.58	3855.06	−2.33
NH_3	0.125730	0.032970	1.018	0.52	1131.99	2.43
CH_4	0.128820	0.038225	1.090	0.31	3110.74	−1.65
HCl	0.137207	0.044970	1.275	0.19	2977.72	−1.19
SiH_4	0.144350	0.038473	1.474	0.03	2243.96	−0.90
CO_2	0.152091	0.069138	1.170	0.64	625.88	−6.35
H_2S	0.149523	0.048134	1.337	0.18	2693.10	−1.44
BeO	0.166871	0.076383	1.358	1.46	1388.73	−5.39
CO	0.156071	0.072803	1.138	0.58	2118.09	−2.11
HNC	0.156828	0.074014	1.177, 0.998	0.50	419.74	−11.01
N_2	0.152013	0.086581	1.105	0.50	2319.99	−1.58
ClOH	0.169299	0.052918	1.720, 0.969	1.42	692.95	−5.85
Cl_2	0.172780	0.074551	2.026	1.22	516.60	−6.50
HCN	0.159017	0.081863	1.161, 1.069	0.44	683.93	−5.64
CH_2O	0.161370	0.085336	1.212, 1.105	0.49	1162.18	−2.74
Cl_2O	0.185949	0.057875	1.725	1.33	667.68	−5.69
C_2H_2	0.164249	0.082493	1.209, 1.066	0.29	538.55	−8.69
FOH	0.182491	0.081106	1.459, 0.972	1.65	881.82	−5.02
FNO	0.187004	0.087779	1.541, 1.142	3.01	498.25	−9.45
CH_2NH	0.169237	0.085535	1.279, 1.093	0.45	3385.05	−1.84
			1.089, 1.025			
C_2H_4	0.173629	0.099145	1.084, 1.336	0.27	918.31	−3.18
H_2N_2	0.178478	0.101637	1.034, 1.257	0.58	1299.06	−2.44
ClNO	0.205134	0.132531	1.143, 2.024	2.68	307.67	−10.68
HNO	0.211678	0.129142	1.221, 1.057	0.79	1491.52	−3.44
CH_2 ($\tilde{a}^1A_1$)	0.227483	0.194202	1.110	0.13	1301.19	−7.52
F_2	0.208954	0.127542	1.437	1.66	883.08	−4.58
P_2	0.197844	0.095907	1.907	0.31	766.88	−1.47
BF	0.199913	0.102910	1.272	0.53	1419.65	0.41
BCl	0.213495	0.102771	1.723	0.31	836.27	−1.25
O_3	0.269978	0.164462	1.291	1.48	667.51	−7.24

Tab. F.3: D_1 and D_2 diagnostics for PBE0 references: dRPA bond distances r and harmonic vibrational frequencies ω are compared to the corresponding CCSD(T) reference values. Only the frequency with the largest percentage error is reported.

Molecule	D_2(dRPA)	D_1(dRPA)	r [Å]	Error [%]	ω [cm^{-1}]	Error [%]
HF	0.099973	0.036226	0.907	−1.00	4285.75	2.58
H$_2$O	0.118778	0.033381	0.964	−1.01	4055.67	2.75
NH$_3$	0.112273	0.030027	1.002	−1.03	1001.50	−9.38
CH$_4$	0.115673	0.035315	1.079	−0.71	3219.68	1.80
HCl	0.122577	0.039021	1.264	−0.67	3072.21	1.94
SiH$_4$	0.126918	0.030415	1.467	−0.47	2291.46	0.99
CO$_2$	0.129445	0.054959	1.157	−0.49	1389.96	2.82
H$_2$S	0.132356	0.042303	1.326	−0.65	1239.92	2.14
BeO	0.136051	0.048549	1.325	−0.99	1554.18	5.89
CO	0.132828	0.057684	1.125	−0.57	2230.14	3.07
HNC	0.133585	0.058659	1.166, 0.989	−0.61	439.34	−6.86
N$_2$	0.134360	0.069832	1.092	−0.71	2125.51	3.93
ClOH	0.137020	0.040759	1.675, 0.954	−1.28	2450.00	5.74
Cl$_2$	0.143149	0.054815	1.983	−0.96	778.27	3.70
HCN	0.139732	0.064179	1.147, 1.062	−0.80	572.93	7.41
CH$_2$O	0.139821	0.065902	1.195, 1.101	−0.93	1851.85	3.65
Cl$_2$O	0.142641	0.040060	1.679	−1.40	749.96	5.93
C$_2$H$_2$	0.144463	0.065565	1.202, 1.058	−0.49	757.60	28.44
FOH	0.141985	0.067865	1.411, 0.958	−1.67	1018.97	9.75
FNO	0.149174	0.058616	1.477, 1.131	−1.29	1936.82	4.21
CH$_2$NH	0.169237	0.109035	1.279, 1.093	−0.92	1129.24	4.15
			1.089, 1.025			
C$_2$H$_4$	0.150159	0.076057	1.075, 1.320	−0.93	1004.46	5.91
H$_2$N$_2$	0.147224	0.078875	1.020, 1.237	−1.04	1614.04	3.17
ClNO	0.165282	0.092465	1.130, 1.947	−1.21	1915.51	4.56
HNO	0.149684	0.063626	1.196, 1.049	−1.31	1705.71	6.59
CH$_2$ (ã^{1}A$_1$)	0.145090	0.077236	1.104	−0.35	2952.18	0.99
F$_2$	0.155028	0.092750	1.384	−2.05	1067.04	15.30
P$_2$	0.169187	0.073497	1.881	−1.06	826.66	6.21
BF	0.163347	0.074929	1.255	−0.77	1465.38	3.64
BCl	0.171168	0.072283	1.710	−0.48	871.98	2.97
O$_3$	0.203907	0.119920	1.249	−1.89	1247.35	17.50
CN$^+$ (ã^{1}Σ$^+$)	0.201529	0.109432	1.167	0.67	2107.56	6.33
C$_2$	0.207375	0.109505	1.236	−0.71	1934.47	4.05

Tab. F.4: D_1 and D_2 diagnostics for the CCSD method using HF references: Bond distances r and harmonic vibrational frequencies ω are compared with the corresponding CCSD(T) reference values. Only the frequency with the largest percentage error is reported.

| Molecule	D_2(CCSD)	D_1(CCSD)	r [Å]	Error [%]	ω [cm^{-1}]	Error [%]
HF	0.117700	0.011520	0.914	−0.24	4215.05	0.88
H_2O	0.125681	0.010717	0.956	−0.25	3881.21	0.97
NH_3	0.130178	0.010545	1.010	−0.23	3513.67	0.90
CH_4	0.134228	0.013188	1.086	−0.12	1360.36	0.94
HCl	0.142087	0.012529	1.270	−0.16	3037.24	0.78
SiH_4	0.146649	0.018627	1.473	−0.08	946.02	1.03
CO_2	0.148959	0.046280	1.156	−0.62	693.37	3.75
H_2S	0.156152	0.018332	1.332	−0.17	1230.33	1.35
BeO	0.158392	0.100262	1.322	−1.18	1568.65	6.87
CO	0.159740	0.038816	1.124	−0.62	2233.87	3.24
HNC	0.169574	0.032089	1.164, 0.993	−0.61	494.06	4.74
N_2	0.170482	0.027761	1.093	−0.65	2437.15	3.39
ClOH	0.166007	0.022927	1.682, 0.960	−0.83	772.18	4.91
Cl_2	0.169091	0.022400	1.993	−0.45	570.90	3.33
HCN	0.179052	0.028904	1.149, 1.064	−0.64	752.17	3.77
CH_2O	0.148636	0.059362	1.200, 1.100	−0.55	1836.59	2.80
Cl_2O	0.175484	0.043992	1.686	−0.97	773.18	9.21
C_2H_2	0.180172	0.030047	1.199, 1.061	−0.54	634.25	7.53
FOH	0.184645	0.033657	1.416, 0.963	−1.33	1002.63	7.99
FNO	0.184613	0.057168	1.461, 1.133	−2.35	596.34	8.38
CH_2NH	0.185920	0.053281	1.266, 1.089	−0.57	1725.41	2.58
			1.085, 1.017			
C_2H_4	0.193309	0.033521	1.080, 1.327	−0.45	978.68	3.19
H_2N_2	0.195891	0.034413	1.026, 1.239	−0.83	1626.32	3.96
ClNO	0.197000	0.061503	1.132, 1.935	−1.84	637.96	4.03
HNO	0.219408	0.038463	1.200, 1.050	−0.92	1673.42	4.58
CH_2 (ã^{1}A$_1$)	0.205803	0.019483	1.107	−0.14	1423.45	1.16
F_2	0.209785	0.028163	1.391	−1.55	1021.09	10.34
P_2	0.206465	0.034593	1.884	−0.90	819.04	5.24
BF	0.222689	0.030087	1.262	−0.28	1430.03	1.14
BCl	0.237401	0.033045	1.716	−0.14	852.69	0.69
O_3	0.257505	0.071522	1.247	−2.02	1272.87	19.90
CN$^+$ (ã$^1\Sigma^+$)	0.365598	0.189252	1.175	1.09	2065.55	4.21
C_2	0.371018	0.085734	1.242	−0.28	1894.99	1.92
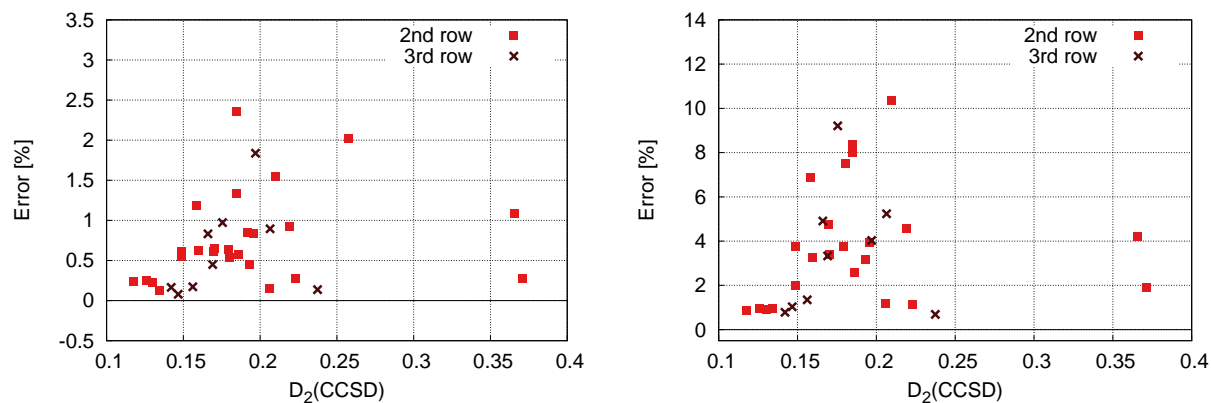
Fig. F.1: D_2 diagnostics for bond lengths (left) and vibrational frequencies (right) for CCSD using a HF reference, corresponding to Table F.4 of Appendix F.
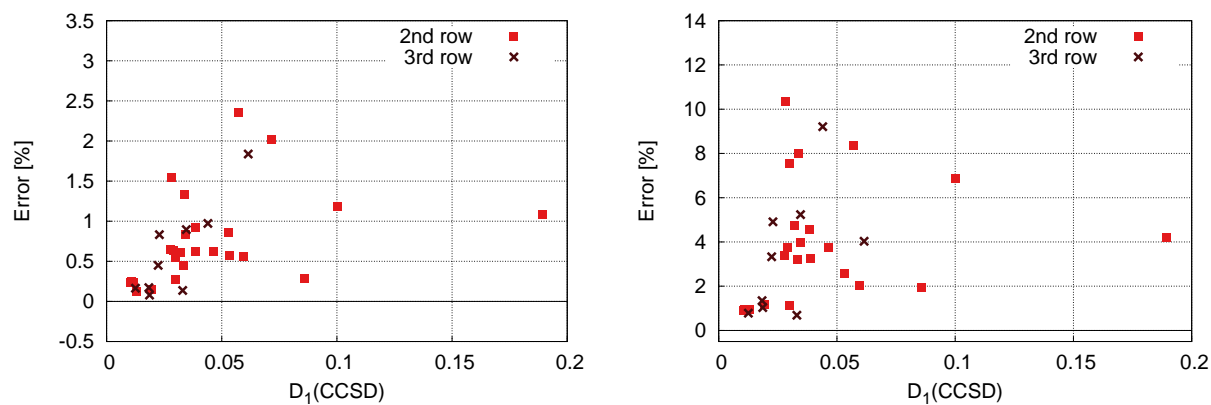

Fig. F.2: D_1 diagnostics for bond lengths (left) and vibrational frequencies (right) for CCSD using a HF reference, corresponding to Table F.4 of Appendix F.
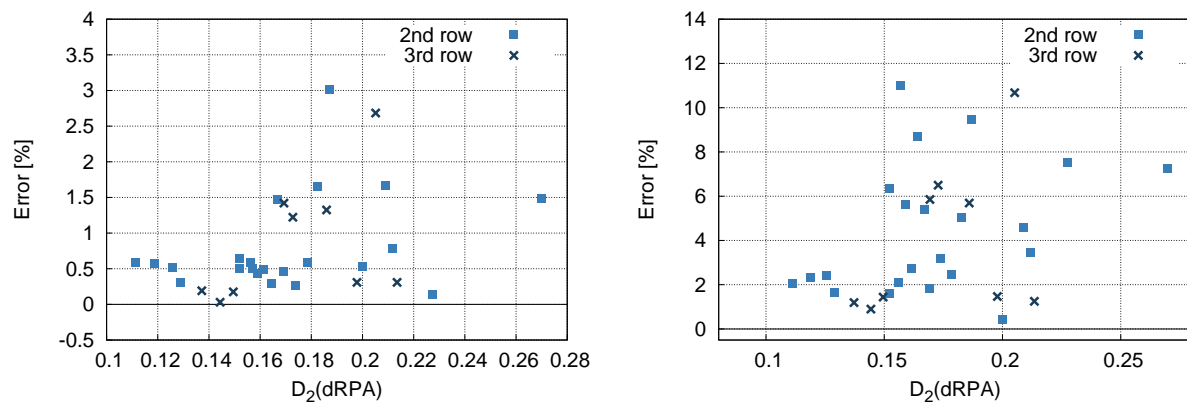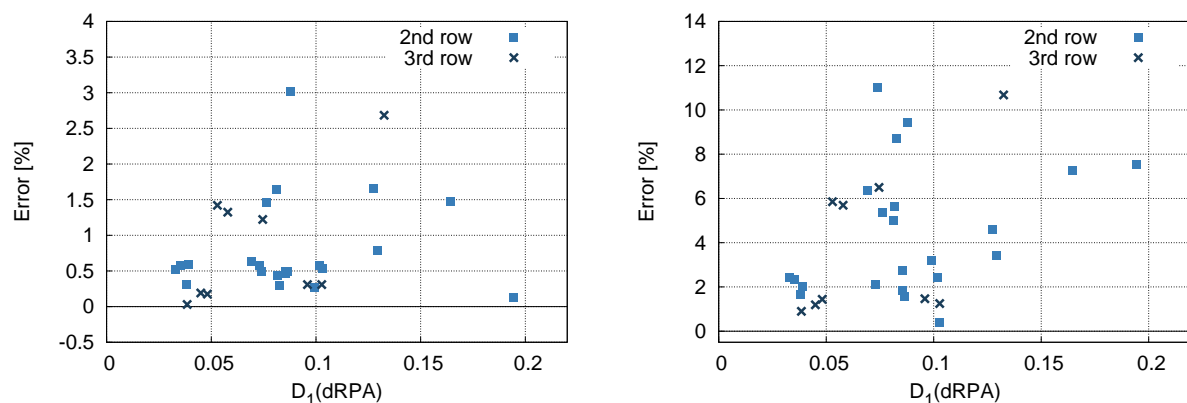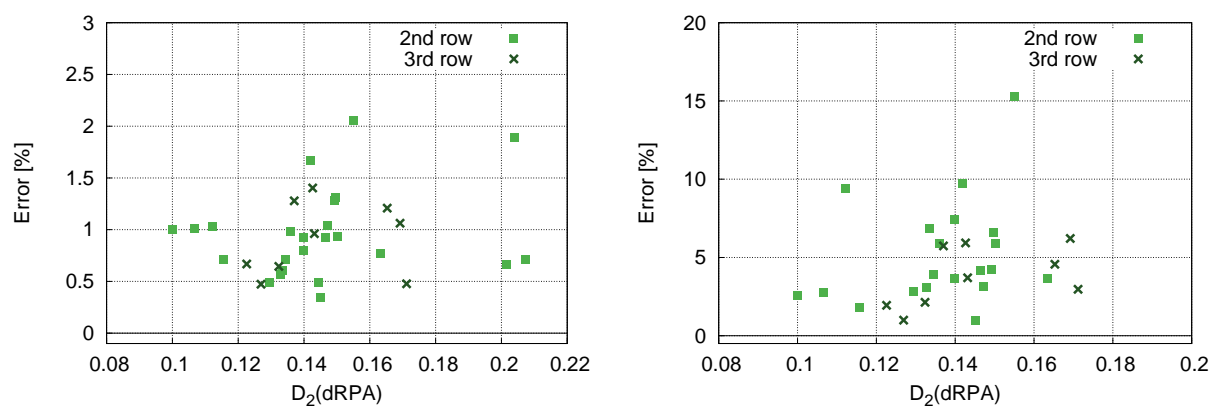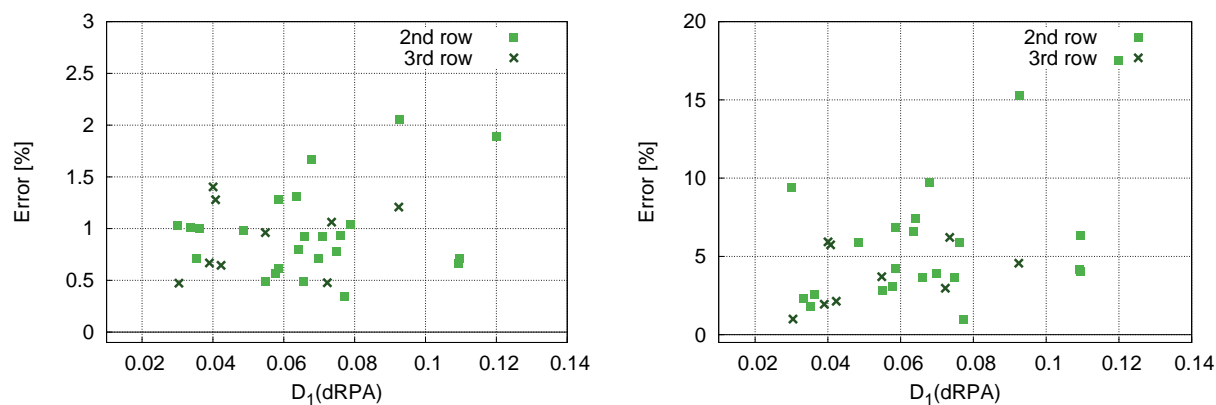

Fig. F.3: D_2 diagnostics for bond lengths and vibrational frequencies for PBE reference determinants.

Fig. F.4: D_1 diagnostics for bond lengths and vibrational frequencies for PBE reference determinants.

Fig. F.5: D_2 diagnostics for bond lengths and vibrational frequencies for PBE0 reference determinants.

Fig. F.6: D_1 diagnostics for bond lengths and vibrational frequencies for PBE0 reference determinants.

Bibliography

[1] G. L. Gutsev, M. D. Mochena, P. Jena, C. W. Bauschlicher Jr., H. Partridge III, *J. Chem. Phys.* **2004,** *121,* 6785.

[2] J. F. Harrison, *Chem. Rev.* **2000,** *100,* 679.

[3] D. Cremer, M. Filatov, V. Polo, E. Kraka, S. Shaik, *Int. J. Mol. Sci.* **2002,** *3,* 604.

[4] N. C. Handy, A. J. Cohen, *Mol. Phys.* **2001,** *99,* 403.

[5] F. Furche, J. P. Perdew, *J. Chem. Phys.* **2006,** *124,* 044103.

[6] M. Dolg, X. Cao, *Chem. Rev.* **2012,** *112,* 403.

[7] H. Eshuis, J. E. Bates, F. Furche, *Theor. Chem. Acc.* **2012,** *131,* 1084.

[8] J. E. Bates, F. Furche, *J. Chem. Phys.* **2013,** *139,* 171103.

[9] M. P. Johansson, I. Warnke, A. Le, F. Furche, *J. Phys. Chem. C* **2014,** *118,* 29370.

[10] X. Ren, P. Rinke, G. E. Scuseria, M. Scheffler, *Phys. Rev. B* **2013,** *88,* 035120.

[11] J. Harl, G. Kresse, *Phys. Rev. Lett.* **2009,** *103,* 056401.

[12] J. Harl, L. Schimka, G. Kresse, *Phys. Rev. B* **2010,** *81,* 115126.

[13] J. Klimes, G. Kresse, *J. Chem. Phys.* **2014,** *140,* 054516.

[14] R. O. Jones, O. Gunnarsson, *Rev. Mod. Phys.* **1989,** *61,* 689.

[15] J. Cerny, P. Hobza, *Phys. Chem. Chem. Phys.* **2007,** *9,* 5291.

[16] S. Grimme, *J. Comput. Chem.* **2004,** *25,* 1463.

[17] S. Grimme, *J. Comput. Chem.* **2006,** *27,* 1787.

[18] S. Grimme, J. Antony, S. Ehrlich, H. Krieg, *J. Chem. Phys.* **2010,** *132,* 154104.

[19] A. Tkatchenko, M. Scheffler, *Phys. Rev. Lett.* **2009,** *102,* 073005.

[20] J. F. Dobson, J. Wang, *Phys. Rev. Lett.* **1999,** *82,* 2123.

[21] A. Szabo, N. S. Ostlund, *Int. J. Quantum Chem.* **1977,** *S11,* 389.

[22] D. C. Langreth, J. P. Perdew, *Phys. Rev. B* **1977,** *15,* 2884.

[23] H. Eshuis, F. Furche, *J. Phys. Chem. Lett.* **2011,** *2,* 983.

[24] X. Ren, P. Rinke, C. Joas, M. Scheffler, *J. Mater. Sci.* **2012,** *47,* 7447.

[25] S. Lebegue, J. Harl, T. Gould, J. G. Ángyán, G. Kresse, J. F. Dobson, *Phys. Rev. Lett.* **2010,** *105,* 196401.

[26] T. Olsen, J. Yan, J. J. Mortensen, K. S. Thygesen, *Phys. Rev. Lett.* **2011,** *107,* 156401.

[27] F. Mittendorfer, A. Garhofer, J. Redinger, J. Klimes, J. Harl, G. Kresse, *Phys. Rev. B* **2011,** *84,* 201401(R).

[28] J. Harl, G. Kresse, *Phys. Rev. B* **2008,** *77,* 045136.

[29] L. Schimka, R. Gaudoin, J. Klimes, M. Marsman, G. Kresse, *Phys. Rev. B* **2013,** *87,* 214102.

[30] J. P. Perdew, A. Ruzsinszky, J. Tao, V. N. Staroverov, G. E. Scuseria, G. I. Csonka, *J. Chem. Phys.* **2005,** *123,* 062201.

[31] J. Tao, J. P. Perdew, V. N. Staroverov, G. E. Scuseria, *Phys. Rev. Lett.* **2003,** *91,* 146401.

[32] J. P. Perdew, K. Burke, M. Ernzerhof, *Phys. Rev. Lett.* **1996,** *77,* 3865.

[33] J. P. Perdew, K. Burke, M. Ernzerhof, *Phys. Rev. Lett.* **1997,** *78,* 1396(E).

[34] C. Adamo, V. Barone, *J. Chem. Phys.* **1999,** *110,* 6158.

[35] A. D. Becke, *J. Chem. Phys.* **1993,** *98,* 5648.

[36] P. Jurecka, J. Sponer, J. Cerny, P. Hobza, *Phys. Chem. Chem. Phys.* **2006,** *8,* 1985.

[37] J. P. Perdew, A. Ruzsinszky, G. I. Csonka, L. A. Constantin, J. Sun, *Phys. Rev. Lett.* **2009,** *103,* 026403.

[38] N. E. Schultz, G. Staszewska, P. Staszewski, D. G. Truhlar, *J. Phys. Chem. B* **2004,** *108,* 4850.

[39] N. Drebov, R. Ahlrichs, *J. Chem. Phys.* **2011,** *134,* 124308.

[40] F. Furche, *Phys. Rev. B* **2001,** *64,* 195120.

[41] D. J. Rowe, *Rev. Mod. Phys.* **1968,** *40,* 153.

[42] D. J. Rowe, *Nucl. Phys.* **1966,** *80,* 209.

[43] G. E. Scuseria, T. M. Henderson, D. C. Sorensen, *J. Chem. Phys.* **2008,** *129,* 231101.

[44] G. E. Scuseria, T. M. Henderson, I. W. Bulik, *J. Chem. Phys.* **2013,** *139,* 104113.

[45] A. Grüneis, M. Marsman, J. Harl, L. Schimka, G. Kresse, *J. Chem. Phys.* **2009,** *131,* 154115.

[46] A. Heßelmann, A. Görling, *Mol. Phys.* **2011,** *109,* 2473.

[47] J. Toulouse, W. M. Zhu, J. G. Ángyán, A. Savin, *Phys. Rev. A* **2010,** *82,* 032502.

[48] T. Olsen, K. S. Thygesen, *Phys. Rev. B* **2013,** *88,* 115131.

[49] T. Olsen, K. S. Thygesen, *J. Chem. Phys.* **2014,** *140,* 164116.

[50] X. Ren, A. Tkatchenko, P. Rinke, M. Scheffler, *Phys. Rev. Lett.* **2011,** *106,* 153003.

[51] J. E. Bates, Dissertation, University of California, Irvine, **2013**.

[52] D. L. Freeman, *Phys. Rev. B* **1977,** *15,* 5512.

[53] J. Klimes, M. Kaltak, E. Maggio, G. Kresse, *J. Chem. Phys.* **2015,** *143,* 102816.

[54] J. Paier, X. Ren, P. Rinke, G. E. Scuseria, A. Grüneis, G. Kresse, M. Scheffler, *New J. Phys.* **2012,** *14,* 043002.

[55] A. Ruzsinszky, I. Y. Zhang, M. Scheffler, *J. Chem. Phys.* **2015,** *143,* 144115.

[56] J. Oddershede, P. Jørgensen, D. L. Yeager, *Comp. Phys. Rep.* **1984,** *2,* 33.

[57] J. Olsen, P. Jørgensen, *J. Chem. Phys.* **1985,** *82,* 3235.

[58] T. Shibuya, J. Rose, V. McKoy, *J. Chem. Phys.* **1973,** *58,* 500.

[59] J. da Providencia, *Nucl. Phys.* **1965,** *61,* 87.

[60] T. Shibuya, V. McKoy, *Phys. Rev. A* **1970,** *2,* 2208.

[61] T. I. Shibuya, V. McKoy, *J. Chem. Phys.* **1971,** *54,* 1738.

[62] T. I. Shibuya, V. McKoy, *J. Chem. Phys.* **1970,** *53,* 3308.

[63] A. Heßelmann, *J. Chem. Phys.* **2011,** *134,* 204107.

[64] T. M. Henderson, G. E. Scuseria, *Mol. Phys.* **2010,** *108,* 2511.

[65] H. Eshuis, J. Yarkony, F. Furche, *J. Chem. Phys.* **2010,** *132,* 234114.

[66] M. Kaltak, J. Klimes, G. Kresse, *Phys. Rev. B* **2014,** *90,* 054115.

[67] M. Kaltak, J. Klimes, G. Kresse, *J. Chem. Theory Comput.* **2014,** *10,* 2498.

[68] K. Burke, *J. Chem. Phys.* **2012,** *136,* 150901.

[69] M. Del Ben, O. Schütt, T. Wentz, P. Messmer, J. Hutter, J. VandeVondele, *Comput. Phys. Commun.* **2015,** *187,* 120.

[70] L. Schimka, J. Harl, A. Stroppa, A. Grüneis, M. Marsman, F. Mittendorfer, G. Kresse, *Nat. Mater.* **2010,** *9,* 741.

[71] TURBOMOLE, TURBOMOLE GmbH, Karlsruhe, V6.6 **2014,** see *www.turbomole.com*.

[72] see CP2K developers group, http://www.cp2k.org/, **2014**.

[73] M. Del Ben, J. Hutter, J. VandeVondele, *J. Chem. Theory Comput.* **2013,** *9,* 2654.

[74] J. Rekkedal, S. Coriani, M. F. Iozzi, A. M. Teale, T. Helgaker, T. B. Pedersen, *J. Chem. Phys.* **2013,** *139,* 081101.

[75] M. Fuchs, X. Gonze, *Phys. Rev. B* **2002,** *65,* 235109.

[76] D. Lu, Y. Li, D. Rocca, G. Galli, *Phys. Rev. Lett.* **2009,** *102,* 206411.

[77] H. F. Schurkus, C. Ochsenfeld, *J. Chem. Phys.* **2016,** *144,* 031101.

[78] A. Luenser, H. F. Schurkus, C. Ochsenfeld, *J. Chem. Theory Comput.* **2017,** ASAP, DOI: 10.1021/acs.jctc.6b01235.

[79] M. Kállay, *J. Chem. Phys.* **2015,** *142,* 204105.

[80] H. Eshuis, F. Furche, *J. Chem. Phys.* **2012,** *136,* 084105.

[81] E. Fabiano, F. Della Sala, *Theor. Chem. Acc.* **2012,** *131,* 1278.

[82] S. F. Boys, F. Bernardi, *Mol. Phys.* **1970,** *19,* 553.

[83] D. Feller, K. A. Peterson, J. Grant Hill, *J. Chem. Phys.* **2011,** *135,* 044102.

[84] J. M. L. Martin, *Chem. Phys. Lett.* **1996,** *259,* 669.

[85] A. Halkier, T. Helgaker, P. Jørgensen, W. Klopper, H. Koch, J. Olsen, A. K. Wilson, *Chem. Phys. Lett.* **1998,** *286,* 243.

[86] J. Toulouse, W. Zhu, A. Savin, G. Jansen, J. G. Ángyán, *J. Chem. Phys.* **2011,** *135,* 084119.

[87] B. G. Janesko, T. M. Henderson, G. E. Scuseria, *J. Chem. Phys.* **2009,** *130,* 081105.

[88] B. G. Janesko, T. M. Henderson, G. E. Scuseria, *J. Chem. Phys.* **2009,** *131,* 034110.

[89] B. Mussard, P. G. Szalay, J. G. Ángyán, *J. Chem. Theory Comput.* **2014,** *10,* 1968.

[90] O. Franck, B. Mussard, E. Luppi, J. Toulouse, *J. Chem. Phys.* **2015,** *142,* 074107.

[91] C. Hättig, W. Klopper, A. Köhn, D. P. Tew, *Chem. Rev.* **2012,** *112,* 4.

[92] W. Klopper, F. R. Manby, S. Ten-no, E. F. Valeev, *Int. Rev. Phys. Chem.* **2006,** *25,* 427.

[93] W. Kutzelnigg, *Theor. Chim. Acta* **1985,** .

[94] W. Klopper, W. Kutzelnigg, *J. Chem. Phys.* **1991,** *94,* 3.

[95] W. Klopper, C. C. M. Samson, *J. Chem. Phys.* **2002,** *116,* 6397.

[96] W. Klopper, W. Kutzelnigg, *J. Mol. Struct. (Theochem)* **1986,** *135,* 339.

[97] W. Klopper, W. Kutzelnigg, *Chem. Phys. Lett.* **1987,** *134,* 17.

[98] W. Kutzelnigg, W. Klopper, *J. Chem. Phys.* **1991,** *94,* 1985.

[99] S. Ten-no, *J. Chem. Phys.* **2004,** *121,* 117.

[100] D. Yamaki, H. Koch, S. Ten-no, *J. Chem. Phys.* **2007,** *127,* 144104.

[101] F. R. Manby, *J. Chem. Phys.* **2003,** *119,* 4607.

[102] E. F. Valeev, *Chem. Phys. Lett.* **2004,** *395,* 190.

[103] D. P. Tew, W. Klopper, *Mol. Phys.* **2010,** *108,* 315.

[104] P. Wind, W. Klopper, T. Helgaker, *Theor. Chim. Acta* **2002,** *107,* 173.

[105] R. A. Bachorz, F. A. Bischoff, A. Glöß, C. Hättig, S. Höfener, W. Klopper, D. P. Tew, *J. Comput. Chem.* **2011,** *32,* 2492.

[106] J. Noga, W. Kutzelnigg, *J. Chem. Phys.* **1994,** *101,* 7738.

[107] H. Fliegl, C. Hättig, W. Klopper, *Int. J. Quantum Chem.* **2006,** *106,* 2306.

[108] H. Fliegl, C. Hättig, W. Klopper, *J. Chem. Phys.* **2006,** *124,* 044112.

[109] C. Neiss, C. Hättig, W. Klopper, *J. Chem. Phys.* **2006,** *125,* 064111.

[110] E. Kordel, C. Villani, W. Klopper, *J. Chem. Phys.* **2005,** *122,* 214306.

[111] S. Höfener, W. Klopper, *Mol. Phys.* **2010,** *108,* 1783.

[112] D. P. Tew, W. Klopper, C. Neiss, C. Hättig, *Phys. Chem. Chem. Phys.* **2007,** *9,* 1921.

[113] D. Bohm, D. Pines, *Phys. Rev.* **1951,** *82,* 625.

[114] D. Pines, D. Bohm, *Phys. Rev.* **1952,** *85,* 338.

[115] D. Bohm, D. Pines, *Phys. Rev.* **1953,** *92,* 609.

[116] A. D. McLachlan, M. A. Ball, *Rev. Mod. Phys.* **1964,** *36,* 844.

[117] A. E. Hansen, T. D. Bouman, *Chem. Phys. Lett.* **1977,** *45,* 326.

[118] A. E. Hansen, T. D. Bouman, *Mol. Phys.* **1979,** *37,* 1713.

[119] J. O. Hirschfelder, *J. Chem. Phys.* **1960,** *33,* 1462.

[120] S. P. A. Sauer, *Molecular Electromagnetism - A Computational Chemistry Approach*; Oxford University Press, Oxford, **2011**.

[121] I. Shavitt, R. J. Bartlett, *Many-Body Methods in Chemistry and Physics: MBPT and Coupled-Cluster Theory*; Cambridge University Press, Cambridge, UK, **2009**.

[122] S. M. Dancoff, *Phys. Rev.* **1950,** *78,* 382.

[123] D. J. Rowe, S. S. M. Wong, *Nucl. Phys. A* **1970,** *153,* 561.

[124] A. L. Fetter, J. D. Walecka, *Quantum Theory of Many-Particle Systems;* McGraw-Hill, New York, **2003**.

[125] P. Ring, P. Schuck, *The Nuclear Many-Body Problem*; Springer, New York, **1980**.

[126] P. Jørgensen, J. Simons, *Second quantization-based methods in quantum chemistry;* Academic Press, New York, **1981**.

[127] O. Christiansen, P. Jørgensen, C. Hättig, *Int. J. Quantum Chem.* **1998,** *68,* 1.

[128] B. Pickup, O. Goscinski, *Mol. Phys.* **1973,** *26,* 1013.

[129] J. Oddershede, P. Jørgensen, *J. Chem. Phys.* **1977,** *66,* 1541.

[130] K. D. Jordan, *Chem. Phys. Lett.* **1975,** *36,* 264.

[131] P. Jørgensen, J. Oddershede, M. A. Ratner, *Chem. Phys. Lett.* **1975,** *32,* 111.

[132] E. S. Nielsen, P. Jørgensen, J. Oddershede, *J. Chem. Phys.* **1980,** *73,* 6238.

[133] M. J. Packer, E. K. Dalskov, T. Enevoldsen, H. J. A. Jensen, J. Oddershede, *J. Chem. Phys.* **1996,** *105,* 5886.

[134] P.-O. Löwdin, *J. Mol. Spectrosc.* **1963,** *10,* 12.

[135] M. Petersilka, U. J. Gossmann, E. K. U. Gross, *Phys. Rev. Lett.* **1996,** *76,* 1212.

[136] E. E. Salpeter, H. A. Bethe, *Phys. Rev.* **1951,** *84,* 1232.

[137] G. Onida, L. Reining, A. Rubio, *Rev. Mod. Phys.* **2002,** *74,* 601.

[138] B. Mussard, D. Rocca, G. Jansen, J. G. Ángyán, *J. Chem. Theory Comput.* **2016,** *12,* 2191.

[139] W. Klopper, personal communication, **2015**.

[140] F. Furche, *J. Chem. Phys.* **2008,** *129,* 114105.

[141] D. C. Langreth, J. P. Perdew, *Solid State Commun.* **1975,** *17,* 1425.

[142] O. Gunnarsson, B. I. Lundqvist, *Phys. Rev. B* **1976,** *13,* 4274.

[143] K. Krause, M. E. Harding, W. Klopper, *Mol. Phys.* **2015,** *113,* 1952.

[144] T. Helgaker, P. Jørgensen, J. Olsen, *Molecular electronic-structure theory*; John Wiley & Sons Inc, Chichester, England, **2000**.

[145] J. G. Ángyán, R. F. Liu, J. Toulouse, G. Jansen, *J. Chem. Theory Comput.* **2011,** *7,* 3116.

[146] W. Klopper, A. M. Teale, S. Coriani, T. B. Pedersen, T. Helgaker, *Chem. Phys. Lett.* **2011,** *510,* 147.

[147] H. B. Callen, T. A. Welton, *Phys. Rev.* **1951,** *83,* 34.

[148] F. Furche, T. Van Voorhis, *J. Chem. Phys.* **2005,** *122,* 164106.

[149] N. Ostlund, M. Karplus, *Chem. Phys. Lett.* **1971,** *11,* 450.

[150] E. A. Sanderson, *Phys. Lett.* **1965,** *19,* 141.

[151] A. Szabo, N. S. Ostlund, *J. Chem. Phys.* **1977,** *67,* 4351.

[152] R. J. Bartlett, M. Musial, *Rev. Mod. Phys.* **2007,** *79,* 291.

[153] G. J. O. Beran, S. R. Gwaltney, M. Head-Gordon, *Phys. Chem. Chem. Phys.* **2003,** *5,* 2488.

[154] I. Lindgren, S. Salomonson, *Int. J. Quantum Chem.* **2002,** *90,* 294.

[155] V. Lotrich, R. J. Bartlett, *J. Chem. Phys.* **2011,** *134,* 184108.

[156] A.-S. Hehn, C. Holzer, W. Klopper, *Chem. Phys.* **2016,** *479,* 160.

[157] G. E. Scuseria, C. L. Janssen, H. F. Schäfer III, *J. Chem. Phys.* **1988,** *89,* 7382.

[158] G. D. Purvis III, R. J. Bartlett, *J. Chem. Phys.* **1982,** *76,* 1910.

[159] G. E. Scuseria, A. C. Scheiner, J. E. Rice, T. J. Lee, H. F. Schaefer III, *J. Chem. Phys.* **1987,** *86,* 2881.

[160] D. Jayatilaka, T. J. Lee, *Chem. Phys. Lett.* **1992,** *199,* 211.

[161] F. Wang, J. Gauss, C. van Wüllen, *J. Chem. Phys.* **2008,** *129,* 064113.

[162] L. Visscher, K. G. Dyall, T. J. Lee, *Int. J. Quantum Chem., Symp.* **1995,** *29,* 411.

[163] J. Oddershede, *Adv. Quantum Chem.* **1978,** *11,* 275.

[164] B. Mussard, P. Reinhardt, J. G. Ángyán, J. Toulouse, *J. Chem. Phys.* **2015,** *142,* 154123.

[165] R. F. Bishop, K. H. Lührmann, *Phys. Rev. B* **1978,** *17,* 3757.

[166] D. P. Tew, W. Klopper, *J. Chem. Phys.* **2005,** *123,* 074101.

[167] J. G. Hill, S. Mazumder, K. A. Peterson, *J. Chem. Phys.* **2010,** *132,* 054108.

[168] J. G. Hill, K. A. Peterson, *Phys. Chem. Chem. Phys.* **2010,** *12,* 10460.

[169] K. E. Yousaf, K. A. Peterson, *J. Chem. Phys.* **2008,** *129,* 184108.

[170] P. Wind, T. Helgaker, W. Klopper, *Theor. Chem. Acc.* **2001,** *106,* 280.

[171] T. Kato, *Commun. Pure Appl. Math.* **1957,** *10,* 151.

[172] D. P. Tew, W. Klopper, *J. Chem. Phys.* **2006,** *125,* 094302.

[173] D. Bokhan, S. Ten-no, J. Noga, *Phys. Chem. Chem. Phys.* **2008,** *10,* 3320.

[174] D. Bokhan, S. Bernadotte, S. Ten-no, *J. Chem. Phys.* **2009,** *131,* 084105.

[175] S. Ten-no, *J. Chem. Phys.* **2007,** *126,* 014108.

[176] D. P. Tew, W. Klopper, C. Hättig, *Chem. Phys. Lett.* **2008,** *452,* 326.

[177] B. G. Janesko, G. E. Scuseria, *Phys. Chem. Chem. Phys.* **2009,** *11,* 9677.

[178] S. Höfener, Dissertation, Karlsruher Institut für Technologie, **2010**.

[179] F. A. Bischoff, Dissertation, Karlsruher Institut für Technologie, **2009**.

[180] A.-S. Hehn, D. P. Tew, W. Klopper, *J. Chem. Phys.* **2015,** *142,* 194106.

[181] A.-S. Hehn, W. Klopper, *J. Chem. Phys.* **2013,** *138,* 181104.

[182] G. Jansen, R. F. Liu, J. G. Angyan, *J. Chem. Phys.* **2010,** *133,* 154106.

[183] T. H. Dunning Jr., *J. Chem. Phys.* **1989,** *90,* 1007.

[184] R. A. Kendall, T. H. Dunning Jr., R. J. Harrison, *J. Chem. Phys.* **1992,** *96,* 6796.

[185] R. Haunschild, W. Klopper, *J. Chem. Phys.* **2012,** *136,* 164102.

[186] F. Weigend, A. Köhn, C. Hättig, *J. Chem. Phys.* **2002,** *116,* 3175.

[187] C. Hättig, *Phys. Chem. Chem. Phys.* **2005,** *7,* 59.

[188] F. Weigend, *J. Comput. Chem.* **2008,** *29,* 167.

[189] K. E. Yousaf, K. A. Peterson, *Chem. Phys. Lett.* **2009,** *476,* 303.

[190] T. Helgaker, W. Klopper, H. Koch, J. Noga, *J. Chem. Phys.* **1997,** *106,* 9639.

[191] D. P. Tew, W. Klopper, *J. Chem. Phys.* **2005,** *123,* 074101.

[192] D. E. Woon, K. A. Peterson, T. H. Dunning Jr., *J. Chem. Phys.* **1998,** *109,* 2233.

[193] T. van Mourik, R. J. Vos, J. H. van Lenthe, F. B. van Duijneveldt, *Int. J. Quantum Chem.* **1997,** *111,* 9248.

[194] F.-M. Tao, Y.-K. Pan, *J. Phys. Chem.* **1991,** *95,* 3582.

[195] W. Klopper, *J. Chem. Phys.* **2001,** *115,* 761.

[196] C. Schwartz, *Phys. Rev.* **1962,** *90,* 1007.

[197] W. Kutzelnigg, J. D. Morgan III, *J. Chem. Phys.* **1992,** *96,* 4484.

[198] W. Kutzelnigg, J. D. Morgan III, *J. Chem. Phys.* **1992,** *97,* 8821.

[199] A. Halkier, T. Helgaker, P. Jørgensen, W. Klopper, J. Olsen, *Chem. Phys. Lett.* **1999,** *302,* 437.

[200] F. Jensen, *Theor. Chem. Acc.* **2000,** *104,* 484.

[201] T. B. Adler, G. Knizia, H.-J. Werner, *J. Chem. Phys.* **2007,** *127,* 221106.

[202] G. Knizia, H.-J. Werner, *J. Chem. Phys.* **2008,** *128,* 154103.

[203] G. Knizia, T. B. Adler, H.-J. Werner, *J. Chem. Phys.* **2009,** *130,* 054104.

[204] A. Köhn, D. P. Tew, *J. Chem. Phys.* **2010,** *132,* 024101.

[205] S. Höfener, *J. Comput. Chem.* **2014,** *35,* 1716.

[206] S. Höfener, D. P. Tew, W. Klopper, T. Helgaker, *Chem. Phys.* **2009,** *356,* 25.

[207] F. Weigend, R. Ahlrichs, *Phys. Chem. Chem. Phys.* **2005,** *7,* 3297.

[208] D. W. Schwenke, *J. Chem. Phys.* **2005,** *122,* 014107.

[209] R. Jurgens-Lutovsky, J. Almlöf, *Chem. Phys. Lett.* **1991,** *178,* 451.

[210] K. Wolinski, P. Pulay, *J. Chem. Phys.* **2003,** *118,* 9497.

[211] J. Deng, P. M. W. Gill, *J. Chem. Phys.* **2011,** *134,* 081103.

[212] A. Köhn, *J. Chem. Phys.* **2009,** *130,* 104104.

[213] M. Hanauer, A. Köhn, *J. Chem. Phys.* **2009,** *131,* 124118.

[214] J. Toulouse, I. C. Gerber, G. Jansen, A. Savin, J. G. Ángyán, *Phys. Rev. Lett.* **2009,** *102,* 096404.

[215] M. Fuchs, Y. M. Niquet, X. Gonze, K. Burke, *J. Chem. Phys.* **2005,** *122,* 094116.

[216] R. A. Bachorz, Dissertation, Universität Karlsruhe (TH), **2009.**

[217] S. Ahnen, A.-S. Hehn, K. D. Vogiatzis, M. A. Trachsel, S. Leutwyler, W. Klopper, *Chem. Phys.* **2014,** *441,* 17.

[218] A. Köhn, D. P. Tew, *J. Chem. Phys.* **2010,** *133,* 174117.

[219] J. Noga, W. Kutzelnigg, W. Klopper, *Chem. Phys. Lett.* **1992,** *199,* 497.

[220] T. Shiozaki, M. Kamiya, S. Hirata, E. F. Valeev, *J. Chem. Phys.* **2008,** *129,* 071101.

[221] A. Köhn, G. W. Richings, D. P. Tew, *J. Chem. Phys.* **2008,** *129,* 201103.

[222] H. Fliegl, W. Klopper, C. Hättig, *J. Chem. Phys.* **2005,** *122,* 084107.

[223] D. P. Tew, W. Klopper, C. Neiss, C. Hättig, *Phys. Chem. Chem. Phys.* **2008,** *10,* 6325 (E).

[224] C. Hättig, D. P. Tew, A. Köhn, *J. Chem. Phys.* **2010,** *132,* 231102.

[225] H. van Aggelen, Y. Yang, W. Yang, *Phys. Rev. A* **2013,** *88,* 030501(R).

[226] D. A. Sirianni, L. A. Burns, C. D. Sherrill, *J. Chem. Theory Comput.* **2017,** *13,* 86.

[227] F. A. Bischoff, S. Wolfsegger, D. P. Tew, W. Klopper, *Mol. Phys.* **2009,** *107,* 963.

[228] E. Papajak, D. G. Truhlar, *J. Chem. Theory Comput.* **2010,** *6,* 597.

[229] E. Papajak, D. G. Truhlar, *J. Chem. Theory Comput.* **2011,** *7,* 10.

[230] A. Halkier, W. Klopper, T. Helgaker, P. Jørgensen, P. R. Taylor, *J. Chem. Phys.* **1999,** *111,* 9157.

[231] K. S. Singwi, M. P. Tosi, R. H. Land, *Phys. Rev.* **1968,** *176,* 589.

[232] Z. D. Yan, J. P. Perdew, S. Kurth, *Phys. Rev. B* **2000,** *61,* 16430.

[233] H. Jiang, E. Engel, *J. Chem. Phys.* **2007,** *127,* 184108.

[234] M. Hellgren, U. von Barth, *Phys. Rev. B* **2007,** *76,* 075107.

[235] A. Ruzsinszky, J. P. Perdew, G. I. Csonka, *J. Chem. Theory Comput.* **2010,** *6,* 127.

[236] A. Heßelmann, A. Görling, *Mol. Phys.* **2010,** *108,* 359.

[237] H.-V. Nguyen, G. Galli, *J. Chem. Phys.* **2010,** *132,* 044109.

[238] N. L. Nguyen, N. Colonna, S. de Gironcoli, *Phys. Rev. B* **2014,** *90,* 045138.

[239] N. Colonna, M. Hellgren, S. de Gironcoli, *Phys. Rev. B* **2014,** *90,* 125150.

[240] N. Colonna, M. Hellgren, S. de Gironcoli, *Phys. Rev. B* **2016,** *93,* 195108.

[241] P. Mori-Sánchez, A. J. Cohen, W. Yang, *Phys. Rev. A* **2012,** *85,* 042507.

[242] K. A. Peterson, T. B. Adler, H.-J. Werner, *J. Chem. Phys.* **2008,** *128,* 084102.

[243] D. P. Tew, W. Klopper, *J. Chem. Phys.* **2006,** *125,* 094302.

[244] U. R. Fogueri, S. Kozuch, A. Karton, J. M. L. Martin, *Theor. Chem. Acc.* **2013,** *132,* 1291.

[245] S. Grimme, A. Hansen, *Angew. Chem. Int. Ed.* **2015,** *54,* 12308.

[246] T. J. Lee, M. Head-Gordon, A. P. Rendell, *Chem. Phys. Lett.* **1995,** *243,* 402.

[247] C. L. Janssen, I. M. B. Nielsen, *Chem. Phys. Lett.* **1998,** *290,* 423.

[248] I. M. B. Nielsen, C. L. Janssen, *Chem. Phys. Lett.* **1999,** *310,* 568.

[249] T. J. Lee, P. R. Taylor, *Int. J. Quantum Chem.* **1989,** *36(S23),* 199.

[250] J. P. Coe, P. Murphy, M. J. Paterson, *Chem. Phys. Lett.* **2014,** *604,* 46.

[251] M. L. Leininger, I. M. B. Nielsen, T. D. Crawford, C. L. Janssen, *Chem. Phys. Lett.* **2000,** *328,* 431.

[252] J. P. Coe, M. J. Paterson, *J. Chem. Theory Comput.* **2015,** *11,* 4189.

[253] C. Hättig, A. Köhn, K. Hald, *J. Chem. Phys.* **2002,** *116,* 5401.

[254] A. Karton, E. Rabinovich, J. M. L. Martin, B. Ruscic, *J. Chem. Phys.* **2006,** *125,* 144108.

[255] A. Karton, S. Daon, J. M. L. Martin, *Chem. Phys. Lett.* **2011,** *510,* 165.

[256] N. E. Schultz, Y. Zhao, D. G. Truhlar, *J. Phys. Chem. A* **2005,** *109,* 11127.

[257] J. S. Sears, C. D. Sherrill, *J. Phys. Chem. A* **2008,** *112,* 3466.

[258] J. S. Sears, C. D. Sherrill, *J. Phys. Chem. A* **2008,** *112,* 6741.

[259] O. Tishchenko, J. Zheng, D. G. Truhlar, *J. Chem. Theory Comput.* **2008,** *4,* 1208.

[260] J. L. Bao, A. Sand, L. Gagliardi, D. G. Truhlar, *J. Chem. Theory Comput.* **2016,** *12,* 4274.

[261] P.-O. Löwdin, *Phys. Rev.* **1955,** *97,* 1474.

[262] M. S. Gordon, M. W. Schmidt, G. M. Chaban, K. R. Glaesemann, W. J. Stevens, C. Gonzalez, *J. Chem. Phys.* **1999,** *110,* 4199.

[263] K. Boguslawski, P. Tecmer, Ö. Legeza, M. Reiher, *J. Phys. Chem. Lett.* **2012,** *3,* 3129.

[264] K. Boguslawski, P. Tecmer, G. Barcza, Ö. Legeza, M. Reiher, *J. Chem. Theory Comput.* **2013,** *9,* 2959.

[265] C. J. Stein, M. Reiher, *Mol. Phys.* **2017,** ASAP, DOI: http://dx.doi.org/10.1080/00268976.2017.1288934.

[266] W. Jiang, N. J. DeYonker, J. J. Determan, A. K. Wilson, *J. Phys. Chem. A* **2012,** *116,* 870.

[267] J. Wang, S. Manivasagam, A. K. Wilson, *J. Chem. Theory Comput.* **2015,** .

[268] T. J. Lee, *Chem. Phys. Lett.* **2003,** *372,* 362.

[269] E. A. Salter, H. Sekino, R. J. Bartlett, *J. Chem. Phys.* **1987,** *87,* 502.

[270] O. Treutler, R. Ahlrichs, *J. Chem. Phys.* **1995,** *102,* 346.

[271] CFOUR program package, see www.cfour.de, **2015**.

[272] J. Gauss, J. F. Stanton, *J. Chem. Phys.* **2002,** *116,* 1773.

[273] A. M. Burow, J. E. Bates, F. Furche, H. Eshuis, *J. Chem. Theory Comput.* **2014,** *10,* 180.

[274] D. S. Ranasinghe, G. A. Peterson, *J. Chem. Phys.* **2013,** *138,* 144104.

[275] P. Deglmann, F. Furche, R. Ahlrichs, *Chem. Phys. Lett.* **2002,** *362,* 511.

[276] P. Deglmann, F. Furche, *J. Chem. Phys.* **2002,** *117,* 9535.

[277] W. Klopper, *Chem. Phys. Lett.* **1991,** *186,* 583.

[278] H.-J. Werner, T. B. Adler, F. R. Manby, *J. Chem. Phys.* **2007,** *126,* 164102.

[279] S. Kedžuch, M. Milko, J. Noga, *Int. J. Quantum Chem.* **2005,** *105,* 929.

[280] R. T. Pack, W. Byers Brown, *J. Chem. Phys.* **1966,** *45,* 556.

[281] M. Ernzerhof, *Chem. Phys. Lett.* **1996,** *263,* 499.

[282] A. Szabo, N. S. Ostlund, *Modern Quantum Chemistry - Introduction to Advanced Electronic Structure Theory*; Dover Publications Inc., New York, **1982**.

[283] W. Klopper, R. A. Bachorz, C. Hättig, D. P. Tew, *Theor. Chem. Acc.* **2010,** *126,* 289.

Acknowledgments